UNIVERSIDADE ESTADUAL DE CAMPINAS
FACULDADE DE ENGENHARIA AGRÍCOLA

MONIQUE PIRES GRAVINA DE OLIVEIRA

Assimilação de dados de monitoramento em tempo real visando melhores estimativas do crescimento vegetal em cultivo protegido

Leveraging data assimilation and monitoring data for improvement of crop growth estimates in protected environments

CAMPINAS

2022

MONIQUE PIRES GRAVINA DE OLIVEIRA

Leveraging data assimilation and monitoring data for improvement of crop growth estimates in protected environments

Assimilação de dados de monitoramento em tempo real visando melhores estimativas do crescimento vegetal em cultivo protegido

Tese apresentada à Faculdade de Engenharia Agrícola da Universidade Estadual de Campinas como parte dos requisitos exigidos para a obtenção do título de Doutora em Engenharia Agrícola, na Área de Agricultura Digital.

Thesis presented to the School of Agricultural Engineering of the University of Campinas in partial fulfillment of the requirements for the degree of Doctor in Agricultural Engineering, in the area of Digital Agriculture.

Supervisor: Prof. Dr. Luiz Henrique Antunes Rodrigues

ESTE EXEMPLAR CORRESPONDE À VERSÃO FINAL DA TESE DEFENDIDA PELA ALUNA MONIQUE PIRES GRAVINA DE OLIVEIRA, E ORIENTADA PELO PROF. DR. LUIZ HENRIQUE ANTUNES RODRIGUES.

CAMPINAS

2022

Ficha catalográfica
Universidade Estadual de Campinas
Biblioteca da Área de Engenharia e Arquitetura
Rose Meire da Silva - CRB 8/5974

OL4l

Oliveira, Monique Pires Gravina de, 1988-
Leveraging data assimilation and monitoring data for improvement of crop growth estimates in protected environments / Monique Pires Gravina de Oliveira. – Campinas, SP : [s.n.], 2022.

Orientador: Luiz Henrique Antunes Rodrigues.
Tese (doutorado) – Universidade Estadual de Campinas, Faculdade de Engenharia Agrícola.

1. Simulação (Computadores). 2. Tomate. 3. Assimilação contínua de dados. I. Rodrigues, Luiz Henrique Antunes, 1959-. II. Universidade Estadual de Campinas. Faculdade de Engenharia Agrícola. III. Título.

Informações para Biblioteca Digital

Título em outro idioma: Assimilação de dados de monitoramento em tempo real visando melhores estimativas do crescimento vegetal em cultivo protegido
Palavras-chave em inglês:
Computer simulation
Tomatoes
Continuous data assimilation
Área de concentração: Agricultura Digital
Titulação: Doutora em Engenharia Agrícola
Banca examinadora:
Luiz Henrique Antunes Rodrigues [Orientador]
Daniel Wallach
Fábio Ricardo Marin
Alim Pedro de Castro Gonçalves
Paulo Rodrigues Peloia
Data de defesa: 04-03-2022
Programa de Pós-Graduação: Engenharia Agrícola

Identificação e informações acadêmicas do(a) aluno(a)
- ORCID do autor: https://orcid.org/0000-0001-7167-4473
- Currículo Lattes do autor: http://lattes.cnpq.br/0521317243890007

Este exemplar corresponde à redação final da **Tese de Doutorado** defendida por **Monique Pires Gravina de Oliveira**, aprovada pela Comissão Julgadora em 04 de março de 2022, na Faculdade de Engenharia Agrícola da Universidade Estadual de Campinas.

Prof. Dr. Luiz Henrique Antunes Rodrigues — Presidente e Orientador

Dr. Alim Pedro de Castro Gonçalves — Membro Titular

Dr. Daniel Wallach — Membro Titular

Dr. Fábio Ricardo Marin — Membro Titular

Dr. Paulo Rodrigues Peloia — Membro Titular

A Ata da defesa com as respectivas assinaturas dos membros encontra-se no SIGA/Sistema de Fluxo de Dissertação/Tese e na Secretaria do Programa da Unidade.

ACKNOWLEDGEMENTS

My doctoral scholarship was funded by grant #2018/12050-6, São Paulo Research Foundation (FAPESP). This study was financed in part by the Coordenação de Aperfeiçoamento de Pessoal de Nível Superior - Brasil (CAPES) - Finance Code 001.

By the end of my Master's degree, I was sure I wanted to tell everyone about self-confidence and about how people around me empowered me, helping me in doing a good job. This is still true, but at this moment, I want to extend my comment to mention my colossal luck to have gotten where I am. It may sound weird to talk about luck in the middle of a pandemic but that is even more evidence, as during the peak of the crisis, I was able to work from home and be protected, while so many were failed by those who could and should have protected them. While life demanded everybody kept moving, I could do so (mostly) from the safety of my home.

Acknowledging luck does not detract from my efforts. Anyone who browses through these pages will be able to see my work, but luck is invisible and should therefore also be acknowledged. And I mean to talk about it because thinking what I achieved could not have fallen apart by just one wrong decision or that I am somehow special and that I deserve what I got, while other people who work just as hard, do not, would be arrogant and ignorant. I was lucky I could do everything I planned, but I am also aware of how there are so many things that were not under my control. All the coincidences — references I found, people I met, small decisions I made or other people made and were out of my power to change — that made this experience even more enriching than what I had in my mind when I began.

And, obviously, I must highlight everyone around me that helped me. I was lucky they were around and that they decided to trust me. Thank you,

Lique, for letting me bloom. For trusting me and teaching me so much about academia. Also, for helping with the funding needed to conduct this research.

Felipe, for all the suggestions and all the support. I never stopped because you have always been there to help me move. Thank you for all your effort to help me go further.

José, Mônica and Valéria, for the support as well. I have been distant and you have always been there for me. You should know it was worthy.

Henrique, my loyal squire, who was up for helping me every time I needed. And Rafaella, for taking care of everything while I was abroad.

Thais, for giving so much when I could give so little back. And being so kind in the process. And never getting (visibly) mad at me even as I (so often) disrespected your maternity leave.

Professor Romis, for giving valuable comments on my work and for carefully listening to my ideas (being the opposite of the terrible academics I met along the way).

Professor Antonio, for the collaboration in the last growth cycle.

Fernando, Matheus and his father, and Yuri and his grandfather, for all the hard work when installing the infrastructure and the sensors used in this research.

Durval Almeida and Carolina Cinto, for aiding with agronomical advice.

Diogo, on whom I have forever been reliant for solving complicated computer stuff. Marcos, for the help with the optimizations, and Gregory, with the PMX.

Leonardo, Gustavo, Gustavo, and Periclão, for aiding with the fieldwork. And Zé Maria, Giovanni, Túlio, Oldeny, and all the staff from Feagri that somehow contributed to this project. Professors Gustavo and Rafael for allowing the use of the labs. Professor Angel, as the head of the institution, for providing the maintenance of the structures.

JD, who opened the doors of his house and received me and was the best housemate I could ever want while living abroad, and Dr. Chuang Zhao, for always helping when I needed.

Stack OverFlow community, for existing, even though replies should not go in the comment area.

Dr. Rafael Ribeiro, for assisting in the initial stages of the project. Unfortunately, the project went in a direction that prevented us from working more closely. I am sure I would have learned a lot.

Dr. Daniel Wallach and Dr. Senthold Asseng, from whom I learned so much during my stay at UF.

Dr. Luís Villani and Dr. Murilo Loiola, for the suggestions in my project thesis committee. And also, Dr. Daniel Wallach, Dr. Fábio Marin, Dr. Alim Gonçalves, and Dr. Paulo Peloia, for reading my thesis and discussing it, helping me in seeing further.

Dr. James W Jones, for providing the code and data for the Reduced State TOMGRO model.

The Fulbright Commission in Brazil, for granting me the Doctoral Dissertation Research Award.

Feagri, for being my Pawnee, and Unicamp, for all the resources to become a better person and a better academic with which it provided me.

“Oh, Lord, please, don’t let me be misunderstood.”

Bennie Benjamin, Horace Ott, and Sol Marcus

“Life goes easy on me. Most of the time.”

Damien Rice

RESUMO

Modelos dinâmicos de crescimento de culturas associados à imensa massa de dados disponíveis têm sido enxergados como parte da resposta ao problema de uma produção agrícola mais eficiente quanto ao uso de recursos. Apesar de tais modelos demandarem etapas de calibração sem as quais seu desempenho preditivo pode ser insuficiente para auxílio na tomada de decisão, o monitoramento em tempo real poderia ser capaz de contornar essa necessidade. Modelos dinâmicos e imagens de satélites têm sido combinados por meio de técnicas de assimilação de dados para diminuição dos erros de predição de variáveis de estado relacionadas ao dossel das culturas, a propriedades do solo ou à produtividade. Em ambientes protegidos, porém, em que o uso de modelos e de sensores permite o monitoramento e a automação de sistemas de controle, de modo que é possível otimizar as condições ambientais visando maior lucratividade da produção, a aplicação de técnicas de assimilação aos dados de monitoramento é pouco explorada. Este projeto teve como objetivo, portanto, determinar o desempenho de técnicas de assimilação de dados utilizando sensoriamento do ambiente e da cultura em uma casa de vegetação, bem como determinar qual a resolução temporal necessária para sua realização e o grau tecnológico necessário para que a abordagem possa ser replicada em condições de produção. Para isso, foram monitorados os fatores meteorológicos de uma casa de vegetação com o cultivo de tomate, bem como o crescimento dos vegetais, por meio de pesagem direta de plantas e do uso de imagens capturadas com câmeras de baixo custo. Por meio de técnicas de estimação de estado como o *Unscented Kalman Filter* e o *Ensemble Kalman Filter*, foi realizada assimilação dos dados no modelo TOMGRO reduzido. Uma vez que o uso dessas técnicas em cultivo protegido não havia sido realizado, foi necessário caracterizar cuidadosamente os elementos que afetam o desempenho dos modelos, bem como dos filtros. Foi observado que: 1. dependendo do modelo de crescimento utilizado, a assimilação de uma variável de estado pode não impactar as demais, como sugerido por análises de sensibilidade, 2. a qualidade das observações é determinante para o bom desempenho das técnicas de assimilação, 3. a assimilação teve melhor desempenho quando houve necessidade de adequar as estimativas a perturbações no crescimento, 4. uma vez que o desempenho dos filtros leve a melhores estimativas da produtividade, não são requeridas observações contínuas. Embora, de modo geral, não tenha sido possível obter desempenhos superiores aos do modelo calibrado, este potencial existe, uma vez que melhores modelos de observações e melhores observações estejam disponíveis.

Palavras-chave: Modelos de crescimento; Assimilação de dados; Cultivo Protegido; Tomate

ABSTRACT

Dynamic crop growth models coupled with the vast amount of available data have been seen as part of the answer to the problem of more resource-efficient agricultural production. Although such models require calibration steps without which their predictive performance may be insufficient to aid decision making, real-time monitoring could be able to overcome this need. Dynamic models and satellite images have been combined using data assimilation techniques to reduce the prediction errors of state variables related to crop canopy, soil properties, or yield. In protected environments, however, where the use of models and sensors allows the monitoring and automation of control systems so that it is possible to optimize environmental conditions for greater production profitability, the assimilation of monitoring data is not explored. This project aimed, then, to determine the performance of data assimilation techniques using environmental and crop sensing in a greenhouse, as well as to determine the acquisition frequency required and the technological level necessary for the approach to be replicated under production conditions. To do so, the meteorological factors of a greenhouse with tomato cultivation were monitored, as well as crop growth, through direct weighing of plants and the use of images captured with low-cost cameras. Using state estimation techniques such as the Unscented Kalman Filter and the Ensemble Kalman Filter, data assimilation in the Reduced State TOMGRO model was performed. Since the use of these techniques in protected cultivation had not been carried out, it was necessary to carefully characterize the elements that affect the performance of the models, as well as the filters. It was observed that: 1. depending on the growth model used, the assimilation of one state variable may not impact the others, as suggested by sensitivity analyses, 2. the quality of observations is crucial for good performance of the assimilation techniques, 3. the assimilation performed better when there was a need to adjust the estimates to growth disturbances, 4. when filters lead to better productivity estimates, continuous observations are not required. Although, in general, it has not been possible to obtain better performances than the calibrated model, this potential exists, as long as better observation models and better-quality observations are available.

Keywords: Crop models; Data assimilation; Protected cultivation; Tomato

LIST OF FIGURES

LIST OF TABLES

TABLE OF CONTENTS

1. INTRODUCTION

The improvement of models of agricultural systems has been widely discussed in the scientific community and has been the subject of special issues of various journals, such as Agricultural Systems (Antle et al., 2017b), European Journal of Agronomy (Wallach and Thorburn, 2017) and Environmental Modelling & Software (Athanasiadis et al., 2015; Holzworth et al., 2014). Researchers expect a new generation of crop growth and development models that can draw on both historical and real-time data (Jones et al., 2017a). As Antle et al. (2017a) point out, in addition to high-resolution historical yield data, which is already available for many growers, there is a vast amount of information available, such as weather forecasts, satellite imagery, thermal imaging and high-resolution spectral data obtained by unmanned aerial vehicles.

Although Antle et al. (2017a) and Jones et al. (2017a) focused mainly on the opportunities for open-field agriculture, the growing demand for food in a context of climate change and shortage of productive land has also required advances in protected cultivation. This has been reflected in the new paradigms of food production, such as vertical farms and urban agriculture, in addition to traditional greenhouses (Graamans et al., 2018; Lawson, 2016; Pinstrup-Andersen, 2017; van Delden et al., 2021). But while the improvement and requirements of models for grasslands, field crops and livestock have been thoroughly discussed, horticultural crops are often not included in crop modeling discussions.

Even as a lot of work has been done in the modeling of the growth and development of greenhouse tomatoes (Heuvelink et al., 2018; Marcelis et al., 1998), assessments that would allow for their wider usage are less frequent, particularly for tropical growth in low-tech greenhouses. For instance, a first arduous and necessary step for the use of crop growth models is calibration of crop specific parameters (Seidel et al., 2018), but for Brazilian growth conditions — either specific cultivars or weather —, no studies have been performed to calibrate these models. And while one could argue the weather variability issues that often lead to different responses to the environment are not present in controlled environments, this is not the case for low- or medium- technology greenhouses (Montero et al., 2019).

It could then be the case that for these environments, one use of the new deluge of data could be to bypass the need for calibration for obtaining good estimates. Steppe (2012) highlighted how sensing data in greenhouses can be used along with mechanistic models to assist in management decisions, so that interventions are connected to the needs of the plant, within the concept of "speaking plant". Observations from continuous monitoring in greenhouses come in multiple forms, such as stem diameters, crop weight, plants' images, but have been explored only by machine learning techniques (Hemming et al., 2020, 2019) even if non-calibrated mechanistic models could assist in providing trends and constraints that could not be observed during growth.

One way to associate sensing data and crop growth process-based models is by data assimilation. Data assimilation is a widely used method in hydrology and meteorology, which consists in combining observed values to the states estimated by the models, taking into account both errors intrinsic to the model and in the observations (Pellenq and Boulet, 2004; Rodell et al., 2004). In the case of crop modeling, data assimilation has been used with remote sensing images to estimate state variables related to crop canopy or soil properties, which has led to better estimates of yield, leaf area index and soil moisture (Dorigo et al., 2007; Jin et al., 2018).

Shifting from the traditional use of satellite images as sources of additional growth information, recent works have explored unmanned aerial vehicles (UAV) and digital images, such as in Yu et al. (2020), to improve yield estimates by assimilating sugarcane height. Linker and Ioslovich (2017) incorporated into the Aquacrop model estimates of canopy cover obtained from digital images of the canopy, as well as data obtained from destructive analysis as biomass observations.

Destructive analysis data has also been used by Ruíz-García et al. (2014) with lettuces and the Nicolet model, but data automatically collected in protected environments has not yet been explored. The lack of studies means it is still unclear what type of growth observation could be useful, particularly if the goal is to obtain better estimates of yield. As some authors (Linker and Ioslovich, 2017; Nearing et al., 2012) observed, assimilation of one variable will not necessarily capture enough information for the model to change yield outcomes. Several challenges and opportunities of data assimilation with remote sensing discussed by recent reviews (Huang et al., 2019a; Jin et al., 2018) would not extrapolate for proximal sensing, as they refer to problems of large areas. However, some of them, such as frequency of assimilation and its impacts on the computational structure required for storing or processing data, would also be present. Furthermore, considering the potential availability of solutions based on this principle, the sources of data for models' environmental inputs and growth observations should come from low-cost sensors, even though these could increase the uncertainty of the inputs, impairing the improvement of estimates.

While assimilation of monitoring data has then the potential to allow for the use of imperfect horticultural growth models, not much is known regarding how it could be used. This work explores if it would be possible to obtain good estimates of tomato growth if real-time observations were assimilated into a non-calibrated tomato model and different approaches to reach this outcome, regarding sources of observations and frequency.

2. OBJECTIVES

To achieve the overall goal of determining if there is an approach to assimilation of monitoring data that could circumvent the need for calibrating a greenhouse-tomato model of growth and development to achieve good estimates of greenhouse tomato growth, there are several goals that must also be achieved:

- Determine how different sources of growth data impact the update of state variables, including yield.
- Determine the difference in performance of data assimilation techniques when environmental inputs and growth data are provided by scientific-grade and by low-cost sensors.
- Assess the impact of assimilation frequency in the uncertainty of estimates obtained by a non-calibrated model subject to growth data assimilation.

3. LITERATURE REVIEW

3.1. Crop models

Briefly, crop models are mathematical representations of plants throughout their growth as affected by the factors that influence said growth, e. g. crop's genetics and the environment. De Vries (1982) proposed three levels of complexity for categorizing crop models: preliminary, comprehensive, or summary models. While the first type contains basic features of the system and aims at a first understanding of the subject, once more knowledge into the processes is gained and imbued into the model, it becomes closer to the second type which, to be made more accessible to others, may then be simplified into the third type, depending on the intended use of the model. Passioura (1996) discussed two other categories, which are related to the intent of their development and use: they could be aimed at farmers, to aid in their decision-making and, for that, understanding of the underlying mechanisms would not be required, or they could be aimed at scientific purposes, which means that the description of mechanisms should be related to theories and validated by hypothesis testing. The first case is generally associated with the terms functional, empirical, statistical and phenomenological and the second, to the terms mechanistic and process-based (Jones et al., 2017b).

Throughout the years, the discipline has evolved to include innovations in data sources, as well as the new requirements of such models. Crop models were no longer standalone tools and became elements of agricultural systems models, through integration across different domains, along with soil, livestock systems, pests and diseases, economic, and landscape and watershed models, enhancing their roles in policy and decision-making (Holzworth et al., 2015; Jones et al., 2017a). And while the first models created could be described as curiosity-driven (Jones et al., 2017b), the denominated "Next Generation of Crop Models" was expected to improve representation of spatial heterogeneity and temporal dynamics, accurately represent the effects of extreme events, incorporate genetics, characterize crop nutrition, include responses to pests and diseases, admit intercrops, crop rotation and livestock production, and comprise economic and social dimensions (Antle et al., 2017a). As Keating and Thorburn (2018) observed, in the past twenty years, research has moved from descriptive and nomothetic contexts to policy and action-driven ones.

This evolution relates to the previously defined categories. While Jones et al. (2017a) state that models are "either functional or mechanistic", Jones et al. (2017b) expand this idea by mentioning how explanatory models may be fully mechanistic, but may also include both mechanistic and functional model **components**. One may also look into Keating and Thorburn

(2018) and how they point to a situation that, right now, in a context of “Big Data” and “Internet of Things”, is more blurred than the allocation of models in such strict categories. They expect a new relationship with data that would increase its role in model use and development through, e. g. model-data fusion and inverse modelling, and new roles for remote and proximal sensing in their initialization and calibration.

Almost twenty-five years ago, a special issue of the journal Scientia Horticulturae covered the existing modeling approaches for fruits, vegetables, and ornamental plants. One question Gary, Jones and Tchamitchian (1998) aimed to clarify was what was expected from crop modeling in horticulture. As others before them (Boote et al., 1996), they mentioned how crop models have value for scientists, growers and policy-makers. For instance, by providing quantitative information regarding crop timing, irrigation, fertilization, crop protection, and climate control, growers would be able to make decisions at the field scale while, on a regional scale, policies could be evaluated from estimations of potential yields, water needs and fertilizer losses. For horticultural models specifically, they mention the diversity of crop management problems: fruit crops and ornamentals, as perennial species, require not only being maintained at high levels of production but also of survival for the following cycle and greenhouses, as another specific cultivation system, can be compared to industrial production systems and crop models may be used in different temporal and spatial scales, allowing for more meticulous management of greenhouses and aiding in crop planning. This management is detailed in the same issue by Lentz (1998) who, when describing the decision levels in the production context, pointed to how crop models could be used to optimize environmental conditions for growth but that would require them to be highly accurate.

However, the improvement of crop models throughout the years that has been thoroughly presented (Holzworth et al., 2015; Jones et al., 2017b) has often been aimed at grasslands, field crops and livestock and has not included horticultural crops, despite belonging to the same field of study. Differently from other crops, there are few studies using tomato growth models to understand production. Berrueta et al. (2020) evaluated greenhouse-grown tomatoes in Uruguay regarding their yield gap, using the Tomsim model to estimate potential growth, presenting management alternatives to reduce the gap and Bojacá, Gil and Cooman (2009) used the Tomgro model to evaluate yield variability in greenhouses in Colombia, but these analyses are not as widespread. However, the community has started directing its attention to the need of advancing modeling of non-staple crops. One example comes from Antle et al. (2017) pointing to how since one of the primary correlates of health in people moving out of hunger is fruit and vegetable consumption, one needs to understand better how they will be affected by climate change.

3.2. Models of greenhouse tomatoes growth and development

After potatoes, tomatoes are the most frequently grown vegetable crops worldwide. As is the case for all crops, tomato yield is not an isolated characteristic, so if the plant does not grow well, it will not have a high yield (Van Ploeg and Heuvelink, 2005). Therefore, models that represent tomato growth and development should be able to characterize the interactions between events and their effects.

Marcelis, Heuvelink and Goudriaan (1998) reviewed horticultural crop models focusing on the representation of growth and development. They discussed the existing approaches for calculating light interception, photosynthesis, respiration, and partitioning, concluding that the larger gaps in modeling these processes lied on the simulation of leaf area development, maintenance respiration, organ abortion, dry mass content and product quality. Among their examples for photosynthesis-based models of tomatoes, they mentioned Tomgro (Dayan et al., 1993a; Gary et al., 1995) and Tomsim (Heuvelink, 1996) models. Heuvelink, Li and Dorais (2018) summarized the subsequent progress in model development for tomatoes. For process-based models (PBM), it mainly consisted of the adaptation of previously existing models CropGro and Aquacrop to also simulate tomato growth (Boote et al., 2012; Katerji et al., 2013; Scholberg et al., 1997).

In both cases, the development is related to the simulation of field-grown tomatoes and, particularly for the case of Cropgro-Tomato, it was motivated by the inability of the previously developed Tomgro model to simulate field-grown tomatoes. McNeal et al. (1995) and Scholberg (1996) explored how they could adapt the model, but branching of the semi-determinate field cultivars impacted the number of nodes in the main stem as well as resulted in faster build-up and decline of leaf canopy in a way that the model did not represent. The Cropgro-Tomato model has recently been evaluated in greenhouse models (Deligios et al., 2017), but it was preliminary and the authors suggest there should be further evaluations. Other process-based models not mentioned include the reduced-state version of the Tomgro Model (Jones et al., 1999), the model developed by Vanthoor et al. (2011), the VegSyst model (Gallardo et al., 2014; Giménez et al., 2013) and the Simple model (Zhao et al., 2019).

The goal of TOMGRO development was to create a dynamic model capable of characterizing tomato responses to the environment aimed at greenhouse control systems (Jones et al., 1991). According to the authors, a model of the biological response, associated with physical models of the environment and the greenhouse control systems, besides information on production costs and crop financial return, allows an optimization approach aiming at greater profit due to the control of environmental conditions. However, the large number of state variables in the model makes it too complex for use in control systems. This led to the development of the Reduced TOMGRO model (Jones et al., 1999), which is an example of using more comprehensive crop models to create reduced form crop models that produce responses needed for specific applications (Jones et al., 2017a).

The model developed by Vanthoor et al. (2011) aimed at the optimization of greenhouse design, capturing the effects on tomato yield of light, carbon dioxide concentration in the air and temperature, including extreme ones. One of their reasons for developing a new model was that previous models were not fully differentiable, which compromised their optimization design goal. The VegSyst model was developed to assist with Nitrogen and irrigation management of greenhouse vegetable crops (Gallardo et al., 2011) and in 2014 was calibrated for tomatoes and incorporated into a decision support system (Gallardo et al., 2014).

The Simple model, recently developed, attempted to address the gap in modeling vegetables, was well as other oil and fiber crops and fruits (Zhao et al., 2019). It has been evaluated on datasets of field-grown tomatoes, but not in greenhouse-grown. While it likely would not be used for controlling the environment, since it uses daily inputs, it could still be useful for estimating yield by the end of the growth cycle. The Simple model exists in the context of the discussion of universal models. While many authors emphasize their limitations, even advising against their development, (Affholder et al., 2012; Boote et al., 1996; Sinclair and Seligman, 1996), it could be the case that after so many years of progress in the field, it is possible to summarize overall growth in a useful albeit limited way. Only further assessments could answer that.

Kuijpers et al. (2019) and Lin, Wei and Xu (2019) aimed at taking advantage of the different representations of similar processes from different models and combined them to obtain accurate growth models. While Monteith (1996) has argued that changes to model structure should be rigorously tested, modular representations of validated processes should not be constrained by these requirements and has been argued throughout the modeling community (Jones et al., 2017b; Vanthoor et al., 2011). Some even emphasize the advantage of this approach as allowing for periodical updates, which would reflect new biological knowledge

(Kim et al., 2019). However, associated to model structure there are often parameters that should be adequately dealt with, as discussed in section 3.3.

Among the limitations of greenhouse tomato models developed thus far, most do not account for water restrictions, as they assume plants are well watered. However, deficit irrigation (DI) has been suggested as a strategy of saving water, even in protected environments, particularly in arid and semi-arid regions (Khapte et al., 2019). Simulation of plant water relations could also be helpful in understanding dry matter content and fresh weights, as indicated by Marcelis, Heuvelink and Goudriaan (1998). Models should also account for salinity (Karlberg et al., 2006), given problems of water quality and the possibility of water reuse. Finally, aspects discussed by Vanthoor et al. (2011) included how tomato quality models could play a role in optimization of the environment as well as how fertigation could influence crop growth.

Heuvelink, Li and Dorais (2018) also mentioned two developments in modeling that build on process-based models: functional-structural plant models (FSPM) and knowledge-and-data-driven models (KDDM). As several fronts of the advance in scientific and decision-making goals are intertwined, this is reflected in the solutions being presented. So, KDDM consist of using elements from both FSPM and machine learning. While there is an expectation of FSPM being used for optimizing greenhouse energy use and crop performance simultaneously (Evers and Marcelis, 2019), this role has been performed by artificial intelligence models. Recently, machine learning models have outperformed traditional growers in the Autonomous Greenhouse Challenge, which in 2018 aimed at optimizing the growth of cucumbers (Hemming et al., 2019) and in 2019, of cherry tomatoes (Hemming et al., 2020). It is becoming clearer that there is room and need for a wide range of modeling approaches. As Van Delden et al. (2021) recently stated, a combination of mechanistic and data-driven models may create an ideal blend of interpretability, which machine learning and artificial intelligence often lacks, and predictive power, for which mechanistic models are often more limited by their calibration requirements and their uncertainties.

3.3. Calibration and uncertainty of crop models

Diving deeper into the discussion of how to represent crop growth and development, one may investigate other aspects intimately related to modeling. In the process of modeling, scientists are faced with choices regarding how to represent model structure. Archontoulis and Miguez (2015) describe non-linear functions for a myriad of processes, e.g. sigmoid curves for growth rate, exponential curves for light distribution and bell curves for soil moisture effects on nitrous oxide emissions.

These representation choices may allow for some flexibility in the form of parameters. Parameters may be understood as properties of the components of a system that are unknown and are not measured directly, and therefore must be estimated using observations of system behavior (Wallach et al., 2019a). In crop models, parameters have a dual role in model structure: to give flexibility to the relationships given uncertainty in measurements and elements of the structure that are unaccounted for, as well as to represent behaviors associated to crop's genetics, which may vary throughout cultivars of the same crop. Wallach (2019) further distinguishes parameters as fixed, which are determined based on the literature and as they do not change, are part of model structure, and calibrated. Kersebaum et al. (2015) attribute the name 'parametrization' to the estimation of fixed parameter values and 'calibration' to the other parameters.

Calibration is often performed by an optimization of goodness-of-fit metric, but how to properly estimate parameters' values is still the object of studies. Seidel et al. (2018) discussed how guidelines could be established to clarify the consequences of the different approaches to choosing which parameters are to be adjusted, the trade-off between parameters compensating for errors throughout the model and their meanings and to discuss approaches to protect against overfitting and proper evaluation of the calibration process. Wallach et al. (2021) have made progress in this discussion for phenology parameters, but the overall need for these guidelines, may be exemplified by a few examples in tomato modeling.

Regarding the methods and overall need for calibration, in Kuijpers et al. (2019) the authors' claimed their approach of interchanging model components was not entirely successful because not all model parameters were identifiable, given calibration based solely on the available weather inputs and observed biomass and yield. They suggest that for a use such as theirs, that rely on the modularity of the model, the model should be calibrated at the process level, but acknowledge it is not always possible to do so. However, their choice of not calibrating any parameters from the new models obtained by the combination of components, using them as they were published, likely affected their conclusions, as calibrated parameter values are only valid for the model configuration that was used for the calibration (Kersebaum et al., 2015). Another issue is the choice of which parameters to calibrate and which to treat as fixed. Vanthoor et al. (2011) treated all parameters — including cardinal temperatures — as fixed. As a likely consequence, the model underestimated crop yield as well as the fruit growth period. The authors note in their discussion how, since temperature effects on crop yield are cultivar-dependent, the model performance could be improved by calibration of the parameters related to the growth inhibition functions, photosynthesis functions and fruit growth period. As for their meaning and the compensation of errors, Vazquez-Cruz et al. (2014) calibrated the Reduced Tomgro model using genetic algorithms, following a sensitivity analysis in which they defined which parameters they would treat as fixed and which they would calibrate. While their approach followed a common flow indicated by Seidel et al. (2018), they did not account for the meaning of the parameters when performing the optimization, ascribing a value larger than 1.0 to the parameter that represents tissue conversion efficiency.

The work from Seidel et al. (2018) was based on a survey aimed at identifying the approaches currently used for calibration and the challenges associated to the process. But even in the cases in which parameters are estimated addressing their concerns, all the different valid approaches may entail different results which would not mean any of the assessments is wrong, but that could imply different results obtained by different approaches may be equally acceptable. How different calibration approaches lead to different results has been discussed in the context of climate change assessments by Angulo et al. (2013) and have been established as affecting significatively the results (Confalonieri et al., 2016).

Since estimates obtained by crop models are not perfect, some uncertainty could be ascribed to them. For Wallach and Thorburn (2017), uncertainty means the distribution of the errors of prediction. By defining the model error (e) as in Equation 1, these distributions may be ascertained in two different ways, depending on the predictor ($f(X\,;\,\theta)$) being treated as fixed or random, a discussion which is at the center of Wallach et al. (2016). If the predictor is treated as fixed, the model error may be ascertained by hindcasts, determining the discrepancy between the prediction and an observed value (Y). If it is not treated as fixed, each of its elements may then be treated as random variables, with several possible values and, therefore, uncertainty in the predictor may have as sources uncertainty in inputs (X), model structure itself ($f(X\,;\,\theta)$) and parameters (θ).

$$e = Y - f(X\,;\,\theta) \qquad \text{Equation 1}$$

Wallach and Thorburn (2017) commented on the different ways of assessing uncertainty, depending on each source. For model structure, a common protocol is to standardize the data for calibration, input data and outputs to be simulated, to ensure that differences in the outcomes arise from differences in model structure. As for parameter- and input-related uncertainty, the central issue refers to the approximation of the distribution. For parameters, one possibility is to sample from a range found in the literature, but a least squares algorithm in calibration would also provide estimates for the distribution of calibrated parameters. For inputs, it is rarely the case that the full range of possibilities may be simulated, so historical weather is often used to represent uncertainty in daily weather, modified by crop management practices, such as sowing date and cycle length. The authors suggested both the need for guidelines for quantifying uncertainty in model structure, parameters, and inputs, and for widespread assessments of prediction uncertainty, so that end-users can determine if the results are sufficiently reliable for their purpose. In the context of yield gap assessments, Schils et al. (2022) already proposed a protocol, which led to a ranking of the uncertainty sources that could allow for prioritizing future efforts to reduce the uncertainty around yield gaps.

Antle et al. (2017) examine model credibility as a factor for model-usage adoption by decision-makers. They assert that model accuracy and uncertainties should be effectively communicated and that strategies for assessing them both are well developed, for instance through uncertainty and sensitivity analysis. For greenhouse tomato models, uncertainty was only explicitly addressed by Cooman and Schrevens (2006) and by Cooman and Schrevens (2007). Cooman and Schrevens (2006) discussed the effects of parameter uncertainty in the outputs of the second version of the Tomgro model. They used a Monte Carlo approach for sampling and their assumed distributions mostly referred to measurements previously performed or values estimated from the literature. Cooman and Schrevens (2007), on the other hand, evaluated the effects of weather input, using two different approaches: factorial and one-at-time. It should be noted that given the context of their evaluation was restricted to the Bogota Plateau, their assessment was likely affected by the choices previously made in the calibration step. In both studies, the authors also aimed at identifying which parameter or input mostly affected the uncertainty of the outputs.

The idea of assessing the contribution of elements of the model, particularly parameters and inputs, to overall uncertainty is expressed by an evaluation denominated sensitivity analysis. In the systematic review by Pianosi et al. (2016), the authors organized the way in which the methods may be categorized according to:

- The purpose of the analysis: if the goal is to identify the order in which the input factors contribute to the output uncertainty (ranking), which are the least relevant factors, that could therefore be fixed (screening), or which region of the input variability space produce significant output values (mapping);

- Computational complexity: the number of model runs required may range from approximate the same number of input factors evaluated to thousands of times this number;
- Sampling approach: if all the factors are sampled at the same time (all-at-a-time) or individually (one-at-a-time);
- Type of analysis: if the method accounts for the entire space of variability of the input factors (global) or only around specific values of the input factors (local).

They also describe each of the most used methods, their advantages and disadvantages, and how they relate to those categories, as well as provide a workflow for performing a sensitivity analysis. When discussing common errors on the subject, Saltelli et al. (2019) highlighted as one of the main problems the use of methodologies that rely on local techniques, which are invalid for nonlinear models and for accounting for interactions. While it is clear that there may be interactions among inputs that are neglected in local analyses, the outcomes of calibration also influence the results, as they are treated as fixed elements. The analysis may then reflect only particular conditions in which the model is to be used, since factors are not all changed at the same time and take only the value defined for that simulation.

Sensitivity analyses strategies for evaluating tomato models have included one-at-a-time approaches (Bertin and Heuvelink, 1993; Jones et al., 1991; Kuijpers et al., 2019) and global ones (Lin et al., 2019; Vazquez-Cruz et al., 2014). Their goals include understanding models' responses to the environment and to parameters (Bertin and Heuvelink, 1993), evaluating if models' responses referred to the same system (Kuijpers et al., 2019) and identifying which parameters should be selected for calibration (Vazquez-Cruz et al., 2014). They have assessed both parameters (Bertin and Heuvelink, 1993; Vazquez-Cruz et al., 2014) and inputs (Bertin and Heuvelink, 1993). Global analyses, on the other hand, do not allow for these detailed evaluations, even though they may point to the most relevant parameters. Vazquez-Cruz et al. (2014) performed a global sensitivity analysis in the parameters of the Reduced Tomgro model and used the EFAST and Sobol methods for calculating the first-order and total effect indexes for each of the five state variables of the model. Their analysis included 17 parameters, ascribing a uniform probability density function for each, and both methods led to similar results as to the highest sensitivities. This algorithmic approach led to different parameters than the ones Jones; Kenig and Vallejos (1999) decided should be calibrated or treated as fixed.

3.4. Data assimilation on crop models

One conclusion drawn from the theoretical evaluation of crop models' misspecification is that as the parameters obtained from calibration with data from one population do not necessarily correspond to the model true parameters values, models should always be calibrated using a sample from the target population for them to show an improved performance (Wallach, 2011). Besides calibration for improving performance, there are also approaches for reducing uncertainty in model estimates. Wallach and Thorburn (2017) summarized them as the improvement of models, using the median of multi-model ensembles, redefining the quantity to be predicted. Evidently, if possible, other alternatives include using more data in the calibration step or higher quality input measurements. But apart from the constraints of what we can call the model framework — which is limited by its inputs, variables, and structure —, including additional measurements could allow for lower prediction errors as well as lower uncertainty in the outputs, since this is an additional information to what is contained in the model (Wallach et al., 2019b). One approach that does that is called data assimilation.

Data assimilation on crop models has often been performed by the integration of remote sensing data into mechanistic models. The subject has been frequently revisited given the evolution in computational capacity and available state estimation techniques (Dorigo et al., 2007; Fischer et al., 1997; Huang et al., 2019a; Jin et al., 2018). Overall, the methods consist in combining estimates from crop models and external observations accounting for their expected errors. The goals of data assimilation works are often connected to the improvement of agricultural systems' models predictive capability, differing in which state variables are assimilated as well as the techniques used and the source of data that constitute the observations that will be assimilated. Recent reviews of data assimilation with crop models (Huang et al., 2019a; Jin et al., 2018) addressed the frequently used methods and their shortcomings, but the following sections aim at expanding some of their discussions regarding the decisions to be made when deciding to use data assimilation techniques.

3.4.1. Methods

The reviews of data assimilation in crop models previously mentioned refer to three types of data assimilation: forcing, calibration and update. As there are several sources for better understanding them, this section will only briefly present the approaches, focusing on strategies for updating. Table 1 includes the equations that summarize the relationships between states, observations and their uncertainties, expressed by their covariances, following the notations and parallels Labbe Jr (2020) used for filters of the Kalman family, i.e., the Kalman Filter (KF), the Extended Kalman Filter (EKF), the Ensemble Kalman Filter (EnKF) and the Unscented Kalman Filter (UKF). Overall, these filters follow a pattern of using the process or model equation to predict the next estimate and updating the estimate by including the information brought by the observation, accounting for the uncertainty present both in the model estimate and the observation. The first step is often called forecast, prior or predict and the second step, update, posterior or analysis. Relevant moments from the update step include the calculation of the residual, which consists in the difference between the estimate and the observation, and of the gain, which corresponds to the weight of the residual when modifying the value estimated by the model, as well as the uncertainty of the outcome. This means that assimilation using filters of the Kalman family requires having a model that establishes a relationship between observation and state, so that they can be compared, and quantifying uncertainty in models and measurements.

Filters' equations and their elements are presented in Table 1 to help make the terms and logic used in the other sections of this work more familiar, but no specific mathematical treatment will be presented. In the predict equations of Table 1, $\mathbf{x}$ and $\mathbf{P}$ are the state mean and covariance, $\mathbf{F}$ is the process function in matrix form — as the filter problem is often solved with matrices operations — while f is the equivalent nonlinear process model or numerical derivative and $\mathbf{Q}$ is the process covariance. In the update equations, $\mathbf{z}$ and $\mathbf{R}$ are the measurement mean and noise covariance, $\mathbf{H}$ is the measurement function while h is the equivalent nonlinear process model or numerical derivative, $\mathbf{y}$ and $\mathbf{K}$ are the residual and Kalman gain. In the UKF, $\boldsymbol{\chi}$ are the sigma points and $\boldsymbol{\mathcal{Y}}$ are the transformed sigma points while $\boldsymbol{w^m}$ and $\boldsymbol{w^c}$ are weights. One approach for generating the ensemble is presented for the EnKF but as it will be commented, there are multiple ways of doing so.

Table 1. Summary of equations used in the Kalman Filter (KF), the Extended Kalman Filter (EKF), the Ensemble Kalman Filter (EnKF) and the Unscented Kalman Filter (UKF).

	KF	EKF	EnKF	UKF
Predict		$\mathbf{F} = \left.\frac{\partial f(\mathbf{x}_t)}{\partial \mathbf{x}}\right\vert_{\mathbf{x}_t}$	$\boldsymbol{\chi} \sim \mathcal{N}(\mathbf{x}_0, \mathbf{P}_0)$	
			$\boldsymbol{\mathcal{Y}} = \mathrm{f}(\boldsymbol{\chi}) + v_Q$	$\boldsymbol{\mathcal{Y}} = \mathrm{f}(\boldsymbol{\chi})$
	$\bar{\mathbf{x}} = \mathbf{F}\mathbf{x}$	$\bar{\mathbf{x}} = \mathrm{f}(\mathbf{x})$	$\bar{\mathbf{x}} = \frac{1}{N}\sum_{1}^{N} \boldsymbol{\mathcal{Y}}$	$\bar{\mathbf{x}} = \sum w^m \boldsymbol{\mathcal{Y}}$
	$\bar{\mathbf{P}} = \mathbf{F}\mathbf{P}\mathbf{F}^{\mathrm{T}} + \mathbf{Q}$	$\bar{\mathbf{P}} = \mathbf{F}\mathbf{P}\mathbf{F}^{\mathrm{T}} + \mathbf{Q}$	$\bar{\mathbf{P}} = \frac{1}{N-1}\sum_{1}^{N} (\boldsymbol{\mathcal{Y}} - \bar{\mathbf{x}})(\boldsymbol{\mathcal{Y}} - \bar{\mathbf{x}})^{\boldsymbol{T}}$	$\bar{\mathbf{P}} = \sum w^c (\boldsymbol{\mathcal{Y}} - \bar{\mathbf{x}})(\boldsymbol{\mathcal{Y}} - \bar{\mathbf{x}})^{\boldsymbol{T}} + \mathbf{Q}$
Update		$\mathbf{H} = \left.\frac{\partial h(\bar{\mathbf{x}}_t)}{\partial \bar{\mathbf{x}}}\right\vert_{\bar{\mathbf{x}}_t}$	$\boldsymbol{\mathcal{Z}} = \mathrm{h}(\boldsymbol{\mathcal{Y}})$	$\boldsymbol{\mathcal{Z}} = \mathrm{h}(\boldsymbol{\mathcal{Y}})$
			$\boldsymbol{\mu}_{\mathbf{z}} = \frac{1}{N}\sum_{1}^{N} \boldsymbol{\mathcal{Z}}$	$\boldsymbol{\mu}_{\mathbf{z}} = \sum w^m \boldsymbol{\mathcal{Z}}$
	$\mathbf{y} = \mathbf{z} - \mathbf{H}\bar{\mathbf{x}}$	$\mathbf{y} = \mathbf{z} - \mathrm{h}(\bar{\mathbf{x}})$	$\mathbf{y} = \mathbf{z} - \boldsymbol{\mathcal{Z}} + v_R$	$\mathbf{y} = \mathbf{z} - \boldsymbol{\mu}_{\mathbf{z}}$
	$\mathbf{S} = \mathbf{H}\bar{\mathbf{P}}\mathbf{H}^{\mathrm{T}} + \mathbf{R}$		$\mathbf{P}_{\mathbf{zz}} = \frac{1}{N-1}\sum_{1}^{N} (\boldsymbol{\mathcal{Z}} - \boldsymbol{\mu}_{\mathbf{z}})(\boldsymbol{\mathcal{Z}} - \boldsymbol{\mu}_{\mathbf{z}})^{\boldsymbol{T}} + \mathbf{R}$	$\mathbf{P}_{\mathbf{zz}} = \sum w^c (\boldsymbol{\mathcal{Z}} - \boldsymbol{\mu}_{\mathbf{z}})(\boldsymbol{\mathcal{Z}} - \boldsymbol{\mu}_{\mathbf{z}})^{\boldsymbol{T}} + \mathbf{R}$
			$\mathbf{P}_{\mathbf{xz}} = \frac{1}{N-1}\sum_{1}^{N} (\boldsymbol{\mathcal{Y}} - \bar{\mathbf{x}})(\boldsymbol{\mathcal{Z}} - \boldsymbol{\mu}_{\mathbf{z}})^{\boldsymbol{T}}$	$\mathbf{P}_{\mathbf{xz}} = \sum w^c (\boldsymbol{\mathcal{Y}} - \bar{\mathbf{x}})(\boldsymbol{\mathcal{Z}} - \boldsymbol{\mu}_{\mathbf{z}})^{\boldsymbol{T}}$
	$\mathbf{K} = \bar{\mathbf{P}}\mathbf{H}^{\mathrm{T}}\mathbf{S}^{-1}$	$\mathbf{K} = \bar{\mathbf{P}}\mathbf{H}^{\mathrm{T}}\left(\mathbf{H}\bar{\mathbf{P}}\mathbf{H}^{\mathrm{T}} + \mathbf{R}\right)^{-1}$	$\mathbf{K} = \mathbf{P}_{\mathbf{xz}}\mathbf{P}_{\boldsymbol{zz}}^{-1}$	$\mathbf{K} = \mathbf{P}_{\mathbf{xz}}\mathbf{P}_{\boldsymbol{zz}}^{-1}$
	$\mathbf{x} = \bar{\mathbf{x}} + \mathbf{K}\mathbf{y}$	$\mathbf{x} = \bar{\mathbf{x}} + \mathbf{K}\mathbf{y}$	$\boldsymbol{\chi} = \bar{\mathbf{x}} + \mathbf{K}\mathbf{y}$	$\mathbf{x} = \bar{\mathbf{x}} + \mathbf{K}\mathbf{y}$
			$\mathbf{x} = \frac{1}{N}\sum_{1}^{N} \boldsymbol{\chi}$	
	$\mathbf{P} = (\mathbf{I} - \mathbf{K}\mathbf{H})\bar{\mathbf{P}}$	$\mathbf{P} = (\mathbf{I} - \mathbf{K}\mathbf{H})\bar{\mathbf{P}}$	$\mathbf{P} = \bar{\mathbf{P}} - \mathbf{K}\mathbf{P}_{\mathbf{zz}}\mathbf{K}^{\mathrm{T}}$	$\mathbf{P} = \bar{\mathbf{P}} - \mathbf{K}\mathbf{P}_{\mathbf{zz}}\mathbf{K}^{\mathrm{T}}$

3.4.1.1. The Kalman Filter (KF)

The main assumptions of the Kalman Filter are that the model estimates and the observations follow a normal distribution, and that the process model and the observation function are linear. Huang et al. (2019a) clarify the linearity requirement stating that if the crop model can be assumed locally linear between adjacent time steps, the standard Kalman Filter could be a viable choice.

Given its restrictions, there are fewer examples of the application of this technique. In some of them, the premise of the filter is used, but with modifications. Instead of calculating the gain, Vazifedoust et al., (2009) tested different values, using the best one as fixed, circumventing the need for identifying the source error values. This approach was repeated by Chen Zhang and Tao (2018), who also normalized simulated and observation values according to the maximum value obtained so that they would be in the same range. Operating in this normalized space allowed them to focus on spatial variability and, in part, trends, instead of absolute values. Later, Chen and Tao (2020) explored more approaches for defining an appropriate value for the fixed gain, by a grid search of an optimal value, as well as exploring historical values.

3.4.1.2. Extended Kalman Filter (EKF)

The Extended Kalman Filter is an adaptation of the Kalman Filter to deal with non-linear cases. To do so, it takes advantage of local linearization by replacing the model and the measurement function by their partial derivatives. The use of this technique is limited, as it requires access to the Jacobian of the model or, in some cases, to an approximation by finite differences that often will not scale to higher dimensions (Huang et al., 2019a), so there are also few examples on crop modeling that apply this technique and most of those which use the method give few details of the implementation. One of the few examples in which there is an explanation of how the filter was used is the work of Linker and Ioslovich (2017). The authors used data from growth experiments of cotton and potatoes aiming at improving estimates of canopy cover and biomass through state assimilation and through the recalibration of three parameters from the Aquacrop model. They used dry biomass direct measurements and the images used as canopy cover observations were digital pictures taken 1.5 m and 2 m above canopy.

Given there were two different approaches for improving estimates, they estimated the covariance matrix of the errors in the state variables in two ways. For the assimilation process, by calculating the difference between the square of the model residuals and the dispersion of the measurements. They chose not to propagate the matrix along the process, given its strong nonlinearity, and recalculated it at each new time of measurement. They justified this choice by claiming the propagation without assimilation of new measurements would only increase the uncertainty related to the linearization and to the unknown initial data of the model errors. For the recalibration process, the matrix was calculated using an assumption that the corresponding standard deviation of each of the chosen parameters is equal to 20% of the current value of corresponding parameter. In their assimilation approach, the H matrix corresponded to the unit matrix, as the measurements directly corresponded to the states and, in the recalibration one, the components of the partial derivatives matrix H were calculated numerically at each instance of canopy cover measurement.

3.4.1.3. Ensemble Kalman Filter (EnKF)

Overall, in the Ensemble Kalman Filter, an ensemble of initial states is generated and each individual ensemble member is propagated through the model until an observation is available. Then the update step is performed individually in each member. This allows for recalculation of the ensemble mean for the states and generation of a new ensemble. The ensemble approach comes from the premise that at least some of the particles will represent the true state. There are, however, different ways of approaching this problem and the elements of uncertainty are intimately connected to other decisions.

- Composition of ensemble elements

Huang et al. (2016) observed that two common methods to generate ensemble members are by directly adding a Gaussian perturbation to the state and by adding a Gaussian perturbation to the uncertain input parameters, which are then used by the model for the simulation. These methods have been explored in different ways. Input perturbation examples come from Lei et al. (2020), who perturbed precipitation and irrigation inputs via multiplicative rescaling with mean-unity lognormally distributed random errors that have a standard deviation equal to 20% of the corresponding input, and from De Wit and Van Diepen (2007), who generated precipitation ensembles based on a highly accurate precipitation dataset that was perturbed with an additive error component and a multiplicative component that generated binary rain or no-rain events on locations in which the records pointed to the absence of precipitation.

In cases in which states are perturbed, Xie et al. (2017) input the initial states and parameters into the CERES-Wheat and, at the beginning of the green-up stage, leaf area index (LAI) and soil moisture were perturbed according to the errors between the field measurements and the simulated LAI and soil moisture. Ines et al. (2013) randomly sampled, at the start of the simulation, values of leaf weight at emergence and plant leaf area at emergence, to increase the variability of the ensemble. Beyond inputs, Lei et al. (2020) also applied direct perturbations to soil moisture states at all depths independently with random errors sampled from a mean-zero, normal distribution with temporally varying standard deviation equal to 10% of the state value, followed by the introduction of a vertical auto-correlation at the different depths.

Researchers have used multiple ways of ascribing uncertainty to parameters. Huang et al. (2016) chose the parameters based on the results of a sensitivity analysis and set the values of the standard deviations of two parameters according to the results of a previous study. Ines et al. (2013) identified which parameters had major influence in the model and, with an uncertainty level of 10%, perturbed each model parameter using a Gaussian distribution, generating ensemble members by randomly sampling model parameter combinations from the perturbed arrays. Zhao, Chen and Shen (2013) even tried to evaluate the impact of using parameter uncertainty to generate the ensembles. They chose one parameter that was mostly correlated to crop yield and ascribed a distribution to it, multiplying its standard deviation by different fixed values. Lu et al. (2021) took advantage of the existing uncertainty in parameters and used this as an artifact to generate ensembles without calibrating the model. They sampled parameters that they called variant as well as a fixed factor to scale phenological parameters for the canopy in a given year.

One issue in perturbing parameters or inputs for generating the ensembles is what Curnel et al. (2011) denominated phenological shift. This effect refers to ensemble members presenting ensemble elements that are in different phenological stages, which leads, at the same point in the simulation, to different modules in the model to be active and, therefore, the assimilation of an observation having a different meaning for each ensemble member.

As for observations, Ines et al., (2013) state that the variance used in the perturbation is based on the uncertainty of the data. But more precisely, Huang et al. (2016) mentions that the standard deviation of the Gaussian white noise error needs to be a realistic value for it to represent the uncertainty of the remotely sensed observation. In section 3.4.2, errors are more thoroughly described, but as an example, Xie et al. (2017) used the errors between the measurements and observations to determine the standard deviations of the observed LAI and soil moisture.

- Ensemble size

The choice of ensemble size is often performed in three different ways: testing, referencing a theoretical result or referencing other assimilation work on the literature. Pellenq and Boulet (2004) affirmed a preliminary study must be performed to find the minimum ensemble size that ensures particles may follow the same trajectory as the true state. They say the number usually corresponds to value above which assimilation results are identical. With this approach, Nearing et al. (2012) showed an example in which the number depended on the goal of the assimilation. The authors tested different values when assimilating LAI and soil moisture aiming at improving estimates of wheat yield, LAI and soil moisture. In the cases of assimilation of the state variable, root mean squared error (RMSE) became stable with a number of elements of 25. In the other cases, the stability came with an ensemble of 100 elements. Lu et al. (2021) evaluated ensemble sizes for simultaneous assimilation of canopy cover and soil moisture from 10 to 400 and overall observed little improvement for more than 200, even though in some years 10 elements were enough for stable results.

Several works, however, refer to the experiences of other authors. Frequently, authors refer to De Wit and Van Diepen (2007) when commenting on their choice for the ensemble size (Bai et al., 2019; Li et al., 2014; Zhao et al., 2013) The work by De Wit and Van Diepen (2007), however, applies to assimilating soil moisture with an ensemble obtained by perturbing precipitation and with an initial state ascribed by sampling a calculated Gaussian acceptable value and it is possible that they do not generalize for other approaches. Additionally, the authors mention that although they observed reduced RMSE in soil moisture estimates, this was not applied to the variance. Despite that, their results were compatible with other results for soil moisture, and recently, Mishra, Cruise and Mecikalski (2021) followed the suggestion from the work of Yin et al. (2015), who theoretically and through an example showed that the ideal ensemble size for assimilating soil moisture is 12, which suggests 50 would be a reasonable estimate in similar situations.

3.4.1.4. Unscented Kalman Filter (UKF)

Similarly to the EnKF, the Unscented Kalman Filter uses the average of an ensemble as the state estimate, instead of the direct estimates provided by the model. However, the ensemble is not just sampled from a distribution. It uses what is called the unscented transform to generate particles — the sigma points — and weights for those particles that, when combined, are more representative of the expected state value. These sigma points are propagated through the non-linear model, which provides more accurate approximations of the mean and covariance matrix of the state vector, and thus more accurate state estimation. (Mansouri et al., 2013).

The Unscented Kalman Filter has been used in the context of crop growth with tomatoes and lettuce. Torres-Monsivais et al., (2017) evaluated the technique along with data simulated with the Reduced State Tomgro model, perturbed by several noise levels, representing measurements. Ruíz-García et al. (2014) used data from destructive analyses of lettuce in a greenhouse to assess uncertainty of the NICOLET model. In the work with tomato, the authors ascribed lower errors to the model and higher to the measurements, which were then subjected to a tuning process, while in the work with lettuce, the values were tuned until reasonable results were obtained.

3.4.2. Errors and uncertainties

How to identify errors in the elements involved in assimilation and their uncertainties is widely discussed by Jin et al. (2018) and Huang et al. (2019a), as they are central in filtering approaches. For crop models, the sources of uncertainty they list include both the issues presented in section 3.3 as well as the difference between simulations and actual growth, which is impacted by pests and diseases. For observations, they mention errors in the measurement themselves and in retrieval methods. In both cases, often their works emphasize aspects of satellite-derived observations, such as errors in spatial data and scale mismatches. This section aims to revisit this topic, with more details and examples on how these uncertainties have been quantified and applied in data assimilation works. Although the discussion in this section focuses on trying to ascribe meaning and understanding the uncertainties, these are filter hyperparameters that may be estimated from data (Wallach et al., 2019b).

3.4.2.1. Observation errors

Overall, data assimilation in crop models rely on observations retrieved from satellite monitoring of Earth’s surface. Dorigo et al. (2007) covered methods used to derive canopy state variables from optical remote sensing data in the visible to near-infrared and shortwave infrared regions. These methods either rely on statistical relationships between the spectral signature and the measured biophysical or biochemical properties of the canopy or they derive the states from the known behaviors of leaf reflectance and radiation propagation through the canopy. Both are used to obtain remote sensing products, which directly estimate the state for the final user. And both remote sensing products and reflectance itself, are used in assimilation. For those products, Huang et al. (2019a) mention how guidelines for uncertainty quantification are still being established by the community and that many EO-derived products have poor or no uncertainty information available. Particularly for satellite-derived leaf area index (LAI) products, Fang et al. (2019) also comment on how given the complexity associated to the retrieval process, a comprehensive quantitative assessment of the quality of LAI products is still missing. In the case of assimilating reflectance or albedo, the crop model is coupled with a radiative-transfer model (RTM), which allows for quantifying uncertainty in the measurements directly (Huang et al., 2019b).

By assimilating products, several works (Huang et al., 2016; Ines et al., 2013; Zhao et al., 2013) are able to consider the assimilation of the product as the assimilation of the state directly, which means the relationship between states and observations may be obtained by the unit matrix, simplifying the approach. However, this choice could affect the outcome as it may lead to bias in the residual and to the cross-variance term not taking any effect of dispersion caused by the observation model into account when determining the gain. Bias in the residual leads the updated estimate to the wrong value and in the gain, to the wrong weight of the residuals in the new estimate. These effects are not often discussed and the only example found that mentions them comes from the work of De Wit and Van Diepen (2007), which makes it explicit that the variance they ascribed to observations did not account for deficiencies in the conversion model itself, later concluding that the value they ascribed to the variance was indeed underestimated. Nevertheless, errors in retrieval have been acknowledged (Jin et al., 2018) and an alternative to avoid them is operating in the measurement space, which leads to avoiding the error in the inversion process (Guo et al., 2018). Additionally, Huang et al. (2019b) used the RTM PROSAIL, arguing this is a good way to avoid the process of regional LAI retrieval and Li et al. (2017) used the PROSAIL model and characterized errors in the observations, pointing to errors from 0.09 to 0.51 $m^2\ m^{-2}$ of error in LAI in the different development stages of wheat.

For those who develop their own measurement functions, they often establish them with empirical relationships and characterize their uncertainty based on field data. So works such as the one by Huang et al. (2016), which converted vegetation indices into LAI, obtained field measurements and used the regression error between LAI field observations and the indices to estimate errors in each phenological stage. As the problems that have been addressed often refer to large areas, estimates of observation uncertainty may be established as the variability across fields. For instance, Zhao, Chen and Shen (2013) understood that neighboring pixels had similar uncertainties for the same period and used the variance among fields as uncertainty of remote sensing LAI.

Other than satellite retrieved data, there are other sources for observations to which error is ascribed in other ways. For instance, Linker and Ioslovich (2017) and Ruíz-García et al. (2014) used destructive measurements of the assimilated state. In the first case, the authors used direct measurements of aboveground biomass of potatoes and cotton and in the second case, of lettuces. As for non-destructive measurements, Linker and Ioslovich (2017) also used pictures taken from 1.5 and 2 m above the crop to determine canopy cover, which, as a fraction of the fraction of the soil surface covered by the canopy, may also be considered a direct measurement of the state. In these cases, errors corresponded to variance from measurements. Data retrieved by unmanned aerial vehicles (UAVs) often have similar limitations as satellites regarding scale, but brings into discussions other aspects, particularly, as cameras are able to capture other types of data. For instance, Yu et al. (2020) used plant height detected by UAVs as well as field measured and discussed the effects of multiple values ascribed to errors, arguing the trial-and-error procedure could provide a guideline when the true field observation error is unknown.

Finally, one relevant aspect refers to how soil-crop systems may not have a constant value for the error. Nearing et al. (2012) explain how the soil moisture observation uncertainty is variable throughout time, since measurement accuracy degrades as vegetation water content increases throughout the season. They ascribed to error measurement a value derived from the relationship between variance in the soil moisture retrieval and this fraction of plant population and plant biomass that corresponds to water. Lei et al. (2020) evaluated a time-varying error for soil moisture observations as a function of LAI. They observed an overall improvement in soil moisture estimates, but also a somewhat less stable DA performance. Also for soil moisture, Mishra; Cruise and Mecikalski (2021), chose a constant error for the observation, but they were aware that the errors in the sensors used behaved in contrasting ways over crop growth stages, and that this choice may have led to errors that were too low in the early growth season and larger later in the season. Lu et al. (2021) used the multi-year average value of the daily standard deviation of the observations from the 4 soil moisture profiles. But for canopy cover, they noted the error varies dramatically during the growing season, with significant variability in the exponential growth stage and the decay period canopy cover, and only marginal when the canopy was near maximum. So, they assumed canopy cover observation error as dynamic, and the standard deviation of the samplings from the different zones on each sampling day was used separately. Li et al. (2017) considered the standard deviation of the LAI observations as 10% of the measured value, based on their observations of LAI, and Curnel et al. (2011) used a coefficient of variation to characterize uncertainty, thus ascribing to this hyperparameter of the filter a value that corresponded to a fraction of the observation.

3.4.2.2. Model errors

As mentioned in section 3.3, model uncertainty may be ascribed to its parameters, inputs, and structure. In the case of Pellenq and Boulet (2004), they had two situations, and the differences in model behavior, regarding soil moisture and biomass, required different approaches for determining sources of model uncertainty. When analyzing the effects of initial input values, they observed that for biomass, as the state value is propagated throughout growth, there is no compensation for previous errors, and errors in the estimates of initial conditions could impact the following behavior. And while for soil water, the reliance on previous values is lower, with shorter "memory" of the system, in the coupled case, the initial water content could strongly impact biomass evolution. As for crop model noise, they assumed there would be at least one parameter set in the ensemble that could satisfactorily reproduce natural conditions. So, they decided by generating ensembles ascribing uncertainty to parameters and to inputs. On the other hand, in the case of soil moisture, since it tends towards low variance and equilibrium, they suggested including model noise as well, which should be nonetheless calibrated to avoid the loss of model integrity. Nearing et al. (2012) evaluated uncertainty in weather inputs, through correlated perturbations in weather time-series. Their results were not conclusive as in one of their systems, the assimilation of LAI improved yield estimates, but not the exclusive assimilation of soil moisture.

Uncertain inputs also manifest through unusual events, which are often not included in models. Therefore, for some authors, an advantage of filter assimilation methods is that they can incorporate these dynamic changes (Li et al., 2014). For example, Hu et al. (2019) improved sugarcane yield estimates by assimilating leaf area index into the SWAP-Wofost model, after the interference in LAI caused by artificial leaf stripping and natural storms, and in Zhao, Chen and Shen (2013), the authors observed high errors when simulating yield for four regions in which meteorological disasters had occurred, which were then reduced to some extent by assimilating observations.

Calibration is an issue that is often mentioned regarding model errors, as it makes the model more consistent with the spatially limited field measurements and calculated uncertainty in parameters could be propagated through the model (Huang et al., 2019a). Kang and Özdoğan (2019) identified that over large areas, calibration is no longer specific for cultivar, sowing dates or management. They commented on how the bias in model estimates this generates leads to violating the assumptions of assimilation techniques that require model errors to have zero means. The authors analyzed the impact of high model bias and uncertainty on yield estimates obtained by LAI assimilation and observed that bias with the same sign for LAI and yield led to lower errors after assimilation than the open-loop reference, while opposite signs led to assimilation enlarging the errors. It is nevertheless the case that before performing assimilation, models are frequently calibrated. Lu et al. (2021) believed the standard was lower, aiming at having an ensemble of non-calibrated simulations that could capture the dynamics of key model states and that its spread reflected the model state variability. Their assimilation of canopy cover and soil moisture was able to improve yield when compared to the no-assimilation case.

3.4.3. Variables

In a way, the largest restrictions to performing data assimilation in crop models are which additional data is available and if the knowledge or ability of how to relate them to models' state variables exists. This is one reason why LAI, canopy cover and soil moisture are frequently explored as observations, as there are several satellite products available for them. But being able to perform data assimilation does not mean that assimilation will be effective. As summarized by Lei et al. (2020), the performance of any data assimilation algorithm is fundamentally related to the strength of the relationship between observations and model states.

For Mishra, Cruise and Mecikalski (2021), assimilation of soil moisture, especially in irrigated areas, led to improvements in yield estimates, which is a very direct relationship, but for Ines et al. (2013), they expected assimilation of soil moisture in the DSSAT-CSM-Maize model to update the rootzone soil moisture, affecting soil nitrogen and, therefore, yield. There is then no guarantee that the included observations will improve estimates. For instance, Linker and Ioslovich (2017) discuss how since the Aquacrop model is water-driven, and as such, solar radiation is not considered explicitly, which may lead to underestimating the effect of canopy cover on crop development. And if assimilation not improving the outcomes is undesirable, it should be noted that it could even have an adverse effect on the estimates, depending on how variables interact with each other. Tewes et al. (2020a) argue that as model complexity rises, sequential update of only one or few state variables could threaten the model's integrity and cause an undefined state of the model, such as when the simulation triggers a new module by reaching a threshold value, but the filter updates the estimate to a value lower than the threshold.

Time-averaged correlation has been suggested as not very helpful when determining best assimilating state variables by Nearing et al. (2012). In their experiments, they point to several cases, using different realistic uncertainty scenarios, in which high correlation is not connected to improvement in yield estimates. Nearing et al. (2018) framed this discussion by relying on concepts of information theory, proposing a method to quantify how efficient data assimilation may be, through the quantification of information content on simulated model states and of the retrieval data relative to the imperfect evaluation data, and then measuring the fraction of this information that is extracted by a given DA implementation or algorithm.

3.4.4. Timing and frequency

An issue that interacts with which variable is going to be assimilated to improve an estimate is at what time of growth and how often should the estimate be updated. Frequently, the discussion is connected to at which moment of the cycle the observation available will be most informative. Dente et al. (2008) evaluated the exclusion of one more precise image and observed that for wheat, within the conditions they observed, the data should include images from either the end of stem elongation stage or the beginning of heading, when the LAI reaches the maximum value. Timing of assimilation in wheat has been widely discussed (Curnel et al., 2011; Dente et al., 2008; Guo et al., 2019; Kang and Özdoğan, 2019; Li et al., 2017; Xie et al., 2017) with some authors reaching the conclusion that images from the whole cycle presented the best results (Kang and Özdoğan, 2019; Li et al., 2017). For sugarcane, on the other hand, Yu et al. (2020) concluded that assimilation of height in the late period of the elongation stage, involving the maximum plant height, can be the most useful, without the need for its sampling over the whole development stage.

As remote sensing observations are often only available with large intervals between them, their assimilation allows for the model to adjust to the updates, but local assimilation of, for example, soil moisture, would present a different situation. Lu et al. (2021) commented on how their use of local probes for monitoring soil moisture allowed for daily assimilation of this state, which likely improved their results. As crop systems models often present daily steps, it is not the case that assimilation would be performed in more frequent intervals, but in other contexts, such as weather forecasts, it has been argued that very frequent updates could insert noise in models, degrading forecasts (He et al., 2020).

4. METHODS

All data used in this work is available at https://doi.org/10.25824/redu/EP4NGO. All code is available in https://github.com/mnqoliveira/data-assimilation-tomato-models.

4.1. Experimental design and data collection

4.1.1. Growth infrastructure

The experiments were conducted in research greenhouses at the School of Agricultural Engineering of the University of Campinas (22º 49' 06” S, 47º 03' 40” W, 635 m altitude). Four cycles of minitomatoes growth were performed (Table 2).

Table 2. Summary of growth cycles for data gathering.

Growth Cycle	Cultivar	Start date	End date
Cycle 0	Seminis – DRC 564	11/jan/2019	04/apr/2019
Cycle 1	Fercam – Milla	12/jul/2019	28/oct/2019
Cycle 2	Feltrin – Carolina	05/nov/2020	12/feb/2021
Cycle 3	Seminis – DRC 564	16/mar/2021	11/jun/2021

- Cycle 0

This growth cycle was conducted in the same setting of Cycles 1 and 2 described below, but as monitoring was not completely established from the beginning, it was treated as a pilot to test the installation of sensors, the irrigation system and to obtain experience in growing the plants.

- Cycle 1 and Cycle 2

These growth cycles were conducted in a research greenhouse with 6.4 m of width, 10.98 m of length, 3.0 m of height from the floor to the gutter and 4.5 m of total height. The greenhouse has a gable roof covered with low density polyethylene of 150 μm width with light diffuser and anti-UV treatment. The ridge of the greenhouse section was oriented North-South. The section was only bounded to the East, by another greenhouse of the same dimensions. Its cooling system consisted of a pad-fan system, activated by a scheduling device. The South-facing side wall was covered with an evaporative cooling pad and an insect screen. Other walls were covered with the same plastic as the cover. Seedlings provided by commercial units were transplanted to polyethylene pots (8 L) filled with coconut fiber approximately 30 days after seeding. They were distanced 1.5m x 0.5m (1.33 plants m^{-2}). Figure 1 shows the overall disposition of pots.

Figure 1. Disposition of the pots in the first research greenhouse, used for cycles one and two.

- Cycle 3

The experiment was conducted in a research greenhouse with dimensions 6.4 m of width, 18 m of length and 3.0 m of height from the floor to the gutter. It has a gable roof covered with low density polyethylene, light diffuser with 150 μm width and anti-UV treatment. The ridge of the greenhouse section was oriented North-South. The section was not bounded in any directions. All walls were covered by an insect screen. Locally cultivated seedlings were transplanted to polyethylene pots (8 L), filled with coconut fiber, distanced 0.9 m x 0.5 m (2.22 plants m^{-2}) approximately 30 days after seeding. Lines of pots were intercalated with lines of nutrient film hydroponic growth (Nutrient Film Technique – NFT), which were not used in this project. Figure 2 shows the environment.

Cycle 3 also included application of neem oil, Bordeaux mixture and lime-sulfur prevent the occurrence of pests and an abamectin-based pesticide (Syngenta's VERTIMEC® 18 EC) after appearance of rust mite.

Figure 2. Disposition of the pots in the second research greenhouse used, for cycle three.

4.1.2. Management practices

All cycles consisted of around 100 days and in all of them plants had reached the highest wire, when the growth was stopped. Management practices (thinning, staking, pruning, pest management and diseases) overall followed the recommendations for hydroponic growth in Alvarenga (2013). Only one stem was grown per pot. Removal of side shoots happened once to three times a week. Leaves were pruned only when their senescence was dominant. Harvest happened when the whole truss was mature. Irrigation consisted of fertigation through a drip irrigation system and while the nutritive solution mainly followed the recommendations in Pires et al. (2011), concentrations were changed according to plants' responses. In Cycles 0 and 1, irrigation length used fixed time through the cycle, but in Cycle 1 the duration proved insufficient by the end of the cycle. In Cycles 2 and 3, total irrigation time was defined as that which would not allow for deficit by the end of the day, to minimize mass fluctuations from one day to the following caused by variation in irrigations. Cycle 1 showed water deficits throughout growth. Cycle 2 suffered with excessive nitrogen fertilization followed by rust mite while Cycle 3 more closely resembled full irrigation and fertilization.

4.1.3. Environmental data

Environmental data was gathered with the sensors from Table 3. They may be characterized as scientific grade (SG) and low-cost (LC). The scientific grade sensors for temperature and relative humidity corresponded to SHT75 transducers protected by porous capsules which, by their turn, were protected by polyvinylchloride tubes coated with aluminum foil. The tubes included downstream fans. The sensors were installed in a hardware platform for wireless sensor networks (Radiuino BE900), with daily backup. For photosynthetically active radiation (PAR), the scientific grade sensors corresponded to quantum sensors Licor LI-190SA with a datalogger Licor LI-1400. Low-cost sensors were connected to Raspberry Pi model B computers.

Table 3. Sensors and frequency of data acquisition used for monitoring the environment.

Variable	Type	Model	Frequency
Air temperature	SG	SHT75	5 minutes
Relative humidity	SG	SHT75	5 minutes
Air temperature	LC	DHT22	5 minutes
Relative humidity	LC	DHT22	5 minutes
Substrate moisture	SG	EC-05	10 minutes
Luminosity	LC	BH1750	5 minutes
Photosynthetically active radiation	SG	LI190SA	15 minutes

Each sensor node was positioned close to one of the monitored plants and each node included two sensors of the same type and for the same variable for redundancy, except for radiation and luminosity, which only include one of each type. As there were differences in the experimental set-ups, they are separately detailed as follows. Sensors were positioned as in Figure 3 for Cycles 0 to 2 and as in Figure 4 for Cycle 3.

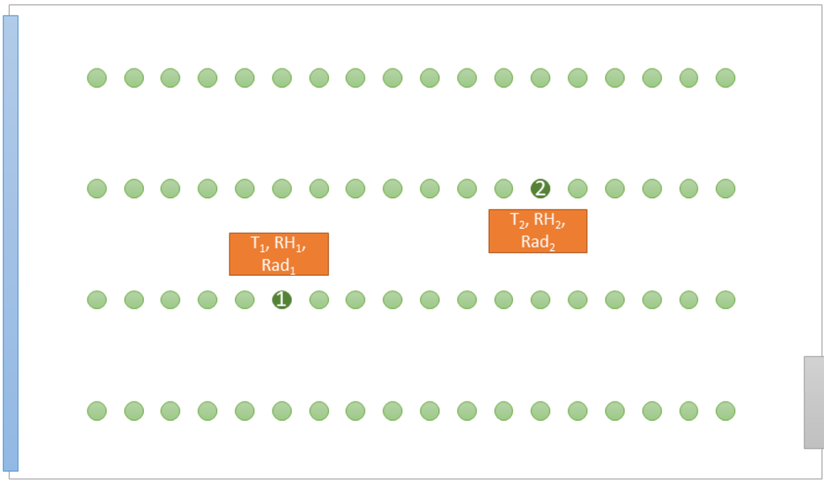

Figure 3. Positions of sensors of temperature (T), relative humidity (RH), and PAR and luminosity (Rad) during growth cycles 0 to 2. Gray rectangle refers to the door and blue rectangle refers to the wet pad. Green circles correspond to the vases. Monitored plants are highlighted in dark green. Distances are at scale.

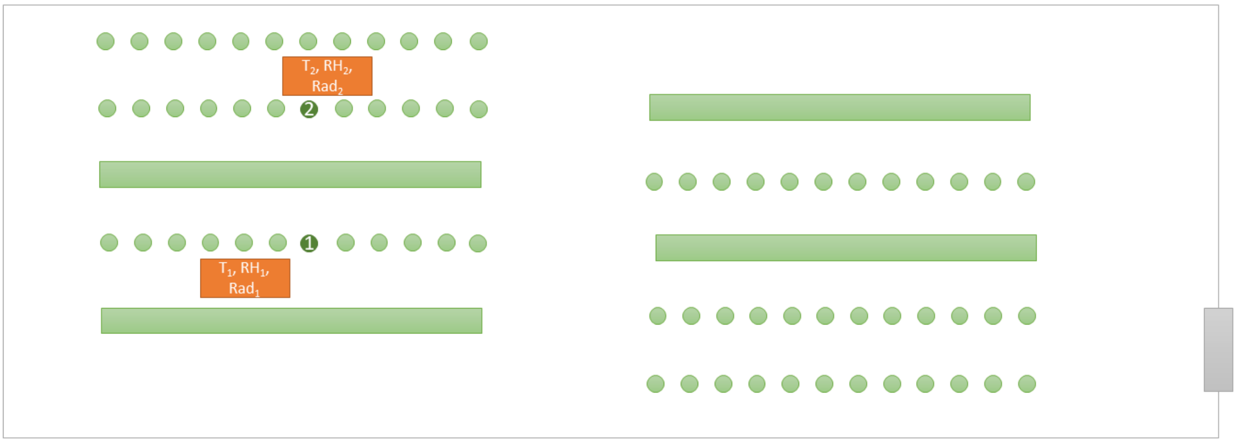

Figure 4. Positions of sensors of temperature (T), relative humidity (RH), and PAR and luminosity (Rad) during growth cycle 3. Gray rectangle refers to the door and green rectangles refer to the NFT grown tomatoes. Green circles correspond to the vases. Monitored plants are highlighted in dark green. Distances are at scale.

4.1.4. Growth data

Plants were characterized by destructive and non-destructive analysis. Destructive data refer to the characterization of dry weight of the plant and leaf area. Every one to three weeks, three plants were removed and used for destructive analysis. Keeping guard plants of the destructed plants was not always possible and could have effects on the results. Plant material was weighted before and after drying for four days or as until constant weight was reached. Leaves, stem and green and mature fruits were separated for weighting. After being weighted, while fresh, leaves were digitized with a scanner. Digitization included a reference of known size. Leaves were cut to accommodate more leaf area simultaneously in the same scan and speed the process. Before starting the removal procedure, plants selected for analysis were first photographed from above and laterally with a cellphone camera.

Non-destructive data refers to the continuous weight monitoring using force transducers HBM S2M with nominal force of 10 N (0.02 % accuracy) and stored in a data logger PMX WGX002, measure card PX455, and to the pictures taken from lateral and superior views, with fixed Raspberry Pi Camera Modules v2, connected to Raspberry Pi Zero.

4.2. Data preprocessing

Data obtained by the environmental sensors and from the weighting system was preprocessed in the R language while images were processed using Python. Environmental data required cleaning of outliers, unit conversions and imputation of missing data, often caused by failures in the sensors.

4.2.1. Environmental data

Outliers were removed from the dataset and treated as missing data. For temperatures, measurements were expected to be higher than -5ºC and lower than 60ºC, for air humidity, larger than 0% and lower than 100%, and for solar radiation or lux, larger than 0 in whichever unit it was measured. All measurements then were aggregated into tens of minutes for imputation. Four imputation approaches were used:

1. Redundancy: Replaced missing value with the measurement from the identical sensor in the same node.

2. Different sensors for the same variable: Replaced missing value with the average measurement from the sensors for the same variable in the same node.

3. Different sensors in different plants: Replaced missing value with the average measurement from all sensors of the same variable from the other node

4. External data: data extracted from the NASA Power database was interpolated through the day using the strategies from Spitters, Toussaint e Goudriaan (1986) and Lizaso et al. (2003) for solar radiation and of Parton e Logan (1981), for temperature.

For temperature and air humidity, they were prioritized in the order 1-2-3-4. For solar radiation, we prioritized as 1-3-2-4, with the premise that differences would be lower between different positions in the greenhouse than between different types of sensors.

In the case of PAR, as the different sensors were not directly equivalent, unit conversion was required. Data from the luxmeters was converted into photosynthetically active radiation [$\mu mol\ s^{-1}\ m^{-2}$] by multiplying measured value by 18 x 10^{-3} $\mu mol\ s^{-1}\ m^{-2}\ lux^{-1}$. (Hall and Scurlock, 1993). When external radiation was used, it was converted from [$MJ\ m^{-2}\ day^{-1}$] of global radiation into [$\mu mol\ s^{-1}\ m^{-2}$] of PAR by multiplying the measurement by 550.6 (Keulen and Dayan, 1993), including a 0.7 factor to account for plastic transmissivity.

4.2.2. System mass

The first step of processing referred to converting weight into mass by dividing the measurements by -9.81 x 10^{-3} $N\ g^{-1}$. Although we attempted to adjust the influence of water as a function of moisture in the substrate, this was not possible. Outliers were not observed, and as measurements were obtained each minute, they were aggregated into hourly observations.

In all growth cycles, as plants were harvested when mature trusses were available, this weight had to be summed to the system mass observation to make it compatible with model's estimate accumulated biomass.

4.2.3. Images

Labeling of the plant organs in the images was done manually, using the software GIMP. Only areas in which there was confidence the organ corresponded to the correct plant were marked, which entailed that if there was uncertainty or occlusion, the area was not marked. Leaves, immature fruits, and mature fruits were colored differently. Figure 5 and Figure 6 show examples in which the original image is being overlayed by the annotations, but it is possible to export only the layers referring to the labels.

Figure 5. Example of non-destructive observation of lateral leaf area and fruit area of sampled plant. Leaves are marked in green, mature fruits are marked in red, and non-mature fruits are marked in yellow. The A4 sheet used as reference is marked in cyan. Obstruction from adjacent plants prevents the identification of all organs corresponding to the plant sampled.

Figure 6. Example of image captured by fixed camera with overlayed labels for plant and reference. Green tomatoes are marked in yellow and leaves are marked in green. Reference is marked in cyan.

The OpenCV library was used to process both the digitized leaves and labeled images. Images contained a reference with known dimensions to be used as scale, which allowed for calculating the relationship between real size and the size in pixels. Table 4 shows how many images were annotated for this study. As for digitized leaf area, the algorithm from the Easy Leaf Area software (Easlon and Bloom, 2014) was used to identify leaves. Two dimensional references in images also allowed for calculating areas and estimating uncertainty in these measurements.

Table 4. Number of images annotated for estimating visible area of organs in pictures in each growth cycle divided by type of observation.

Cycle	Monitoring	Calibration
Cycle 1	170	53
Cycle 2	167	44
Cycle 3	148	36

4.3. Model implementation and calibration

4.3.1. The Reduced TOMGRO model

This study uses the Reduced State Tomgro (RT) model, which is a summary model from the TOMGRO model, aimed at being used in greenhouse control systems. In summary, the model has only five state variables: number of nodes, leaf area index, aboveground dry biomass, fruit dry biomass and mature fruit dry biomass. Based on hourly temperature and photosynthetically active solar radiation data, the model quantifies the growth and development of the tomato plant when water and nutrients do not limit growth. Development is indicated by the number of nodes, and growth, by the other states. The leaf area index influences photosynthesis, which, along with respiration, determines total carbohydrates available for growth of aboveground biomass and fruit biomass. The RT model, which has its variables and parameters further detailed in Jones et al. (1999), is therefore a simple model that does not include root growth or irrigation, and this simplicity may help in a first approach. An overview of its equations and parameters may be seen in Appendix A.

The RT model used in this work was implemented in the Python language, using Jones et al. (1991), Jones et al. (1999), and the spreadsheet provided by Dr James W Jones as sources. The difference equations were integrated by the Euler method. Having access to the spreadsheet used by the authors allowed for observing the equations as implemented, as well as the original data. By running the code written for this work with the original input data and by using the same strategy for calibration — minimizing the squared errors of one variable at a time —, the same parameters and outputs were obtained for all five datasets: Avignon, Lake City and all three from Gainesville. The simulation outputs in Figure 7, Figure 8 and Figure 9 were obtained using the Python implementation and represent the results in Figures 1, 3 and 5 in Jones et al. (1999).

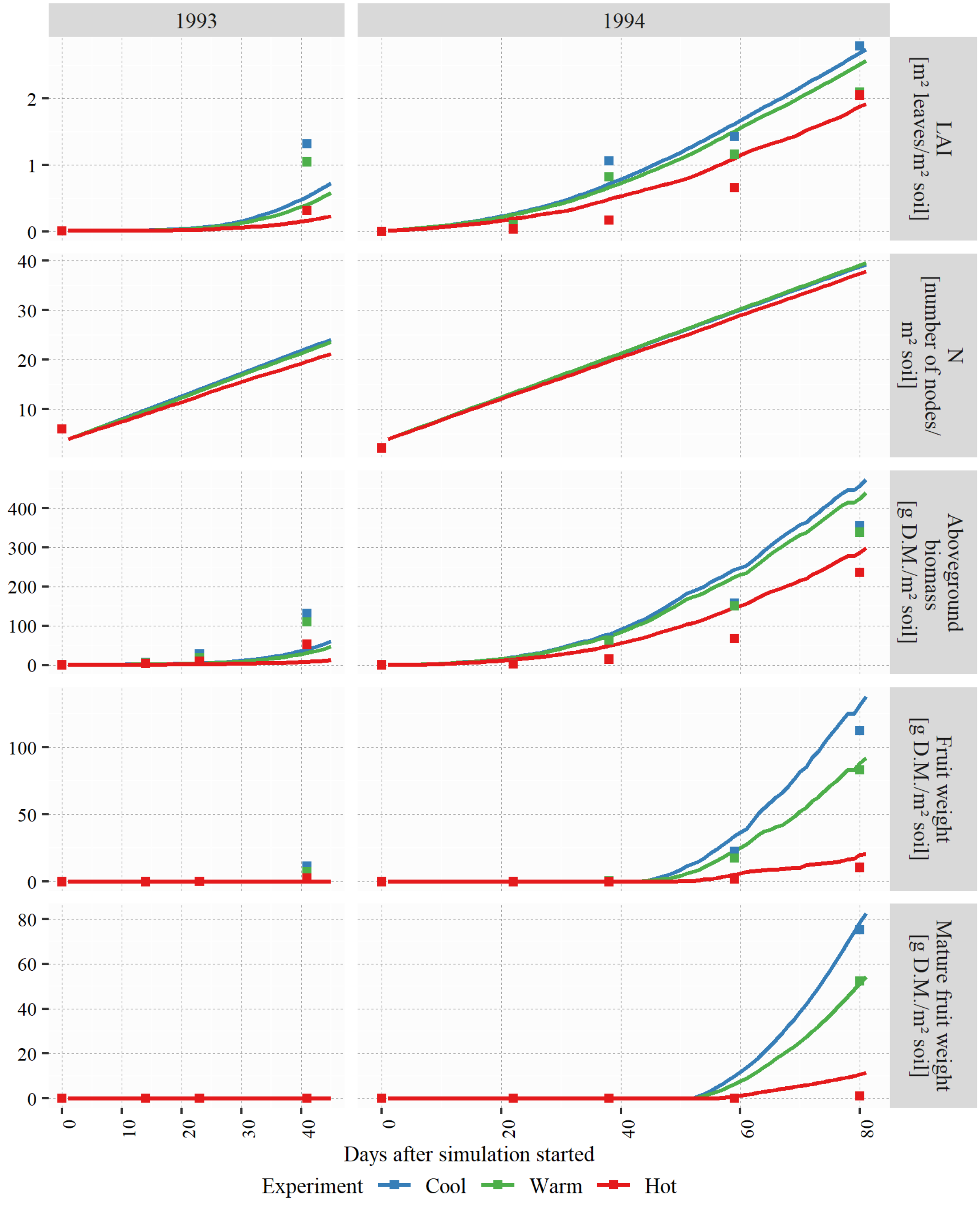

Figure 7. Results from simulation with the Python implementation using Gainesville data. Squares represent observations from destructive analyses.

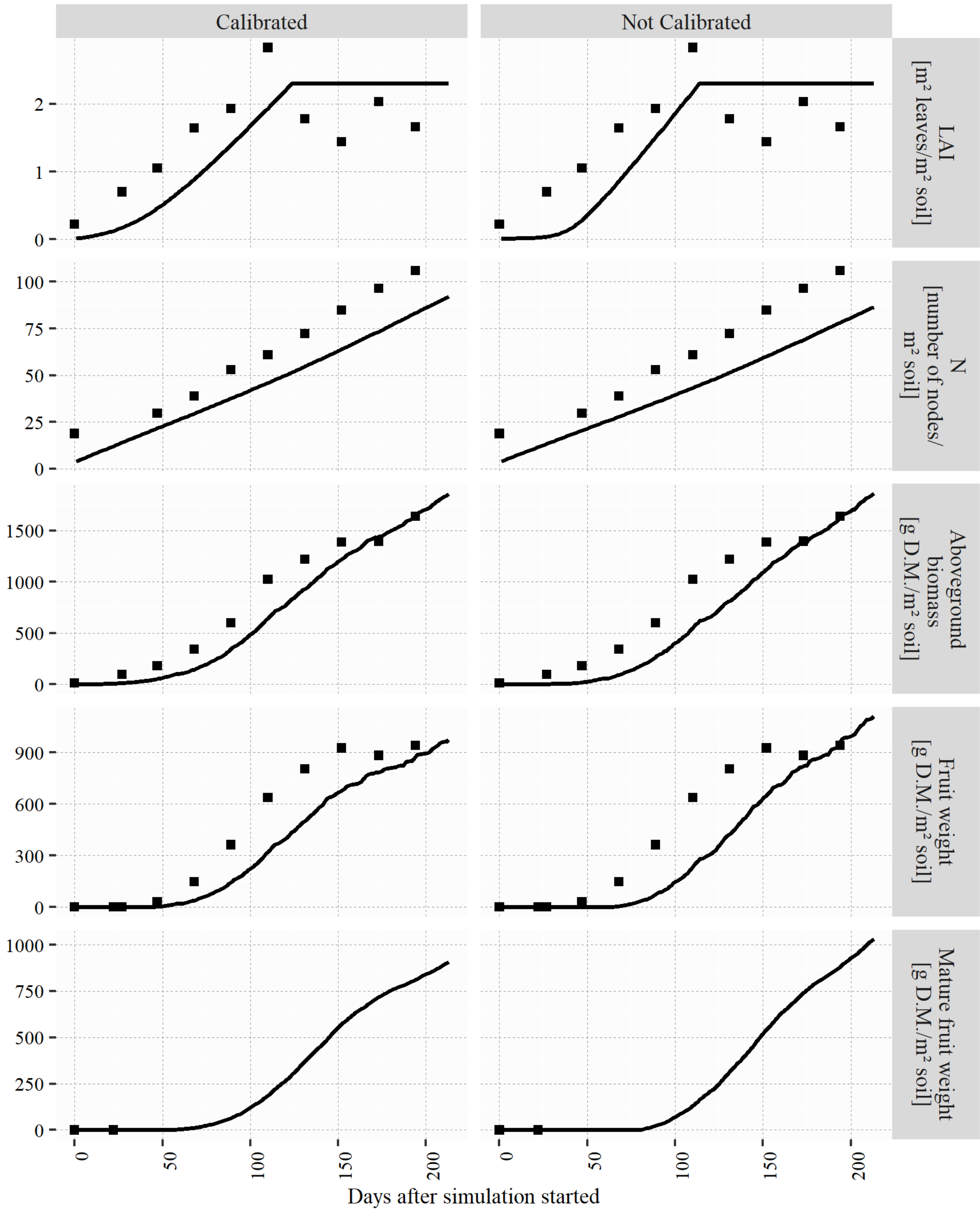

Figure 8. Results from simulation with the Python implementation using Avignon data. Squares represent observations from destructive analyses.

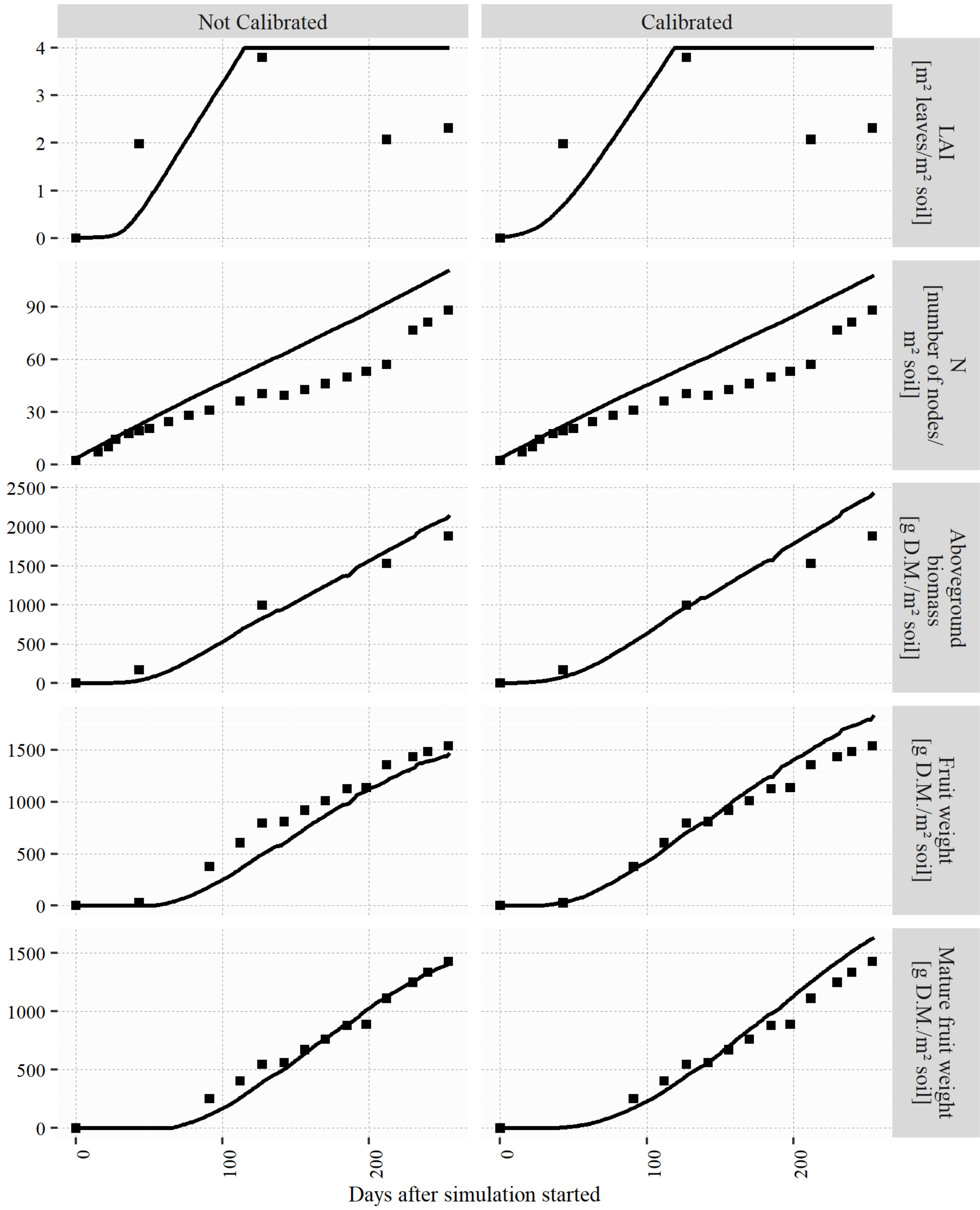

Figure 9. Results from simulation with the Python implementation using Lake City data. Squares represent observations from destructive analyses.

4.3.2. Calibration

Jones et al. (1999) calibrated parameters for the Reduced-State Tomgro sequentially, minimizing the sum of the squared error for LAI, fruits, mature fruits, and aboveground biomass, with a total of 10 parameters being calibrated. However, as values of one variable may inform on the other, optimizing all parameters simultaneously would also be a valid approach.

In this study, from all parameters assessed in the sensitivity analysis, the ones with largest total sensitivity indexes for each state variable, including number of nodes, were adjusted in two ways: by minimizing an error metric using a global optimization algorithm and by visually determining good adjustments of growth curves to the observed values in the destructive analyses. Although the second approach was informative, to make the work more reproducible, optimization was adopted.

The error metric used in optimization was the root square of the sum of squared errors, which were calculated by the difference of log-transformed observations and estimates. Transformation was applied to compensate for the differences in magnitudes of the state variables. The root square was used to smooth the effect of extreme error values.

Data from the destructive analyses was used to calibrate the Reduced Tomgro model. Given there were three different cycles, each with different conditions, a calibrated run used data from the respective cycle. Non-calibrated runs used parameters from the original Gainesville calibration. Regardless of calibration, input data such as maximum leaf area or plant density referred to data from the evaluated cycle.

4.4. Model uncertainty and sensitivity analyses

An uncertainty analysis was performed to identify values which could be ascribed to filters' hyperparameters, both for inputs and for parameters. The assessment was also used to identify which parameters should be calibrated and perturbed in ensemble generation.

4.4.1. Uncertainty ascribed to parameters

A wide range of weather series, referring to Campinas historical data, was used to assess parameters across several ranges of external factors. Since environmental inputs are intimately correlated, instead of randomly generating them, multiple examples were drawn from actual weather series.

For each of the 20 years selected and 4 planting dates with a length of 160 days, the model was run with parameter ranges from Appendix A sampled following Saltelli's extension of the Sobol sequence[1]. Inputs refer to historical weather of the Campinas. While temperature

[1] Sampling used SALib library (Herman and Usher, 2017)

is maintained as is, assuming natural or mechanical ventilation, radiation is reduced to 70%, ascribed to cover material transmissivity. CO_2 was sampled to represent modifications to the environment either by accumulation or depletion. While keeping the internal temperature the same as the outside led to unlikely low temperatures, we assumed a passive low-tech greenhouse, in which these problems exist.

Total number of runs accounted for the combinations of one thousand samples of each parameter. The maximum value of the leaf area index, or its equivalent of intercepted solar radiation, is an input in the model and was included in the analysis (Appendix A) as it is intimately related to canopy photosynthesis and, therefore, growth, in all models.

4.4.2. Uncertainty ascribed to input variables

Parameters’ values refer to the ones obtained in the calibration of Cycle 3. As for weather inputs, variations should be consistent with minor variability across the time-series, as the parameters used could not be valid if weather inputs differ by much from the calibration condition. So, to account for autocorrelation between adjacent values, as well as between variables, but taking into account that measurement error could in fact lead to incompatible measurements, the sampling strategy applied a uniform change to the series from Saltelli's extension of the Sobol sequence with normal distribution, zero mean, to account for positive and negative changes, and a standard deviation that could correspond to variability within a greenhouse, roughly 5% of the average observation. Radiation and carbon dioxide concentrations were bounded to a minimum of zero. Total number of runs was 50 thousand to account for the combinations of 10 thousand samples of each variable.

4.5. Modeling the relationship of observed variables to state variables

Observation models were created from data obtained from plants subjected to destructive and non-destructive analyses. The modeling strategy focused on obtaining simple empirical relationships, and the generalized least squares method was used to account for the heteroscedasticity and correlation between residues. To avoid data leakage, despite the different growth conditions, data from the cycle was not used to obtain the relationship that would be used in that cycle. All observations obtained per plant were multiplied by plant density to make units compatible with the states in the model.

We used area extracted from lateral and top images to determine the leaf area index, fruit area extracted from lateral images to infer fruit dry mass and weight as determined by the weighting system to infer aboveground biomass. In this last case, we performed a conversion that would consider the difference caused by roots depending on development stage, and the difference from fresh to dry biomass. It was not possible to address changes in water content in the system plant-substrate-water.

4.6. Data assimilation

The algorithms for data assimilation were based on the FilterPy library[2], and modified as needed. To account for this being a first approach, and as data for obtaining observation models was limited, only one variable was assimilated at a time. In this work, three state variables were estimated: aboveground dry biomass, leaf area index and fruit dry biomass.

As the processes represented by the model are non-linear, two techniques were adopted — Ensemble Kalman Filter and Unscented Kalman Filter— and their hyperparameters and additional requirements are described below. In all cases, variance in the measurements was determined as the variance of the indirect observations of the calibration samples. While we are aware that this corresponds to partial leakage, we believe this was the best way to provide an estimate for these filter parameters.

4.6.1. Overall assimilation approach

4.6.1.1. UKF

This method requires specifications of uncertainty that were ascribed as following. Uncertainty in the initial states was determined as the variance of the samples analyzed in the transplanting day. Uncertainty in the model was determined as the absolute error calculated by the difference between observations of the states in the calibration samples in the cycle and the simulated value of the uncalibrated model. The technique also has hyperparameters for sampling the sigma points, but they were kept as the default from FilterPy.

4.6.1.2. EnKF

For the EnKF, uncertainty in the process depend on the ensemble generation process. In this study, it was ascribed to a model parameter, by adding a perturbation sampled from a normal distribution with zero mean and standard deviation of 10% of the parameter value. The parameter depended on the state variable being assimilated: for leaf area index, the maximum

[2] https://filterpy.readthedocs.io/en/latest/

leaf area expansion per node was perturbed, for aboveground biomass, the leaf quantum efficiency, and for fruit biomass, the maximum partitioning of new growth to fruit. The number of elements in the ensemble was tested and defined as 100.

4.6.2. Assessment of influence from low-cost sensors

Growth data from Cycle 3 was used to calibrate the model and simulations from the calibrated model with the weather data from all four cycles were then treated as the truth of an artificial dataset. The simulations of fruit and mature fruit biomass were perturbed by gaussian noise sampled from a distribution of zero mean and standard deviation corresponding to 10%, 30% and 50% of the simulated truth. The perturbed simulations were treated as observations and the EnKF was used to assimilate them using the non-calibrated model as source of model estimates. In this case, ensembles were generated by perturbation of weather inputs corresponding to 10% of the measured input. The procedure was repeated 20 times to avoid biasing the results due to sampling. An additional random perturbation — N(1, 0.09) — was included in the observations and represents the variability of the sampling noise.

4.6.3. Determination of temporal resolution

We used images captured every other day as the full set of observations. Data from the weighting system was captured each minute and was then averaged in the hour and data from between 4 am and 5 am, before sunrise in all cycles, was used as the observation for each day. We then subsampled these observations to determine the effect of frequency. Subsampling was applied to the observations and corresponded to using 50% and 10% of the data available in the cycle. To avoid results being biased by sampling, the procedure was performed 20 times. One of the repetitions was sampled in regular intervals through the cycle and the others were randomly sampled.

5. RESULTS AND DISCUSSION

5.1. Data

As detailed in the methods section, this work required growing tomatoes and characterizing growth cycles through monitoring the environment as well as plants. Data gathering was then quite laborious and there was an improvement in the quality of data obtained in Cycles 2 and 3, when compared to Cycles 0 and 1. It is not expected for this difference to have an impact on the assimilation results, but as it appears through the work, it will be further commented on the following sections. One reason for the difference is that it was only possible to identify issues after processing raw data, which, by its turn, required data gathering to write the scripts to process and analyze the results.

5.1.1. Weather

The curves from Figure 10 show the summaries of daily environmental data in the greenhouse, which correspond to the final value ascribed to the scientific grade instruments, after processing, and that were used in the simulations. For solar radiation, as a reference, external solar radiation is included. This reference suggests there may have been an interference with measured values especially in Cycle 1, but possibly in Cycle 2, indicated by the different trends of the measurements. In Cycle 1, there is a step reduction in the measured value that was possibly caused by the height in which the sensor was placed being lower than the plants' maximum height, subjecting the sensors to shadows. In Cycle 2, there is no such reduction but there is a trend of decline in the measurement that is not observed for the external radiation. The difference in this case, however, could be ascribed to the conversions of PAR and global radiation not being very accurate and relying on more information than the approximations used allowed for. Nevertheless, the values overall correspond to daily integrals ranging from 6 to 16 MJ PAR m^{-2} day^{-1}, or 12 to 32 MJ m^{-2} day^{-1} of global radiation, which is considered above the minimum required — 0.85 MJ m^{-2} day^{-1} — for flowering (Alvarenga, 2013).

As for temperatures, they were within a range considered appropriate for tomato growth pointed by Alvarenga (2013) — 10°C to 34°C — during the most part of growth cycles. But the author also points to specific ranges in developmental stages that are more narrow and often minimum temperatures were larger than those recommended, i.e., 18°C to 24°C during flowering, 14°C to 17°C during the nights and 19°C to 24°C during the days in the fructification phase and 20°C to 24°C for maturity. As Cycles 1 and 2 used a cooling system, there were few days in which maximum temperatures exceeded the more general recommendations. The highest observed temperature in Cycle 2 refers to a day in which an electrical issue led the ventilation and refrigerating systems to shut down for a few hours. The average being closer to minimum temperatures in Cycle 2 suggests that maximum daily temperatures were mostly exceptions during the day, before the cooling system was activated. Higher relative humidity through the cycle also suggests there was more interference from the system, even though this also meant that for this environmental variable, ideal conditions were not maintained for tomato growth. For Cycle 3, maximum temperatures in the initial stages could not be circumvented, but it does not seem to have damaged growth. Cycle 3 also presented the largest differences in measurements of the different nodes and as Node 2 reached highest temperatures, this was accompanied by the lowest relative humidity measurements.

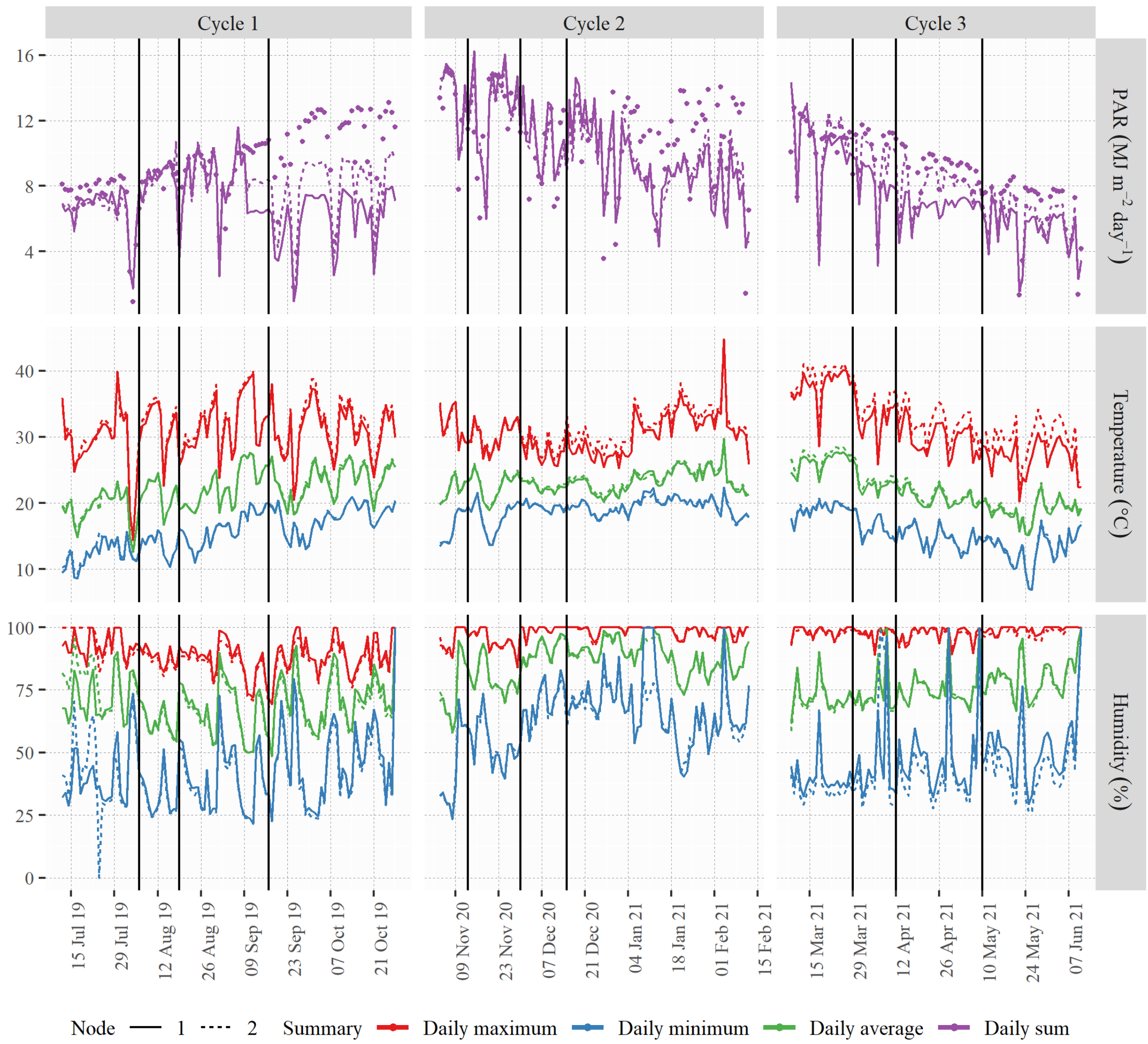

Figure 10. Summary of environmental data after processing, for the growth cycles with complete data gathering. External daily radiation included as reference and represented by the points. Vertical lines refer to the approximate dates of change in the development stage (flowering, appearance of fruits and maturity).

Figure 11 and Figure 12 show the results from imputation strategies used in each sensor node for hourly data. In these two figures, percentage imputed refers to the fraction of the total observations in that hour that was extracted from another source to reach the scheduled number of observations. As mentioned in the description of growth infrastructure in section 4.1.1, not all sensors were installed in Cycle 0, which is why it required imputation from external data and, afterward, replacement from one sensor to the other. In the other cycles, the indicated imputation for solar radiation refers to data from the night, in which the schedule from the quantum sensors logger interrupted data gathering, but as this only refers to data after sunset and before sunrise, it just included replacement by zeros. Data from low-cost sensors in Node 2 also required imputation in Cycle 1. As no redundancy was available for luxmeters, it used data from the other node. On the other hand, for half of the cycle, it relied on the other sensor for temperature and, later, on data from the SHT75 transductors. Although it was not possible to fix the issues during growth, it was later fixed for the following growth cycle.

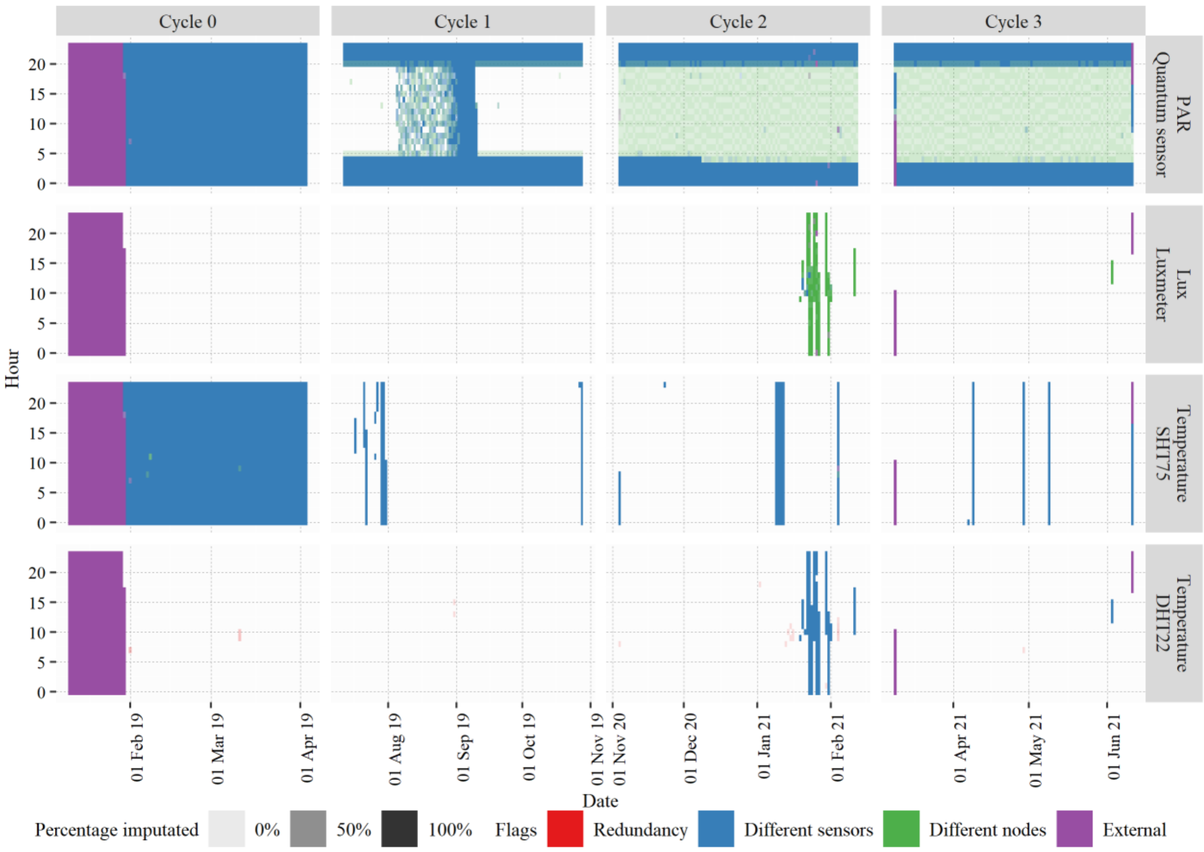

Figure 11. Map of imputations performed in sensors of Node 1. Each pair (x, y) refers to one hour in each of the days in the different cycles. The vertical left axis indicates the hour in the day. Colors are mapped into the different strategies of imputation. The amount of data required to be estimated, relatively to the number of measurements expected in the hour, is shown by transparency in the respective square.

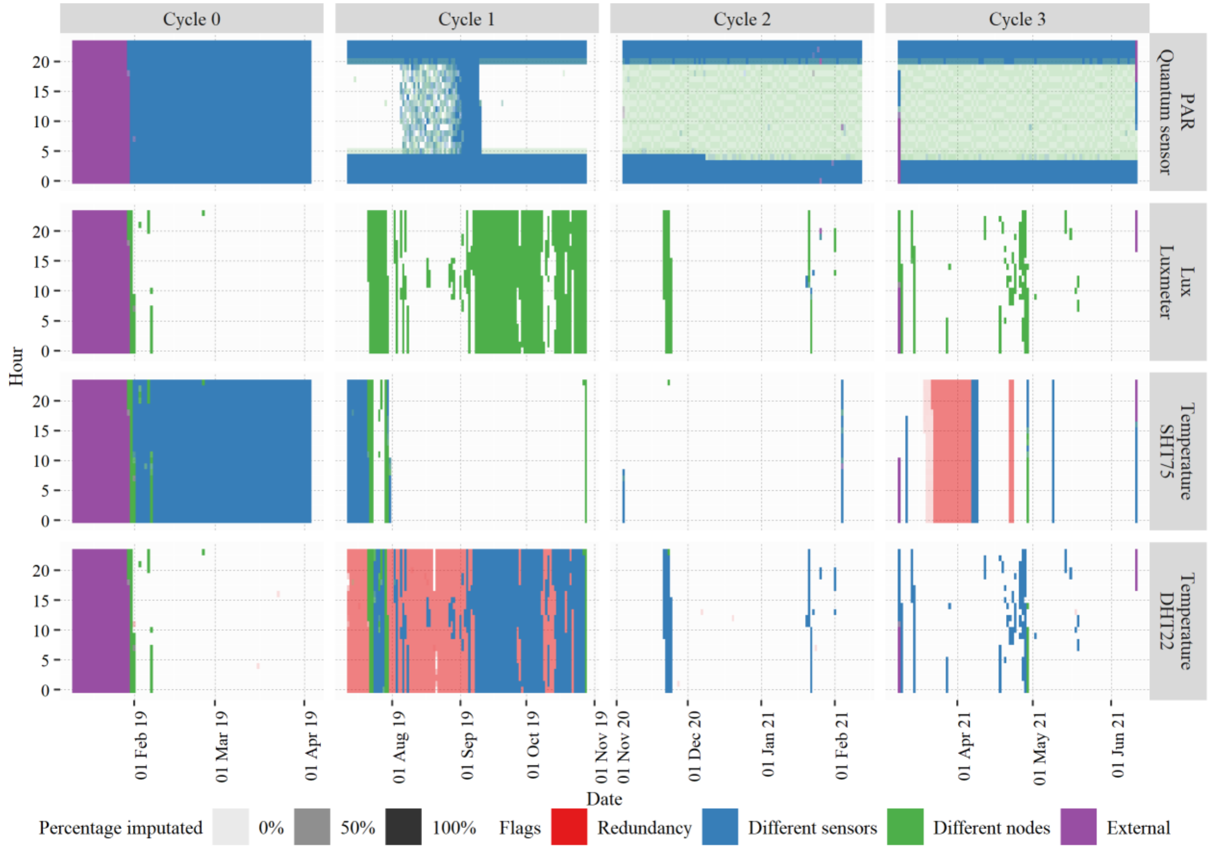

Figure 12. Map of imputations performed in sensors of Node 2. Each pair (x, y) refers to one hour in each of the days in the different cycles. The vertical left axis indicates the hour in the day. Colors are mapped into the different strategies of imputation. The amount of data required to be estimated, relatively to the number of measurements expected in the hour, is shown by transparency in the respective square.

As imputation sometimes used data from other sensors, it is reasonable to assess the correspondence between their measurements. Figure 13 and Figure 14 show the relationship between the raw measurements from different sensors. These results suggest that using data from one sensor as replacement for missing measurements of the other was adequate. Although the relationship between luxmeters and quantum sensors is not as good as the one of temperature sensors, it is reasonable to admit that for the few cases in which they were necessary, mainly for Cycle 2, this replacement should be acceptable.

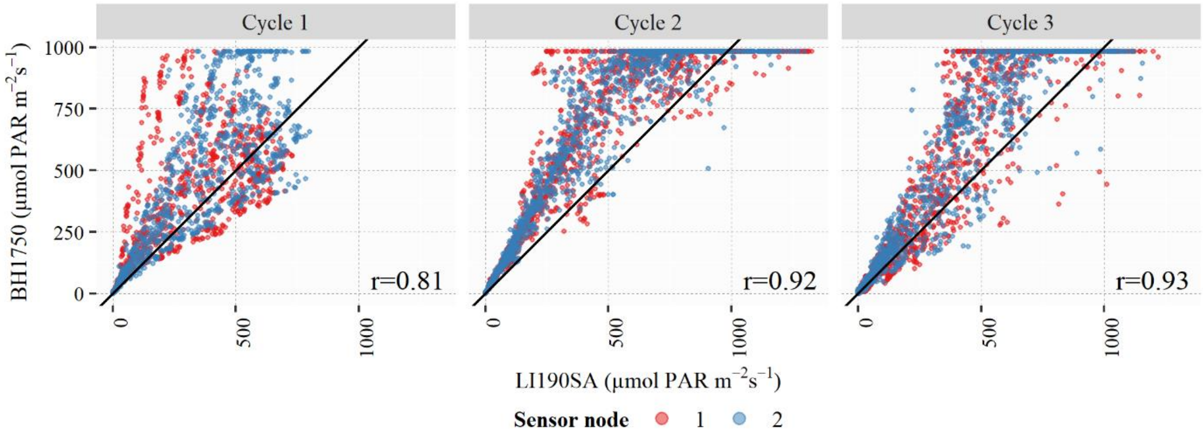

Figure 13.Scatterplots of relationships between measurements of PAR converted from data obtained by BH1750 luxmeters and measurements of PAR obtained by LI190SA quantum sensors.

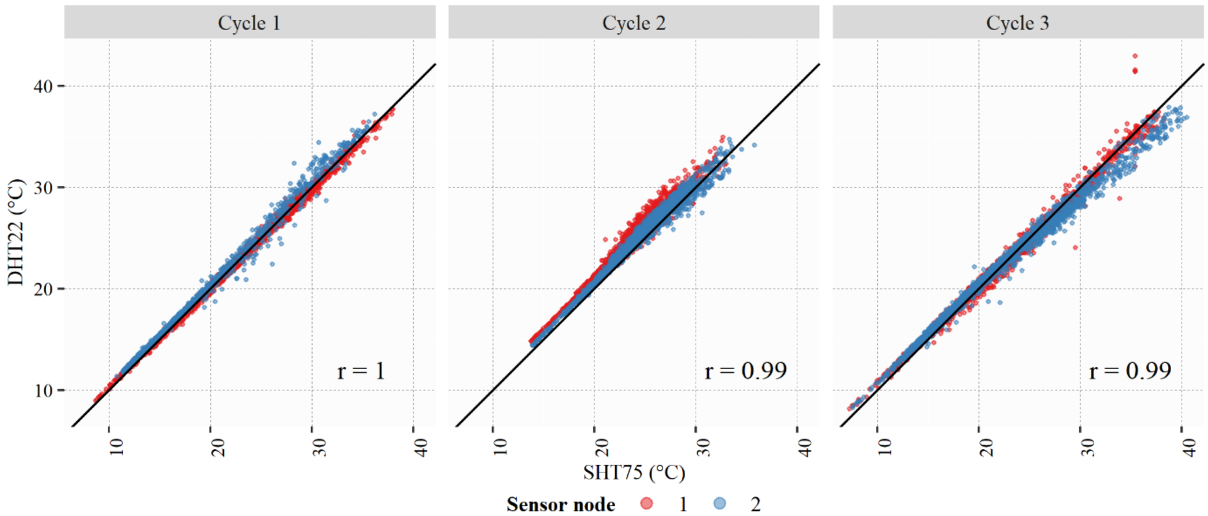

Figure 14. Scatterplots of relationships between measurements of temperature obtained by DHT22 sensors and measurements of temperature obtained by SHT75 transductors.

5.1.2. Plant growth

The three cycles presented different developments, caused by differences in management, which were explored in this work: the first may be characterized by low irrigation, subjecting plants to water deficit, the second, by an excess of nitrogen fertilization and an attack of tomato rust mite by the end of the cycle, and the third cycle was conducted closer to full water and fertilization. The following sections detail how these differences impacted the outcomes, as well as how they relate to the previously presented environmental data. But before commenting on the meaning of the outcomes, the methods used for growth characterization merit some comments.

Leaf area measurement by digitization of leaves with a scanner (Figure 15) is dependent on how the expected leaf area was defined in the code. For instance, Li et al. (2020) generated a gray image by doubling the weight of the green component in the RGB image, while Easlon and Bloom (2014) first defined a minimum green level and then used ratios, i.e. green/red (G/R) and green/blue (G/B), to identify the leaves. In this work, the latter approach achieved better results. But as the script focused on identifying green leaves, leaf area was mostly represented as green LAI, which may not be what the developers of the crop model intended. This work used only thresholding and other basic RGB processing and more advanced algorithms could have improved separation. However, from what was observed in the results, it should not lead to vastly different outcomes, as one problem would be detecting yellow parts on the leaves, but these often appeared in a moment that the model was no longer very sensitive to differences in LAI values, as will be discussed ahead.

Figure 15. Example of leaf scan from Cycle 3, including the contour obtained automatically, which was used to calculate the area corresponding to leaf in the picture.

In this study, we used the size reference included for unit conversion, to estimate errors in the method, as its area was often known (Table 5). These errors do not extrapolate for the errors in the identification of leaves, as the thresholds for leaves and the reference are different, but they indicate the errors of conversion, since when the reference was misidentified, it propagates into the conversion calculation. The largest errors observed in Cycle 1 were likely caused by the reference being black, which was difficult to separate from the shadows of the scanner. An additional aspect analyzed was that the largest errors were more prevalent in images from the beginning of the cycle, in which increases would not amount to major differences in the final value.

Table 5. Average and standard deviation of the relative error [%] in reference area measurement for digitized leaves.

	Monitoring*	Calibration
Cycle 1	5.1 ± 1.3	5.5 ± 7.4
Cycle 2	3.8 ± 2.1	2.6 ± 2.5
Cycle 3	0.8 ± 1.8	4.6 ± 1.4

* Final value, when they were subjected to destructive analyses.

Regarding the areas of monitored plants, as data gathering was also a learning process, references in Cycle 1 were ascribed to fixed and known measurements of objects in the environment in almost all pictures. In Cycle 2, the reference for the view from above in monitored plants was higher than the references in calibration, since only later it would be detected later that plants' leaves would cover the reference. This should lead to underestimation of the area in monitored plants, in comparison to the calibration plants. Similarly to the case of digitized leaf area, two-dimensional references allowed for estimating error in the area of the reference (Table 6).

Table 6. Average and standard deviation of the relative error [%] in reference area measurement.

Growth Cycle	Position	Monitoring	Calibration
Cycle 1	Above	-	-
	Lateral	-	4.4±3.2
Cycle 2	Above	1.5 ± 1.5	2.2±3.4
	Lateral	4.0 ± 3.1	3.0 ±3.0
Cycle 3	Above	2.4 ± 2.2	4.7±4.4
	Lateral	1.9 ± 2.0	2.8±1.7

Another type of data obtained when monitoring growth refers to the measurements from the weighting system. In this case, an attempt was made at establishing a relationship between moisture and the voltage measured by a soil moisture sensor. This would allow for quantifying the amount of water in the substrate and subtract it from the system, identifying the mass that corresponded only to the plant. The calibration attempt, however, led to poor relationships as the substrate is very porous and the relationships seemed quite dependent on the degree of compaction of the substrate in the vase. As it was understood that measured values could suffer additional interference from plant growth, as identified by Kang, Van Iersel e Kim (2019), attempts to quantify water in the system were abandoned.

To avoid interference from irrigation and evapotranspiration, another decision referred at what time the measurements would be made. We used the standard deviation of hourly measurements, which naturally pointed to fewer changes before sunrise, and measurements between 4 and 5 am were then used. However, this decision would likely not have substantially influenced the results, as Figure 16 suggests.

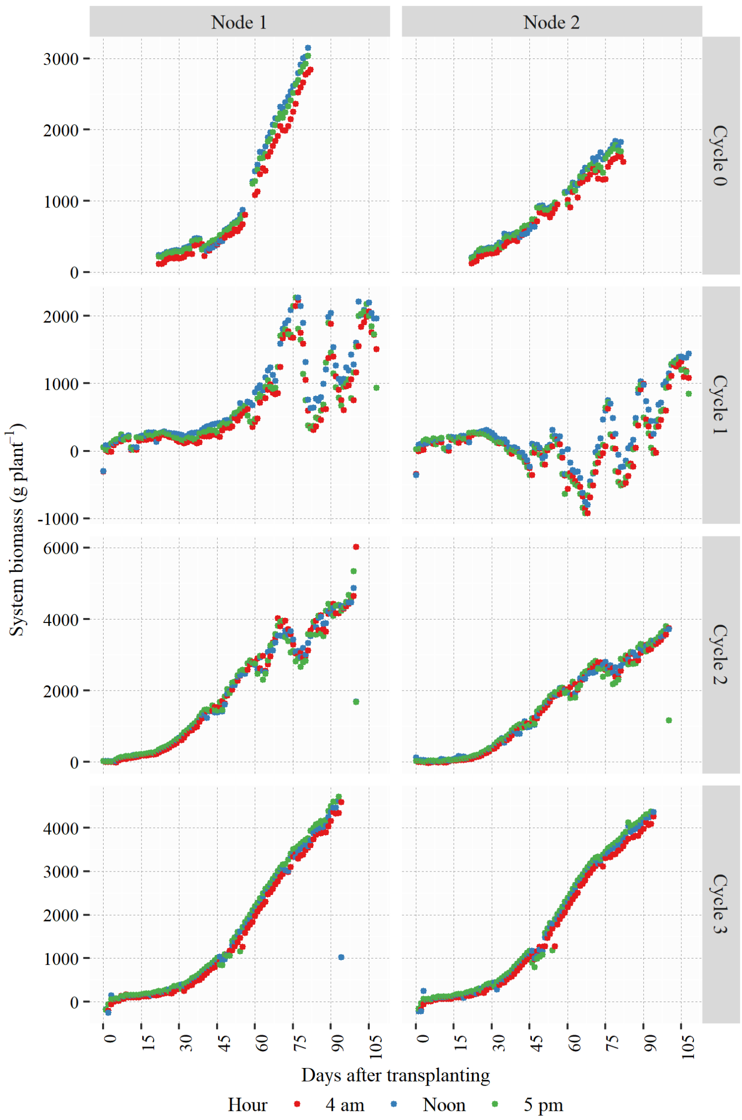

Figure 16. Daily observations of system weight with measurement time defined in different hours of the day.

The direct or indirect approaches used for growth characterization led to curves that were compatible with each cycle characteristic. Figure 17 shows the curves related to leaf area, either identified in photos or by digitization of leaves, and Figure 18 shows the curves related to biomass, either total or exclusively from fruits. In Figure 17, there is a difference in leaf area per plant and leaf area index, as the second case is influenced by plant density. In Cycle 3, the smaller distance between lines led to higher plant density and, therefore, higher leaf area index, even though the final values of plant leaf area were similar to the ones in Cycle 2. The overlap between plants influence photosynthesis and therefore should not be disregarded, but this issue is further explored in the simulation section. The rust mite attack led to lower leaf area and higher variability in this variable in plants sampled by the end of the Cycle 2. On the other hand, excess nitrogen led to a steeper curve for leaf area in the same growth cycle.

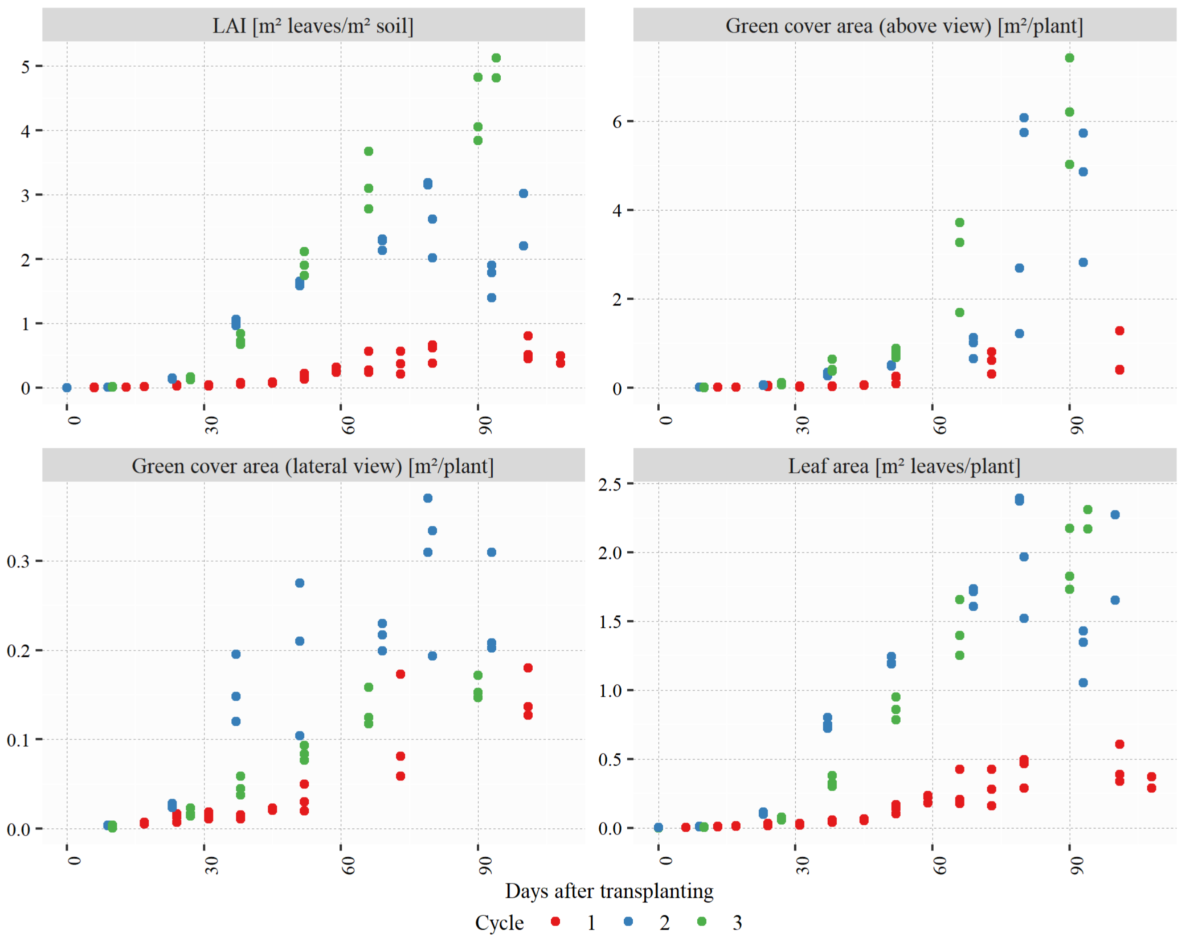

Figure 17.Characterization of leaf area identified in the scans and in pictures of calibration samples. LAI corresponds to leaf area multiplied by plant density.

Despite the similar values for plant leaf area, plants in Cycle 2 had much higher green cover from the lateral view. This was possibly caused by the shape of the leaves, which were curled, leading to more visible areas being detected in pictures. It should be noted that the areas identified in lateral images are much lower than the total leaf area of the plant and while images from above show more compatible magnitudes, they capture not only growth but also proximity to the camera.

Data from the destructive analyses point to smaller plants, with lower leaf area in Cycle 1 and lower biomass, caused by restricted irrigation. It is interesting that despite the restrictions, fruit production was not as largely affected and the opposite of what happened in Cycle 2 was observed, with most of the final biomass being composed by fruits, instead of leaves and stem. On the other hand, despite similar leaf areas from Cycles 2 and 3 and similar aboveground biomass, the previously mentioned excess nitrogen was also the probable cause of the lower fruit mass in Cycle 2.

In Heuvelink (1995), the experiments which provided data for the development of the Tomsim model and their results are described. The author grew the cultivar Counter, mostly in optimal conditions, also for around 100 days. The author reported that total dry weight, which includes harvested fruits, ranged from 94 g plant^{-1} to 488 g plant^{-1}. The wide range of biomass can be attributed to the different planting dates, which subjected some experiments to low radiation intensity. The results are similar to the ones observed in this study for Cycles 2 and 3. Although biomass in this study did not include picked leaves, for monitored plants, which were the last observed values, no removal of leaves was performed, so they are comparable. With few exceptions, in their work, fruits comprised between 50 and 60% of total dry biomass, which was different from even the best case of this study, in which this percentage was of about 30%.

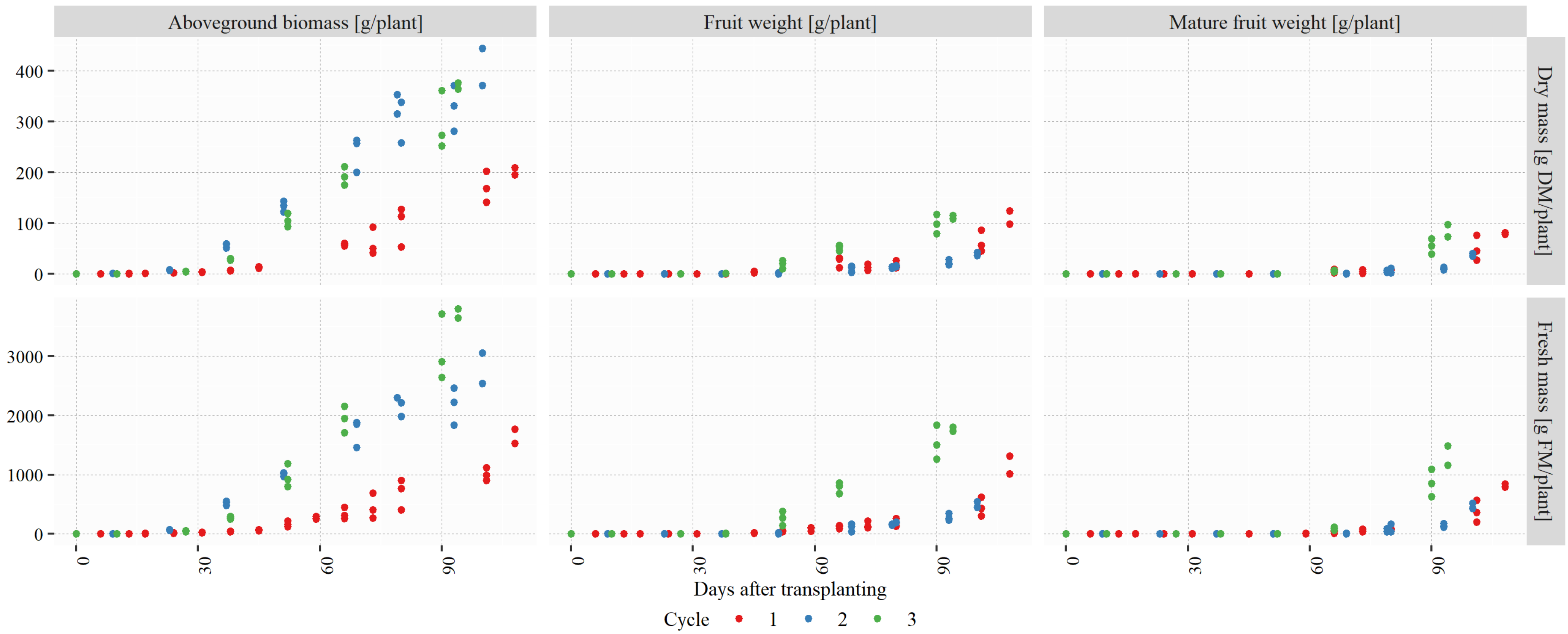

Figure 18. Characterization of plant biomass of calibration samples in each growth cycle.

Overall, growth from monitored plants, measured indirectly through pictures and through the weight system, was similar to the growth of other plants in the environment (Figure 19). Areas corresponding to leaves and fruits extracted from the images obtained with cellphones were compatible with the ones extracted from images obtained by the fixed cameras. Growth trends are noticeable, but are also very sensitive to lighting and occlusion, which often explains the discontinuities. As few observations were obtained for mature fruits, they were not included.

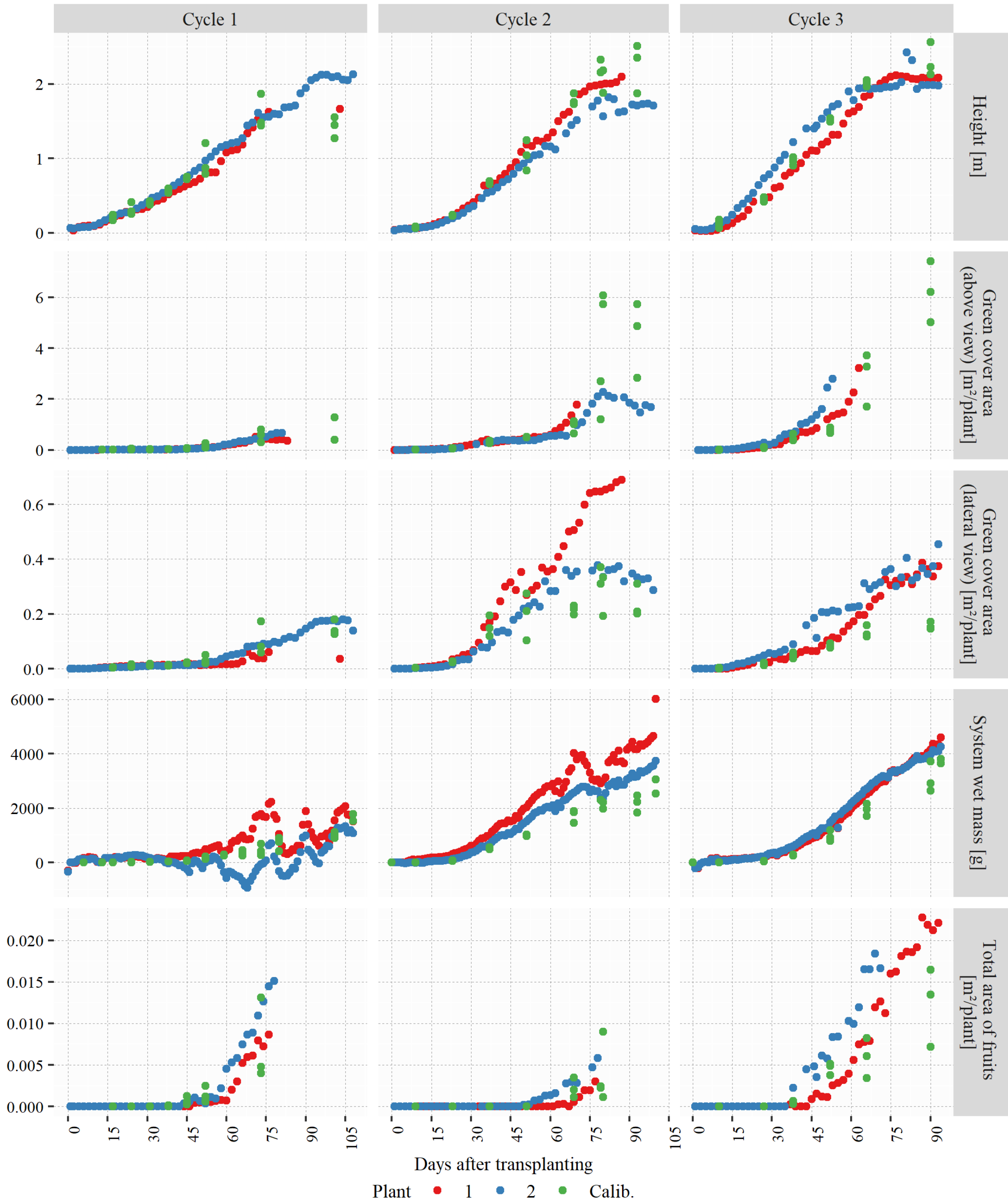

Figure 19. Times-series of observations from monitored plants and values for the same variables from the calibration samples. For the weighting system, values for the calibration samples refer to aboveground fresh mass, with the last calibration observations corresponding to the monitored plants.

When areas of the lateral view of monitored plants were larger than from calibration data, this effect likely can be attributed to occlusion, as monitored plants were slightly dislocated from the planting line, for example for Cycle 3 and Plant 1 in Cycle 2, and the visibility of plants used in calibration was affected by adjacent plants (Figure 5). On the other hand, for calibrated plants, we note that visible area in Cycle 3 is equivalent to the visible area in Cycle 1, even if in the latter, maximum leaf area per plant reached an average of 0.44 m^2 leaves/plant and in Cycle 1, 1.91 m^2 leaves/plant, as indicated in Figure 19. This was likely a consequence of fewer leaves reducing the complexity of annotations in the environment of Cycle 1.

In Figure 19, height was included with two purposes: as a reference of information extracted from pictures in a comprehensible unit, but also to show how monitored plants having their growth interrupted earlier than plants used in calibration is particularly noticeable in Cycle 3, as their heights remain constant by the end of the cycle. Curves of area of fruits in Cycles 1 and 2 are interrupted before the end of the cycle because as plants were harvested, observations did not correspond to total fruit mass any longer and were not compatible with the principle of accumulated biomass used in the growth model. In the green cover area identified from the above view, interruption often refers to the plant reaching the camera and occupying all visible area, being no longer informative. The very low values observed in Cycle 1 for the above view may be connected not only to lower leaf area, but also to a slight dislocation of the camera, so that it did not fully capture the plant.

As for the system wet mass, one can observe how the first cycle corresponded to unstable mass values, mostly corresponding to the amount of irrigation applied. In the second and third cycles, these fluctuations are less prevalent. In those cycles, we can observe values from monitored plants are larger than for calibrated samples as roots are included in the system. Their accommodation of more water also increases total mass.

5.2. Model uncertainty and sensitivity analysis

5.2.1. Parameters

Figure 20 shows the interannual variability of the total sensitivity index of parameters for all state variables, as well as its progress through growth. The largest total sensitivity indices mean the largest fraction of the variance observed on the output is ascribed to that parameter, so a change in a parameter index through growth means the fraction is different for the same parameter in different moments. These differences were expected. As plants respond to the environment, it is natural that differences in weather should impact what process is affecting growth the most and, therefore, the calculated index. Similarly, as growth progresses, what impacts a state variable the most changes, as partitioning changes the dynamics of carbon allocation. While it could be the case that for indeterminate growth of tomatoes, after reaching a certain stage, changes in indices should not be very substantial, weather variability may still affect the indices, as progress in season also means changes in the weather, leading to the high variability still observed in indices by the end of the cycle. So, while one can guide themselves by the average, it should be clear that different years could lead to different outcomes in which parameters would impact simulations the most.

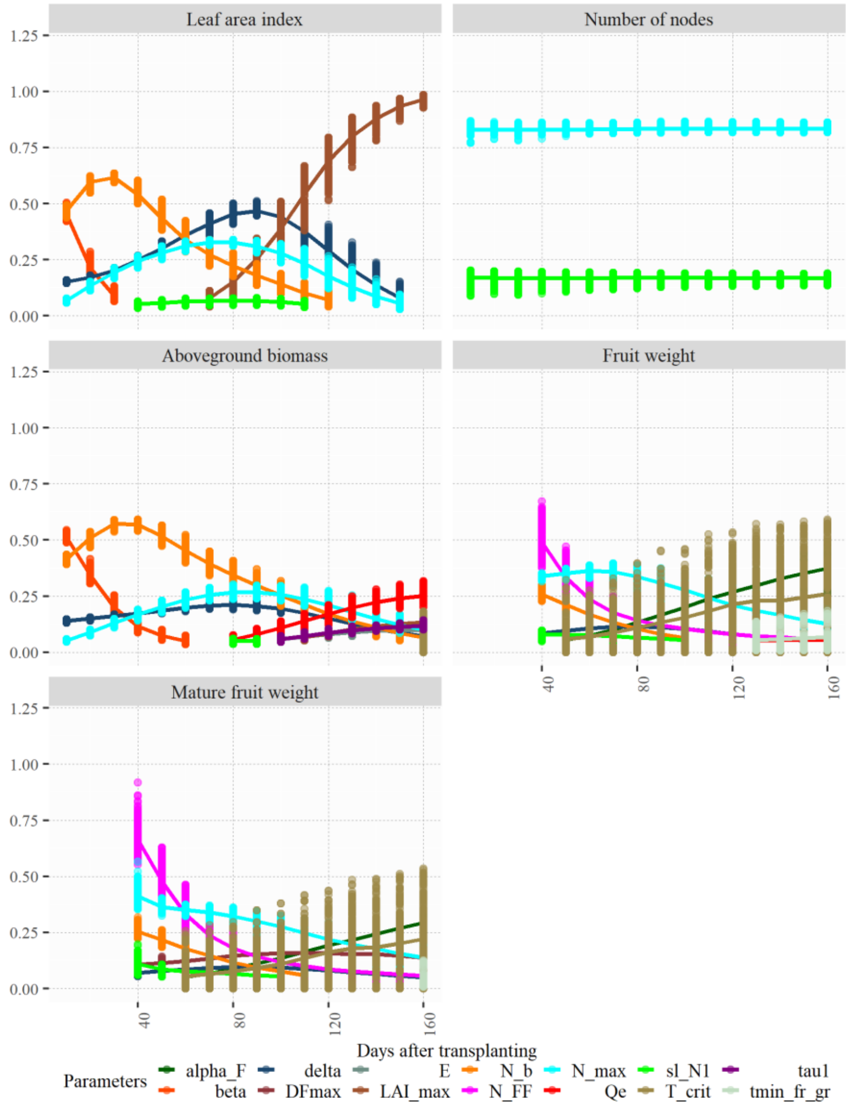

Figure 20. Total effect sensitivity indices of yield to models' parameters for the Reduced Tomgro model with the Campinas historical weather dataset. Parameters' full names are presented in the Appendix A. Lines correspond to the average index value while dots correspond to the results in each scenario assessed. Only averages larger than 0.05 are shown. For fruits, the X axis starts at 40 days after transplanting as before often there is a lot of instability in the averages.

Instead of using the parameters indicated in Jones, Kenig and Vallejos (1999), these results led to selecting ten parameters for calibration (Table 7). The criteria for selection included being relevant not only to the state variable whose equation included the parameter, but also other state variables. For instance, differently from those authors, we included the calibration of parameters from the equation of number of nodes as it was clearly relevant for all variables and, in the worst case, its value would remain unchanged. On the other hand, ranking the highest indices pertaining to the state variable's equation led to choosing alpha_F, delta and Qe as parameters to generate the ensembles of fruit biomass, leaf area index and aboveground biomass, respectively.

Table 7. List of parameters identified for calibration.

Original parameters*	Parameters	State variable equation
-	N_max	Number of nodes
belta, delta, N_b	belta, delta and N_b	Leaf area index
Vmax	Q_e	Aboveground biomass
alpha_F, T_crit, V, N_FF	alpha_F, T_crit and N_FF	Fruit biomass
DFMax and K_F	DFMax and K_F	Mature fruit biomass

*Parameters calibrated in Jones, Kenig and Vallejos (1999).

In Figure 21, one of the eighty assessed weather time-series was used to exemplify the impact of different parameters on the simulation of the different state variables. It shows the curves of the resulting simulations using the maximum or minimum value of the most important parameters, considering the average index through the cycle. Multiple curves appear as a result of the combinations present after sampling using Saltelli's extension of the Sobol sequence. One can see how important parameters either lead to very different outcomes or, in the case the outcomes are similar, a clear divide existed at some point during growth, disappearing afterward. This disappearance does not entail that a parameter should not be adjusted if it is no longer appearing as important by the end of the cycle. In this case, an error on its estimation could lead to systematic bias that no longer would affect variability in the outcome. Vazquez-Cruz et al. (2014) performed a similar analysis, but as sensitivity indices are mostly quantifying effects that are relative from one parameter to the other, and since in their case they allowed for ranges of parameters representing percentages to be larger than 1, the results are not comparable.

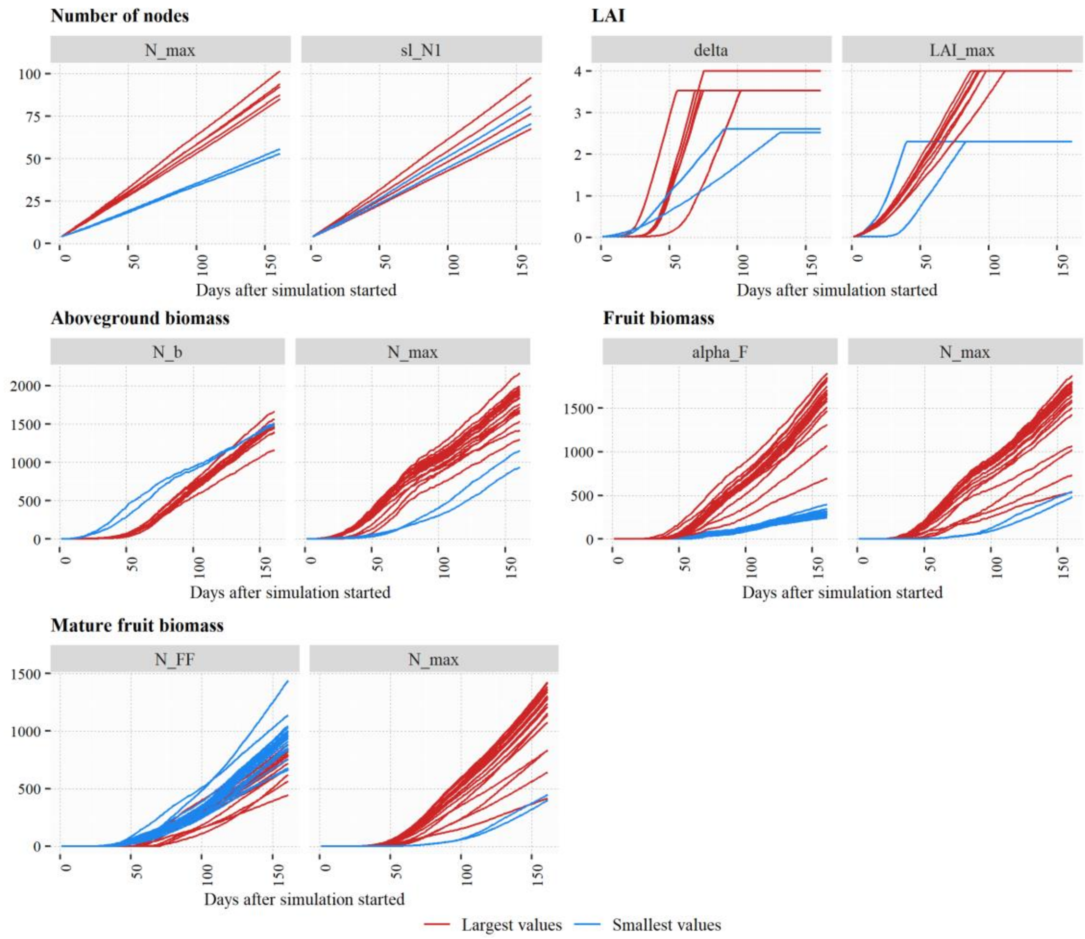

Figure 21. Simulations using maximum and minimum values of selected parameters with highest average total sensitivity index, for one weather scenario in Campinas for each state variable simulated by the Reduced Tomgro model.

5.2.2. Input variables

In this case, sensitivity analysis results are more limited. Since there is an interaction between parameters and the weather, we could not assess the impact of environmental factors without a robust calibration process, that accounted for different weather conditions. These indices also reflect more of the external conditionals and bottlenecks than the parameters' case. Figure 22 shows the results of the sensitivity analysis considering perturbations in the measurements of environmental variables in Cycle 3. Overall, temperatures dominate the results and are the most relevant for all state variables, but for aboveground biomass, as growth progresses, solar radiation becomes more relevant than temperatures and this could be either because temperatures became lower by the end of this cycle, leading to less variability caused by this input, or because solar radiation is also lower and changing its values would impact more simulations' outcomes.

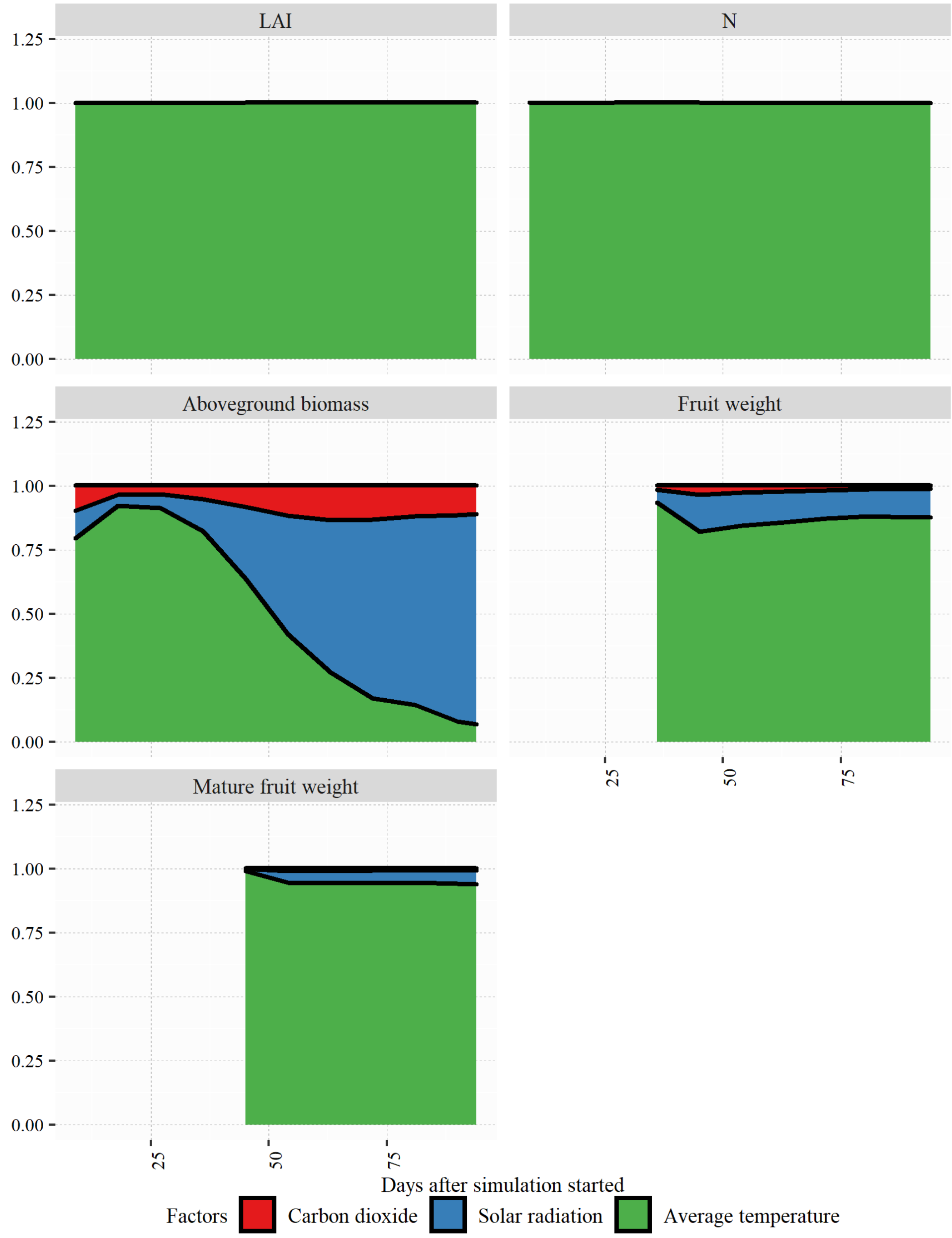

Figure 22. Total effect sensitivity indices of input factors on variables simulated by the Reduced Tomgro model. Values not shown refer to the absence of variability on the variable by that point in growth.

Figure 23 shows an example of the effect of the largest perturbations assessed. As the disturbances were sampled from normal distributions, the results shown refer to perturbations larger than 18% in the observed input. It shows that aboveground biomass would be affected by solar radiation and that fruits would be severely affected by temperature. One can also see the point of the effects of one factor being relative to the other in the different assessments of each state variable. While the change in magnitude of fruit biomass caused by the high importance of temperature would be of 200% percent more, in the case of number of nodes, it would affect the results by 13%, even though they both present similar total sensitivity indices.

The model ascribes little effect to temperature in the calculation of biomass rate, mainly relating to the indirect effect of temperature on leaf area and effect on photosynthesis, while it directly affects fruits by the same effects as well as the indirect effects on nodes and direct effects on fruit abortion. Although overall temperatures were the most relevant variables, this analysis showed how errors in solar radiation measurements could clearly impact biomass, leading to the indices in Figure 22. Given it is easier to increase the number of measurements of temperatures than of solar radiation, therefore reducing its uncertainty, solar radiation was chosen when perturbing an input was required for assimilation.

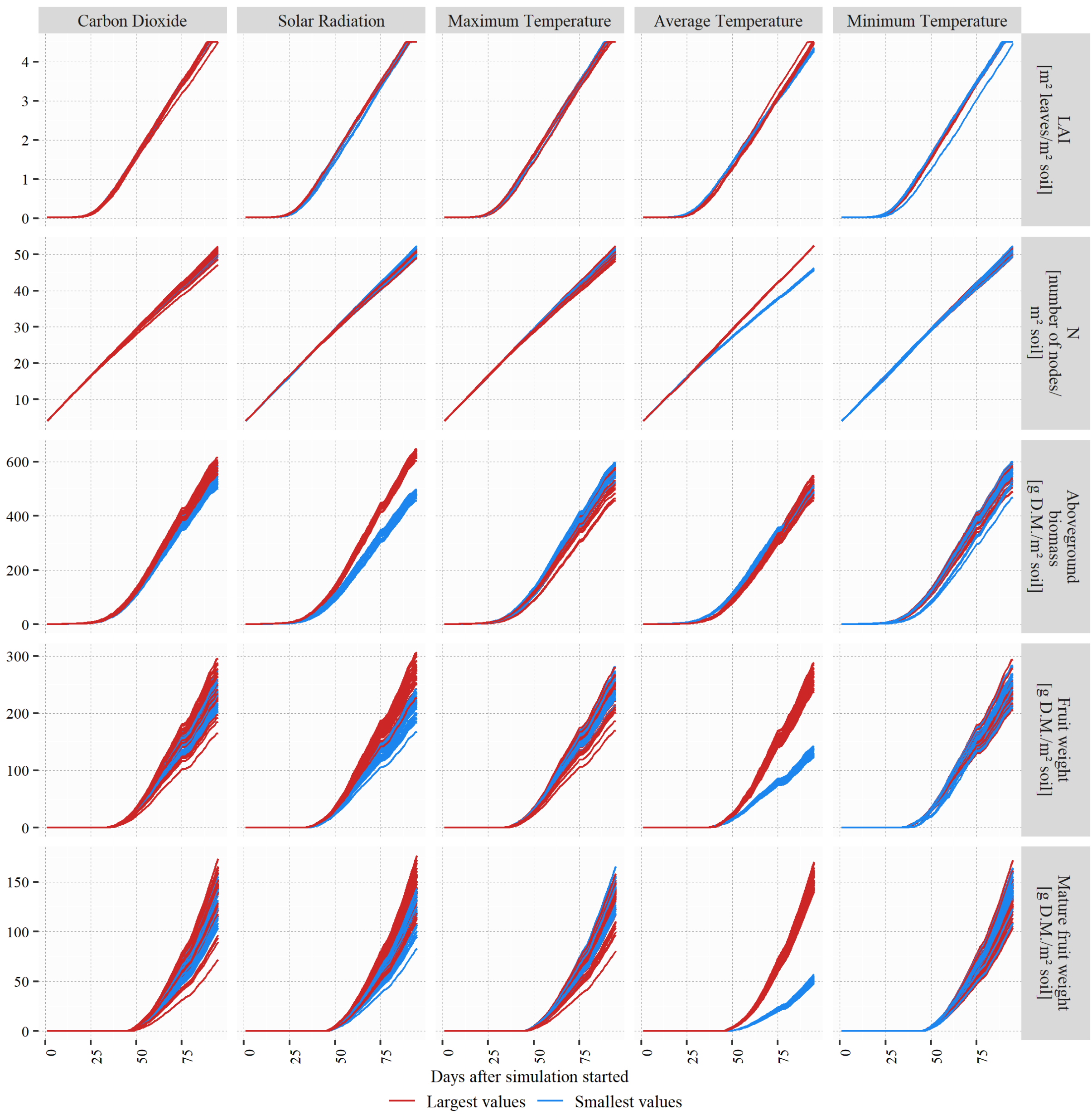

Figure 23. Simulations using maximum and minimum values of all input factors with highest total sensitivity index, for data of one node of Cycle 3, for each state variable simulated by the Reduced Tomgro model.

5.3. Model implementation and calibration

As mentioned in section 4.3.1, the Python implementation was able to reach the original results, when using the same strategy of calibration. As the strategy used in this study was different in multiple different ways — parameters from all variables were optimized simultaneously with a different error metric and algorithm, as well as different parameters were chosen for calibration — the simulation outcomes were also different, although not substantially (Figure 24). The shapes of the LAI curves became slightly steeper and aboveground biomass and fruit biomass were no longer overestimated, with a slight underestimation of mature fruits.

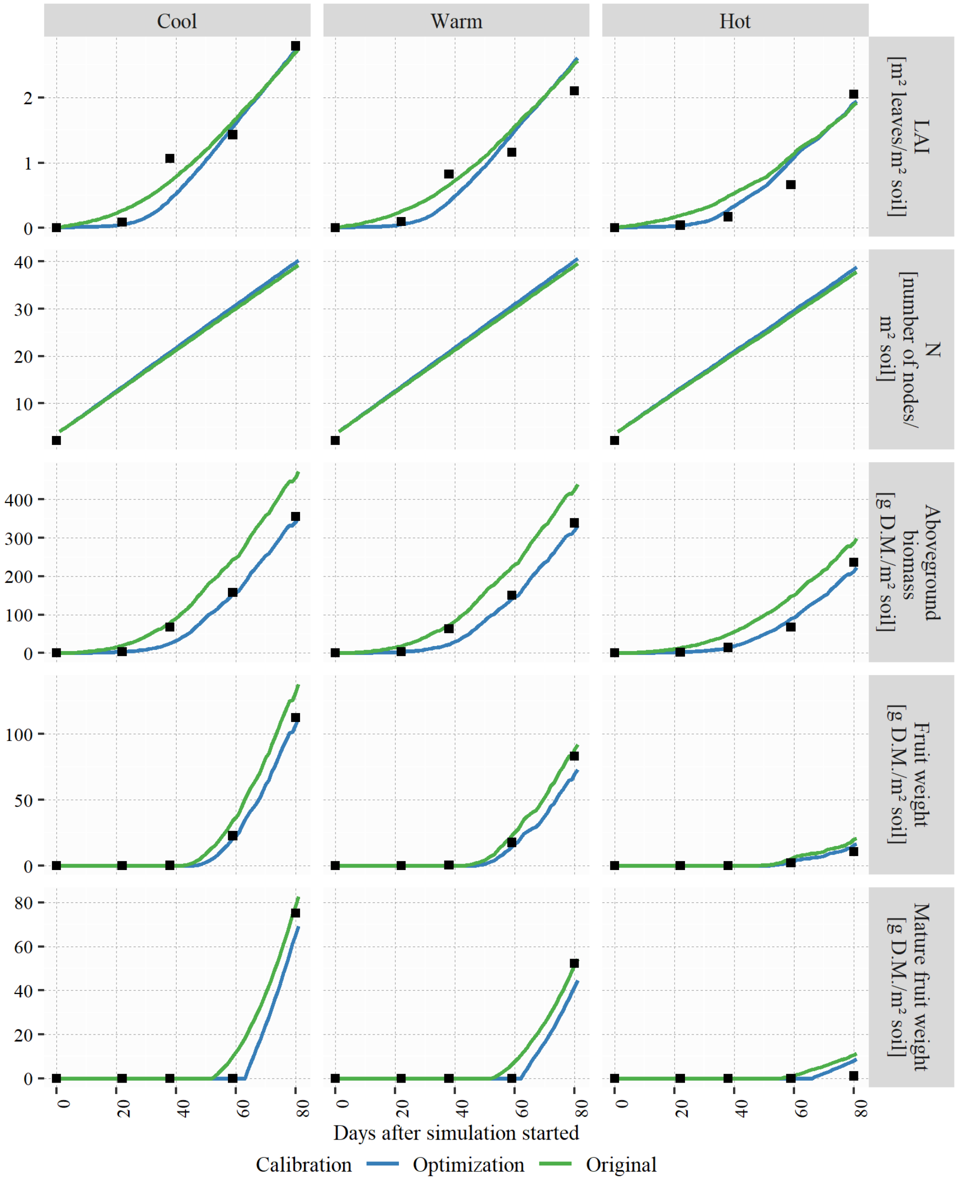

Figure 24. Results for the simulation using the Reduced Tomgro model with Gainesville input data with different approaches for calibration of parameters. Squares represent data used in calibration.

For Campinas, the different approaches, in this case manual adjustment and global optimization, led to differences especially in mature fruit weight (Figure 25), which was caused by the optimization exploring the low samples of day 66, as the metric used gave a lot more weight to it than to the final observations. The curve representing number of nodes suggests either the parameter used or the process could be reassessed to best describe plant development. On the other hand, although the maximum value allowed for the parameter was of 0.7, the optimization algorithm changed the parameter from 0.5 to 0.57 nodes day^{-1}, likely given the influence of the other variables, observed previously in Figure 20.

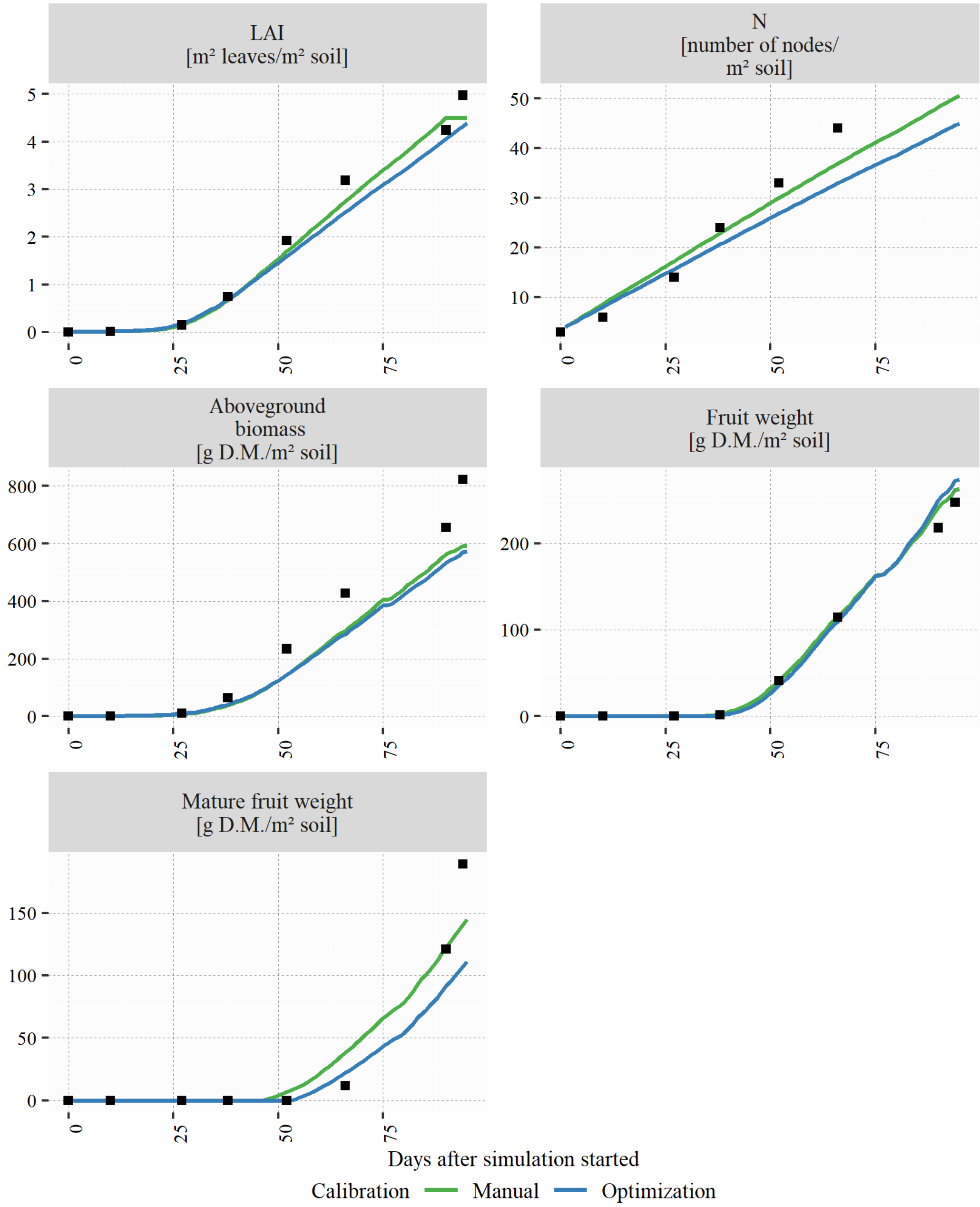

Figure 25.Results for the simulation using the Reduced Tomgro model with input data from the third growth cycle in Campinas and different approaches for calibration of parameters. Squares represent data used in calibration.

Both approaches underestimated aboveground biomass, even as Qe, the leaf quantum efficiency, was increased from 0.08 to 0.09 μmol CO_2 fixed μmol photon $^{-1}$. In their work, Vazquez-Cruz et al. (2014) ascribed a value of 2.07 to the parameter representing the ratio of biomass to photosynthate available for growth, which could suggest they also observed problems in achieving compatible results between the leaf area available and the aboveground biomass and their optimization led to amplifying biomass to reduce the errors. But it could also be an issue with the solar radiation data obtained in this study, although there is no identified reason as to why Cycle 3 would have had this type of problem.

Another issue that should be noted regarding using this model for the growth cycles observed is that as the model developed for optimal growth, it could have been the case that it would not accurately represent Cycles 1 and 2. However, Figure 26 indicates the model showed flexibility and was able to be adjusted well for most variables in all cycles. Low biomass in Cycle 1 was accompanied by changes in the magnitudes of the other state variables, even though it led to a larger underestimation of biomass than the non-calibrated model. One more remarkable exception is the case of fruits for Cycle 2, as the inhibition was caused by a change in partitioning and the model could not, naturally, capture this effect. In all cycles, the observations referring to the number of nodes used for calibration did not include data collected after the removal of apical meristem. It can be also noted in Figure 26 that the model was able to capture, as in Bojacá, Gil and Cooman (2009), the effects of differences in the environment mentioned in section 5.1.1, leading to slightly different curves for each node.

Given the reasonable results, even when compared with other approaches, for consistency and reproducibility, the optimization method was adopted through the remaining steps. Modeling is also further discussed in Appendix C.

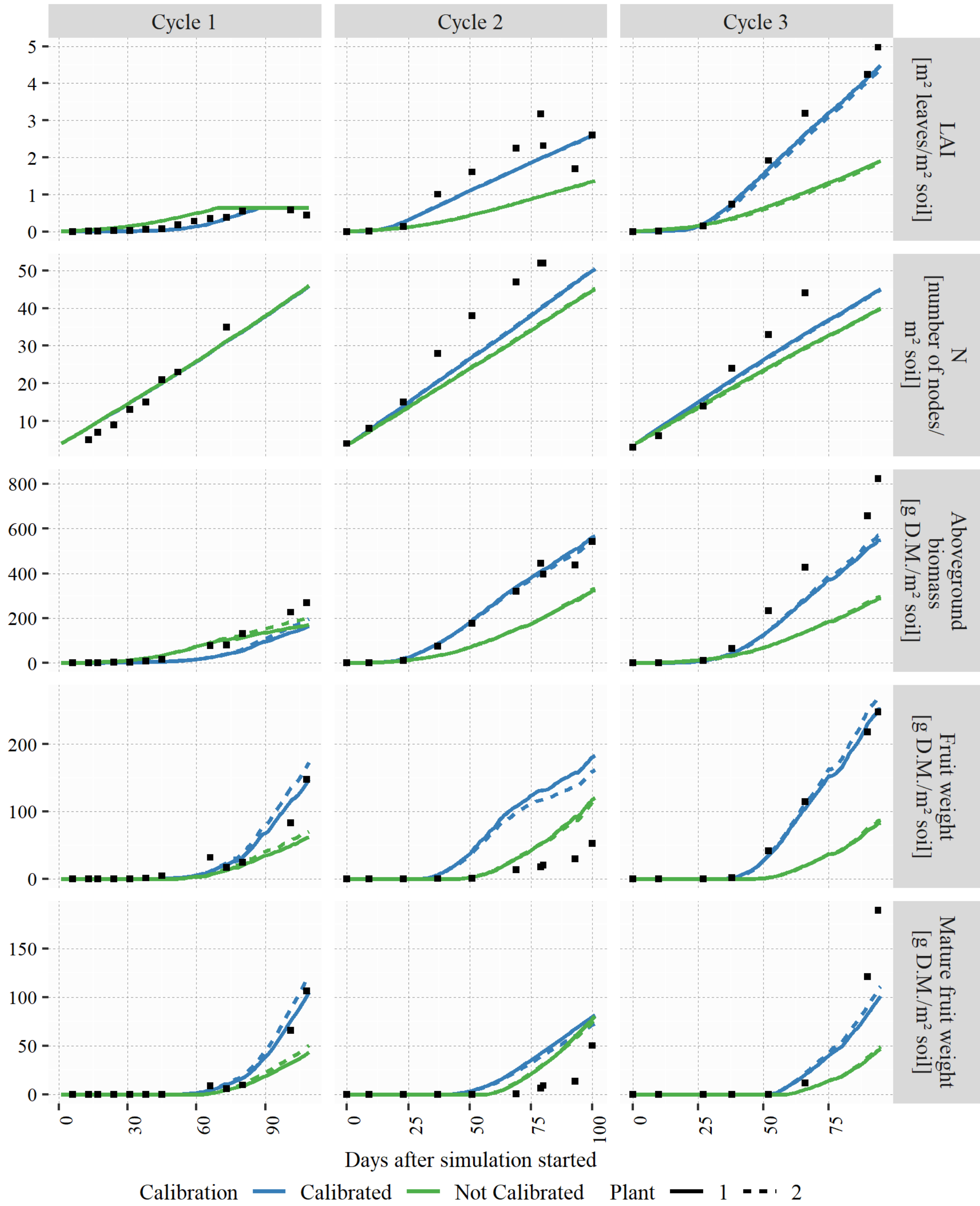

Figure 26. Simulation with optimized calibration for Campinas in all complete cycles. Squares represent data used in calibration.

5.4. Modeling the relationship of observed variables to variables of interest

In the case of assimilation for large areas using remote sensing images as the source of observations, several products are already available. For example, Fang et al. (2019) presents an overview of global LAI products and Jiang et al. (2020) evaluate two soil moisture products. This step, however, was still needed in this study, as there is no established relationship between the non-destructive observations used and the state variables to be updated (Figure 27).

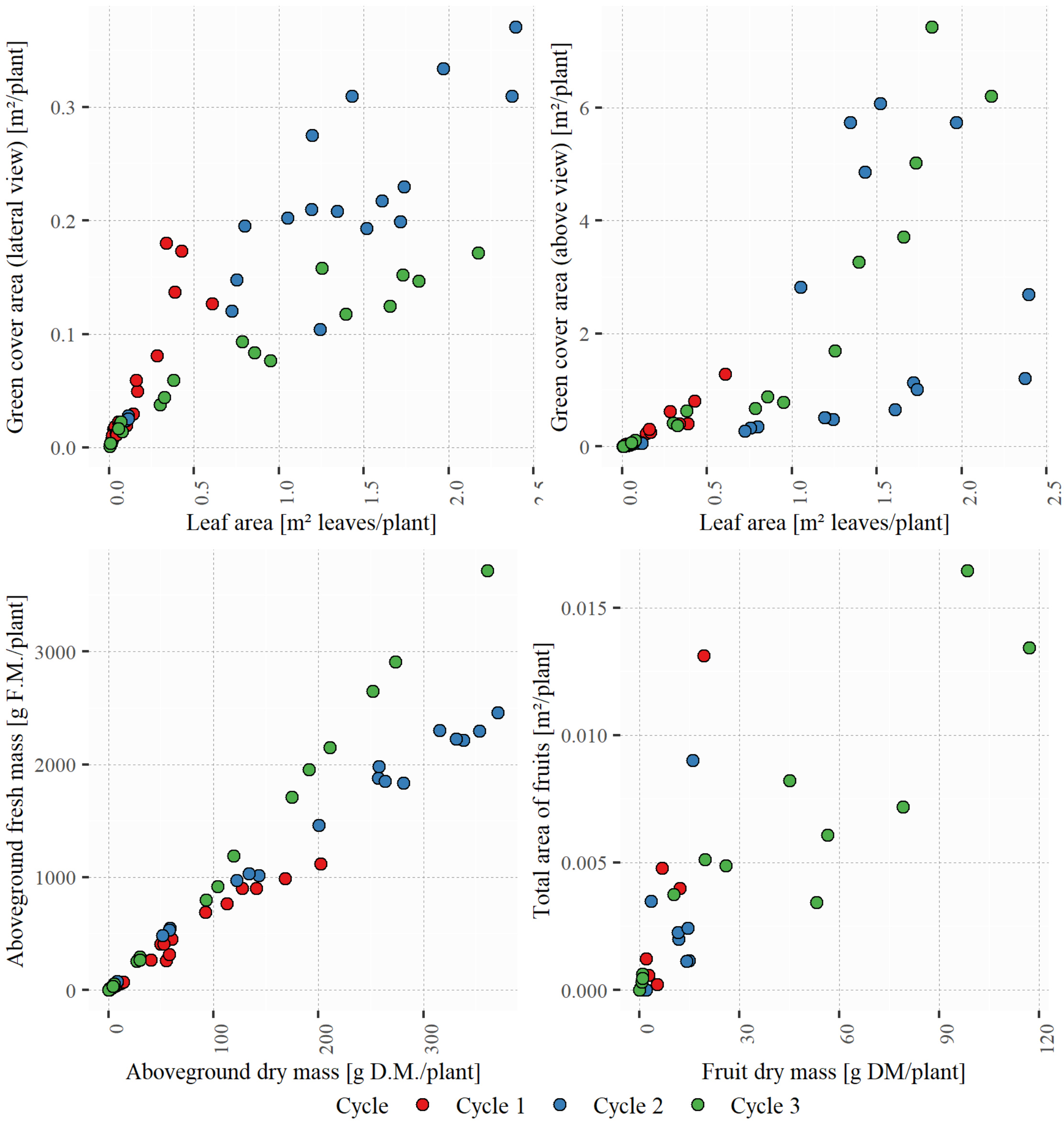

Figure 27. Scatterplots of relationships between observations of plants used in the destructive analyses, used for the development of observation models. Observations that refer to an area were extracted from images and aboveground fresh mass was obtained by weighting plants before drying.

While the original goal of this study aimed at proposing a relationship that could lead to the dismissal of future calibration, reaching it was not possible, as the different conditions in each cycle led to different growth patterns. Nevertheless, one can see (Table 8) that even as these differences existed, the models obtained had similar slopes, with the largest range being for the equation obtained for fruits in Cycle 3. As the conversion of fruit biomass is the only case in which the slope and intercept present similar magnitude, the differences in the intercept also affect this outcome. These differences affected assimilation as will be discussed, but the other results suggest it should be possible to generate a model that can be generalized if conditions are similar. It also suggests that even linear methods could be explored. Nyakwende; Paull and Atherton (1997) explored polynomial relationships to quantify leaf area of tomato plants younger than 40 days through images, but linear relationships are frequently explored to relate vegetation indexes and LAI or canopy cover (Betbeder et al., 2016; Dorigo et al., 2007; Tenreiro et al., 2021).

Table 8. Equations derived from calibration data for observation models, i.e., conversion of state variable into the equivalent observation.

Growth Cycle	Equation	State variable	Observed variable
Cycle 1	$wf\_lat = 1.19 \times 10^{-4} \times W_f + 1.97 \times 10^{-3}$	W_f	Area Wf
Cycle 2	$wf\_lat = 1.31 \times 10^{-4} \times W_f + 1.77 \times 10^{-3}$		
Cycle 3	$wf\_lat = 3.34 \times 10^{-4} \times W_f + 1.36 \times 10^{-4}$		
Cycle 1	$w\_fm = 8.32 \times W + 4.74 \times 10^{-1}$	W	W_fm
Cycle 2	$w\_fm = 7.81 \times W - 5.26 \times 10^{-1}$		
Cycle 3	$w\_fm = 6.90 \times W + 6.79 \times 10^{-1}$		
Cycle 1	$lai\_lat = 1.42 \times 10^{-1} \times LAI + 3.44 \times 10^{-3}$	LAI	GC Lat
Cycle 2	$lai\_lat = 2.54 \times 10^{-1} \times LAI + 2.97 \times 10^{-3}$		
Cycle 3	$lai\_lat = 2.26 \times 10^{-1} \times LAI + 4.75 \times 10^{-3}$		
Cycle 1	$lai\_abv = 9.87 \times 10^{-1} \times LAI + 5.74 \times 10^{-4}$		GC Abv
Cycle 2	$lai\_abv = 1.30 \times LAI - 1.28 \times 10^{-3}$		
Cycle 3	$lai\_abv = 1.16 \times LAI - 4.81 \times 10^{-4}$		

W_f: dry mass of fruits [g m^{-2}], W: aboveground dry biomass [g m^{-2}], LAI: leaf area index [m^{-2} m^{-2}], Area Wf: area of fruits on images [m^{-2} m^{-2}], W_fm: aboveground fresh mass [m^{-2} m^{-2}], GC Lat: area of leaves identified on images from lateral view [m^{-2} m^{-2}], GC Abv: area of leaves identified on images from the above view [m^{-2} m^{-2}].

Table 9 shows the metrics from the observation models after excluding data from the cycle. While correlations are compatible with what is visible from the scatterplots, error metrics point to large uncertainties. Since these models are used to convert the state variable into the same unit of the observation, they should be evaluated in the observations' unit. And while an error of 0.40 g FM m^{-2} may be considered very small when compared to the mass of the weighting system, the opposite is true for an error of 0.61 m^2 m^{-2} for the area visible on images. This larger error was likely caused by the different behaviors from the three growth cycles. Mean Absolute Percentage Errors confirm that the error in the unseen cycle is very large and suggest that using these models to convert state variables in the assimilation may lead to lower efficiency of the process. The issues previously discussed regarding the determination of all these measurements likely affected this step, and improvements in them should also reduce the errors in the models. However, while large, it is not uncommon for remote sensing LAI products used in assimilation to reach errors larger than 0.5 m^2 m^{-2}. Fang et al. (2019) report validation

RMSE errors from moderate and high-resolution leaf area index products for crops ranging from 0.2 to 0.8 m^2 m^{-2}.

In the case of mature fruit biomass, which was not explored here as there were not enough observations to develop the models, obtaining good relationships should be a lot easier, as occlusion by leaves is minimized by pruning practices.

Table 9. Standard error (SE), mean absolute percentage error (MAPE) and coefficient of determination (R^2) from each observation model for data from each cycle. SE is reported from training in the other cycles and MAPE is reported from validation in the same cycle.

Assimilated variable		LAI	LAI	W	Wf
Observed Variable		GC Abv [m^2 m^{-2}]	GC Lat [m^2 m^{-2}]	W_fm [g FM m^{-2}]	Area Wf [m^2 m^{-2}]
Cycle 1	SE (training)	0.988	0.311	0.395	0.062
Cycle 2		0.597	0.613	0.339	0.084
Cycle 3		0.921	0.436	0.257	0.252
Cycle 1	R^2 (training)	0.64	0.73	0.94	0.81
Cycle 2		0.86	0.82	0.98	0.77
Cycle 3		0.44	0.87	0.99	0.36
Cycle 1	MAPE (validation)	30 %	41 %	34 %	373 %
Cycle 2		122 %	55 %	29 %	82 %
Cycle 3		26 %	113 %	58 %	122 %

*Observations as: GC Lat: green cover (lateral view), GC Abv: green cover (above view), W_fm fresh mass from destructive analyses, Area Wf: total area of fruits.

5.5. Data assimilation

Pellenq and Boulet (2004) posed four questions that guide this discussion: if the assimilation of a particular observation improves all components of the simulation; if calibration errors can be compensated by tuning state variables instead of parameters; what the optimum frequency of measurements is and what the most suitable assimilation strategy (noise specification, assimilation method, etc.) to fulfill a particular goal is. The first three will be commented on section 5.5.1 and are expanded in Appendix D and Appendix E. The last one is commented on section 5.5.2. Section 5.5.3 will explore the idea of using low-cost environmental sensors as a source of input data given observations with reasonably low errors are available.

5.5.1. Overall assimilation results

For very precise measurements, the techniques will basically replace estimates by measurements. Their advantage comes when models and measurements alike are noisy. Table 10 highlights the cases in which RMSE of the growth cycle for a state variable was lower with assimilation of that variable than without, regardless of calibration. Overall, calibration led to the lowest errors, but in almost all cases, assimilation slightly improved the results when the model was not calibrated. No technique was consistently better either across variables or across growth cycles.

Table 10. Average root mean squared error [g m^{-2}] for estimates of state variables updated with data from different sources with the Unscented Kalman Filter and the Ensemble Kalman Filter, and from the model without assimilation with and without calibration.

State variable	Filter	Assim. state	Obs. variable*	Cycle 1	Cycle 2	Cycle 3
LAI	None – Calib.	-	-	0.08	0.53	0.31
	None – Not Calib.	-	-	0.17	1.17	1.76
	EnKF	LAI	GC Lat	**0.08**	**0.70**	1.83
	UKF			**0.10**	**0.69**	1.83
	EnKF		GC Abv	**0.07**	**1.07**	**0.80**
	UKF			**0.09**	**1.07**	**1.71**
W	None – Calib.		-	42.4	29.8	124.8
	None – Not Calib.	-	-	30.8	148.8	275.4
	EnKF	W	W_fm_full	64.8	**59.1**	**142.9**
	UKF	W		66.6	**65.2**	**123.8**
Wf	None – Calib.	-	-	15.9	82.7	12.4
	None – Not Calib.	-	-	25.8	34.8	90.1
	EnKF	Wf	Area Wf	**24.1**	**33.2**	**88.7**
	UKF	Wf		**23.6**	**16.3**	**86.2**

*Observations as: GC Lat: green cover (lateral view), GC Abv: green cover (above view), W_fm_full: weighting system, Area Wf: total area of fruits. Bold numbers refer to root mean squared errors lower than the larger RMSE between the non-calibrated and calibrated error.

Although calibration is expected to improve model performance, this was not observed in some cases, as growth did not correspond to the situation for which the model was developed. In Cycle 1, in which total biomass and leaf area were affected by irrigation, the optimization used in calibration could not determine parameters that would generate compatible estimates between these two variables. In Cycle 2, similarly, excessive nitrogen led to much lower fruit production, and this effect was not properly captured by the parameters selected. Assimilation results in both cases depended on the quality of observations. In Cycle 1, in which the system biomass was affected by irrigation, the large errors also led to poor estimates and, therefore, the best results came from the non-calibrated simulation. In Cycle 2, on the other hand, assimilation of the images led to the adjustment of the estimates to the lower values that actually happened.

The errors in the weighting system of Cycle 1 were a particularity of that growth cycle, but since it should be the most precise measurement, it led to the largest improvements, and the results in Cycle 2 were very similar to the calibrated estimates, while on Cycle 3, errors were reduced in almost 50%. The improvement not being higher in Cycle 3 is likely caused by the same reason that led to the underestimation of biomass after calibration, as the model cannot simulate higher rates of biomass with the inputs that were used or with its current structure.

As for the uncertainties in observations from images that were discussed in the previous sections, they would affect all image-based assimilation. However, as these are permeated through the observation models, one should look to the models with lower validation errors (Table 9) to better understand this potential. In this case, the best example comes from using the pictures from above and the EnKF to estimate the leaf area index in Cycle 3. The large error by the end of the cycle is possibly caused by the absence of images, which led the model to simulate based on the last available update. It could also be noted that for Cycles 1 and 2, assimilation of images led to estimates as good as the ones obtained by calibration.

As some comments require more clarity of what happened in the simulations, Figure 28 to Figure 31 show the curves of assimilation of the different observations. Two remarks refer to the assimilation of fruit area. In Figure 28, observations of fruit area in Cycle 3 were apparently barely used, and the assimilated curve closely resembles the simulation without calibration. This is likely caused by the slope in the observation model presented in section 5.3. Figure 19 showed that monitored plants in Cycle 3 had the largest areas of fruits by the end of the growth cycle. Still, the scatterplot from Figure 27 shows how a model obtained with data from the other two cycles would likely underestimate the fruit mass observation. So, when the estimated fruit biomass value was converted to the equivalent observation, the difference in magnitude of what was estimated by the model and the observation would not be captured in the residual calculation.

In Cycle 2, the calibrated model performed poorly, but UKF assimilation of fruit area in images partially improved the yield results (Figure 28). This was also observed for fruit biomass itself, but it is not necessarily the case that improvement of one state variable will cascade into improving the other. It should be noted that conversion by observation models also led to negative estimates, which is another point to the necessity of improving such models.

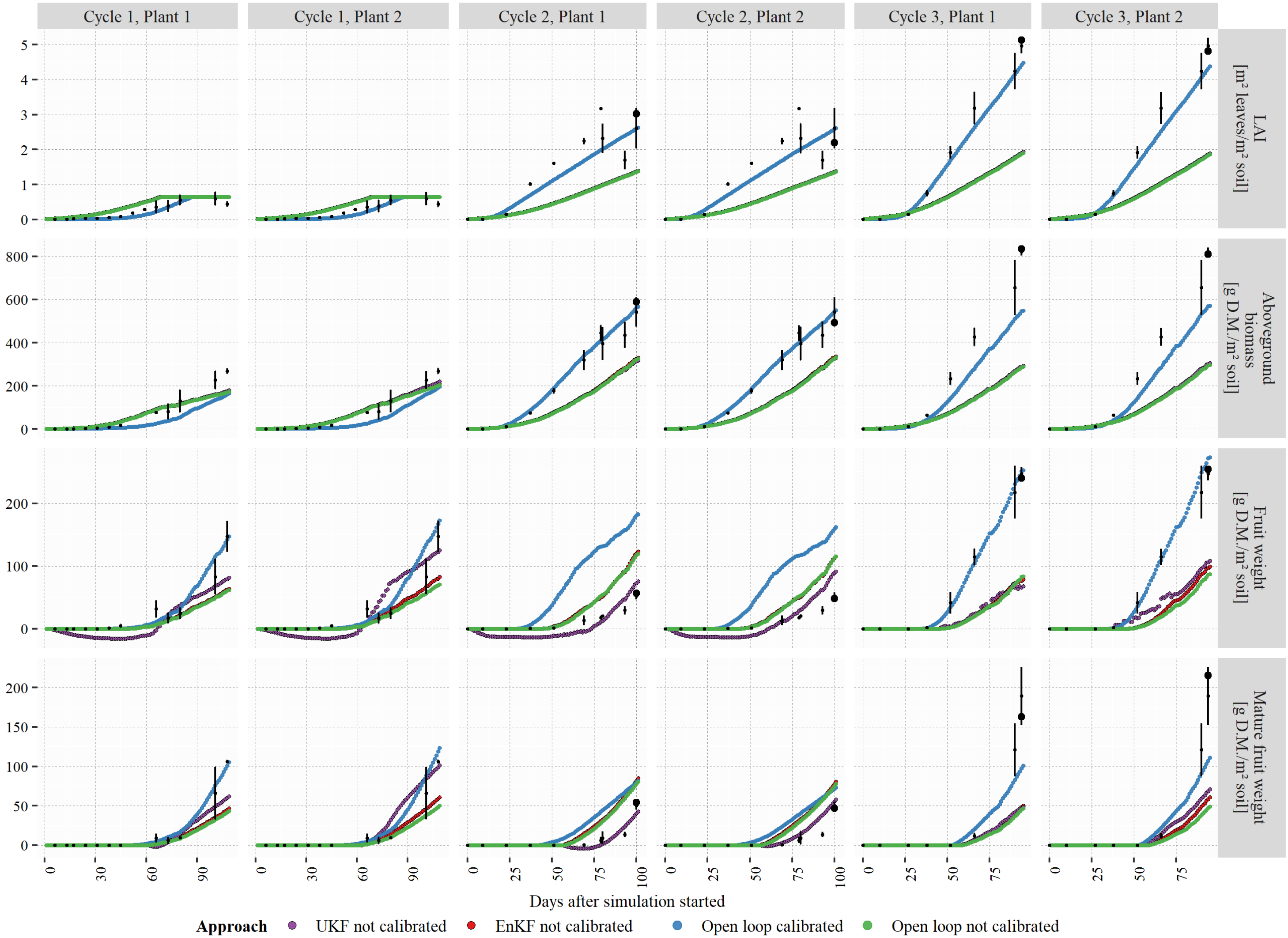

Figure 28. Growth curves for each monitored plant as estimated by the different techniques used for assimilation of indirect observations of fruit biomass, by the Reduced Tomgro with calibration and by the Reduced Tomgro without calibration. Dots refer to the values determined by destructive measurements, and the bar represents the associated standard deviation. The final value for the monitored plant is represented by a larger dot.

When analyzing the results focusing on yield, overall, assimilation of either leaf area (Figure 29 and Figure 30) or aboveground biomass (Figure 31) did not improve the estimates as much as assimilation of fruit area. Metrics for this analysis are presented in Appendix B. This is likely connected to leaf area index being more relevant in the beginning of growth, as also seen in section 5.2.1, so that after light interception saturation, other factors are more relevant (Heuvelink et al., 2005). One issue regarding assimilation of images of leaves using the UKF is the visible decrease in the estimates by the end of the growth. This was caused by the sampling of the unscented transform leading to some sigma points reaching the maximum leaf area defined as an input and the others not doing so, in a way that the average between them led to values that were lower than the previous. Changes in the filters' parameters that would reduce the spread of the sigma points could have solved this issue.

Finally, it is particularly interesting to observe an effect that happened in the assimilation of aboveground biomass using the weighting system. Even though it thoroughly improved aboveground biomass, it had an adverse effect on fruit dry biomass. Because the Reduced Tomgro model calculates fruit biomass based on photosynthesis and respiration, instead of as a fraction of aboveground biomass, the increase in biomass may lead to an increase in respiration that is not compensated by an increase in photosynthesis through LAI, thus decreasing assimilates available for fruits.

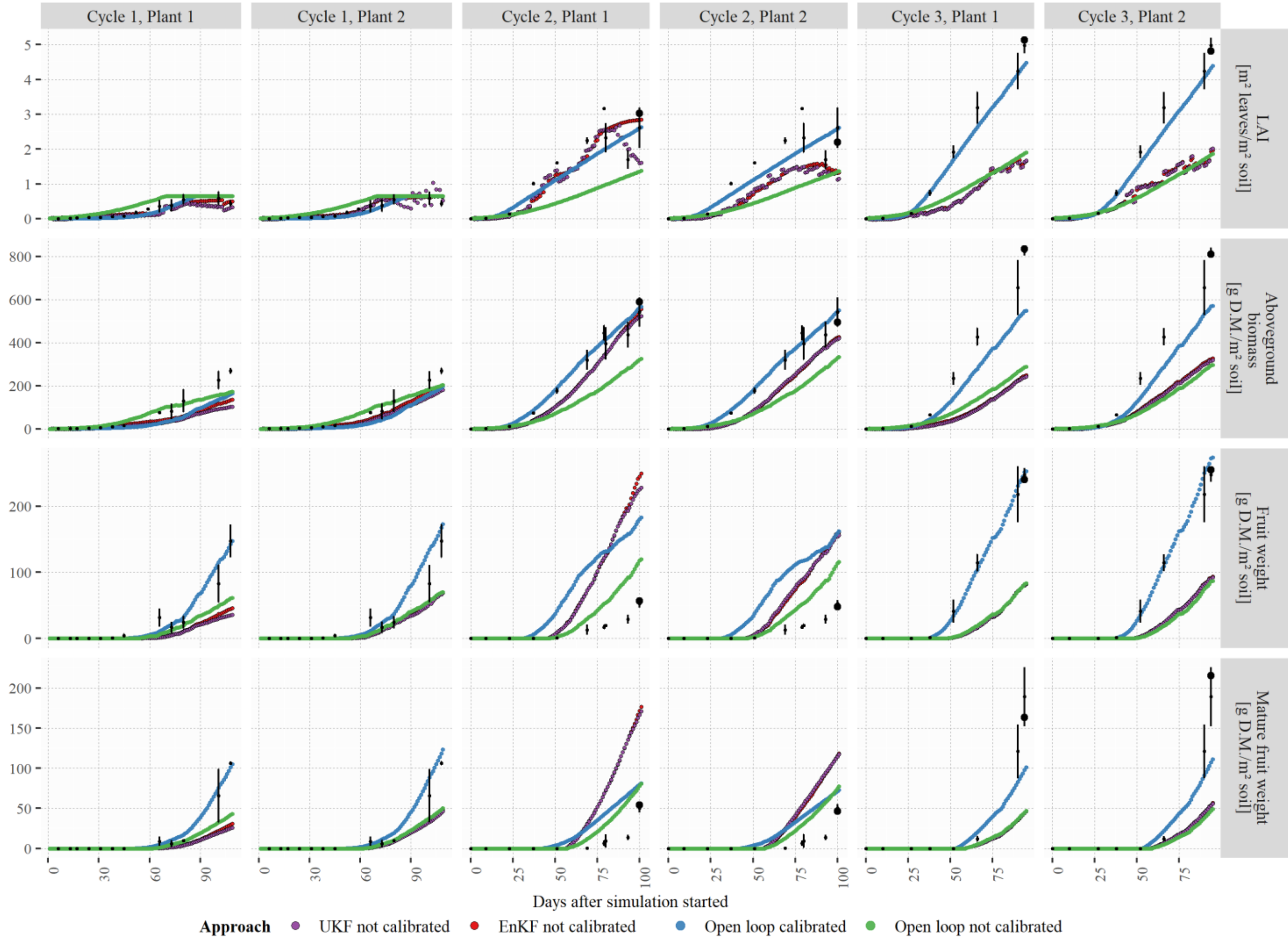

Figure 29. Growth curves for each monitored plant as estimated by the different techniques used for assimilation of indirect observations of leaf area index, by the Reduced Tomgro with calibration and by the Reduced Tomgro without calibration. Observations in this case corresponded to pictures taken from lateral view. Dots refer to the values determined by destructive measurements, and the bar represents the associated standard deviation. The final value for the monitored plant is represented by a larger dot.

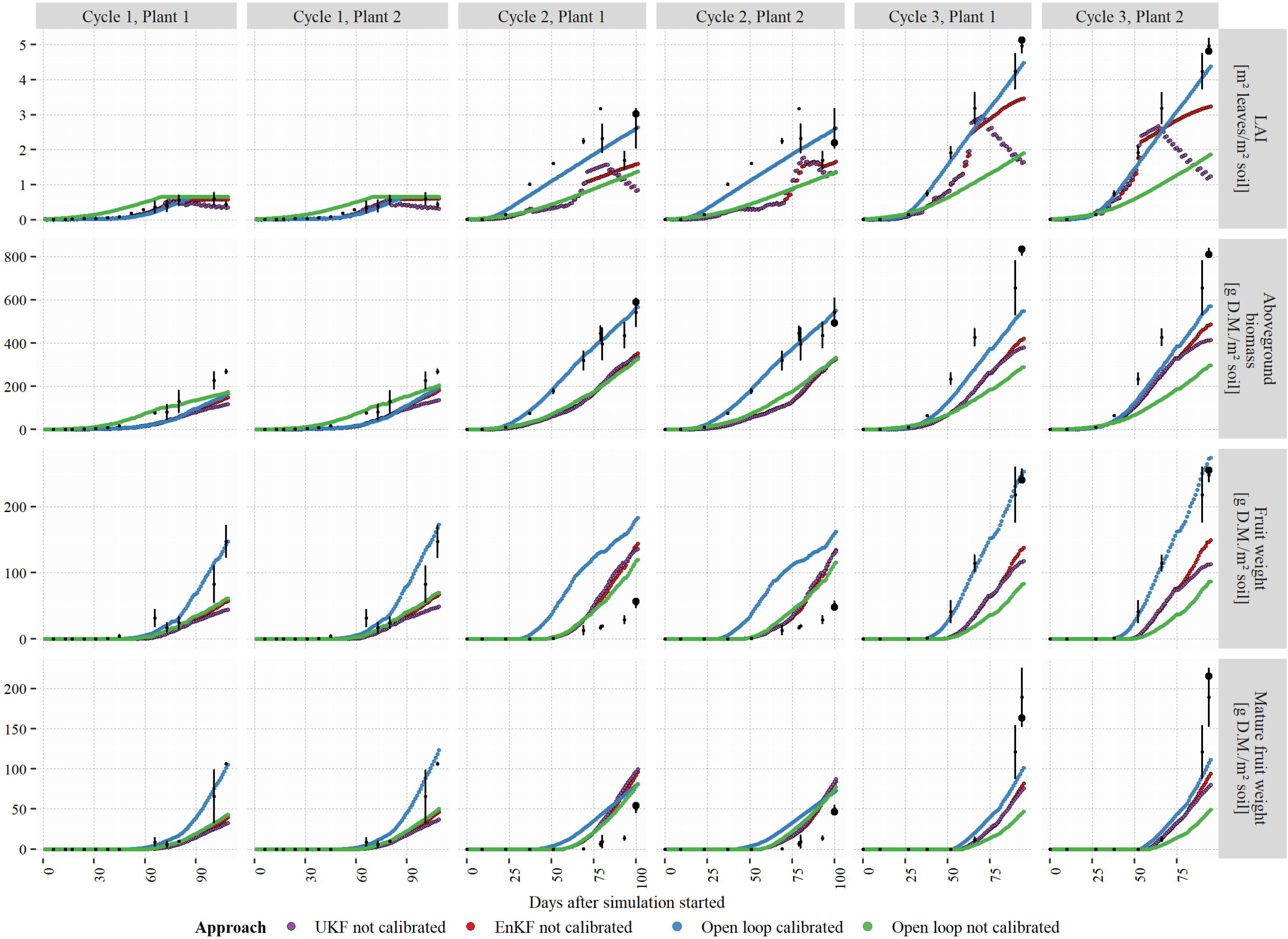

Figure 30. Growth curves for each monitored plant as estimated by the different techniques used for assimilation of indirect observations of leaf area index, by the Reduced Tomgro with calibration and by the Reduced Tomgro without calibration. Observations in this case corresponded to pictures taken from above view. Dots refer to the values determined by destructive measurements, and the bar represents the associated standard deviation. The final value for the monitored plant is represented by a larger dot.

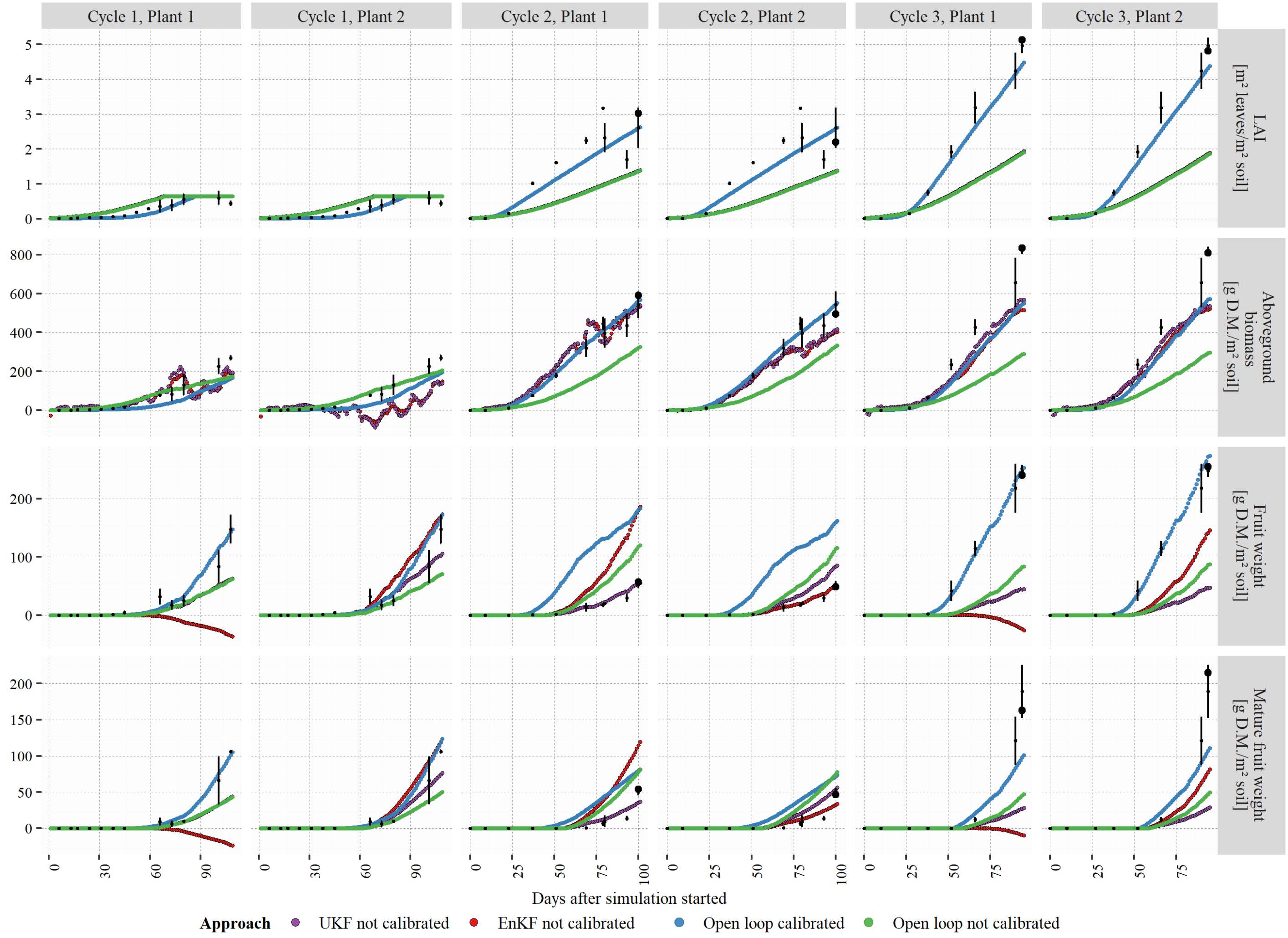

Figure 31. Growth curves for each monitored plant as estimated by the different techniques used for assimilation of indirect observations of aboveground biomass, by the Reduced Tomgro with calibration and by the Reduced Tomgro without calibration. Observations in this case corresponded to pictures taken from lateral view. Dots refer to the values determined by destructive measurements, and the bar represents the associated standard deviation. The final value for the monitored plant is represented by a larger dot.

5.5.2. Temporal resolution

It could be the case that for inaccurate measurements, fewer observations could lead to similar outcomes of using all available data. Figure 32 shows the results for assimilation using the UKF and its impact on yield, including all the observed RMSE in the repeated simulations. By reducing the frequency, ranges increase, because the usefulness of observations is not equal across time, and since later observations are often connected to poorer data quality, as the environment becomes more complex. Therefore, while fewer observations may lead to lower errors in most simulations, and the minimum observed RMSE in the multiple sampling is often similar to the one obtained using all observations, inferior results, i.e., larger errors, may also occur. This means that if the cost of acquiring and storing them is not high, using more observations — in the context of very uncertain observations and model estimates — is likely the best strategy.

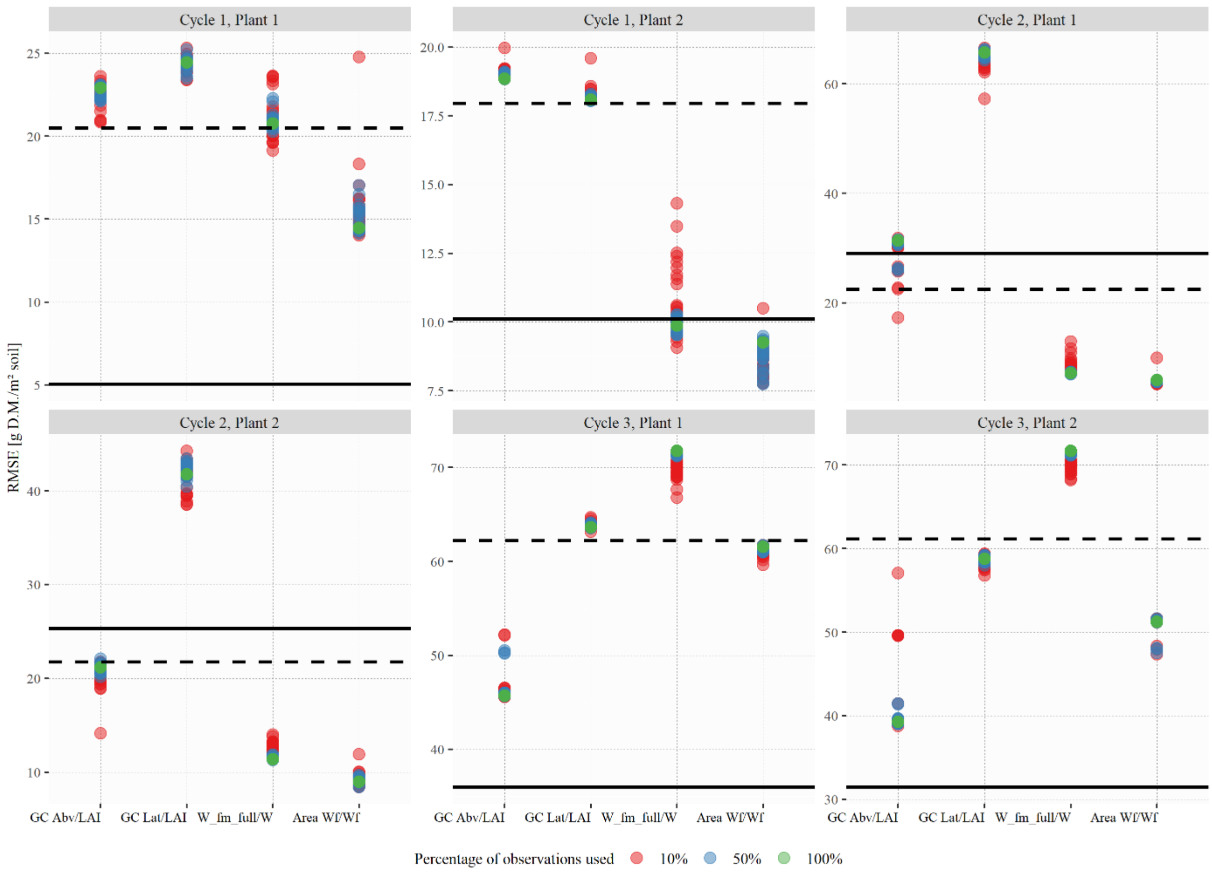

Figure 32. Root mean squared error [g m^{-2}] for yield estimates assimilating data from different sources with the Unscented Kalman Filter for all the twenty samplings of the dataset. Horizontal solid line corresponds to the error of the simulation without calibration and horizontal dashed line, to the simulation with calibration. Observations as: GC Lat/LAI: green cover (lateral view) for leaf area index, GC Abv/LAI: green cover (above view) for leaf area index, W_fm_full/W: weighting system for aboveground biomass, Area Wf/Wf: total area of fruits for fruit dry biomass.

5.5.3. Low-cost sensors

The use of low-cost sensors increases the uncertainty in model inputs and therefore in model variance. From results in section 5.2.2, one can see average temperatures affect all state variables the most, while solar radiation mainly affects aboveground biomass. However, it could also be seen in Figure 13 that the only relationship that could be compromised by changing the sensor would be that of photosynthetically active radiation. And given the systematic error in the estimation of aboveground biomass, this uncertainty was explored to generate the ensembles and data from the low-cost sensors was used as input. As assimilation was performed in the non-calibrated model, uncertainty was already deemed very large and there should be no large influence from micrometeorological data. It could be the case, however, that by using uncertainty in the inputs as the driver for the ensembles, the difference of performance across sensors could be mitigated.

Table 11 presents the errors from this strategy, both with assimilation of simulated observations of fruits and of mature fruits. Simulations using any of the two sensors either already presented large differences (Cycles 1 and 2) or almost no difference (Cycles 0 and 3), so to satisfy the premise of the analysis, these differences should be lower after assimilation. This was not clearly observed and, in particular, results were not consistent across variables or growth cycles. As for the effectiveness of assimilation, overall, only minor improvements were observed with one positive exception for the assimilation of mature fruits in Cycle 2 and one negative exception for the assimilation of fruits in Cycle 0.

Table 11. Average root mean squared error (RMSE) of yield estimates for all the executions of assimilation of fruit and mature fruit biomass using the Ensemble Kalman Filter and luxmeters (L) or quantum sensors (Q) for the input of solar radiation.

	No assim.		10%		30%		50%	
Growth Cycle/Sensor	L	Q	L	Q	L	Q	L	Q
Variable				Wf				
Cycle 0	14.16	13.84	12.71	12.38	13.05	12.73	20.29	20.16
Cycle 1	9.81	15.62	7.66	13.82	8.33	14.51	8.39	14.57
Cycle 2	42.35	49.64	39.33	47.62	39.49	47.87	39.51	47.90
Cycle 3	18.39	20.09	16.63	18.37	16.64	18.39	16.64	18.39
Variable				Wm				
Cycle 0	14.16	13.84	9.92	9.67	9.92	9.67	9.92	9.67
Cycle 1	9.81	15.62	4.50	8.77	4.50	8.77	4.50	8.77
Cycle 2	42.35	49.64	27.20	37.53	27.20	37.53	27.20	37.53
Cycle 3	18.39	20.09	11.53	14.42	11.53	14.42	11.53	14.42

The absence of impact of assimilation could have been caused by the approach used for generating the ensemble. Seemingly, ascribing the uncertainty to radiation input data was not enough to shift the outcomes, regardless of noise level in the observations. The low variance in the ensemble led assimilation towards the simulated value. Figure 33 and Figure 34 show the differences in the observation covariance, the state covariance in the ensemble and the gain through growth after assimilation of fruits and of mature fruits observations, respectively. It is possible to note that in comparison to the covariance, the observation covariance is much larger in all cycles, leading the gain to have a low value.

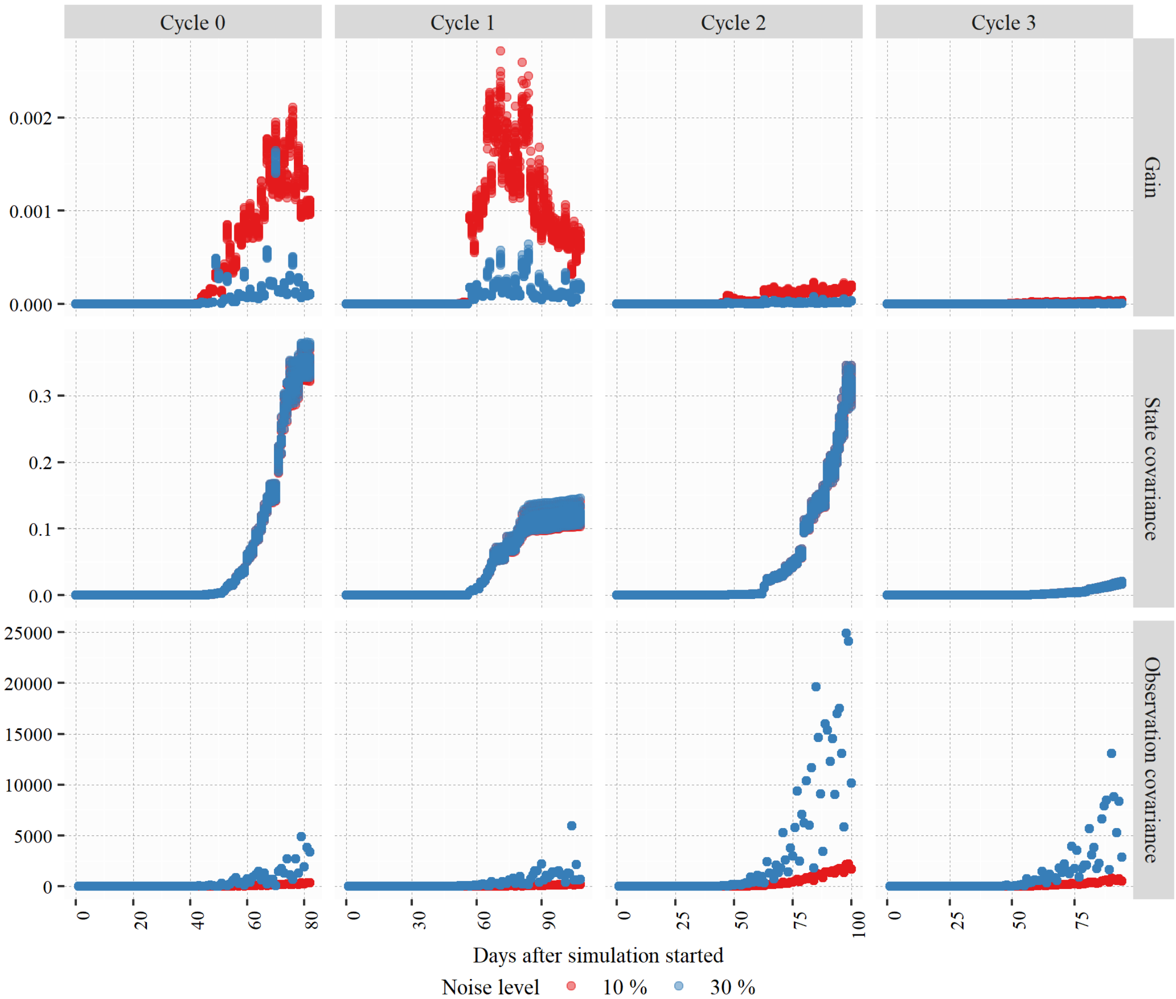

Figure 33. Evolution of filter hyperparameters on the assimilation of fruit biomass with different noise levels for the observations using the low-cost sensor as source of solar radiation input.

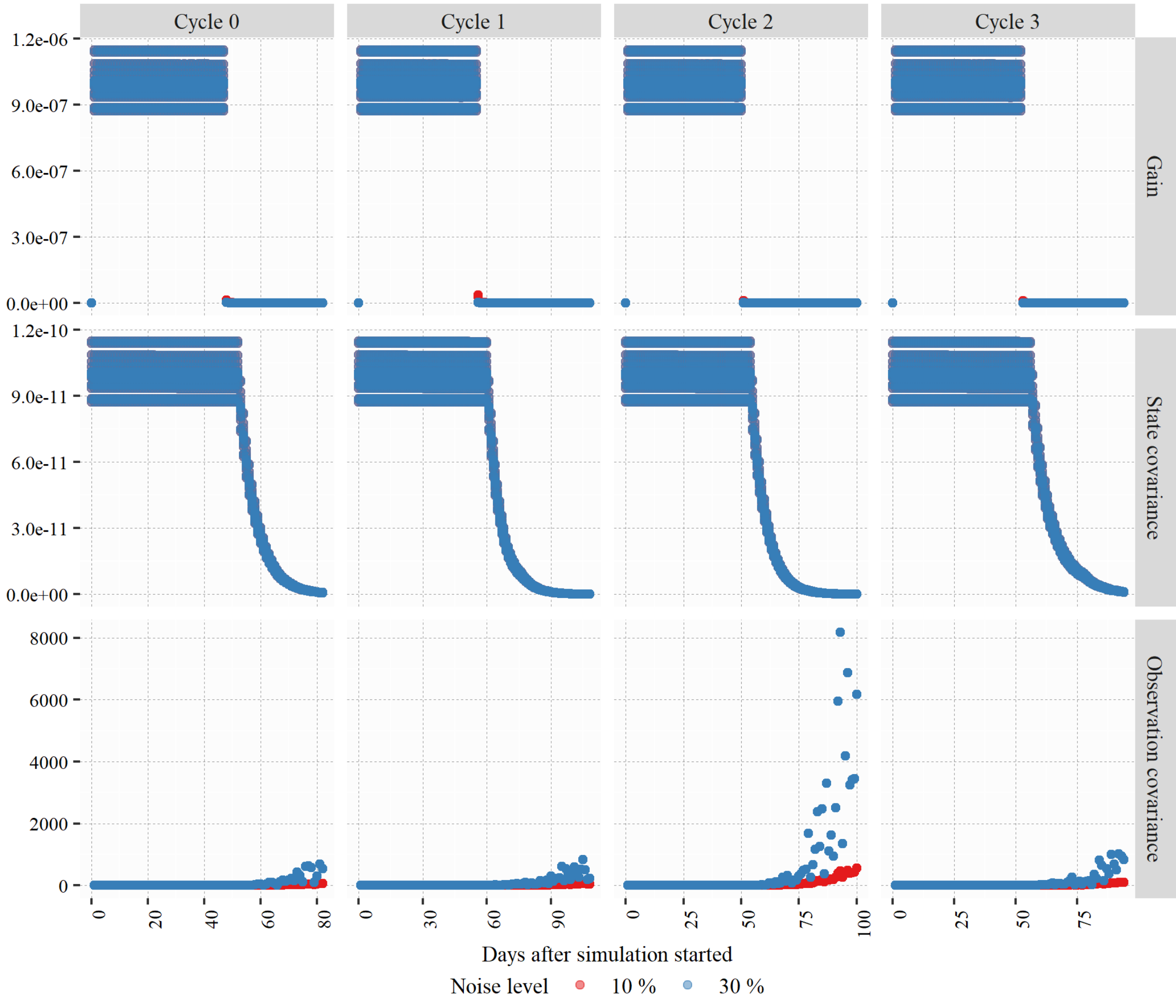

Figure 34. Evolution of filter hyperparameters on the assimilation of mature fruit biomass with different noise levels for the observations using the low-cost sensor as source of solar radiation input.

6. FINAL REMARKS AND CONCLUSION

Modeling is a common strategy to aide in decision-making in multiple fields of study. Crop modeling relies on agronomical and biological research to unveil the mechanisms that lead to crop growth and development, considering the different environmental and management inputs. Recent developments in data gathering and processing led to an expectation of this new deluge of potential information to accelerate knowledge discovery and its application in the modeling processes. Although much of this expectation has been directed to empirical models, through deep learning and machine learning techniques, there is a gap on the use of state estimation approaches in lower spatial scale contexts.

This study covered aspects of the data assimilation framework of research, redirecting previous knowledge of assimilation in large areas with satellite images. But several intermediate steps were required before achieving the goal of assimilation: crop management, data gathering, model understanding, implementation and calibration, and determination of observation models. Apart from the crop management, which was certainly challenging and led to the unintended different outcomes across cycles, the first step relates to data gathering. Regarding environmental data, as data imputation and processing were required, these steps would provide the complete hourly environmental datasets required by the growth model, but they also add uncertainty to the model estimates in a way that could not be quantified. It is not expected for the results from the uncertainty analyses or calibration to have been affected by this step, as in all cycles, few cases required imputation. Uncertainty associated with measurements are certainly present in plant annotations as well. Even as a lot of care was taken in the process, often with two persons responsible for each image, it cannot be guaranteed that there are no errors, especially for green areas. While unfortunately these uncertainties may have negatively affected the results of the work, one positive aspect of uncertainty being an overarching theme of this study was to lead to a more comfortable relationship with its presence either in model estimates or in observations.

When reviewing the literature to contextualize and better understand the problem treated in this study, a few questions arose. Is there any understanding of how the assimilation of one state variable may impact the frequently desired outcome of improving yield estimates? Is there any suggestion of how to characterize the uncertainties involved in the process? This motivated the work in the Appendix E, in which these questions were explored. As there was no protocol established for data assimilation and, especially given assimilation in protected environments being a new subject of research, different approaches were evaluated.

As the use of data assimilation in protected environments is new, how much work has already been done on the subject and could be used as basis for this study was scarce. This study had to validate models used on greenhouse growth, identifying which parameters should be calibrated, to obtain the observation models, and to determine how to ascribe uncertainty to the parameters of the filters. This means that the potential uncovered in this study may be further explored by more research.

Destructive analyses suggested that it was possible to obtain good estimates of fruit growth through pictures even when parts of the plant were occluded. At the same time, the outcomes of assimilation with artificial observations of fruit growth suggested good improvements of yield estimates are possible from assimilating fruit data directly. There is then a potential of data assimilation with fruits images as a source of observation for better yield estimates in protected environments. The use of photos from smartphones as non-destructive measurements in commercial settings has been previously proposed (Li et al., 2020) and is subject of research on its own. This could be a step in the direction of enhancing production planning, as well as of controlling the system for optimized production and resource usage. By enabling the use of this technology for small growers, they could leverage benefits of crop models, such as planning and optimizing resources.

It should be remembered that the model used in this study did not include irrigation or other aspects that are relevant to the management of tomato growth, such as fertilization supplemental lighting. But when the focus is not yield, although other variables are not as appropriate for assimilation, they could be informative for other model states and possibly, management. There is no established method for assessing which variables would be informative, and some points with this regard have been made in section 3.4.3. Some hints of how to perform this assessment come from the sensitivity analysis performed in this study, as it showed the lower influence of parameters from leaf area on yield and that the most relevant parameters were connected to fruit biomass estimation. Perhaps an approach could be devised that would be able to explore pairs of state variables within valid values to assess how one variable could affect the other. The outcome would be a combination of sensitivity analysis of state variables, weather (as it is likely unknown), but of model bias as well, as the assessment of Kang and Özdoğan (2019) showed how it could affect results. Ines et al. (2013) concluded that weather conditions expected during the growing season could provide information as to when a variable is best to be assimilated, and this would include a beneficial constraint in the analyses, as the historical assessment led to longer processing time in the sensitivity analysis of this study.

Another way of seeing the problem of improving estimates could have been by using real-time calibration of parameters. Indirect observations have been used for calibration (Richetti et al., 2019) and they would lead to a more permanent improvement of model estimates, without relying on observations. And as data assimilation is characterized by the three strategies — forcing, update and recalibration — there is already an overlap between strategies, particularly update and recalibration, as well as discussions that convey this approach. The recalibration strategy often relies on optimization methods, similarly to calibration so the novelty would come from taking advantage of filters. Yu et al. (2020) used a smoother to ensure the consistency between states and parameters, assimilating all available observations simultaneously. Shadrin et al. (2020) suggested the use of an extended state vector which included parameters from a logistic S-curve which would characterize growth in a controlled environment using the Extended Kalman Filter. Zhang et al. (2021) used an approach they called Informed Particle Filter as they used a sensitivity analysis to determine parameters that would be included in the extended state vector as well as included bounds to the estimates of the filter.

The mention of Particle Filters leads to another possible expansion of this study that includes the exploration of other techniques or modifications. For instance, Particle Filters would account for non-Gaussian distribution of errors. But it is the case that even the techniques used in this study have also been adapted in other works for improvement in some respects, e. g., EnKF adaptations to not perturb observations aiming at minimizing the risk of pairing LAI observations with unusual planting date (Ines et al., 2013) or to include inflation parameters to perturb the ensemble to avoid filter divergence (Ines et al., 2013; Xie et al., 2017), the constant gain in the Kalman Filter, previously mentioned, that according to Chen, Zhang and Tao (2018) alleviated the effect of filter divergence. Gruber; De Lannoy and Crow (2019) used an adaptive approach, i.e., one that would try to estimate state variables and their error statistics simultaneously, based on the Kalman Filter.

One aspect of filters that could not be explored is the reduction in the uncertainty of the estimate. As the magnitudes of errors were very large — consider the error in the estimate of a non-calibrated model, or the errors of more than 100% in the validation of the observation models —, there is little added to the knowledge of how the approach would perform by analyzing the outcomes in detail. But as the filters act as a weighted average, there could be room for a sensitivity analysis of the gain, to assess the expected improvement of estimates given the expected uncertainty in measurements and model estimates, in cases in which errors are expected to be much larger in one estimate than the other.

This study aimed at using data assimilation to circumvent the need for calibration of a tomato growth model. Overall, while assimilation of observations only slightly improved estimates obtained by models, regardless of the source of observation being of very high quality, such as minute observations of plant weight, or indirect observations of plant growth through images, in some cases there were remarkable improvements when compared to the non-calibrated model, especially when the observation error is low. Data assimilation seemed especially valuable to adjust estimates in growth cycles in which potential growth was not observed. However, the ability to extend the approach for other users rely on the availability of good and generalizable observation models.

When assessing sensors of different accuracy levels for providing weather inputs, the approach was inconclusive. In some cases, lower errors were indeed observed, but the results were not consistent through all the experiments assessed. Finally, in the conditions analyzed, we observed that when the goal is to assess the effect of assimilation on yield, although lower frequency can lead to lower errors, it could also lead to larger errors, likely depending on the timing of the assimilated observation.

7. LITERATURE CITED

Affholder, F., Tittonell, P., Corbeels, M., Roux, S., Motisi, N., Tixier, P., Wery, J., 2012. Ad hoc modeling in agronomy: What have we learned in the last 15 years? Agron. J. 104, 735–748. https://doi.org/10.2134/agronj2011.0376

Alvarenga, M.A.R., 2013. Tomate: produção em campo, casa de vegetação e hidroponia, 2nd ed. Editora Universitária de Lavras, Lavras.

Angulo, C., Rötter, R., Lock, R., Enders, A., Fronzek, S., Ewert, F., 2013. Implication of crop model calibration strategies for assessing regional impacts of climate change in Europe. Agric. For. Meteorol. 170, 32–46. https://doi.org/10.1016/j.agrformet.2012.11.017

Antle, J.M., Basso, B., Conant, R.T., Godfray, H.C.J., Jones, J.W., Herrero, M., Howitt, R.E., Keating, B.A., Munoz-Carpena, R., Rosenzweig, C., Tittonell, P., Wheeler, T.R., 2017a. Towards a new generation of agricultural system data, models and knowledge products: Design and improvement. Agric. Syst. 155, 255–268. https://doi.org/10.1016/j.agsy.2016.10.002

Antle, J.M., Jones, J.W., Rosenzweig, C., 2017b. Next generation agricultural system models and knowledge products: Synthesis and strategy. Agric. Syst. 155, 179–185. https://doi.org/10.1016/j.agsy.2017.05.006

Archontoulis, S. V., Miguez, F.E., 2015. Nonlinear Regression Models and Applications in Agricultural Research. Agron. J. 107, 786–798. https://doi.org/10.2134/agronj2012.0506

Athanasiadis, I.N., Janssen, S., Holzworth, D., Thorburn, P.J., Donatelli, M., Snow, V., Hoogenboom, G., White, J.W.W.W., Athanasiadis, I.N., Janssen, S., Donatelli, M., Snow, V., Hoogenboom, G., White, J.W.W.W., Thorburn, P.J., Holzworth, D., Thorburn, P.J., Donatelli, M., Snow, V., Hoogenboom, G., White, J.W.W.W., 2015. Thematic issue on agricultural systems modelling and software - Part II. Environ. Model. Softw. 62, 274–275. https://doi.org/10.1016/j.envsoft.2014.11.003

Bai, T., Wang, S., Meng, W., Zhang, N., Wang, T., Chen, Y., Mercatoris, B., 2019. Assimilation of Remotely-Sensed LAI into WOFOST Model with the SUBPLEX Algorithm for Improving the Field-Scale Jujube Yield Forecasts. Remote Sens. 11, 1945. https://doi.org/10.3390/rs11161945

Berrueta, C., Heuvelink, E., Giménez, G., Dogliotti, S., 2020. Estimation of tomato yield gaps for greenhouse in Uruguay. Sci. Hortic. (Amsterdam). 265, 109250. https://doi.org/10.1016/j.scienta.2020.109250

Bertin, N., Heuvelink, E., 1993. Dry-matter production in a tomato crop: Comparison of two simulation models. J. Hortic. Sci. 68, 995–1011. https://doi.org/10.1080/00221589.1993.11516441

Betbeder, J., Fieuzal, R., Baup, F., 2016. Assimilation of LAI and Dry Biomass Data From Optical and SAR Images Into an Agro-Meteorological Model to Estimate Soybean Yield. IEEE J. Sel. Top. Appl. Earth Obs. Remote Sens. 9, 2540–2553. https://doi.org/10.1109/JSTARS.2016.2541169

Bojacá, C.R., Gil, R., Cooman, A., 2009. Use of geostatistical and crop growth modelling to assess the variability of greenhouse tomato yield caused by spatial temperature variations. Comput. Electron. Agric. 65, 219–227. https://doi.org/10.1016/j.compag.2008.10.001

Boote, K.J., Jones, J.W., Pickering, N.B., 1996. Potential uses and limitations of crop models. Agron. J. 88, 704–716. https://doi.org/10.2134/agronj1996.00021962008800050005x

Boote, K.J., Rybak, M.R., Scholberg, J.M.S., Jones, J.W., 2012. Improving the CROPGRO-Tomato Model for Predicting Growth and Yield Response to Temperature. Hortscience 47, 1038–1049.

Chen, Y., Tao, F., 2020. Improving the practicability of remote sensing data-assimilation-based crop yield estimations over a large area using a spatial assimilation algorithm and ensemble assimilation strategies. Agric. For. Meteorol. 291, 108082. https://doi.org/10.1016/j.agrformet.2020.108082

Chen, Y., Zhang, Z., Tao, F., 2018. Improving regional winter wheat yield estimation through assimilation of phenology and leaf area index from remote sensing data. Eur. J. Agron. 101, 163–173. https://doi.org/10.1016/J.EJA.2018.09.006

Confalonieri, R., Orlando, F., Paleari, L., Stella, T., Gilardelli, C., Movedi, E., Pagani, V., Cappelli, G., Vertemara, A., Alberti, L., Alberti, P., Atanassiu, S., Bonaiti, M., Cappelletti, G., Ceruti, M., Confalonieri, A., Corgatelli, G., Corti, P., Dell'Oro, M., Ghidoni, A., Lamarta, A., Maghini, A., Mambretti, M., Manchia, A., Massoni, G., Mutti, P., Pariani, S., Pasini, D., Pesenti, A., Pizzamiglio, G., Ravasio, A., Rea, A., Santorsola, D., Serafini, G., Slavazza, M., Acutis, M., 2016. Uncertainty in crop model predictions: What is the role of users? Environ. Model. Softw. 81, 165–173. https://doi.org/10.1016/J.ENVSOFT.2016.04.009

Cooman, A., Schrevens, E., 2007. Sensitivity of the Tomgro Model to Solar Radiation Intensity, Air Temperature and Carbon Dioxide Concentration. Biosyst. Eng. 96, 249–255. https://doi.org/10.1016/J.BIOSYSTEMSENG.2006.10.011

Cooman, A., Schrevens, E., 2006. A Monte Carlo Approach for estimating the Uncertainty of Predictions with the Tomato Plant Growth Model, Tomgro. Biosyst. Eng. 94, 517–524. https://doi.org/10.1016/j.biosystemseng.2006.05.005

Curnel, Y., de Wit, A.J.W., Duveiller, G., Defourny, P., 2011. Potential performances of remotely sensed LAI assimilation in WOFOST model based on an OSS Experiment. Agric. For. Meteorol. 151, 1843–1855. https://doi.org/10.1016/j.agrformet.2011.08.002

Dayan, E., van Keulen, H., Jones, J.W., Zipori, I., Shmuel, D., Challa, H., 1993a. Development, calibration and validation of a greenhouse tomato growth model: I. Description of the model. Agric. Syst. 43, 145–163. https://doi.org/10.1016/0308-521X(93)90024-V

Dayan, E., van Keulen, H., Jones, J.W.W., Zipori, I., Shmuel, D., Challa, H., 1993b. Development, calibration and validation of a greenhouse tomato growth model: II. Field calibration and validation. Agric. Syst. 43, 165–183. https://doi.org/10.1016/0308-521X(93)90025-W

De Vries, F.W.T.P., 1982. Phases of development of models, in: Simulation of Plant Growth and Crop Production. Pudoc, pp. 20–25.

de Wit, A.J.W., van Diepen, C.A., 2007. Crop model data assimilation with the Ensemble Kalman filter for improving regional crop yield forecasts. Agric. For. Meteorol. 146, 38–56. https://doi.org/10.1016/j.agrformet.2007.05.004

Deligios, P.A., Cossu, M., Murgia, L., Sirigu, A., Urracci, G., Pazzona, A., Pala, T., Ledda, L., 2017. Modeling tomato growth and production in a photovoltaic greenhouse in southern Italy, in: Acta Horticulturae. International Society for Horticultural Science, pp. 203–210. https://doi.org/10.17660/ActaHortic.2017.1182.24

Dente, L., Satalino, G., Mattia, F., Rinaldi, M., 2008. Assimilation of leaf area index derived from ASAR and MERIS data into CERES-Wheat model to map wheat yield. Remote Sens.

Environ. 112, 1395–1407. https://doi.org/10.1016/j.rse.2007.05.023

Dorigo, W.A., Zurita-Milla, R., de Wit, A.J.W., Brazile, J., Singh, R., Schaepman, M.E., 2007. A review on reflective remote sensing and data assimilation techniques for enhanced agroecosystem modeling. Int. J. Appl. Earth Obs. Geoinf. 9, 165–193. https://doi.org/10.1016/j.jag.2006.05.003

Easlon, H.M., Bloom, A.J., 2014. Easy Leaf Area: Automated digital image analysis for rapid and accurate measurement of leaf area. Appl. Plant Sci. 2, 1400033. https://doi.org/10.3732/apps.1400033

Evers, J.B., Marcelis, L.F.M., 2019. Functional—structural plant modeling of plants and crops, in: Boote, K. (Ed.), Advances in Crop Modelling for a Sustainable Agriculture. Burleigh Dodds Science Publishing Limited, Cambridge, pp. 45–68. https://doi.org/10.19103/AS.2019.0061.02

Fang, H., Baret, F., Plummer, S., Schaepman-Strub, G., 2019. An Overview of Global Leaf Area Index (LAI): Methods, Products, Validation, and Applications. Rev. Geophys. 57, 739–799. https://doi.org/10.1029/2018RG000608

Fischer, A., Kergoat, L., Dedieu, G., 1997. Coupling Satellite Data with Vegetation Functional Models: Review of Different Approaches and Perspectives Suggested by the Assimilation Strategy. Remote Sens. Rev. 15, 283–303. https://doi.org/10.1080/02757259709532343

Gallardo, M., Giménez, C., Martínez-Gaitán, C., Stöckle, C.O., Thompson, R.B., Granados, M.R., 2011. Evaluation of the VegSyst model with muskmelon to simulate crop growth, nitrogen uptake and evapotranspiration. Agric. Water Manag. 101, 107–117. https://doi.org/10.1016/j.agwat.2011.09.008

Gallardo, M., Thompson, R.B., Giménez, C., Padilla, F.M., Stöckle, C.O., 2014. Prototype decision support system based on the VegSyst simulation model to calculate crop N and water requirements for tomato under plastic cover. Irrig. Sci. 32, 237–253. https://doi.org/10.1007/s00271-014-0427-3

Gary, C., Barczi, J.F., Bertin, N., Tchamitchian, M., 1995. Simulation of individual organ growth and development on a tomato plant: a model and a user-friendly interface. Acta Hortic. 199–206. https://doi.org/10.17660/ActaHortic.1995.399.23

Gary, C., Jones, J.., Tchamitchian, M., 1998. Crop modelling in horticulture: state of the art. Sci. Hortic. (Amsterdam). 74, 3–20. https://doi.org/10.1016/S0304-4238(98)00080-6

Giménez, C., Gallardo, M., Martínez-Gaitán, C., Stöckle, C.O., Thompson, R.B., Granados, M.R., 2013. VegSyst, a simulation model of daily crop growth, nitrogen uptake and evapotranspiration for pepper crops for use in an on-farm decision support system. Irrig. Sci. 31, 465–477. https://doi.org/10.1007/s00271-011-0312-2

Graamans, L., Baeza, E., van den Dobbelsteen, A., Tsafaras, I., Stanghellini, C., 2018. Plant factories versus greenhouses: Comparison of resource use efficiency. Agric. Syst. 160, 31–43. https://doi.org/10.1016/j.agsy.2017.11.003

Gruber, A., De Lannoy, G., Crow, W., 2019. A Monte Carlo based adaptive Kalman filtering framework for soil moisture data assimilation. Remote Sens. Environ. 228, 105–114. https://doi.org/10.1016/J.RSE.2019.04.003

Guo, C., Tang, Y., Lu, J., Zhu, Y., Cao, W., Cheng, T., Zhang, L., Tian, Y., 2019. Predicting wheat productivity: Integrating time series of vegetation indices into crop modeling via sequential assimilation. Agric. For. Meteorol. 272–273, 69–80.

https://doi.org/10.1016/J.AGRFORMET.2019.01.023

Guo, C., Zhang, L., Zhou, X., Zhu, Y., Cao, W., Qiu, X., Cheng, T., Tian, Y., 2018. Integrating remote sensing information with crop model to monitor wheat growth and yield based on simulation zone partitioning. Precis. Agric. 19, 55–78. https://doi.org/10.1007/s11119-017-9498-5

Hall, O.D., Scurlock, J.M.O., 1993. Biomass production and data, Photosynthesis and Production in a Changing Environment: afield and laboratory manual. Springer Netherlands, Dordrecht. https://doi.org/10.1007/978-94-011-1566-7

He, H., Lei, L., Whitaker, J.S., Tan, Z., 2020. Impacts of Assimilation Frequency on Ensemble Kalman Filter Data Assimilation and Imbalances. J. Adv. Model. Earth Syst. 12. https://doi.org/10.1029/2020MS002187

Hemming, S., de Zwart, F. de, Elings, A., Petropoulou, A., Righini, I., 2020. Cherry tomato production in intelligent greenhouses-sensors and ai for control of climate, irrigation, crop yield, and quality. Sensors (Switzerland) 20, 1–30. https://doi.org/10.3390/s20226430

Hemming, S., de Zwart, F., Elings, A., Righini, I., Petropoulou, A., 2019. Remote Control of Greenhouse Vegetable Production with Artificial Intelligence—Greenhouse Climate, Irrigation, and Crop Production. Sensors 19, 1807. https://doi.org/10.3390/s19081807

Herman, J., Usher, W., 2017. SALib: An open-source Python library for Sensitivity Analysis. J. Open Source Softw. 2, 97. https://doi.org/10.21105/joss.00097

Heuvelink, E., 1996. Tomato growth and yield: quantitative analysis and synthesis.

Heuvelink, E., 1995. Growth, development and yield of a tomato crop: periodic destructive measurements in a greenhouse. Sci. Hortic. (Amsterdam). 61, 77–99. https://doi.org/10.1016/0304-4238(94)00729-Y

Heuvelink, E., Bakker, M.J., Elings, A., Kaarsemaker, R., Marcelis, L.F.M., 2005. Effect of leaf area on tomato yield. Acta Hortic. 691, 43–50. https://doi.org/10.17660/ActaHortic.2005.691.2

Heuvelink, E., Li, T., Dorais, M., 2018. Crop growth and yield., in: Heuvelink, E. (Ed.), Tomatoes. CABI, Wallingford, pp. 89–136. https://doi.org/10.1079/9781780641935.0089

Holzworth, D., Athanasiadis, I.N., Janssen, S., Donatelli, M., Snow, V., Hoogenboom, G., White, J.W., Thorburn, P.J., 2014. Thematic issue on agricultural systems modelling and software – Part I. Environ. Model. Softw. 62, 326. https://doi.org/10.1016/j.envsoft.2014.11.003

Holzworth, D.P., Snow, V., Janssen, S., Athanasiadis, I.N., Donatelli, M., Hoogenboom, G., White, J.W., Thorburn, P., 2015. Agricultural production systems modelling and software: Current status and future prospects. Environ. Model. Softw. 72, 276–286. https://doi.org/10.1016/j.envsoft.2014.12.013

Hu, S., Shi, L., Huang, K., Zha, Y., Hu, X., Ye, H., Yang, Q., 2019. Improvement of sugarcane crop simulation by SWAP-WOFOST model via data assimilation. F. Crop. Res. 232, 49–61. https://doi.org/10.1016/j.fcr.2018.12.009

Huang, J., Gómez-Dans, J.L., Huang, H., Ma, H., Wu, Q., Lewis, P.E., Liang, S., Chen, Z., Xue, J.-H., Wu, Y., Zhao, F., Wang, J., Xie, X., 2019a. Assimilation of remote sensing into crop growth models: Current status and perspectives. Agric. For. Meteorol. 276–277, 107609. https://doi.org/10.1016/j.agrformet.2019.06.008

Huang, J., Ma, H., Sedano, F., Lewis, P., Liang, S., Wu, Q., Su, W., Zhang, X., Zhu, D., 2019b. Evaluation of regional estimates of winter wheat yield by assimilating three remotely sensed reflectance datasets into the coupled WOFOST–PROSAIL model. Eur. J. Agron. 102, 1–13. https://doi.org/10.1016/J.EJA.2018.10.008

Huang, J., Sedano, F., Huang, Y., Ma, H., Li, X., Liang, S., Tian, L., Zhang, X., Fan, J., Wu, W., 2016. Assimilating a synthetic Kalman filter leaf area index series into the WOFOST model to improve regional winter wheat yield estimation. Agric. For. Meteorol. 216, 188–202. https://doi.org/10.1016/j.agrformet.2015.10.013

Ines, A.V.M., Das, N.N., Hansen, J.W., Njoku, E.G., 2013. Assimilation of remotely sensed soil moisture and vegetation with a crop simulation model for maize yield prediction. Remote Sens. Environ. 138, 149–164. https://doi.org/10.1016/J.RSE.2013.07.018

Jiang, B., Su, H., Liu, K., Chen, S., 2020. Assessment of remotely sensed and modelled soil moisture data products in the U.S. Southern great plains. Remote Sens. 12, 1–20. https://doi.org/10.3390/rs12122030

Jin, X., Kumar, L., Li, Z., Feng, H., Xu, X., Yang, G., Wang, J., 2018. A review of data assimilation of remote sensing and crop models. Eur. J. Agron. 92, 141–152. https://doi.org/10.1016/j.eja.2017.11.002

Jones, J.W., Antle, J.M., Basso, B., Boote, K.J., Conant, R.T., Foster, I., Godfray, H.C.J., Herrero, M., Howitt, R.E., Janssen, S., Keating, B.A., Munoz-Carpena, R., Porter, C.H., Rosenzweig, C., Wheeler, T.R., 2017a. Toward a new generation of agricultural system data, models, and knowledge products: State of agricultural systems science. Agric. Syst. 155, 269–288. https://doi.org/10.1016/j.agsy.2016.09.021

Jones, J.W., Antle, J.M., Basso, B., Boote, K.J., Conant, R.T., Foster, I., Godfray, H.C.J., Herrero, M., Howitt, R.E., Janssen, S., Keating, B.A., Munoz-Carpena, R., Porter, C.H., Rosenzweig, C., Wheeler, T.R., 2017b. Brief history of agricultural systems modeling. Agric. Syst. 155, 240–254. https://doi.org/10.1016/j.agsy.2016.05.014

Jones, J.W., Dayan, E., Allen, L.H., Van Keulen, H., Challa, H., 1991. A dynamic tomato growth and yield model (TOMGRO). Trans. ASAE 34, 0663–0672. https://doi.org/10.13031/2013.31715

Jones, J.W., Kenig, A., Vallejos, C.E., 1999. Reduced state-variable tomato growth model. Trans. ASAE 42, 255–265. https://doi.org/10.13031/2013.13203

Kang, S., van Iersel, M.W., Kim, J., 2019. Plant root growth affects FDR soil moisture sensor calibration. Sci. Hortic. (Amsterdam). 252, 208–211. https://doi.org/10.1016/j.scienta.2019.03.050

Kang, Y., Özdoğan, M., 2019. Field-level crop yield mapping with Landsat using a hierarchical data assimilation approach. Remote Sens. Environ. 228, 144–163. https://doi.org/10.1016/J.RSE.2019.04.005

Karlberg, L., Ben-Gal, A., Jansson, P.E., Shani, U., 2006. Modelling transpiration and growth in salinity-stressed tomato under different climatic conditions. Ecol. Modell. 190, 15–40. https://doi.org/10.1016/j.ecolmodel.2005.04.015

Katerji, N., Campi, P., Mastrorilli, M., 2013. Productivity, evapotranspiration, and water use efficiency of corn and tomato crops simulated by AquaCrop under contrasting water stress conditions in the Mediterranean region. Agric. Water Manag. 130, 14–26. https://doi.org/10.1016/j.agwat.2013.08.005

Keating, B.A., Thorburn, P.J., 2018. Modelling crops and cropping systems—Evolving purpose, practice and prospects. Eur. J. Agron. 100, 163–176. https://doi.org/10.1016/j.eja.2018.04.007

Kersebaum, K.C.C., Boote, K.J.J., Jorgenson, J.S.S., Nendel, C., Bindi, M., Frühauf, C., Gaiser, T., Hoogenboom, G., Kollas, C., Olesen, J.E.E., Rötter, R.P.P., Ruget, F., Thorburn, P.J.J., Trnka, M., Wegehenkel, M., 2015. Analysis and classification of data sets for calibration and validation of agro-ecosystem models. Environ. Model. Softw. 72, 402–417. https://doi.org/10.1016/j.envsoft.2015.05.009

Keulen, H. Van, Dayan, E., 1993. TOMGRO- a greenhouse-tomato simulation model.

Khapte, P.S., Kumar, Pradeep, Burman, U., Kumar, Praveen, 2019. Deficit irrigation in tomato: Agronomical and physio-biochemical implications. Sci. Hortic. (Amsterdam). 248, 256–264. https://doi.org/10.1016/J.SCIENTA.2019.01.006

Kim, S.-H., Hsiao, J., Kinmonth-Schultz, H., 2019. Advances and improvements in modeling plant processes, in: Boote, K. (Ed.), Advances in Crop Modelling for a Sustainable Agriculture. Burleigh Dodds Science Publishing, Cambridge, pp. 3–44. https://doi.org/10.19103/AS.2019.0061.01

Kuijpers, W.J.P., van de Molengraft, M.J.G., van Mourik, S., van ’t Ooster, A., Hemming, S., van Henten, E.J., 2019. Model selection with a common structure: Tomato crop growth models. Biosyst. Eng. 187, 247–257. https://doi.org/10.1016/j.biosystemseng.2019.09.010

Labbe Jr, R.R., 2020. Kalman and Bayesian Filters in Python, 2nd ed.

Lawson, L., 2016. Agriculture: Sowing the city. Nature 540, 522–524. https://doi.org/10.1038/540522a

Lei, F., Crow, W.T., Kustas, W.P., Dong, J., Yang, Y., Knipper, K.R., Anderson, M.C., Gao, F., Notarnicola, C., Greifeneder, F., McKee, L.M., Alfieri, J.G., Hain, C., Dokoozlian, N., 2020. Data assimilation of high-resolution thermal and radar remote sensing retrievals for soil moisture monitoring in a drip-irrigated vineyard. Remote Sens. Environ. 239, 111622. https://doi.org/10.1016/j.rse.2019.111622

Lentz, W., 1998. Model applications in horticulture: a review. Sci. Hortic. (Amsterdam). 74, 151–174. https://doi.org/10.1016/S0304-4238(98)00085-5

Li, C., Adhikari, R., Yao, Y., Miller, A.G., Kalbaugh, K., Li, D., Nemali, K., 2020. Measuring plant growth characteristics using smartphone based image analysis technique in controlled environment agriculture. Comput. Electron. Agric. 168. https://doi.org/10.1016/j.compag.2019.105123

Li, H., Chen, Z., Liu, G., Jiang, Z., Huang, C., 2017. Improving Winter Wheat Yield Estimation from the CERES-Wheat Model to Assimilate Leaf Area Index with Different Assimilation Methods and Spatio-Temporal Scales. Remote Sens. 9, 190. https://doi.org/10.3390/rs9030190

Li, Y., Zhou, Q., Zhou, J., Zhang, G., Chen, C., Wang, J., 2014. Assimilating remote sensing information into a coupled hydrology-crop growth model to estimate regional maize yield in arid regions. Ecol. Modell. 291. https://doi.org/10.1016/j.ecolmodel.2014.07.013

Lin, D., Wei, R., Xu, L., 2019. An Integrated Yield Prediction Model for Greenhouse Tomato. Agronomy 9, 873. https://doi.org/10.3390/agronomy9120873

Linker, R., Ioslovich, I., 2017. Assimilation of canopy cover and biomass measurements in the crop model AquaCrop. Biosyst. Eng. 162, 57–66.

https://doi.org/10.1016/j.biosystemseng.2017.08.003

Lizaso, J.I., Batchelor, W.D., Westgate, M.E., Echarte, L., 2003. Enhancing the ability of CERES-Maize to compute light capture. Agric. Syst. 76, 293–311. https://doi.org/10.1016/S0308-521X(02)00003-3

Lu, Y., Chibarabada, T.P., Ziliani, M.G., Onema, J.K., Mccabe, M.F., Sheffield, J., 2021. Assimilation of soil moisture and canopy cover data improves maize simulation using an under-calibrated crop model. Agric. Water Manag. 252, 106884. https://doi.org/10.1016/j.agwat.2021.106884

Mansouri, M., Dumont, B., Destain, M.-F., 2013. Modeling and prediction of nonlinear environmental system using Bayesian methods. Comput. Electron. Agric. 92, 16–31. https://doi.org/10.1016/j.compag.2012.12.013

Marcelis, L.F.., Heuvelink, E., Goudriaan, J., 1998. Modelling biomass production and yield of horticultural crops: a review. Sci. Hortic. (Amsterdam). 74, 83–111. https://doi.org/10.1016/S0304-4238(98)00083-1

McNeal, B.L., Scholberg, J.M.S., Jones, J.W., Stanley, C.D., Csizinsky, A.A., Obreza, T.A., 1995. Application of a greenhouse tomato-growth model (TOMGRO) to field-grown tomato. Soil Crop Sci. Soc. Florida.

Mishra, V., Cruise, J.F., Mecikalski, J.R., 2021. Assimilation of coupled microwave / thermal infrared soil moisture profiles into a crop model for robust maize yield estimates over Southeast United States. Eur. J. Agron. 123, 126208. https://doi.org/10.1016/j.eja.2020.126208

Monteith, J.L., 1996. The quest for balance in crop modeling. Agron. J. 88, 695–697. https://doi.org/10.2134/agronj1996.00021962008800050003x

Montero, J.I., Zhang, Y., Yang, Q., Ke, X., 2019. Advances in greenhouse design, in: Marcelis, L.F.M., Heuvelink, E. (Eds.), Achieving Sustainable Greenhouse Cultivation. Burleigh Dodds Science Publishing Limited, Cambridge, pp. 17–52. https://doi.org/10.19103/AS.2019.0052.02

Nearing, G., Yatheendradas, S., Crow, W., Zhan, X., Liu, J., Chen, F., 2018. The Efficiency of Data Assimilation. Water Resour. Res. https://doi.org/10.1029/2017WR020991

Nearing, G.S., Crow, W.T., Thorp, K.R., Moran, M.S., Reichle, R.H., Gupta, H. V., 2012. Assimilating remote sensing observations of leaf area index and soil moisture for wheat yield estimates: An observing system simulation experiment. Water Resour. Res. 48. https://doi.org/10.1029/2011WR011420

Nyakwende, E., Paull, C.J., Atherton, J.G., 1997. Non-destructive determination of leaf area in tomato plants using image processing. J. Hortic. Sci. 72, 255–262. https://doi.org/10.1080/14620316.1997.11515512

Parton, W.J., Logan, J.A., 1981. A model for diurnal variation in soil and air temperature. Agric. Meteorol. 23, 205–216. https://doi.org/10.1016/0002-1571(81)90105-9

Passioura, J.B., 1996. Simulation models: Science, snake oil, education, or engineering? Agron. J. 88, 690–694. https://doi.org/10.2134/agronj1996.00021962008800050002x

Pellenq, J., Boulet, G., 2004. A methodology to test the pertinence of remote-sensing data assimilation into vegetation models for water and energy exchange at the land surface. Agronomie 24, 197–204. https://doi.org/10.1051/agro:2004017

Pianosi, F., Beven, K., Freer, J., Hall, J.W., Rougier, J., Stephenson, D.B., Wagener, T., 2016. Sensitivity analysis of environmental models: A systematic review with practical workflow. Environ. Model. Softw. 79, 214–232. https://doi.org/10.1016/j.envsoft.2016.02.008

Pinstrup-Andersen, P., 2017. Is it time to take vertical indoor farming seriously? Glob. Food Sec. 0–1. https://doi.org/10.1016/j.gfs.2017.09.002

Pires, R.C. de M., Furlani, P.R., Ribeiro, R.V., Bodine Junior, D., Sakai, E., Lourencao, A.L., Torre Neto, A., 2011. Irrigation frequency and substrate volume effects in the growth and yield of tomato plants under greenhouse conditions. Sci. Agric. 68, 400–405. https://doi.org/10.1590/S0103-90162011000400002

Ramirez, A., Rodriguez, F., Berenguel, M., Heuvelink, E., Ramírez, A., Rodríguez, F., Berenguel, M., Heuvelink, E., 2004. Calibration and validation of complex and simplified tomato growth models for control purposes in the Southeast of Spain. Acta Hortic. 654, 147–154. https://doi.org/10.17660/ActaHortic.2004.654.15

Richetti, J., Boote, K.J., Hoogenboom, G., Judge, J., Johann, J.A., Uribe-Opazo, M.A., 2019. Remotely sensed vegetation index and LAI for parameter determination of the CSM-CROPGRO-Soybean model when in situ data are not available. Int. J. Appl. Earth Obs. Geoinf. 79, 110–115. https://doi.org/10.1016/j.jag.2019.03.007

Rodell, M., Houser, P.R., Jambor, U., Gottschalck, J., Mitchell, K., Meng, C.-J., Arsenault, K., Cosgrove, B., Radakovich, J., Bosilovich, M., Entin, J.K., Walker, J.P., Lohmann, D., Toll, D., 2004. The Global Land Data Assimilation System. Bull. Am. Meteorol. Soc. 85, 381–394. https://doi.org/10.1175/BAMS-85-3-381

Ruíz-García, A., López-Cruz, I.L., Ramírez-Arias, A., Rico-Garcia, E., 2014. Modeling uncertainty of greenhouse crop lettuce growth model using Kalman Filtering. Acta Hortic. 1037, 361–368. https://doi.org/10.17660/ActaHortic.2014.1037.44

Saltelli, A., Aleksankina, K., Becker, W., Fennell, P., Ferretti, F., Holst, N., Li, S., Wu, Q., 2019. Why so many published sensitivity analyses are false: A systematic review of sensitivity analysis practices. Environ. Model. Softw.

Schils, R.L.M., van Voorn, G.A.K., Grassini, P., van Ittersum, M.K., 2022. Uncertainty is more than a number or colour: Involving experts in uncertainty assessments of yield gaps. Agric. Syst. 195, 103311. https://doi.org/10.1016/J.AGSY.2021.103311

Scholberg, J., 1996. Adaptive use of crop growth models to simulate the growth of field-grown tomato.

Scholberg, J.M.S., Boote, K.J., Jones, J.W., McNeal, B.L., 1997. Adaptation of the CROPGRO model to simulate the growth of field-grown tomato, in: Applications of Systems Approaches at the Field Level. Systems Approaches for Sustainable Agricultural Development. Springer, Dordrecht, pp. 135–151. https://doi.org/10.1007/978-94-017-0754-1_9

Seidel, S.J.J., Palosuo, T., Thorburn, P., Wallach, D., 2018. Towards improved calibration of crop models – Where are we now and where should we go? Eur. J. Agron. 94, 25–35. https://doi.org/10.1016/j.eja.2018.01.006

Shadrin, D., Podladchikova, T., Ovchinnikov, G., Pavlov, A., Pukalchik, M., Somov, A., 2020. Kalman Filtering for Accurate and Fast Plant Growth Dynamics Assessment, in: 2020 IEEE International Instrumentation and Measurement Technology Conference (I2MTC). IEEE, pp. 1–6. https://doi.org/10.1109/I2MTC43012.2020.9129053

Sinclair, T.R., Seligman, N.G., 1996. Crop modeling: From infancy to maturity. Agron. J. 88, 698–704. https://doi.org/10.2134/agronj1996.00021962008800050004x

Spitters, C.J.T., Toussaint, H.A.J.M., Goudriaan, J., 1986. Separating the diffuse and direct component of global radiation and its implications for modeling canopy photosynthesis Part I. Components of incoming radiation. Agric. For. Meteorol. 38, 217–229. https://doi.org/10.1016/0168-1923(86)90060-2

Steppe, K., 2012. Plant sensors and models: Getting the dialogue started. Acta Hortic. 957, 277–280.

Tenreiro, T.R., García-Vila, M., Gómez, J.A., Jiménez-Berni, J.A., Fereres, E., 2021. Using NDVI for the assessment of canopy cover in agricultural crops within modelling research. Comput. Electron. Agric. 182, 106038. https://doi.org/10.1016/j.compag.2021.106038

Tewes, A., Hoffmann, H., Krauss, G., Schäfer, F., Kerkhoff, C., Gaiser, T., 2020. New Approaches for the Assimilation of LAI Measurements into a Crop Model Ensemble to Improve Wheat Biomass Estimations. Agronomy 10, 446. https://doi.org/10.3390/agronomy10030446

Torres-Monsivais, J.C., López-Cruz, I.L., Ruíz-García, A., Ramírez-Arias, J.A., Peña-Moreno, R.D., 2017. Data assimilation to improve states estimation of a dynamic greenhouse tomatoes crop growth model. Acta Hortic. 433–440. https://doi.org/10.17660/ActaHortic.2017.1170.53

van Delden, S.H., SharathKumar, M., Butturini, M., Graamans, L.J.A., Heuvelink, E., Kacira, M., Kaiser, E., Klamer, R.S., Klerkx, L., Kootstra, G., Loeber, A., Schouten, R.E., Stanghellini, C., van Ieperen, W., Verdonk, J.C., Vialet-Chabrand, S., Woltering, E.J., van de Zedde, R., Zhang, Y., Marcelis, L.F.M., 2021. Current status and future challenges in implementing and upscaling vertical farming systems. Nat. Food 2, 944–956. https://doi.org/10.1038/s43016-021-00402-w

Van Ploeg, D., Heuvelink, E., 2005. Influence of sub-optimal temperature on tomato growth and yield: a review. J. Hortic. Sci. Biotechnol. 80, 652–659. https://doi.org/10.1080/14620316.2005.11511994

Vanthoor, B.H.E., de Visser, P.H.B., Stanghellini, C., van Henten, E.J., 2011. A methodology for model-based greenhouse design: Part 2, description and validation of a tomato yield model. Biosyst. Eng. 110, 378–395. https://doi.org/10.1016/j.biosystemseng.2011.08.005

Vazifedoust, M., van Dam, J.C., Bastiaanssen, W.G.M., Feddes, R.A., 2009. Assimilation of satellite data into agrohydrological models to improve crop yield forecasts. Int. J. Remote Sens. 30, 2523–2545. https://doi.org/10.1080/01431160802552769

Vazquez-Cruz, M.A., Guzman-Cruz, R., Lopez-Cruz, I.L., Cornejo-Perez, O., Torres-Pacheco, I., Guevara-Gonzalez, R.G., 2014. Global sensitivity analysis by means of EFAST and Sobol' methods and calibration of reduced state-variable TOMGRO model using genetic algorithms. Comput. Electron. Agric. 100, 1–12. https://doi.org/10.1016/j.compag.2013.10.006

Wallach, D., 2019. Dealing with uncertainty in crop models, in: Boote, K.J. (Ed.), Advances in Crop Modelling for a Sustainable Agriculture. Burleigh Dodds Science Publishing, Cambridge, pp. 419–448. https://doi.org/10.19103/AS.2019.0061.21

Wallach, D., 2011. Crop Model Calibration: A Statistical Perspective. Agron. J. 103, 1144–1151. https://doi.org/10.2134/agronj2010.0432

Wallach, D., Makowski, D., Jones, J.W., Brun, F., 2019a. Basics of Agricultural System Models, in: Wallach, D., Makowski, D., Jones, J.W., Brun, F. (Eds.), Working with Dynamic Crop Models. Elsevier, pp. 3–43. https://doi.org/10.1016/B978-0-12-811756-9.00001-0

Wallach, D., Makowski, D., Jones, J.W., Brun, F., 2019b. Data Assimilation for Dynamic Models, in: Wallach, D., Makowski, D., Jones, J.W., Brun, F. (Eds.), Working with Dynamic Crop Models. Elsevier, pp. 487–518. https://doi.org/10.1016/B978-0-12-811756-9.00014-9

Wallach, D., Palosuo, T., Thorburn, P., Hochman, Z., Gourdain, E., Andrianasolo, F., Asseng, S., Basso, B., Buis, S., Crout, N., Dibari, C., Dumont, B., Ferrise, R., Gaiser, T., Garcia, C., Gayler, S., Ghahramani, A., Hiremath, S., Hoek, S., Horan, H., Hoogenboom, G., Huang, M., Jabloun, M., Jansson, P.-E., Jing, Q., Justes, E., Kersebaum, K.C., Klosterhalfen, A., Launay, M., Lewan, E., Luo, Q., Maestrini, B., Mielenz, H., Moriondo, M., Nariman Zadeh, H., Padovan, G., Olesen, J.E., Poyda, A., Priesack, E., Pullens, J.W.M., Qian, B., Schütze, N., Shelia, V., Souissi, A., Specka, X., Srivastava, A.K., Stella, T., Streck, T., Trombi, G., Wallor, E., Wang, J., Weber, T.K.D., Weihermüller, L., de Wit, A., Wöhling, T., Xiao, L., Zhao, C., Zhu, Y., Seidel, S.J., 2021. The chaos in calibrating crop models: Lessons learned from a multi-model calibration exercise. Environ. Model. Softw. 145, 105206. https://doi.org/10.1016/j.envsoft.2021.105206

Wallach, D., Thorburn, P., Asseng, S., Challinor, A.J., Ewert, F., Jones, J.W., Rötter, R., Ruane, A., 2016. Estimating model prediction error: Should you treat predictions as fixed or random? Environ. Model. Softw. 84, 529–539. https://doi.org/10.1016/j.envsoft.2016.07.010

Wallach, D., Thorburn, P.J., 2017. Estimating uncertainty in crop model predictions: Current situation and future prospects. Eur. J. Agron. 88, A1–A7. https://doi.org/10.1016/j.eja.2017.06.001

Xie, Y., Wang, P., Bai, X., Khan, J., Zhang, S., Li, L., Wang, L., 2017. Assimilation of the leaf area index and vegetation temperature condition index for winter wheat yield estimation using Landsat imagery and the CERES-Wheat model. Agric. For. Meteorol. 246, 194–206. https://doi.org/10.1016/J.AGRFORMET.2017.06.015

Yin, J., Zhan, X., Zheng, Y., Hain, C.R., Liu, J., Fang, L., 2015. Optimal ensemble size of ensemble Kalman filter in sequential soil moisture data assimilation. Geophys. Res. Lett. 42, 6710–6715. https://doi.org/10.1002/2015GL063366

Yu, D., Zha, Y., Shi, L., Jin, X., Hu, S., Yang, Q., 2020. Improvement of sugarcane yield estimation by assimilating UAV-derived plant height observations. Eur. J. Agron. 121, 126159. https://doi.org/10.1016/j.eja.2020.126159

Zhang, T., Su, J., Liu, C., Chen, W.H., 2021. State and parameter estimation of the AquaCrop model for winter wheat using sensitivity informed particle filter. Comput. Electron. Agric. 180, 105909. https://doi.org/10.1016/j.compag.2020.105909

Zhao, C., Liu, B., Xiao, L., Hoogenboom, G., Boote, K.J., Kassie, B.T., Pavan, W., Shelia, V., Kim, K.S., Hernandez-Ochoa, I.M., Wallach, D., Porter, C.H., Stockle, C.O., Zhu, Y., Asseng, S., 2019. A SIMPLE crop model. Eur. J. Agron. 104, 97–106. https://doi.org/10.1016/j.eja.2019.01.009

Zhao, Y., Chen, S., Shen, S., 2013. Assimilating remote sensing information with crop model using Ensemble Kalman Filter for improving LAI monitoring and yield estimation. Ecol.

Modell. 270, 30–42. https://doi.org/10.1016/j.ecolmodel.2013.08.016

Appendix A — Model Equations and Parameters of the Reduced-State Tomgro Model

The model calculates growth and development of tomatoes mostly based on the equations below. The model is represented by five difference equations of the states number of nodes (N), leaf area index (LAI), aboveground dry biomass (W), fruit dry biomass (W_f) and mature fruit dry biomass (W_m). It uses photosynthetically active solar radiation (PPFD) and temperatures (T) as inputs. Their parameters are presented in Table 12**.**

$$\frac{dN}{dt} = N_m \cdot f_N(T) \qquad \text{Equation 2}$$

$$\frac{dLAI}{dt} = \rho \cdot \delta \cdot \lambda(T_d) \cdot \frac{e^{[\beta(N-N_b)]}}{1 + e^{[\beta(N-N_b)]}} \cdot \frac{dN}{dt} \qquad \text{Equation 3}$$

$$GR_{net} = \mathrm{E} \cdot \left(P_g - R_m\right) \cdot [1 - f_R(N)] \qquad \text{Equation 4}$$

$$R_m = \sum Q_{10}^{(T-20)} \cdot r_m \cdot (W - W_m)\,\mathrm{dt} \qquad \text{Equation 5}$$

$$P_g = \sum \left\{ \frac{\mathrm{D} \cdot LF_{max} \cdot \mathrm{PGRED(T)}}{K} \cdot \ln\left[\frac{(1-m) \cdot LF_{max} + Q_e \cdot \mathrm{K} \cdot \mathrm{PPFD}}{(1-m) \cdot LF_{max} + Q_e \cdot \mathrm{K} \cdot \mathrm{PPFD} \cdot \mathrm{e}^{-\mathrm{K \cdot LAI}}}\right] \right\} \qquad \text{Equation 6}$$

$$\frac{dW}{dt} = GR_{net} - p_1 \cdot \rho \cdot \frac{dN}{dt} \qquad \text{Equation 7}$$

$$\frac{dW}{dt}_{max} = \frac{dW_F}{dt} + \{(V_{max} - p\}_1) \cdot \rho \cdot \frac{dN}{dt} \qquad \text{Equation 8}$$

$$\mathrm{g}\left(T_{daytime}\right) = 1.0 - 0.154 \cdot \left(T_{daytime} - T_{CRIT}\right) \qquad \text{Equation 9}$$

$$\frac{dW_F}{dt} = GR_{net} \cdot \alpha_F \cdot f_F(T_d) \cdot \left[1 - e^{\vartheta-(N-N_{FF})}\right] \cdot g\left(T_{daytime}\right) \qquad \text{Equation 10}$$

$$\frac{dW_M}{dt} = D_F\{(T\}_d) \cdot (W_F - W_M) \qquad \text{Equation 11}$$

For the sensitivity analyses performed, all parameters from Table 12 were sampled within a uniform distribution, in which Lim. 1 is the lower value and Lim. 2 is the upper value. Sources used as references for bounds estimates were: (1) (Jones et al., 1999); (2) (Jones et al., 1991); (3) (Jones et al., 1999), spreadsheet; (4) (Dayan et al., 1993b); (5) (Ramirez et al., 2004); (6) (Marcelis et al., 1998).

Table 12. Parameters from the Reduced Tomgro model.

Parameter	Fixed?	Lim. 1	Lim. 2	Sources
delta (δ) – Maximum leaf area expansion per node [m^2 leaf $node^{-1}$]	N	0.03	0.07	(1), (3), (5)
beta (β) – Coefficient in expolinear equation [$node^{-1}$]	N	0.1	0.5	(1), (3), (5)
N_b (N_b) – Project of linear segment of LAI vs N to horizontal axis [node]	N	10	25	(1), (3), (5)
alpha_F (α_F) – Maximum partitioning of new growth to fruit [fraction d^{-1}]	N	0.50	0.95	(1), (3), (5)
V (ϑ) – transition coefficient between vegetative and full fruit growth [$node^{-1}$]	N	0.1	0.27	(1), (3)
N_FF (N_{FF}) – nodes per plant when first fruit appears [node]	N	10	25	(1), (3)
T_crit (T_{CRIT}) – Mean daytime temperature above which fruit abortion starts [˚C]	N	22	29	(1), (3), (5)
K_F – development time from first fruit to first ripe fruit [node]	N	4	8	(1), (3)
DFmax – Average development rate used to move fruits from green to mature stage [d^{-1}]	N	0.02	0.10	(1), (3)
Vmax (V_{max}) – Maximum increase in vegetative tissue d.w. growth per node [g dw $node^{-1}$]	N	6.0	9.0	(1), (3), (5)
tmaxPg – Temperature below which photosynthesis decreases from maximum [oC]	Y	34	40	(2)
N_max (N_m)– Maximum rate of node appearance (at optimal temperatures) [node d^{-1}]	Y	0.4	0.7	(1), (3), (5)
Qe (Q_e) – Leaf quantum efficiency [μmol (CO_2 fixed) μmol $(photon)^{-1}$]	Y	0.055	0.09	(1), (3), (5)
tmin_fr_gr – Minimum temperature that affects fruit growth [˚C]	Y	6	10	(3)
sl_N1 – Parameter to modify node development rate [˚C^{-1}]	Y	0.02	0.03	(1), (3)
sl_N2 – Parameter to modify node development rate [˚C^{-1}]	Y	0.04	0.06	(1), (3)
sl_R – Parameter to modify partitioning of biomass to roots [$nodes^{-1}$]	Y	0.003	0.0035	(3)
tau1 – Carbon dioxide use efficiency [μmol (CO_2)/m^2 s ppm (CO_2)]	Y	0.06	0.1	(1), (3), (5)
tau2 – Carbon dioxide use efficiency for concentrations larger than 350 ppm [μmol CO_2 $(m^2 \text{ s ppm } CO_2)^{-1}$]	Y	0.058	0.1	(3)
TSlop – Parameter to reduce rate of leaf area expansion [˚C]	Y	18.54	22.66	(3)
E – Growth efficiency, ratio of biomass to photosynthate available for growth [g d.w. g^{-1}CH2O]	Y	0.6	0.8	(1), (3), (5)
K – Light extinction coefficient	Y	0.5	0.8	(1), (3), (6)
p_1 (p_1) – Loss of leaf d.w. per node after LAI_max is reached [g leaf $node^{-1}$]	Y	1.5	2.5	(1)
LAImax [m^2 m^{-2}]	Input	2.3	4.0	(1)

Representation in parenthesis refer to how they were presented in Equations Equation 2 to Equation 11.

Appendix B — ERROR METRICS

Table 13. Root mean squared error [g m^{-2}] from estimates of the state variable updated with data from different sources with the Unscented Kalman Filter and the Ensemble Kalman Filter, and from the model without assimilation with and without calibration.

State variable	Filter	Assim. state	Obs. variable*	Cycle 1		Cycle 2		Cycle 3	
				Plant 1	Plant 2	Plant 1	Plant 2	Plant 1	Plant 2
LAI	None – Calib.	-	-	-0.21	-0.21	-0.02	0.00	0.49	0.58
	None – Not Calib.	-	-	-0.21	-0.21	1.23	1.24	3.07	3.11
	EnKF	LAI	GC Lat	**-0.15**	**-0.16**	**1.02**	**0.94**	**1.47**	**1.55**
	UKF			**0.11**	**0.10**	**1.02**	1.27	3.35	3.76
	EnKF		GC Abv	**-0.05**	**-0.20**	**1.02**	1.29	3.34	**3.05**
	UKF			**0.13**	-0.21	**1.02**	1.48	3.33	**2.99**
W	None – Calib.		-	103.68	71.86	-25.10	-8.96	273.74	250.47
	None – Not Calib.	-	-	95.80	64.69	216.12	209.09	533.57	525.46
	EnKF	W	W_fm_full	**70.38**	127.88	**36.69**	**122.14**	**297.01**	**311.92**
	UKF	W		**75.84**	134.96	**5.74**	**128.88**	**257.07**	**290.18**
Wf	None – Calib.	-	-	-0.19	-25.18	-130.49	-109.63	-5.73	-26.20
	None – Not Calib.	-	-	85.70	76.98	-67.59	-63.32	164.10	160.55
	EnKF	Wf	Area Wf	**81.53**	**72.63**	**-54.75**	**-57.27**	169.09	**159.52**
	UKF	Wf		**67.98**	**24.55**	**-20.28**	**-36.60**	181.41	**141.26**

*Observations as: GC Lat: green cover (lateral view), GC Abv: green cover (above view), W_fm_full: weighting system, Area Wf: total area of fruits. Bold numbers refer to root mean squared errors lower than the larger RMSE between the non-calibrated and calibrated error.

Table 14. Root mean squared error [g m^{-2}] from estimates of yield updated with data from different sources with the Unscented Kalman Filter and the Ensemble Kalman Filter, and from the model without assimilation with and without calibration.

Filter	Assim. state	Obs. variable*	Cycle 1		Cycle 2		Cycle 3	
			Plant 1	Plant 2	Plant 1	Plant 2	Plant 1	Plant 2
None – Calib.	-	-	5.05	10.11	29.05	25.34	36.00	31.49
None – Not Calib.	-	-	20.48	17.95	22.45	21.72	62.21	61.12
EnKF	LAI	GC Abv	22.51	20.02	**26.17**	**19.35**	**46.95**	**40.83**
UKF			24.59	23.01	**29.04**	**21.19**	**49.05**	**46.43**
EnKF		GC Lat	25.54	19.22	65.40	40.92	63.77	**58.46**
UKF			27.15	20.24	64.35	41.75	63.62	**58.76**
EnKF	W	W_fm_full	44.70	**10.25**	35.88	7.59	89.27	**47.51**
UKF		-	20.76	**9.85**	7.19	11.40	71.73	71.65
EnKF	Wf	Area Wf	**19.76**	**14.79**	**22.89**	**21.78**	**61.27**	**56.49**
UKF			**14.47**	**9.26**	**5.91**	**8.99**	**61.55**	**51.25**

*Observations as: GC Lat: green cover (lateral view), GC Abv: green cover (above view), W_fm_full: weighting system, Area Wf: total area of fruits. Bold numbers refer to root mean squared errors lower than the larger RMSE between the non-calibrated and calibrated error.

Appendix C — Delving into the performance of greenhouse tomato growth models

Abstract

Models can be powerful tools to aid decision-making, but depending on the crop and location of production, their use is incipient. For greenhouse tomatoes growth, a lot has been done in model development, but there is more that could be done to allow for their use in low-tech environments. This work aims at discussing a few options for tomato modeling of greenhouse grown tomatoes, focusing on aspects of their uncertainties. We have implemented code for models of greenhouse tomato growth — the Reduced State Tomgro model and the model developed by Vanthoor and colleagues — and evaluated them in two distinct locations. We also evaluated the ability of a determinate growth tomato model — the Simple model — to represent indeterminate growth. We showed both models developed for protected environments may be deemed adequate to represent indeterminate growth in both locations assessed, albeit some improvement may be required for calibration, and that the model for field-grown tomatoes requires a few adaptations. We also showed that interannual weather variability affect parameter importance more than which location was evaluated. We observed that errors in the most important parameters may impact the outcome very substantially. This knowledge about those models may enhance the understanding of their uncertainties and applications that require such evaluations, such as calibration, will benefit from these analyses.

C1. Introduction

Almost twenty-five years ago, Marcelis et al. (1998) reviewed horticultural crop models focusing on their representation of growth and development processes. They discussed the existing approaches for calculating light interception, photosynthesis, respiration, and partitioning, concluding that the larger gaps in modeling these processes lied on the simulation of leaf area development, maintenance respiration, organ abortion, dry mass content and product quality. Among their examples for photosynthesis-based models of tomatoes, they mentioned Tomgro (Dayan et al., 1993a; Gary et al., 1995) and Tomsim (E Heuvelink, 1996). Heuvelink et al. (2018) summarized the subsequent progress in model development for tomatoes. For process-based models (PBM), it mainly consisted of the adaptation of previously existing models CropGro and Aquacrop to also simulate tomato growth (Boote et al., 2012; Katerji et al., 2013; Scholberg et al., 1997).

In both cases, the development was related to the simulation of field-grown tomatoes that, for the case of Cropgro-Tomato, was motivated by the inability of the previously developed Tomgro model to simulate field-grown tomatoes. McNeal et al. (1995) and Scholberg (1996) explored how they could adapt the model, but branching of the semi-determinate field cultivars impacted the number of nodes in the main stem as well as resulted in faster build-up and decline of leaf canopy in a way that Tomgro did not account for. The Cropgro-Tomato model has recently been evaluated under greenhouse conditions (Deligios et al., 2017), but it was a preliminary study and the authors suggested there should be further evaluations. Other process-based models not mentioned in Heuvelink et al. (2018) include the reduced-state version of the Tomgro Model (Jones et al., 1999) the model developed by Vanthoor et al. (2011), VegSyst (Gallardo et al., 2014; Giménez et al., 2013) and the Simple model (Zhao et al., 2019). Their developments are ascribed to multiple reasons, including previous models having an excessive number of parameters (Jones et al., 1999) or not being fully differentiable and being valid on a limited temperature range (Vanthoor et al., 2011), and to assist with N and irrigation management of greenhouse vegetable crops (Gallardo et al., 2011).

When Gary et al. (1998) commented on the advantage of modeling growth and development of fruits, vegetables, and ornamental plants, they mentioned, as others before them (Boote et al., 1996), how crop models could have value for scientists, growers and policy-makers. They also mentioned greenhouses as a specific cultivation system, that could be compared to industrial production systems, in which crop models could be used in different temporal and spatial scales, aiding in online control systems and crop planning. Since that work was published, models developed for greenhouse tomatoes have been integrated in control systems that include from temperature and humidity (Rodríguez et al., 2015) to lighting and heating (Katzin et al., 2020; Kuijpers et al., 2021; Righini et al., 2020). Other benefits for growers from PBMs relate to uncovering knowledge regarding plant growth. Berrueta et al. (2020) used the Tomsim model to estimate potential yield from the daily dry matter production in Uruguay, and then evaluated the yield gap of greenhouse growers, and Bojacá et al. (2009) used the Tomgro model to evaluate yield variability in greenhouses in Colombia. All this potential, however, has not been reflected in overall assessments of horticultural models.

The improvement and requirements of models for grasslands, field crops and livestock has been thoroughly discussed by Jones et al. (2017). Despite belonging to the same agricultural field of study, horticultural crops are often not included in crop modeling discussions. Granted, this has not halted progress in the horticultural modeling community, which has advanced in complex functional-structural plant modeling which, as expected by Evers and Marcelis (2019), could be used for optimizing greenhouse energy use and crop performance simultaneously. But while these advances happen, aspects such as uncertainty and model comparison are less frequently addressed in the already existing models, even when the goals of the wider community include quantifying issues of food security, nutrition and the need for change in diets to reduce greenhouse gases emissions (Antle et al., 2017; Mbow et al., 2019).

Among greenhouse tomato growth models, most evaluations refer to the Tomsim or the comprehensive Tomgro model (Bertin and Heuvelink, 1993; Dayan et al., 1993b; E. Heuvelink, 1996; Heuvelink, 1999; Heuvelink and Bertin, 1994) with the other models previously mentioned, accounting for fewer studies (Lin et al., 2019; Ramirez et al., 2004; Vazquez-Cruz et al., 2014). The Simple model, developed to address the gap in modeling vegetables, oil and fiber crops and fruits, has been evaluated on field-grown tomatoes, but not in greenhouse-grown, and no assessment of its performance for indeterminate growth has been done for tomatoes. As for uncertainty analysis, which is performed in order to assess a model's credibility (Antle et al., 2017), they are often limited and sensitivity analyses are mostly local, without or only partially accounting for non-linearities and interactions (Bertin and Heuvelink, 1993; Cooman and Schrevens, 2007, 2006; Heuvelink and Bertin, 1994; Ramirez et al., 2004; Vanthoor et al., 2011; Vazquez-Cruz et al., 2014).

Finally, while several publications point to the usage in high-technology greenhouses (Katzin et al., 2020; Kuijpers et al., 2021; Righini et al., 2020), there is a great fraction of the environments that are defined as low-tech (Montero et al., 2019) and these have not been the focus of those analyses. By evaluating models on those conditions and making them more available, these production settings could have more to rely on than solely data-driven models.

There are several fronts in which greenhouse tomato growth models may be brought closer to the broader discussions of the community. This work aims to do that by analyzing two greenhouse tomato growth models, assessing their ability to represent growth and their uncertainties in two different locations. We also evaluate the Simple model in the context of protected cultivation of tomatoes.

C2. Materials and methods

C2.1 Data

Field data used in this work was obtained from experiments used in the development of the Reduced Tomgro Model (Jones et al., 1999) and from an experiment performed in a low technology plastic greenhouse in Brazil[3], respectively from Gainesville, Florida, United States, and Campinas, São Paulo, Brazil. Historical radiation and air temperature were gathered from the NASA POWER Data Access Viewer, Single Point Data Access Tool. Solar radiation interpolation throughout the day used the equations in Spitters et al. (1986) and Lizaso et al. (2003) and air temperature interpolation, the equations in Parton and Logan (1981).

C2.2 Models

Three models were used in this work: the Reduced-State Tomgro Model, the model presented in Vanthoor et al. (2011), which we call Vanthoor model, and the Simple model. Code for all models was written and run in Python 3.8 and is available in an only repository, as is the remainder of the code used in this work[4]. The Reduced Tomgro implementation used (Jones et al., 1999, 1991) as sources and the spreadsheet provided by Dr James W Jones. The R code for the SIMPLE model was also shared by the team and along with the information in Zhao et al. (2019), it was used to rewrite the code. Source codes and original data allowed for a more thorough validation of the models. The Vanthoor model implementation was based in the simplified version by Katzin et al. (2020) and in the supplementary material from Vanthoor et al. (2011).

C2.3 Calibration

Both the Reduced-State Tomgro and the Simple model are explicit about which parameters should be calibrated and which are treated as fixed. For the Vanthoor model, while the authors treated in their validation all parameters related to the growth inhibition and photosynthesis functions and fruit growth period as fixed, they acknowledged these parameters

[3] Data available at https://doi.org/10.25824/redu/EP4NGO
[4] https://github.com/mnqoliveira/data-assimilation-tomato-models

probably should be calibrated. For the Simple model, to represent indeterminate growth and postpone senescence, we allowed the maturity parameter to reach upper limits larger than the ones observed in Zhao et al. (2019).

All parameters available for calibration are described in Supplementary Material 1. As field data was limited, not all of them were included in calibration, to avoid over-parameterization. The results of the sensitivity analysis of parameters in section 2.4.1 were used to select those that would be calibrated. Fixed parameters that were included refer to our assessment of the possibility of them being calibrated for greenhouse-grown tomatoes. Calibration followed the approach of minimizing the root square of squared error of the difference of log-transformed observations and estimates, using a global optimization algorithm. All parameters were calibrated simultaneously.

C2.4 Uncertainty and sensitivity analysis

Uncertainty analysis in this work has two goals. The first one is to determine which parameters affect state variables the most throughout the cycle. The other goal is aimed at determining the effect of uncertainty in weather inputs, which could be ascribed to internal variability in a greenhouse or measurement errors. Even though uncertainty and variability are different concepts, they could be ascertained through the same strategy. These different goals require different approaches. In both cases, the number of runs was increased until stable results for the sensitivity indices were obtained.

C2.4.1 Parameters and inputs

A wide range of weather series, referring to the studied locations, was used to assess parameters across several ranges of external factors. Since environmental inputs are intimately correlated, instead of randomly generating these, multiple examples were drawn from actual weather series.

For each time-series of the 20 years selected and 4 planting dates with a length of 160 days, the model was run with parameter values from Supplementary Material 1 sampled following Saltelli's extension of the Sobol sequence[5]. Inputs refer to historical weather of the Campinas and Gainesville regions. While temperature is maintained as is, assuming natural or mechanical ventilation, radiation is reduced to 70%, ascribed to cover material transmissivity.

[5] Sampling used SALib library (Herman and Usher, 2017).

CO_2 was sampled to represent modifications to the environment either by accumulation or depletion. While keeping the internal temperature the same as the outside led to unlikely low temperatures, we assumed passive low-tech greenhouse, in which these problems exist.

Total number of runs accounted for the combinations of five thousand samples of each parameter. The maximum value of the leaf area index, or its equivalent of intercepted solar radiation, is an input in all models and was included in the analysis as it is intimately related to canopy photosynthesis and, therefore, growth, in all models. For the Vanthoor model, the input that corresponds to the beginning of the generative phase was also included.

C2.4.2 Greenhouse internal variability

Parameters' values refer to the ones obtained in the calibration of each original dataset (Gainesville and Campinas). As for weather inputs, variations should be consistent with minor variability across the time-series, as the parameters used could not be valid if weather inputs differ by much from the calibration condition. So, to account for autocorrelation between adjacent values, as well as between variables, but also considering that measurement error could in fact lead to incompatible measurements, the sampling strategy applied a uniform change to the series. This perturbation was drawn from Saltelli's extension of the Sobol sequence with normal distribution, with zero mean, to account for positive and negative changes, and a standard deviation of 0.05, which would then be multiplied and added to the measured values. Radiation and carbon dioxide concentrations were bounded to a minimum value of zero. Total number of runs was of 50 thousand to account for the combinations of 10 thousand samples of each variable, i.e. average, maximum and minimum temperatures, solar radiation and carbon dioxide concentration.

C3. RESULTS

C3.1 Model comparison

Overall, both models developed for greenhouse tomatoes were able to capture the trends and magnitudes of all variables in both datasets (Figure 1). The Reduced Tomgro Model adequately represented leaf area index and fruit biomass in all datasets, but while it also adequately represented aboveground biomass and mature fruit biomass in the Gainesville dataset, this did not happen in the Campinas dataset, in which it underestimated both variables. The Vanthoor model underestimated all variables in all datasets, except for fruit biomass in the

Campinas dataset. The expected effect on fruit biomass caused by instant temperatures should have been observed in the Gainesville dataset, which included different temperature scenarios, but this was not the case and all three experiments had approximately the same estimates.

The absence of this effect may be associated to the calibration approach used. On the one hand, it led to results for the Reduced Tomgro model in the Gainesville dataset that are compatible with the ones previously obtained by the models' developers. On the other hand, to reach the observed curves in the Vanthoor model, calibration led to parameters that do not properly represent the meaning ascribed to them. As optimal temperatures are expressed by combining two curves, parameters that characterize them were changed so that optimal ranges were no longer observed in both datasets. It also led to the maximum instantaneous temperature parameter to be equal to the twenty-four-hour average, which is not representative of the intended effect.

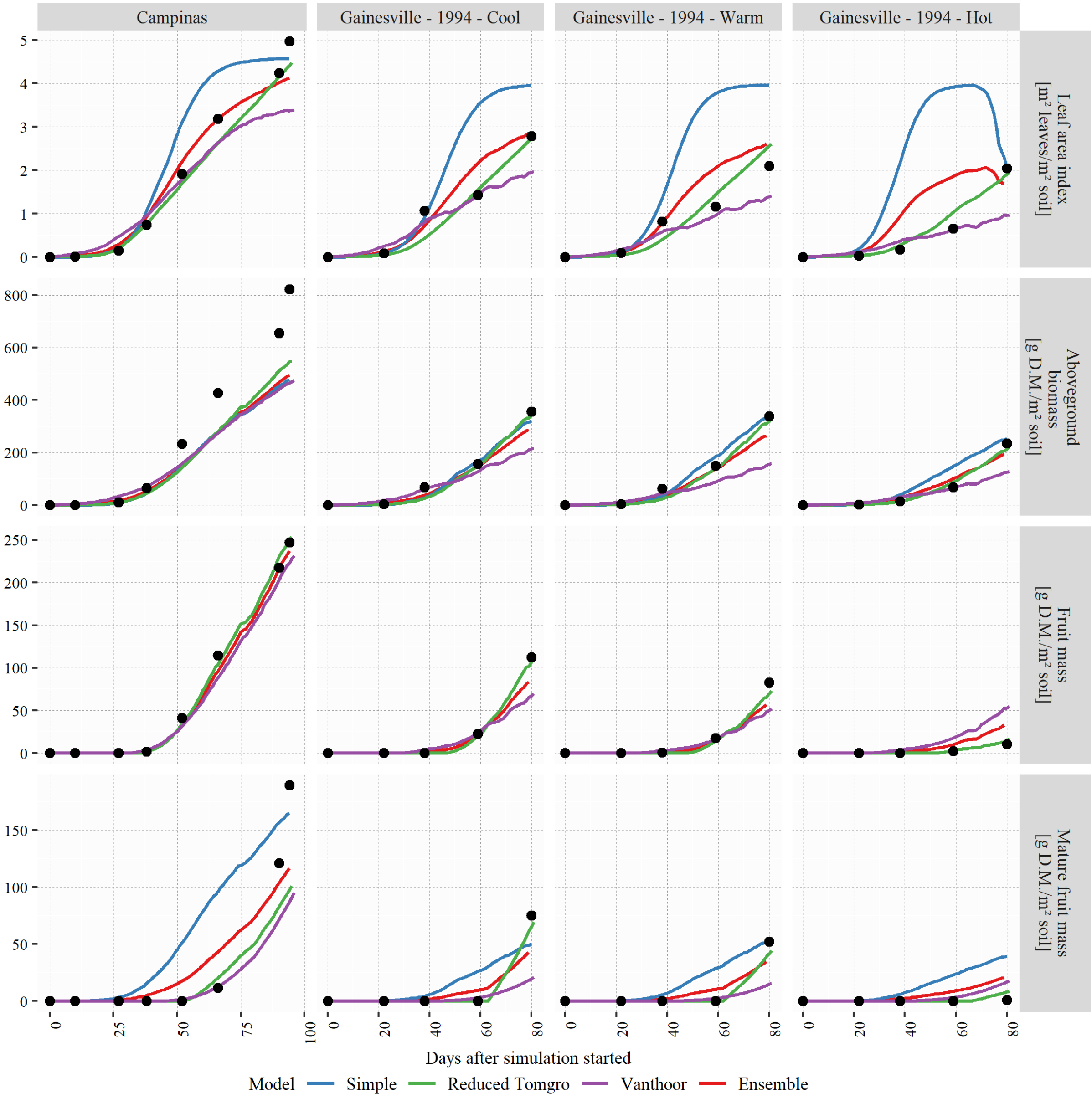

Figure 1. Model comparison after calibration. Black dots refer to the average of measured values and lines refer to simulations performed in the respective environments.

The Simple model was not able to adjust to observed values in the Gainesville dataset, seemingly because to be able to optimize both biomass accumulation and solar radiation interception simultaneously, the model often reached maximum values of the fraction of intercepted radiation, which was not observed in the experiments. Although it tracked the magnitude of the equivalent leaf area in the Campinas dataset, it also underestimated biomass. As the yield is estimated as a fixed fraction of biomass, calibration of the harvest index may adjust the final value observed. However, as the advantages of indeterminate growth models include estimates of intermediate harvests, this fixed relationship would suggest that mature fruits are available through all growth, overestimating mature fruit availability in the first months.

By averaging models' daily outputs into an ensemble, the shortcomings were smoothed into good estimates. Although the outputs for aboveground biomass in Campinas, could not be improved, as it was underestimated by all models, the ensemble results were better than the ones obtained by the Vanthoor model in Gainesville.

C3.2 Uncertainty and sensitivity analysis

C3.2.1 Model parameters

Sensitivity analyses in model parameters show mainly two results: different locations may show similar patterns for indices and interannual weather variability may impact the importance of a parameter more than its location. Figure 2 shows the total sensitivity index calculated for the Reduced Tomgro model, Figure 3, for the Vanthoor model and Figure 4, for the Simple model. We focus on mature fruit mass estimates to limit the number of variables. Supplementary Material 2 includes state variables beyond yield.

In both Vanthoor and Reduced Tomgro models, the most important parameters are connected to the effect of high temperatures in yield. In the Reduced Tomgro model, this effect is seen in the importance of *T_crit*, which is the mean daytime temperature above which fruit abortion starts, and in the Vanthoor model, in the importance of *ksMaxTCan* and *ksMaxTCan24*, which govern the upper limits of optimal temperatures. The other pronounced effect is of development and partitioning, noticed in the *DFmax* and *alpha_F*, in the Reduced Tomgro model, parameters which govern moving fruits from green to mature stage and partitioning to fruits from available carbohydrates, respectively, and in *ttsum* and *nDev* in the Vanthoor model, parameters connected to fruit appearance and to the beginning of harvest. From the inputs included, the Vanthoor model was the most affected, with *ttsum* having the largest importance through the whole cycle and *laiMax* appearing by the end of the evaluated period.

As the models were developed with different approaches, the Reduced Tomgro model with its individual equations for each state variable shows influence of parameters that can be ascribed to other state variables, such as *N_max*, which influences the rate of node appearance. Meanwhile, in the Vanthoor model, this distinction is not as pronounced and apart from the maximum leaf area, which could be connected to the leaf area state variable, other parameters influence all variables simultaneously. This is a consequence of the model being a pool of carbohydrates that is distributed to plant organs.

As for the Simple model, even though yield is only calculated by the end of the cycle, we can observe the progress in the indices, as if the growth is considered indeterminate. The same effect of parameters related to temperatures (*I50A* and *T_base*) being more or as important than the constant attributed to partitioning (*HI*) is observed.

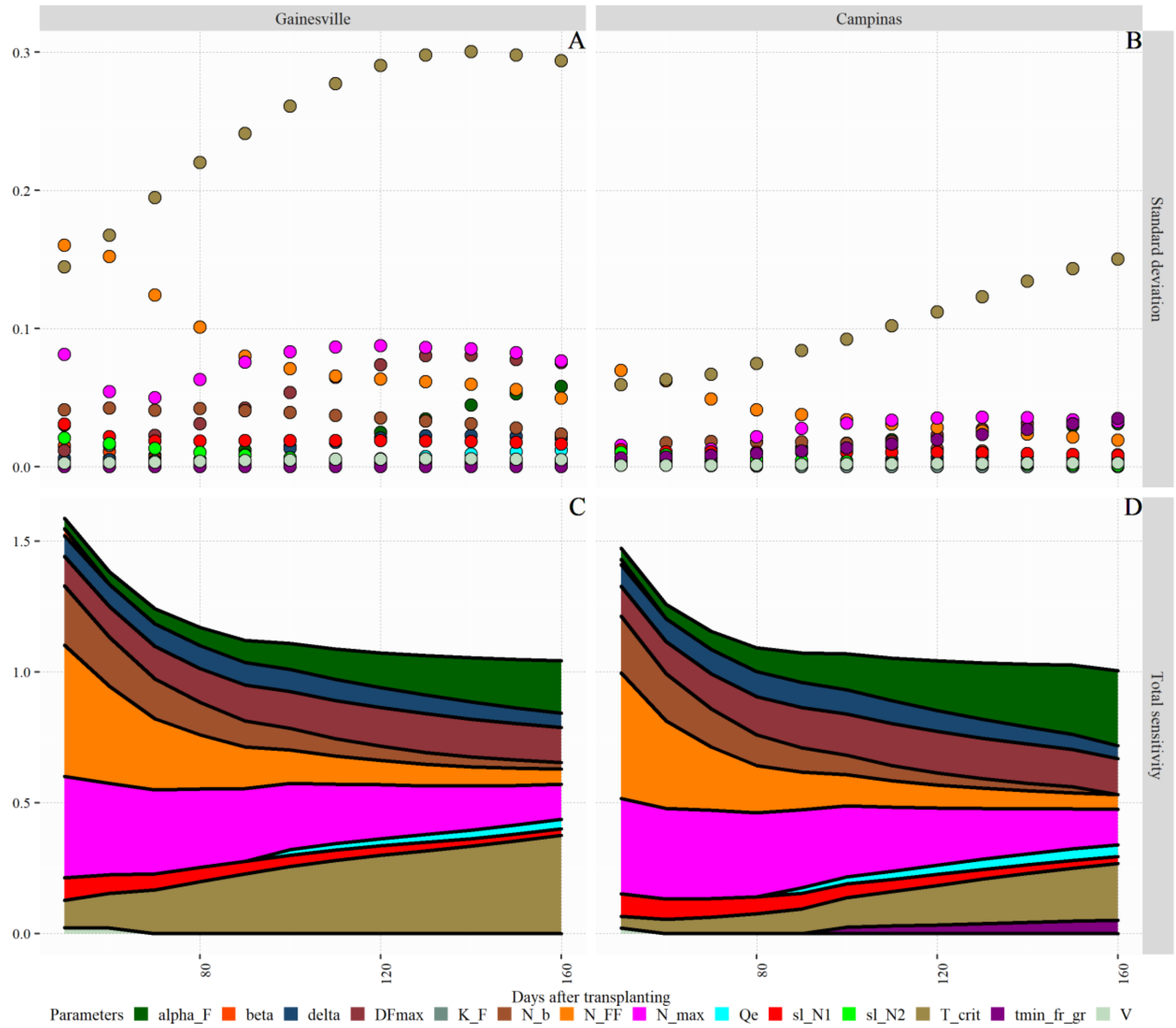

Figure 2. Total effect sensitivity indices of yield to models' parameters for the Reduced Tomgro model with the Gainesville (panels A and C) and Campinas (panels B and D) historical weather datasets. Parameters' full names are presented in the Supplementary Material. The upper graphs (A and B) refer to the standard deviation of the total sensitivity index in all the scenarios evaluated. The lower graphs (C and D) refer to the average total sensitivity index for each parameter through the cycle. Only averages larger than 0.02 are shown. The X axis starts at 40 days after transplanting as before often there is a lot of instability in averages.

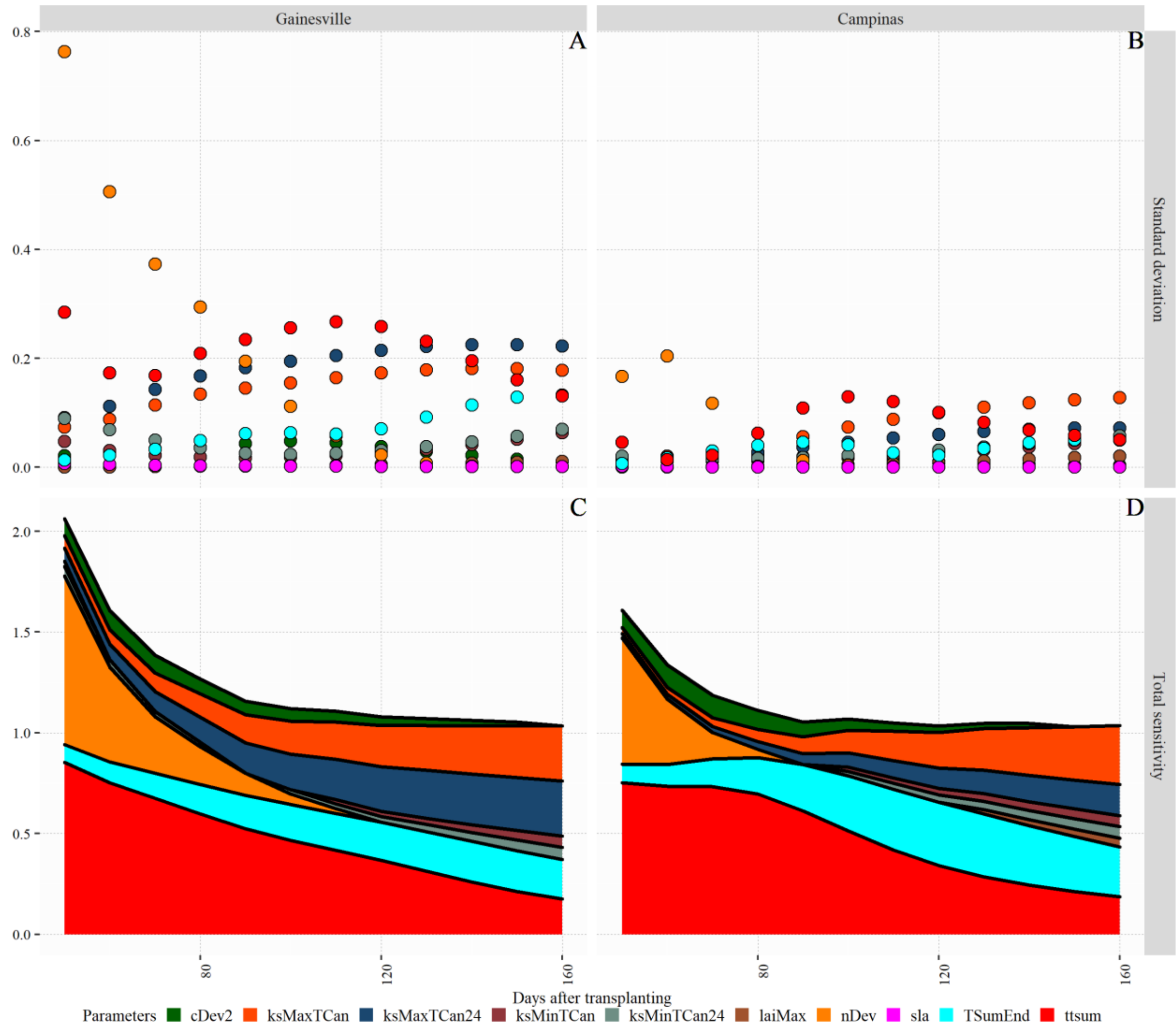

Figure 3. Total effect sensitivity indices of yield to models' parameters for the Vanthoor model with the Gainesville (panels A and C) and Campinas (panels B and D) historical weather datasets. Parameters' full names are presented in the Supplementary Material. The upper graphs (A and B) refer to the standard deviation of the total sensitivity index in all the scenarios evaluated. The lower graphs (C and D) refer to the average total sensitivity index for each parameter through the cycle. Only averages larger than 0.02 are shown. The X axis starts at 40 days after transplanting as before often there is a lot of instability in averages.

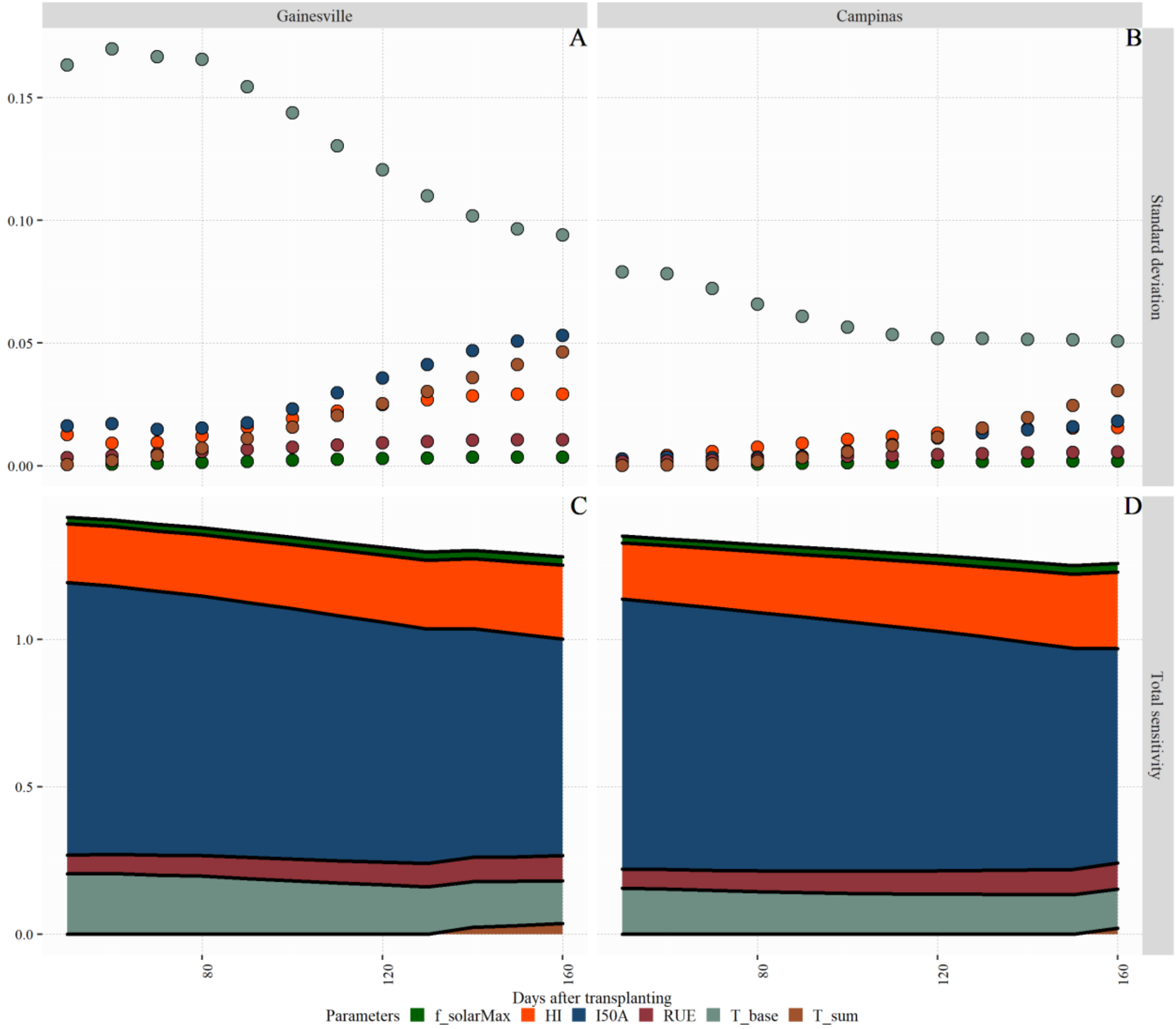

Figure 4. Total effect sensitivity indices of yield to models' parameters for the Simple model with the Gainesville (panels A and C) and Campinas (panels B and D) historical weather datasets. Parameters' full names are presented in the Supplementary Material. The upper graphs (A and B) refer to the standard deviation of the total sensitivity index in all the scenarios evaluated. The lower graphs (C and D) refer to the average total sensitivity index for each parameter through the cycle. Only averages larger than 0.02 are shown. The X axis starts at 40 days after transplanting as before often there is a lot of instability in the averages.

Figures 2 to 4 show the standard deviation of the index across years. The largest standard deviations are observed in the Vanthoor model in the Gainesville dataset, likely since most parameters evaluated are related to temperatures and those are the most affected variables when comparing weather inputs from different years and locations. For the *ttsum* parameter, the standard deviation is larger than 0.2 in Gainesville, when its value is about 0.5 and may signify that the combination of season-year impacts more the index than when comparing to Campinas. In the Reduced Tomgro model, the largest standard deviations are observed for *T_crit*, which is directly related to environmental conditions, as well as *N_FF* and *N_max*, parameters connected to the number of nodes, which evolve based solely on temperatures.

Largest standard deviation connected to temperature is also observed in the Simple model and the parameter *I50A*, as it is also connected to cumulative temperature.

The largest total sensitivity indices mean the largest fraction of the variance observed on the output is ascribed to that parameter, so a change in a parameter index through growth means the fraction is different for the same parameter in different moments. Figure 5 shows one example of the different curves obtained for yields in one random weather scenario if the maximum or minimum value of the most important parameters — considering the average index through the cycle — are used. One can see how important parameters either lead to very different outcomes or, in the case the outcomes are similar, a clear divide existed at some point during growth, disappearing afterward. One example comes from *ttsum* in the Vanthoor model which creates differences in the beginning of the cycle, but not by the end.

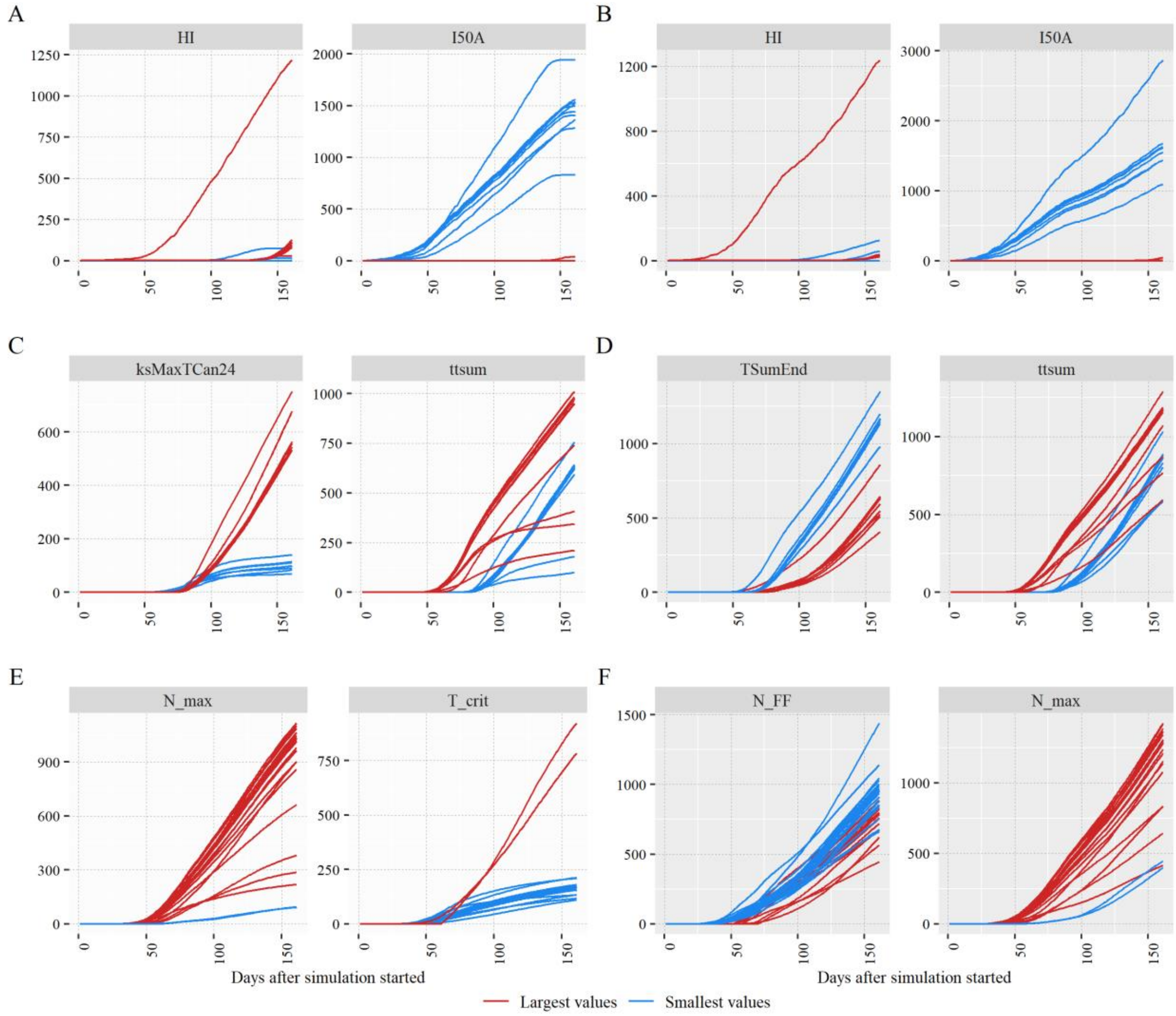

Figure 5. Simulations of yield using maximum and minimum values of selected parameters with highest total sensitivity index for one weather scenario. The lighter background refers to results in Gainesville weather (A, C and E) and the darker background, in Campinas (B, D and F). First line (A and B) refers

to outcomes of the Simple model, second line (C and D), to the Vanthoor model and third line (E and F), to the Reduced Tomgro model.

C3.2.1 Weather inputs

We focus on the results from the Reduced Tomgro (Figure 6) and the Vanthoor (Figure 7) models, which more closely resembled observed growth and development patterns. Sensitivity indices in this case represent which environmental measurements, if slightly different, would affect model outcomes the most. The results from these analyses are intimately connected both to the way state variables are represented in the models and to the environmental conditions. For example, leaf area index in the Reduced Tomgro model is defined by an equation that solely relies on the temperature while in the Vanthoor model, it is converted from biomass destined to the leaves. It is to be expected that for leaf area, solar radiation and carbon dioxide affect more the leaf area outcomes in the Vanthoor model than in the Reduced Tomgro model, even though, in both cases, temperatures dominate the variance in the results, leading to higher indices. As for the environment, one can notice how temperatures become more relevant for aboveground biomass as the scenarios in the Gainesville dataset move from Cool to Warm, and since solar radiation and carbon dioxide concentrations remained the same, this effect reflects how the results from one factor are relative to the other.

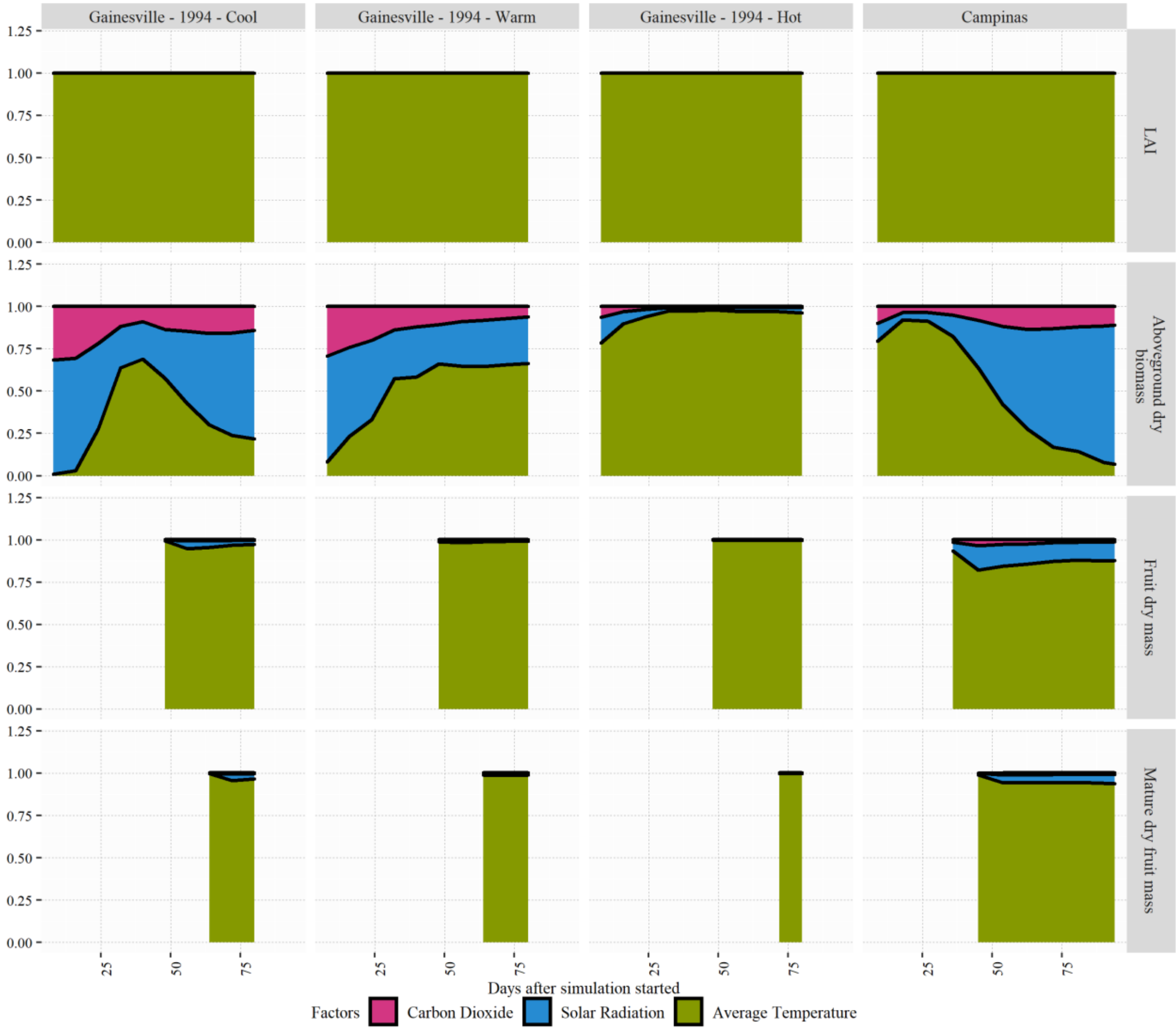

Figure 6. Total effect of input factors on variables simulated by the Reduced Tomgro model. Values not shown refer to the absence of variability on the variable by that point in growth.

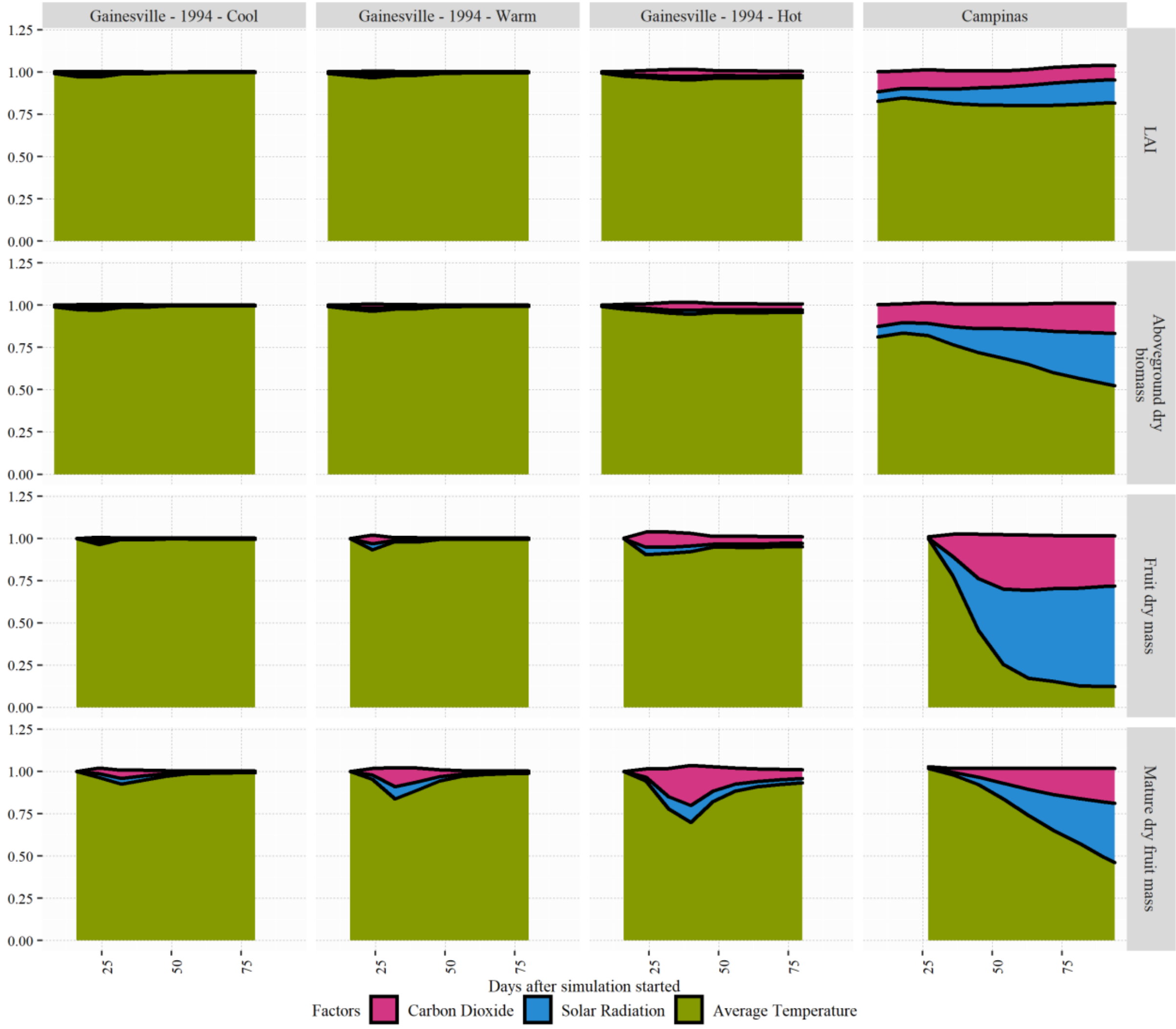

Figure 7. Total effect sensitivity indices of input factors on variables simulated by the Vanthoor model. Values not shown refer to the absence of variability on the variable by that point in growth.

In the Campinas dataset, one can also observe how there is a shift in the importance of solar radiation for aboveground biomass in the Reduced Tomgro model, as well as for fruit weight in the Vanthoor model. These could mean that, in fact, larger errors in solar radiation measurements could impact those variables more, but it could also reflect how lower temperatures were being recorded by the end of the cycle so that the perturbations applied did not impact the outcome as much as the ones of other variables. Either way, both models were not as sensitive to changes in carbon dioxide in the environment, although the Vanthoor model was more influenced by this input. It should be noted that carbon dioxide was estimated by concentrations outside the greenhouse, so these results could be improved by measured values.

Table 1 exemplifies the differences in yield caused by extreme values of the parameters. As the disturbances were sampled from normal distributions, the results shown refer to perturbations larger than 18% in the observed input. As suggested by the total sensitivity index, average temperature has a large impact on yield in both models.

Table 1. Summary of uncertainty in yield, characterized by the range of observed values, caused by artificial systematic errors in input measurements, as simulated by the perturbation of measured inputs.

Model	Factor	City	Minimum yield [g DM m^{-2}]	Maximum yield [g DM m^{-2}]
Reduced Tomgro	Average temperature	Campinas	51.8	155.2
	Solar radiation		118.6	147.8
	CO_2		127.9	135.7
	Average temperature	Gainesville - Cool	51.4	97.2
	Solar radiation		51.5	73.1
	CO_2		61.5	64.7
Vanthoor	Average temperature	Campinas	51.4	97.2
	Solar radiation		91.0	146.0
	CO_2		95.5	134.7
	Average temperature	Gainesville - Cool	2.7	84.2
	Solar radiation		68.1	88.4
	CO_2		74.2	84.8

C4. DISCUSSION

C4.1 Model comparison

Models for indeterminate growth of tomato plants have been developed and are being used to different degrees of support in production, but with fewer examples for low-technology greenhouses. Our qualitative evaluation showed they are able to describe overall growth, but we can observe biases in the estimates, which are amplified when converted to fresh mass, which is the quantity of interest (Marcelis et al., 1998). On the other hand, there is also an issue that these models represent cumulative harvests, accumulating errors as well, and the impact on each harvest would not be as large.

Model structure of the evaluated greenhouse-tomato models are quite different as, for the Vanthoor model, each state variable may influence the other, as available carbohydrates are drawn for the organs from the same pool. The Reduced Tomgro model is constituted by individualized equations and up to a point, it is possible to show good adjustment to a variable and not to other. For instance, fruit biomass does not rely explicitly on aboveground biomass, as it recalculates available carbohydrates, which could explain the good fit for this variable in the Campinas dataset, but not for aboveground biomass. Temperature effects seemed to have been captured in the Reduced Tomgro model, leading to high temperatures for impacting fruit establishment, but not in the Vanthoor model, as observed in the Gainesville dataset.

While we expect calibration to account for accommodating differences in cultivars, for example the original optimal growth range in the Vanthoor model which is 18 °C to 22 °C, being different from Brazilian recommendations from 20 °C to 25 °C (Alvarenga, 2013), we also observed other issues in the process. For example, optimization for the error metric used led to underestimating mature fruit biomass, as low observations in one day had larger weight than the others, but this was a limitation of simultaneously accounting for all variables, as required by the structure of the Vanthoor model. As previously mentioned, the parameters that account for optimal temperatures led to values that would always penalize the conversion of carbohydrates in the buffer to plant organ growth. We also decided for allowing one parameter accounting for development rate *TSumEnd* to reach much larger values than the whole cycle, to accommodate for the case of the process not being fully represented. Another decision that could have influenced the results was to approximate total biomass as 90% of the calculated biomass, to exclude root biomass, which is calculated in the model along with stem biomass.

The Simple model showed promising results in the Campinas dataset, but it should be adapted to fully accommodate indeterminate growth, i.e., after the initial vegetative phase, inflorescences appear indefinitely after every three leaves, leading to an expo-linear growth pattern (Heuvelink et al., 2018; Heuvelink and Okello, 2018). Although the model uses a daily step and provides estimates of yield for all the cycle, the proportion between total biomass and accumulated mature fruit mass changes through growth, before the effect of vegetative mass from the beginning is negligible, so a harvest index may not be defined for shorter cycles. A second aspect is that the parameter *T_sum* is related to reaching physiological maturity, but also determines the beginning of senescence. The result for LAI in the hot scenario of the Gainesville dataset properly identifies senescence of leaves, which exists, but as the model was not defined for indeterminate growth, it does not represent senescence of old leaves and pruning being compensated by new growth, so that leaf area is expected to remain approximately constant. Finally, in the Gainesville dataset, to be able to reach total biomass, the model also reached the maximum fraction of intercepted solar radiation, which could have also been compensated by modifying radiation use efficiency (RUE). This is treated in the model as a species parameter, and at first, it could be considered fixed. But it is possible that the value could be adjusted from

1.05 g MJ total radiation^{-1} (2.1 g MJ PAR^{-1}) to 2 g MJ total radiation^{-1}, closer to the observed in the Hortsyst and Vegsyst models (Gallardo et al., 2014), in which it was defined as 4.01 g MJ PAR^{-1}. This change is also supported by Higashide and Heuvelink (2009) and Heuvelink et al. (2018), who pointed to light use efficiency value for modern greenhouse cultivar ranging from 3.3 to 3.5 g MJ PAR^{-1}.

These three different model structures also showed an example in which one may take advantage of model ensembles for improvement of predictive performance. For example, aspects in which the Simple model poorly represented indeterminate tomato growth were compensated by the ability of other models to do so. And while the other models underestimated yield in Campinas, the Simple model was able to help increase the estimates.

C4.2 Uncertainty and sensitivity analyses of parameters

Observing changes in parameters' sensitivity indices through growth was of interest for two reasons. The first is that as our sensitivity analyses informed calibration, observing parameters that impacted the outcomes through the whole cycle allowed for choosing and adjusting parameters that would influence how a model would represent the different state variables. The other reason is that as this is an example of indeterminate growth, fruit and mature fruit weight show different behaviors at least before the stabilization of continuous harvesting.

Changes in indices through the cycles are expected, as plants develop and given different weather, they develop in different rates. For indeterminate growth of tomatoes, it could also be expected that after reaching a certain stage in growth, for similar weather conditions, changes in indices should not be very substantial. And as we are concerned here with protected cultivation, different weather conditions could be highly reduced as more control over the environment is possible. But since this is not always the case for low-technology greenhouses, weather variability may affect the indices, as progress in season also means changes in the weather, leading to the high variability still observed in indices by the end of the cycle.

The structure of the Reduced Tomgro model leads to very few points in which one state variable depend on the other, differently from the Vanthoor model. This seemingly leads to other state variables not influencing yield as much. This does not entail that a parameter should not be adjusted if it is no longer appearing as important by the end of the cycle. In this case, an error on its estimation could lead to systematic bias that no longer affect variability in the outcome. This is observed for phenology parameters, which for example, if they lead to earlier fruit production, fruit biomass may be systematically increased. This also suggests that timing of sampling may affect calibration results and that good quality or more observations for the different state variables at different moments of the cycle may be desirable. On the other hand, we included the leaf area input as it is harder for growers to determine and we wanted to assess how it could impact results. While leaf area progress estimates would be harmed, if the goal is determining yield, the results seem to allow for using the model even if this information is not precisely defined. In the case of both greenhouse tomato models, if maximum leaf area is reached before fruit growth, yield will not be affected, otherwise, only first trusses are supposed to be affected and would not sum up to large differences. This is likely connected to leaf area index being more relevant in the beginning of growth, so that after light interception saturation, other factors are more relevant (Heuvelink et al., 2005).

Another aspect of our analysis refers to the choice of performing global sensitivity analyses, which had two motives: interactions among factors are neglected in local analyses, but also that the outcomes of calibration influence local analyses, as those parameters are treated as fixed elements. Local analysis may then reflect only the conditions associated to calibration. As we observed, even for the same location, models may have very different outcomes in different years, as they rely more on different parameters. Variability shows how calibration that works for one year may not work for the other as an optimization may reach low values for the cost function without ascribing the best value for a parameter if in that environment it does not affect the result as much. While our analysis ascribed uncertainty to all parameters and this could lead to unrealistic noise, because living systems contain homeostatic regulations that dampen variations (Gary et al., 1998), it is the case that determining parameters values without directly measuring them could input this noise into the estimates and our choice was to take this issue into account. We also discuss total sensitivity and this is more prone to include combinations that could not exist, which were not excluded from the analysis as this is difficult to estimate.

C4.3 Uncertainty and sensitivity analyses of weather

From the perspective of internal variability, it is to be expected that radiation and carbon dioxide do not vary much in a naturally or mechanically ventilated greenhouse, but as temperatures may, and we can observe that yield is sensitive to average temperature, we note that models can characterize the effects of this variability. From the perspective of errors in measurement, the more extreme environmental conditions are, the more likely they will impact outcomes if wrongly measured. In the conditions evaluated, we noted that temperatures dominate yield estimates, which is interesting given they are more easily measured and including more sensors to reduce the error could be feasible.

C5.CONCLUSION

In this work, we explored, through the steps of calibration, uncertainty, and sensitivity analyses, how models would perform in low- or medium-technology greenhouses. We showed that for these environments, greenhouse-grown tomato models may show high uncertainty in their parameters, to the point of substantially changing the outcome of a simulation if they are wrongly determined. In the same sense, if there is no limitation to growth caused by the environmental factors, temperature is the factor with highest total sensitivity index, which is positive given including more measurements to reduce uncertainty or bias in the value is less costly than including more measurements of solar radiation.

Although we were able to perform simulations that closely resembled observed values, more attention may be required to the calibration step, as simultaneous calibration with a global optimization algorithm is leading to parameters that do not correspond to their expected meaning.

C6.ACKNOWLEDGEMENTS

This study was financed in part by the Coordenação de Aperfeiçoamento de Pessoal de Nível Superior - Brasil (CAPES) - Finance Code 001, by grant #2018/12050-6, São Paulo Research Foundation (FAPESP) and by the Fulbright Commission in Brazil, through the Fulbright Foreign Student Program. Data were in part obtained from the NASA Langley Research Center (LaRC) POWER Project funded through the NASA Earth Science/Applied Science Program. We also thank Dr James W Jones for providing access to the spreadsheet that was originally used to perform model calculations.

C7.LITERATURE CITED

Alvarenga, M.A.R., 2013. Tomate: produção em campo, casa de vegetação e hidroponia, 2nd ed. Editora Universitária de Lavras, Lavras.

Antle, J.M., Basso, B., Conant, R.T., Godfray, H.C.J., Jones, J.W., Herrero, M., Howitt, R.E., Keating, B.A., Munoz-Carpena, R., Rosenzweig, C., Tittonell, P., Wheeler, T.R., 2017. Towards a new generation of agricultural system data, models and knowledge products: Design and improvement. Agric. Syst. 155, 255–268. https://doi.org/10.1016/j.agsy.2016.10.002

Berrueta, C., Heuvelink, E., Giménez, G., Dogliotti, S., 2020. Estimation of tomato yield gaps for greenhouse in Uruguay. Sci. Hortic. (Amsterdam). 265, 109250. https://doi.org/10.1016/j.scienta.2020.109250

Bertin, N., Heuvelink, E., 1993. Dry-matter production in a tomato crop: Comparison of two simulation models. J. Hortic. Sci. 68, 995–1011. https://doi.org/10.1080/00221589.1993.11516441

Bojacá, C.R., Gil, R., Cooman, A., 2009. Use of geostatistical and crop growth modelling to assess the variability of greenhouse tomato yield caused by spatial temperature variations. Comput. Electron. Agric. 65, 219–227. https://doi.org/10.1016/j.compag.2008.10.001

Boote, K.J., Jones, J.W., Pickering, N.B., 1996. Potential uses and limitations of crop models. Agron. J. 88, 704–716. https://doi.org/10.2134/agronj1996.00021962008800050005x

Boote, K.J., Rybak, M.R., Scholberg, J.M.S., Jones, J.W., 2012. Improving the CROPGRO-Tomato Model for Predicting Growth and Yield Response to Temperature. Hortscience 47, 1038–1049.

Cooman, A., Schrevens, E., 2007. Sensitivity of the Tomgro Model to Solar Radiation Intensity, Air Temperature and Carbon Dioxide Concentration. Biosyst. Eng. 96, 249–255. https://doi.org/10.1016/J.BIOSYSTEMSENG.2006.10.011

Cooman, A., Schrevens, E., 2006. A Monte Carlo Approach for estimating the Uncertainty of Predictions with the Tomato Plant Growth Model, Tomgro. Biosyst. Eng. 94, 517–524. https://doi.org/10.1016/j.biosystemseng.2006.05.005

Dayan, E., van Keulen, H., Jones, J.W., Zipori, I., Shmuel, D., Challa, H., 1993a. Development, calibration and validation of a greenhouse tomato growth model: I. Description of the model. Agric. Syst. 43, 145–163. https://doi.org/10.1016/0308-521X(93)90024-V

Dayan, E., van Keulen, H., Jones, J.W.W., Zipori, I., Shmuel, D., Challa, H., 1993b. Development, calibration and validation of a greenhouse tomato growth model: II. Field calibration and validation. Agric. Syst. 43, 165–183. https://doi.org/10.1016/0308-521X(93)90025-W

Deligios, P.A., Cossu, M., Murgia, L., Sirigu, A., Urracci, G., Pazzona, A., Pala, T., Ledda, L., 2017. Modeling tomato growth and production in a photovoltaic greenhouse in southern

Italy, in: Acta Horticulturae. International Society for Horticultural Science, pp. 203–210. https://doi.org/10.17660/ActaHortic.2017.1182.24

Evers, J.B., Marcelis, L.F.M., 2019. Functional—structural plant modeling of plants and crops, in: Boote, K. (Ed.), Advances in Crop Modelling for a Sustainable Agriculture. Burleigh Dodds Science Publishing Limited, Cambridge, pp. 45–68. https://doi.org/10.19103/AS.2019.0061.02

Gallardo, M., Giménez, C., Martínez-Gaitán, C., Stöckle, C.O., Thompson, R.B., Granados, M.R., 2011. Evaluation of the VegSyst model with muskmelon to simulate crop growth, nitrogen uptake and evapotranspiration. Agric. Water Manag. 101, 107–117. https://doi.org/10.1016/j.agwat.2011.09.008

Gallardo, M., Thompson, R.B., Giménez, C., Padilla, F.M., Stöckle, C.O., 2014. Prototype decision support system based on the VegSyst simulation model to calculate crop N and water requirements for tomato under plastic cover. Irrig. Sci. 32, 237–253. https://doi.org/10.1007/s00271-014-0427-3

Gary, C., Barczi, J.F., Bertin, N., Tchamitchian, M., 1995. Simulation of individual organ growth and development on a tomato plant: a model and a user-friendly interface. Acta Hortic. 199–206. https://doi.org/10.17660/ActaHortic.1995.399.23

Gary, C., Jones, J.., Tchamitchian, M., 1998. Crop modelling in horticulture: state of the art. Sci. Hortic. (Amsterdam). 74, 3–20. https://doi.org/10.1016/S0304-4238(98)00080-6

Giménez, C., Gallardo, M., Martínez-Gaitán, C., Stöckle, C.O., Thompson, R.B., Granados, M.R., 2013. VegSyst, a simulation model of daily crop growth, nitrogen uptake and evapotranspiration for pepper crops for use in an on-farm decision support system. Irrig. Sci. 31, 465–477. https://doi.org/10.1007/s00271-011-0312-2

Herman, J., Usher, W., 2017. SALib: An open-source Python library for Sensitivity Analysis. J. Open Source Softw. 2, 97. https://doi.org/10.21105/joss.00097

Heuvelink, E., 1999. Evaluation of a Dynamic Simulation Model for Tomato Crop Growth and Development. Ann. Bot. 83, 413–422. https://doi.org/10.1006/anbo.1998.0832

Heuvelink, E, 1996. Tomato growth and yield: quantitative analysis and synthesis.

Heuvelink, E., 1996. Dry Matter Partitioning in Tomato: Validation of a Dynamic Simulation Model. Ann. Bot. 77, 71–80. https://doi.org/10.1006/anbo.1996.0009

Heuvelink, E., Bakker, M.J., Elings, A., Kaarsemaker, R., Marcelis, L.F.M., 2005. Effect of leaf area on tomato yield. Acta Hortic. 691, 43–50. https://doi.org/10.17660/ActaHortic.2005.691.2

Heuvelink, E., Bertin, N., 1994. Dry-matter partitioning in a tomato crop: Comparison of two simulation models. J. Hortic. Sci. 69, 885–903. https://doi.org/10.1080/14620316.1994.11516525

Heuvelink, Ep., Li, T., Dorais, M., 2018. Crop growth and yield., in: Heuvelink, E. (Ed.), Tomatoes. CABI, Wallingford, pp. 89–136. https://doi.org/10.1079/9781780641935.0089

Heuvelink, Ep, Okello, R.C.O., 2018. Developmental processes, in: Heuvelink, E. (Ed.), Tomatoes. CABI.

Higashide, T., Heuvelink, E., 2009. Physiological and morphological changes over the past 50 years in yield components in tomato. J. Am. Soc. Hortic. Sci. 134, 460–465. https://doi.org/10.21273/jashs.134.4.460

Jones, J.W., Antle, J.M., Basso, B., Boote, K.J., Conant, R.T., Foster, I., Godfray, H.C.J., Herrero, M., Howitt, R.E., Janssen, S., Keating, B.A., Munoz-Carpena, R., Porter, C.H., Rosenzweig, C., Wheeler, T.R., 2017. Toward a new generation of agricultural system data, models, and knowledge products: State of agricultural systems science. Agric. Syst. 155, 269–288. https://doi.org/10.1016/j.agsy.2016.09.021

Jones, J.W., Dayan, E., Allen, L.H., Van Keulen, H., Challa, H., 1991. A dynamic tomato growth and yield model (TOMGRO). Trans. ASAE 34, 0663–0672. https://doi.org/10.13031/2013.31715

Jones, J.W., Kenig, A., Vallejos, C.E., 1999. Reduced state-variable tomato growth model. Trans. ASAE 42, 255–265. https://doi.org/10.13031/2013.13203

Katerji, N., Campi, P., Mastrorilli, M., 2013. Productivity, evapotranspiration, and water use efficiency of corn and tomato crops simulated by AquaCrop under contrasting water stress conditions in the Mediterranean region. Agric. Water Manag. 130, 14–26. https://doi.org/10.1016/j.agwat.2013.08.005

Katzin, D., van Mourik, S., Kempkes, F., van Henten, E.J., 2020. GreenLight – An open source model for greenhouses with supplemental lighting: Evaluation of heat requirements under LED and HPS lamps. Biosyst. Eng. 194, 61–81. https://doi.org/10.1016/j.biosystemseng.2020.03.010

Kuijpers, W.J.P., Katzin, D., van Mourik, S., Antunes, D.J., Hemming, S., van de Molengraft, M.J.G., 2021. Lighting systems and strategies compared in an optimally controlled greenhouse. Biosyst. Eng. 202, 195–216. https://doi.org/10.1016/j.biosystemseng.2020.12.006

Lin, D., Wei, R., Xu, L., 2019. An Integrated Yield Prediction Model for Greenhouse Tomato.

Agronomy 9, 873. https://doi.org/10.3390/agronomy9120873

Lizaso, J.I., Batchelor, W.D., Westgate, M.E., Echarte, L., 2003. Enhancing the ability of CERES-Maize to compute light capture. Agric. Syst. 76, 293–311. https://doi.org/10.1016/S0308-521X(02)00003-3

Marcelis, L.F.., Heuvelink, E., Goudriaan, J., 1998. Modelling biomass production and yield of horticultural crops: a review. Sci. Hortic. (Amsterdam). 74, 83–111. https://doi.org/10.1016/S0304-4238(98)00083-1

Mbow, C., Rosenzweig, C., Barioni, L.G., Benton, T.G., Herrero, M., Krishnapillai, M., Liwenga, E., Pradhan, P., Rivera-Ferre, M.G., Sapkota, T., Tubiello, F.N., Xu, Y., 2019. Food security, in: Shukla, P.., Skea, J., Calvo Buendia, E., Masson-Delmotte, V., Pörtner, H.-O., Roberts, D.C., Zhai, P., Slade, R., Connors, S., van Diemen, R., Ferrat, M., Haughey, E., Luz, S., Neogi, S., Pathak, M., Petzold, J., Portugal Pereira, J., Vyas, P., Huntley, E., Kissick, K., Belkacemi, M., Malley, J. (Eds.), Climate Change and Land: An IPCC Special Report on Climate Change, Desertification, Land Degradation, Sustainable Land Management, Food Security, and Greenhouse Gas Fluxes in Terrestrial Ecosystems.

McNeal, B.L., Scholberg, J.M.S., Jones, J.W., Stanley, C.D., Csizinsky, A.A., Obreza, T.A., 1995. Application of a greenhouse tomato-growth model (TOMGRO) to field-grown tomato. Soil Crop Sci. Soc. Florida.

Montero, J.I., Zhang, Y., Yang, Q., Ke, X., 2019. Advances in greenhouse design, in: Marcelis, L.F.M., Heuvelink, E. (Eds.), Achieving Sustainable Greenhouse Cultivation. Burleigh Dodds Science Publishing Limited, Cambridge, pp. 17–52. https://doi.org/10.19103/AS.2019.0052.02

Parton, W.J., Logan, J.A., 1981. A model for diurnal variation in soil and air temperature. Agric. Meteorol. 23, 205–216. https://doi.org/10.1016/0002-1571(81)90105-9

Ramirez, A., Rodriguez, F., Berenguel, M., Heuvelink, E., Ramírez, A., Rodríguez, F., Berenguel, M., Heuvelink, E., 2004. Calibration and validation of complex and simplified tomato growth models for control purposes in the Southeast of Spain. Acta Hortic. 654, 147–154. https://doi.org/10.17660/ActaHortic.2004.654.15

Righini, I., Vanthoor, B., Verheul, M.J., Naseer, M., Maessen, H., Persson, T., Stanghellini, C., 2020. A greenhouse climate-yield model focussing on additional light, heat harvesting and its validation. Biosyst. Eng. 194, 1–15. https://doi.org/10.1016/j.biosystemseng.2020.03.009

Rodríguez, F., Berenguel, M., Guzmán, J.L., Ramírez-Arias, A., 2015. The greenhouse dynamical system, in: Advances in Industrial Control. Springer International Publishing, pp. 9–97. https://doi.org/10.1007/978-3-319-11134-6_2

Scholberg, J., 1996. Adaptive use of crop growth models to simulate the growth of field-grown tomato.

Scholberg, J.M.S., Boote, K.J., Jones, J.W., McNeal, B.L., 1997. Adaptation of the CROPGRO model to simulate the growth of field-grown tomato, in: Applications of Systems Approaches at the Field Level. Systems Approaches for Sustainable Agricultural Development. Springer, Dordrecht, pp. 135–151. https://doi.org/10.1007/978-94-017-0754-1_9

Spitters, C.J.T., Toussaint, H.A.J.M., Goudriaan, J., 1986. Separating the diffuse and direct component of global radiation and its implications for modeling canopy photosynthesis Part I. Components of incoming radiation. Agric. For. Meteorol. 38, 217–229. https://doi.org/10.1016/0168-1923(86)90060-2

Vanthoor, B.H.E., de Visser, P.H.B., Stanghellini, C., van Henten, E.J., 2011. A methodology for model-based greenhouse design: Part 2, description and validation of a tomato yield model. Biosyst. Eng. 110, 378–395. https://doi.org/10.1016/j.biosystemseng.2011.08.005

Vazquez-Cruz, M.A., Guzman-Cruz, R., Lopez-Cruz, I.L., Cornejo-Perez, O., Torres-Pacheco, I., Guevara-Gonzalez, R.G., 2014. Global sensitivity analysis by means of EFAST and Sobol' methods and calibration of reduced state-variable TOMGRO model using genetic algorithms. Comput. Electron. Agric. 100, 1–12. https://doi.org/10.1016/j.compag.2013.10.006

Wallach, D., Thorburn, P., Asseng, S., Challinor, A.J., Ewert, F., Jones, J.W., Rötter, R., Ruane, A., 2016. Estimating model prediction error: Should you treat predictions as fixed or random? Environ. Model. Softw. 84, 529–539. https://doi.org/10.1016/j.envsoft.2016.07.010

Zhao, C., Liu, B., Xiao, L., Hoogenboom, G., Boote, K.J., Kassie, B.T., Pavan, W., Shelia, V., Kim, K.S., Hernandez-Ochoa, I.M., Wallach, D., Porter, C.H., Stockle, C.O., Zhu, Y., Asseng, S., 2019. A SIMPLE crop model. Eur. J. Agron. 104, 97–106. https://doi.org/10.1016/j.eja.2019.01.009

SUPPLEMENTARY MATERIAL C1

Table 2. Parameters from the Reduced Tomgro model.

Parameter	Fixed?	Calibrated?	Lim. 1	Lim. 2	Sources
delta – Maximum leaf area expansion per node [m^2 leaf $node^{-1}$]	N	Y	0.03	0.07	(1), (3), (5), Estimated
beta – Coefficient in expolinear equation [$node^{-1}$]	N	Y	0.1	0.5	(1), (3), (5), Estimated
N_b – Project of linear segment of LAI vs N to horizontal axis [node]	N	Y	10	25	(1), (3), (5), Estimated
alpha_F – Maximum partitioning of new growth to fruit [fraction d^{-1}]	N	Y	0.50	0.95	(1), (3), (5), Estimated
V – transition coefficient between vegetative and full fruit growth [$node^{-1}$]	N	N	0.1	0.27	(1), (3), Estimated
N_FF – nodes per plant when first fruit appears [node]	N	Y	10	25	(1), (3), Estimated
T_crit – Mean daytime temperature above which fruit abortion starts [° C]	N	Y	22	29	(1), (3), (5), Estimated
K_F - development time from first fruit to first ripe fruit [node]	N	Y	4	8	(1), (3), Estimated
DFmax – Average development rate used to move fruits from green to mature stage [d^{-1}]	N	Y	0.02	0.10	(1), (3), Estimated
V_{max} – Maximum increase in vegetative tissue d.w. growth per node [g dw $node^{-1}$]	N	N	6.0	9.0	(1), (3), (5), Estimated
tmaxPg – Temperature below which photosynthesis decreases from maximum [°C]	Y	N	34	40	(2), Estimated
N_max - Maximum rate of node appearance (at optimal temperatures) [node d^{-1}]	Y	Y	0.4	0.7	(1), (3), (5), Estimated

Qe – Leaf quantum efficiency [μmol (CO_2 fixed) μmol (photon) $^{-1}$]	Y	Y	0.055	0.09	(1), (3), (5), Estimated
tmin_fr_gr – Minimum temperature that affects fruit growth [^{o} C]	Y	N	6	10	(3), Estimated
sl_N1 – Parameter to modify node development rate [$^o C^{-1}$]	Y	N	0.02	0.03	(1), (3), Estimated
sl_N2 – Parameter to modify node development rate [$^o C^{-1}$]	Y	N	0.04	0.06	(1), (3), Estimated
sl_R – Parameter to modify partitioning of biomass to roots [$nodes^{-1}$]	Y	N	0.003	0.0035	(3), Estimated
tau1 - Carbon dioxide use efficiency [μmol (CO_2)/m^2 s ppm(CO_2)]	Y	N	0.06	0.1	(1), (3), (5), Estimated
tau2 - Carbon dioxide use efficiency for concentrations larger than 350 ppm [μmol CO_2 (m^2 s ppm CO_2)$^{-1}$]	Y	N	0.058	0.1	(3), Estimated
TSlop - Parameter to reduce rate of leaf area expansion [^{o} C]	Y	N	18.54	22.66	(3), Estimated
E – Growth efficiency, ratio of biomass to photosynthate available for growth [g d.w. $g^{-1} CH_2O$]	Y	N	0.6	0.8	(1), (3), (5), Estimated
K – light extinction coefficient	Y	N	0.5	0.8	(1), (3), (6)
p_1 - Loss of leaf d.w. per node after LAI_max is reached [g leaf $node^{-1}$]	Y	N	1.5	2.5	(1), Estimated
LAImax [m^2 m^{-2}]	Input	Input	2.3	4.0	(1)

All parameters were sampled within a uniform distribution, in which Lim. 1 is the lower value and Lim. 2 is the upper value. Non-calibrated parameters were only included in the sensitivity analysis. References: (1) (Jones et al., 1999); (2) (Jones et al., 1991); (3) (Jones et al., 1999), spreadsheet; (4) (Dayan et al., 1993b); (5) (Ramirez et al., 2004); (6) (Marcelis et al., 1998); (7) (Zhao et al., 2019); (8) (Vanthoor et al., 2011)

Table 3. Parameters from the Simple model.

Parameter	Fixed?	Calibrated?	Lim. 1	Lim. 2	Source

T_{sum} – Thermal time until crop maturity [ºC]	N	Y	2500	5000	(7), Estimated
HI – Potential harvest index	N	Y	0.10	0.80	(7), Estimated
I50A – Cumulative temperature requirement for leaf area development to intercept 50% of radiation [ºC d]	N	Y	200	3000	(7), Estimated
RUE – Radiation use efficiency (aboveground only and without respiration) [g MJ^{-1}]	Y	Y	0.8	2	(7)
T_base – Base temperature for phenology development and growth [ºC]	Y	Y	4	15	(7), (8)
T_opt – Optimal temperature for biomass growth [ºC]	Y	N	23	30	(7), Estimated
T_heat – Threshold temperature to start accelerating senescence from heat stress [ºC]	Y	Y	40	50	(7), Estimated
T_ext – The extreme temperature threshold when RUE becomes 0 due to heat stress [ºC]	Y	Y	30	34	(7), Estimated
fSolarMax [-]	Input	Input	0.65	0.99	(1)

All parameters were sampled within a uniform distribution, in which Lim. 1 is the lower value and Lim. 2 is the upper value. Non-calibrated parameters were only included in the sensitivity analysis. References: (1) (Jones et al., 1999); (2) (Jones et al., 1991); (3) (Jones et al., 1999), spreadsheet; (4) (Dayan et al., 1993b); (5) (Ramirez et al., 2004); (6) (Marcelis et al., 1998); (7) (Zhao et al., 2019); (8) (Vanthoor et al., 2011)

Table 4. Parameters from the Vanthoor model.

Parameter	Fixed?	Calibrated?	Lim. 1	Lim. 2	Source
K1 – light extinction coefficient	Y	N	0.5	0.8	(1), (3), (6)
ksMinTCan24 – Parameter to adjust curve of 24 hour mean crop growth inhibition [°C]	N	Y	8	18	(8), Estimated

ksMaxTCan24 – Parameter to adjust curve of 24 hour mean crop growth inhibition [°C]	N	Y	22	30	(8), Estimated
ksMinTCan – Parameter to adjust curve of instantaneous crop growth inhibition [°C]	N	Y	5	18	(8), Estimated
ksMaxTCan – Parameter to adjust curve of instantaneous crop growth inhibition [°C]	N	Y	22	32	(8), Estimated
cDev2 - Fruit development rate coefficient 2 [s^{-1} $°C^{-1}$]	Y	Y	1×10^{-8}	1.3×10^{-8}	(8), Estimated
cMaxBufFruit2 - Maximum fruit set regression coefficient 2 [fruits $plant^{-1}$ s^{-1} $°C^{-1}$]	Y	N	7×10^{-7}	8×10^{-7}	(8), Estimated
sla - Specific leaf area m^2 {leaf} mg^{-1} {CH_2O}	N	Y	2.4×10^{-5}	7.5×10^{-5}	(2), (8)
TSumEnd - Temperature sum when fruit growth rate is at full potential °C d	N	Y	800	2500	(8), Estimated
ttsum – Thermal time until the start of generative phase [ºC d^{-1}]	Input	Y	-900	-300	(8), Estimated
LAImax [m^2 m^{-2}]	Input	Input	2.3	4.0	(1)

All parameters were sampled within a uniform distribution, in which Lim. 1 is the lower value and Lim. 2 is the upper value. Non-calibrated parameters were only included in the sensitivity analysis. References: (1) (Jones et al., 1999); (2) (Jones et al., 1991); (3) (Jones et al., 1999), spreadsheet; (4) (Dayan et al., 1993b); (5) (Ramirez et al., 2004); (6) (Marcelis et al., 1998); (7) (Zhao et al., 2019); (8) (Vanthoor et al., 2011)

SUPPLEMENTARY MATERIAL C2

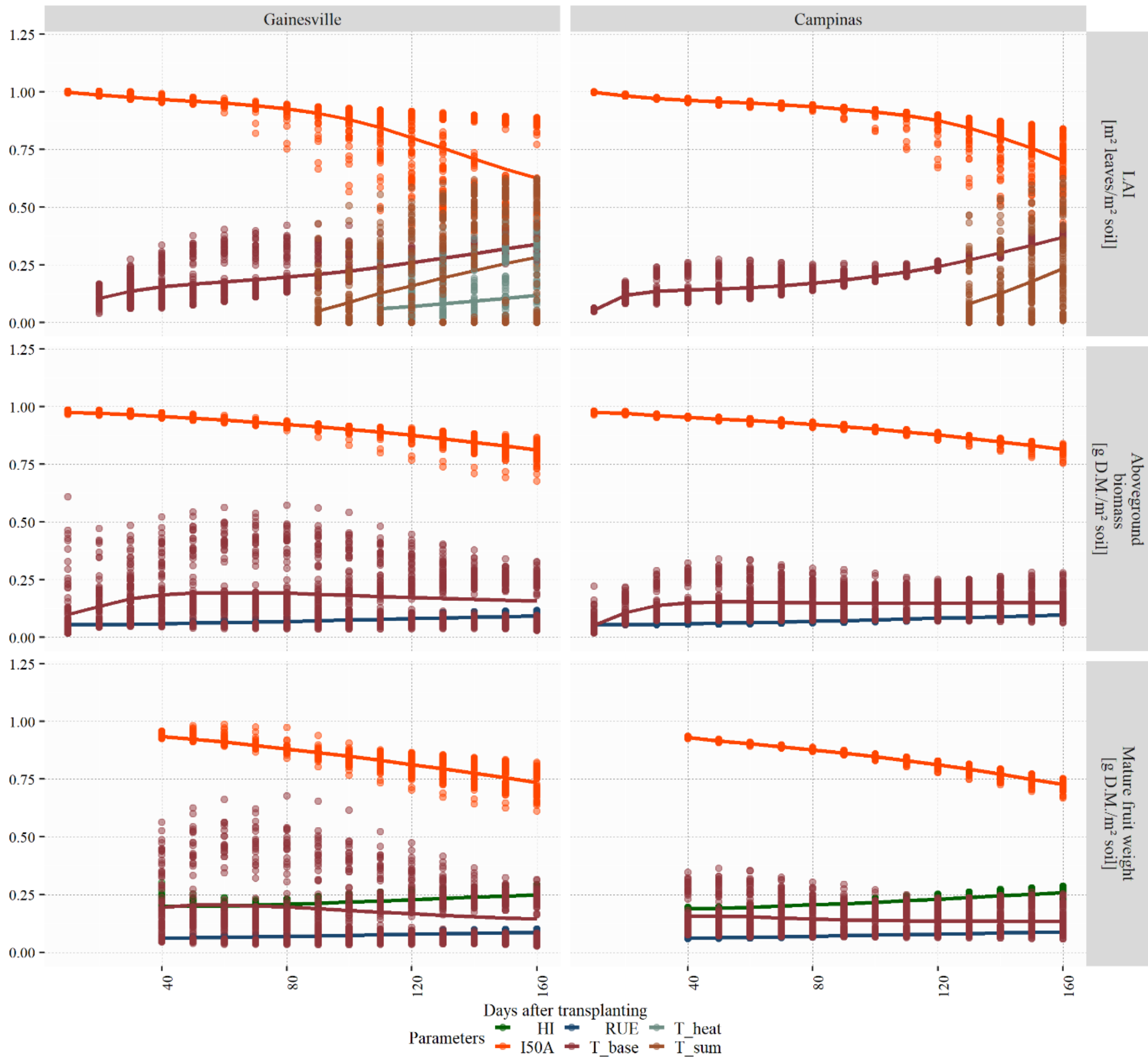

Figure 8. Total effect sensitivity indices of yield to models' parameters for the Simple model with the Campinas and Gainesville historical weather datasets. Parameters' full names are presented in the Supplementary Material. Lines correspond to the average index value while dots correspond to the results in each scenario assessed. Only parameters with averages larger than 0.05 are shown. For fruits, the X axis starts at 40 days after transplanting as before often there is a lot of instability in the averages.

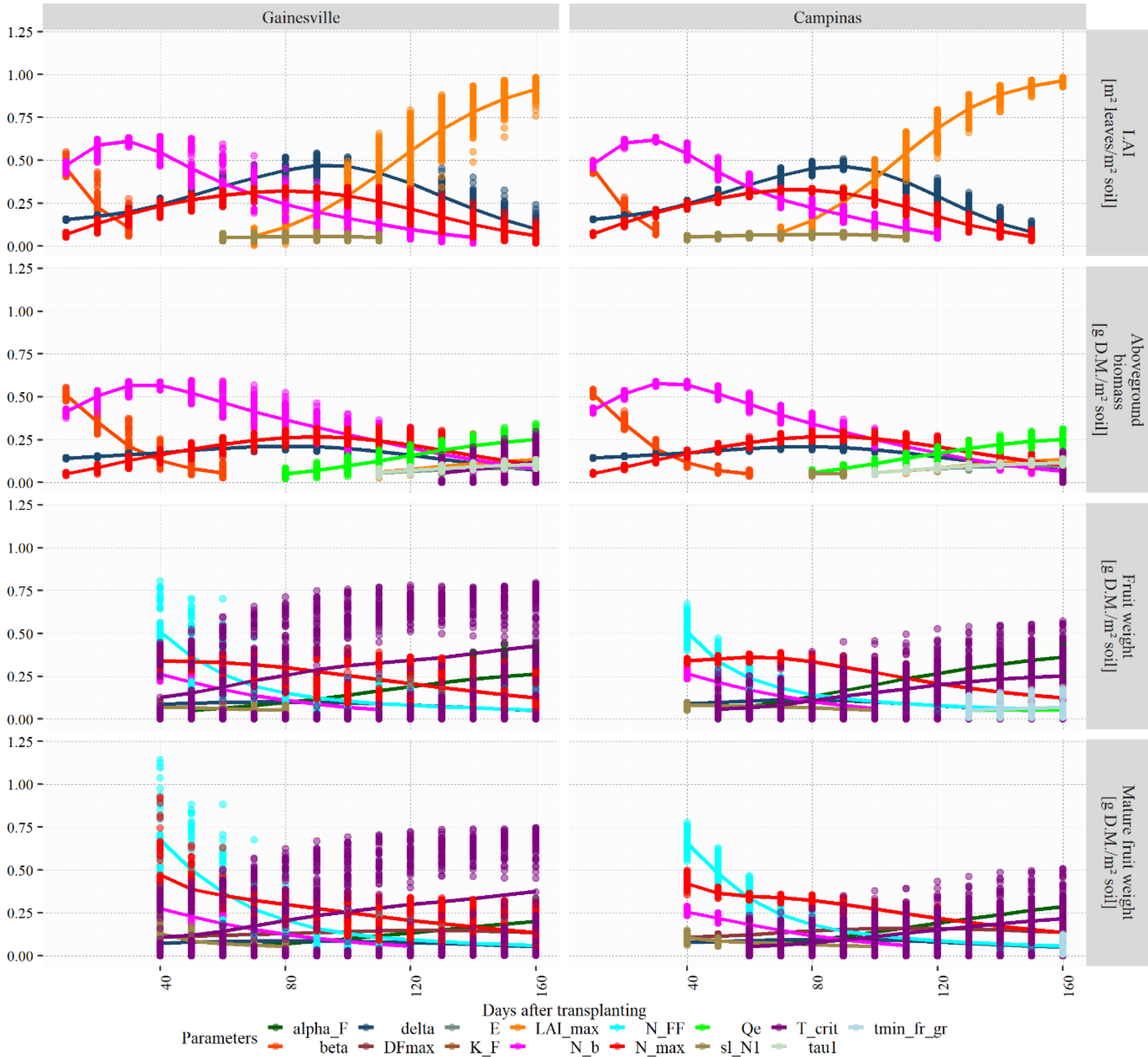

Figure 9. Total effect sensitivity indices of yield to models' parameters for the Reduced Tomgro model with the Campinas and Gainesville historical weather datasets. Parameters' full names are presented in the Supplementary Material. Lines correspond to the average index value while dots correspond to the results in each scenario assessed. Only averages larger than 0.05 are shown. For fruits, the X axis starts at 40 days after transplanting as before often there is a lot of instability in the averages.

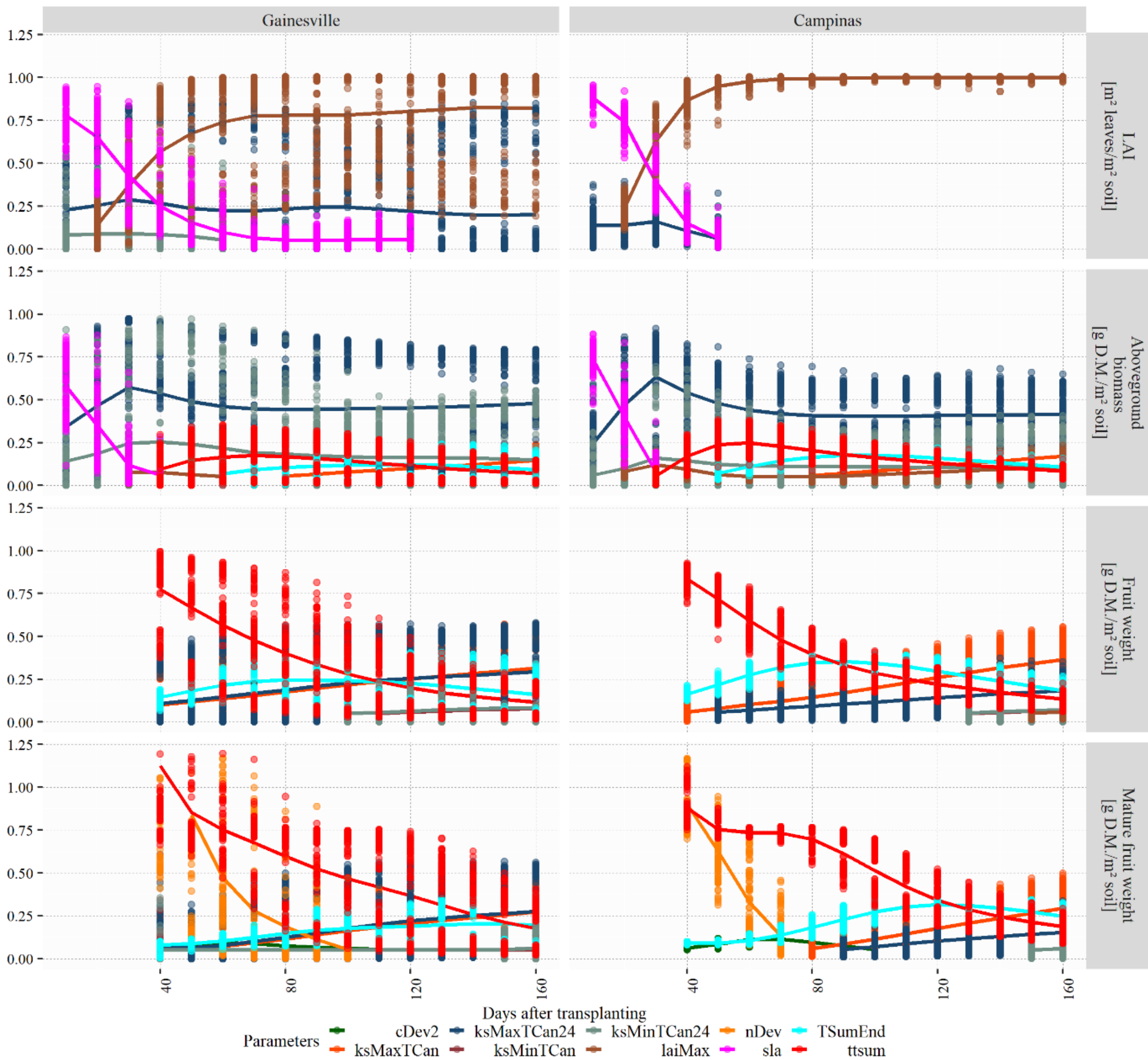

Figure 10. Total effect sensitivity indices of yield to models' parameters for the Vanthoor model with the Campinas and Gainesville historical weather datasets. Parameters' full names are presented in the Supplementary Material. Lines correspond to the average index value while dots correspond to the results in each scenario assessed. Only averages larger than 0.05 are shown. For fruits, the X axis starts at 40 days after transplanting as before often there is a lot of instability in the averages.

Appendix D — LEVERAGING DATA FROM REAL-TIME MONITORING IN CROP MODELS

ABSTRACT

Researchers using crop models have been devising new roles for data and crop modeling based on the availability of data and the new techniques available for modeling. From the various techniques available, modeling may be tackled by data-driven methods or through a process-based approach. And process-based or mechanistic models may take advantage from real-time observations through data assimilation. This work provides a case study of data assimilation in a protected environment, capturing tomato growth data from different sources. We updated growth estimates of the Reduced State TOMGRO model, by assimilating observational data obtained through the continuous monitoring of plant mass and images captured by low-cost cameras, using the Unscented Kalman Filter and the Ensemble Kalman Filter. These techniques had not been used yet in the protected cultivation of tomatoes, so it was necessary to develop the observation models as well, establishing the relationship between the observed variables and the ones estimated by the process-based model. We observed that the quality of observations and of observation models is crucial for good performance of the assimilation techniques. We also observed that the assimilation performed better than calibrated models when there was a need to adjust the estimates to growth disturbances and that when filters lead to better productivity estimates, continuous observations may not be required. Our results show great potential in the new contexts of the internet of things (IoT) in agriculture, vertical farming, and digital twins.

KEYWORDS

Data assimilation, greenhouse, crop model, proximal sensing

D1. INTRODUCTION

Traditionally, crop growth data has been used with crop models from their development to calibration performed prior to their use. There are, however, new roles envisioned for it in crop modeling that are premised on its abundance and quality. For example, Keating and Thorburn (2018) mentioned a new relationship with data that would increase its role in model use and development through, e.g. model-data fusion and inverse modeling, and new roles for remote and proximal sensing in their initialization and calibration.

Data assimilation is a widely used method in hydrology and meteorology which consists in combining observed values to the states estimated by models, taking into account the uncertainty that exists in model estimates and observations (Pellenq and Boulet, 2004). In the case of crop modeling, data assimilation has been used with remote sensing images to update state variables related to crop canopy or soil properties, obtaining better estimates of yield, leaf area index, and soil moisture (Dorigo et al., 2007; Jin et al., 2018). Recent reviews of data assimilation in crop modeling suggest the Ensemble Kalman Filter and the Particle Filter as the most frequent algorithms used (Huang et al., 2019; Jin et al., 2018).

These reviews also point out to the limitations of current approaches, such as those relating to their use in large areas, as this application has mostly been limited its application to the temporal and spatial resolutions of satellites. Recent works have explored unmanned aerial vehicles (UAV) and digital images, such as in Yu et al. (2020), to improve yield estimates by assimilating sugarcane height. Linker and Ioslovich (2017) incorporated into the Aquacrop model estimates of canopy cover obtained from digital images of the canopy, as well as data obtained from destructive analysis as biomass observations. Destructive analysis data has also been used by Ruíz-García et al. (2014) with lettuces and the Nicolet model.

In the case of vegetables and other crops usually grown in greenhouses and other protected environments, it is possible to monitor vegetation growth more intensely than in large areas. Consequently, it becomes possible to perform assimilation with automatic observations obtained at greater temporal and spatial resolutions, as van Mourik et al. (2019) have done for monitoring greenhouse environments.

Automatic plant-related measurement in protected environments has been applied to obtain different kinds of information, as a few examples show. Growers monitoring plant growth through load cells had been registered in the Netherlands by de Koning and Bakker (1992) and has been suggested by works such as Helmer et al. (2005) and Lee and Son (2019), and in Chen et al. (2016) for plant factories. Automatic measurement has also been suggested for determining water demand (De Graaf et al., 2004). Finally, automatic plant-related measurement has the potential to be used for crafting digital twins, which may be defined as “a dynamic representation of a real-life object […] that can be used to monitor, analyze and simulate current and future states of and interventions on these objects, using data integration, artificial intelligence and machine learning.” (Verdouw et al., 2021).

The assimilation of these observations could enhance a broad range of modeling strategies, from those that rely on feedback information from sensors (Marcelis et al., 2000), to the ones relying on machine learning methods for dealing with real-time data, such as Gong et al. (2021), Hemming et al. (2020) and Hemming et al. (2019). In their recent review of the status of vertical farming systems, van Delden et al. (2021) comment on how sensor-informed artificial intelligence (AI) can be used to update self-learning dynamic growth prediction models that are partially process-based and partially data-driven as a strategy to increase radiation use efficiency. However, both models and measurements still retains an aspect of uncertainty, which data assimilation techniques can address.

Since data assimilation with data from diverse sources could prove useful in this different environment, leveraging the intense monitoring as well as crop models, our goal was to perform a first approach of data assimilation in a greenhouse tomato growth model, evaluating its potential to improve estimates from a non-calibrated model. With data retrieved in a production-like environment, we obtained the observation models required for assimilation. Using the Reduced State Tomgro model (Jones et al., 1999), we obtained estimates of tomato growth, which were combined by data assimilation techniques with data extracted from images and from a weighting system.

D2. MATERIAL AND METHODS

D2.1 Crop model

This work uses the Reduced State Tomgro (RT) model, which is a summary model from the TOMGRO model, aimed at being used in greenhouse control systems. The RT models growth of tomatoes when water and nutrients are not limiting factors. In summary, the model has only five state variables — number of nodes, leaf area index, aboveground dry biomass, fruit dry biomass and mature fruit dry biomass — and was developed to control the environment. Based on hourly temperature and photosynthetically active solar radiation data, the model quantifies the growth and development of the tomato plant when water and nutrients do not limit growth. Development is indicated by the number of nodes, and growth, by the other states. The leaf area index influences photosynthesis, which, along with respiration, determines total carbohydrates available for growth of aboveground biomass and fruit biomass. The RT model, which has its variables and parameters further detailed in Jones et al. (1999), is therefore a simple model that does not include root growth or irrigation, and this simplicity may help in a first approach.

The RT model used in this paper was implemented in the Python language, using Jones et al. (1991), Jones et al. (1999), and the spreadsheet provided by Dr James W Jones as sources. The difference equations were integrated by the Euler method. All code used in this work, including the model code, is available in https://github.com/mnqoliveira/data-assimilation-tomato-models.

D2.2 Data sources

The experiments were conducted in research greenhouses at the School of Agricultural Engineering of the University of Campinas (22º 49' 06” S, 47º 03' 40” W, 635 m altitude)[6]. Three cycles of cherry tomato growth were performed (Table 1).

Table 1. Growth cycles for data gathering.

Growth Cycle	Cultivar	Start date	End date
Cycle 01	Fercam - Milla	12/jul/2019	28/oct/2019
Cycle 02	Feltrin - Carolina	05/nov/2020	12/feb/2021
Cycle 03	Seminis - DRC-564	09/mar/2021	11/jun/2021

Two kinds of environmental data were measured: air temperature and photosynthetically active radiation. The sensors for temperature were SHT75 transducers protected by porous capsules which, by their turn, were protected by tubes of polyvinylchloride tubes coated with aluminum foil. The tubes included downstream fans. The sensors were installed in a hardware platform for wireless sensor networks (Radiuino BE900), with daily backup. For measurements of photosynthetically active radiation (PAR), we used quantum sensors Licor LI-190SA with a datalogger Licor LI-1400.

Plants were characterized by destructive analysis and by non-destructive observations. Non-destructive data refers to the pictures taken from side and superior views, by fixed Raspberry Pi Camera Modules v2, connected to Raspberry Pi Zero. It also refers to the continuous — every

[6] Description and data are submitted as a data article.

minute — weight monitoring using force transducers HBM S2M with nominal force of 10 N (0.02 % accuracy) and stored in a data logger PMX WGX002, measure card PX455.

Destructive data refers to the characterization of dry weight of the plant and leaf area. In intervals of one to three weeks, three plants were removed from the greenhouse. Leaves, fruits, stem, and mature fruits were separated for weighting. Before being weighted, leaves were digitized with a scanner. Digitization included a reference of known size. Plant material was weighted before and after drying for four days or as until constant weight was reached.

Before removal, those plants were first photographed from above and laterally with a smartphone camera, and all pictures included references of known size. Labeling of the plant organs in the images was done manually, using the software GIMP. Marking was done only in areas in which there was certainty the organ corresponded to the correct plant; if there was uncertainty or occlusion, the area was not marked. The organs were colored differently, and were then detected by a script in python, also included in the repository previously mentioned. The corresponding area was scaled by using the reference. Fruit area refers to the area of mature and immature fruits. All data is available at https://doi.org/10.25824/redu/EP4NGO.

The three cycles presented different developments, which are explored in this work: the first may be characterized by low irrigation, subjecting plants to water deficit, the second, by an excess of nitrogen fertilization and an attack of tomato rust mite by the end of the cycle, and the third cycle was conducted closer to full water and fertilization.

D2.3 Model calibration

Data from the destructive analyses was used to calibrate the Reduced Tomgro model. Calibration followed the approach of minimizing the relative squared error using a global optimization algorithm. Given there were three different cycles, each with different conditions, a calibrated run used data from the respective cycle. Non-calibrated runs used data from the original Gainesville calibration. We also used the calibration of the cycle with full fertilization and irrigation as a manner of incorporating particularities of growth of cherry tomatoes in tropical conditions, providing a basis for assimilation in the two other cycles. Regardless of calibration, input data such as maximum leaf area or plant density referred to data from the evaluated cycle.

D2.4 Observation models

Observation models were created from data obtained from plants subjected to destructive and non-destructive analyses. Our modeling strategy focused on obtaining simple empirical relationships, and the generalized least squares method was used to account for the heteroscedasticity and correlation between residues. To avoid data leakage, despite the different growth conditions, data from the cycle was not used to obtain the relationship that would be used in that cycle. All observations obtained per plant were multiplied by plant density to make units compatible with the states in the model.

We used area extracted from lateral and top images to determine the leaf area index, fruit area extracted from lateral images to infer fruit dry mass and weight as determined by the weighting system to infer aboveground biomass. In this last case, we performed a conversion that would consider the difference caused by roots depending on development stage, and the difference from fresh to dry biomass.

D2.5 Data assimilation

Two assimilation techniques were used: Ensemble Kalman Filter (EnKF) and Unscented Kalman Filter (UKF). These approaches require specifications of uncertainty that were ascribed as following. Uncertainty in the initial states was determined as the variance of the samples analyzed in the transplanting day. For the EnKF, uncertainty in the process was ascribed to a model parameter, depending on the state variable being assimilated. Uncertainty in the model for the UKF was determined as the absolute error, calculated by the difference between observations of the states in the calibration samples in the cycle and the simulated value of the uncalibrated model. Variance in the measurements was determined as the standard deviation of the indirect observations of the calibration samples. While we are aware that this corresponds to partial leakage, we believe this was the best way to provide an estimate for these filter parameters. In this work, three state variables were estimated: aboveground dry biomass, leaf area index and fruit dry biomass.

D2.6 Frequency of assimilation

We used images captured every other day as the full set of observations. Data from the weighting system was captured each minute and averaged in the hour. Data from between 4 am and 5 am, before sunrise in all cycles, was used as the observation for each day. We then subsampled these observations to determine the effect of frequency. Subsampling was applied to the observations, and corresponded to using 50% and 10% of the data available in the cycle. To avoid results being biased by sampling, the procedure was performed 20 times. One of the repetitions was sampled in regular intervals through the cycle, and the others were randomly sampled.

D2.7 Evaluation

Since our goal was to determine how much the non-calibrated model estimates could be improved by assimilating observations from different sources, we evaluated our approach by calculating the root mean squared error through the cycle, using samples from destructive analysis, comparing non-calibrated, calibrated, and filtered series. We also compared the last estimated value for the states from the assimilation and the final measured value for the monitored plants.

D3. RESULTS

D3.1 Plant monitoring

Overall, growth from monitored plants, measured indirectly through pictures and through the weight system, was similar to the growth of other plants in the environment (Figure 1). Areas corresponding to leaves and fruits extracted from the images obtained with cellphones were compatible with the ones extracted from images obtained by the fixed cameras. Growth trends are noticeable, but are also very sensitive to lighting and occlusion, which often explains the discontinuities.

When areas of the lateral view of monitored plants were larger than from calibration data, this effect likely can be attributed to occlusion, as monitored plants were slightly dislocated from the planting line, for example for Cycle 3 and Plant 1 in Cycle 2, and the visibility of plants used in calibration was affected by adjacent plants (Figure 2). On the other hand, for calibrated plants, we note that visible area in Cycle 3 is equivalent to the visible area in Cycle 1. This happened despite maximum leaf area per plant reached an average of 0.44 m^2 leaves/plant in Cycle 3 and in Cycle 1, 1.91 m^2 leaves/plant. This was likely a consequence of fewer leaves reducing the complexity of annotations in the environment of Cycle 1.

In Figure 1, height was included with two purposes: as a reference of information extracted from pictures in a comprehensible unit, but also to show how monitored plants having their growth interrupted earlier than plants used in calibration is particularly noticeable in Cycle 3, as their heights remain constant by the end of the cycle.

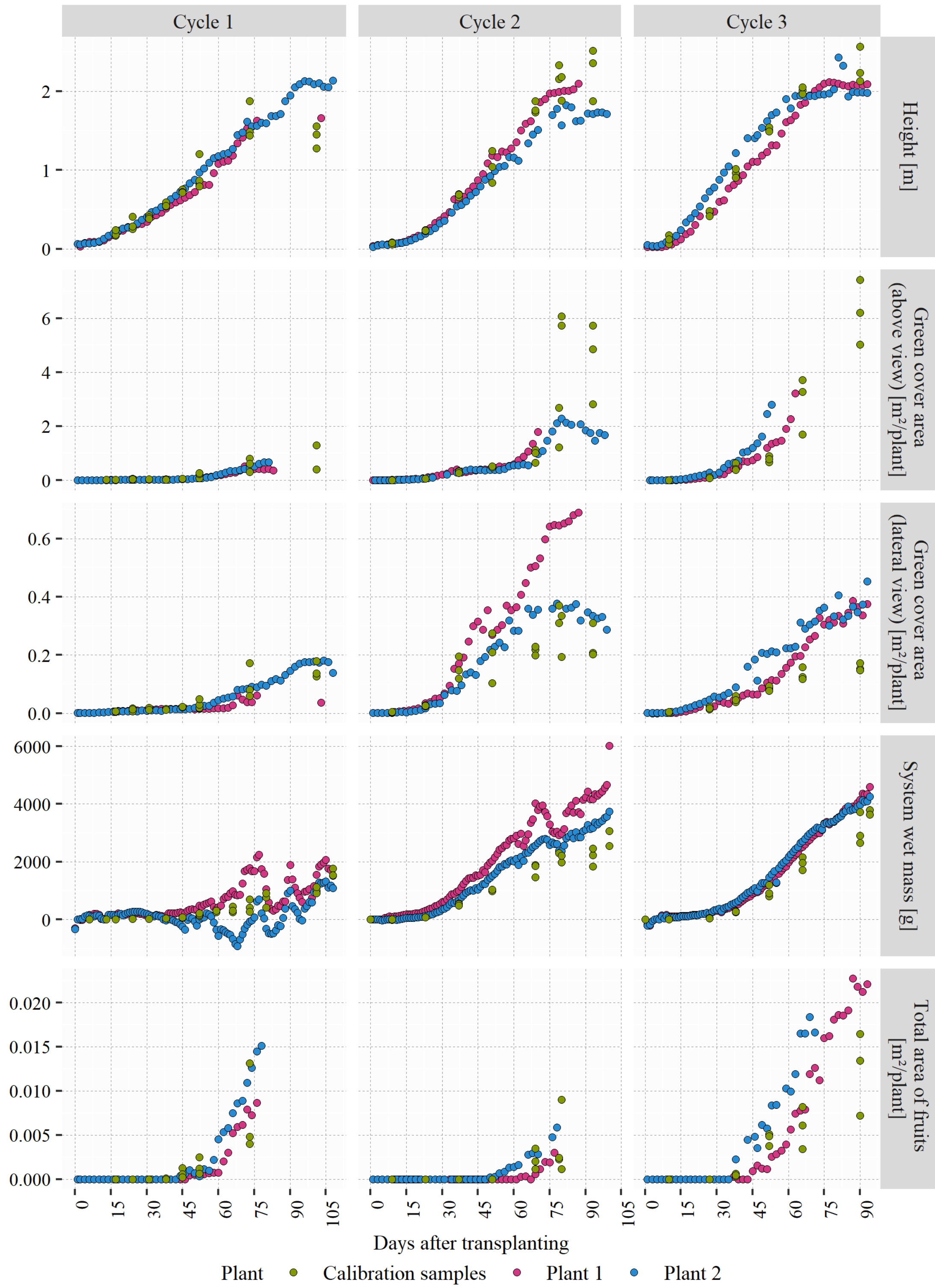

Figure 1. Times-series of observations from monitored plants and values for the same variables from the calibration samples. For the weighting system, values for the calibration samples refer to aboveground fresh mass and last observations from aboveground data correspond to the monitored plants.

Curves of area of fruits in Cycles 1 and 2 are interrupted before the end of the cycle because as plants were harvested, observations did not correspond to total fruit mass any longer and were not compatible with the principle of accumulated biomass used in the growth model. In the green cover area identified from the above view, interruption often refers to the plant reaching the camera and occupying all visible area, being no longer informative. The very low values observed in Cycle 1 for the above view may be connected not only to lower leaf area, but also to a slight dislocation of the camera, so that it did not fully capture the plant.

As for the system wet mass, one can observe how the first cycle corresponded to unstable mass values, mostly corresponding to the amount of irrigation applied. In the second and third cycles, these fluctuations are less prevalent. In those cycles, we can observe values from monitored plants are larger than for calibrated samples as roots are included in the system. Their accommodation of more water also increases total mass.

Figure 2. Example of non-destructive observation of lateral leaf area and fruit area of sampled plant. Leaves are marked in green, mature fruits are marked in red, and non-mature fruits are marked in yellow. The A4 sheet used as reference is marked in cyan. Obstruction from adjacent plants prevents the identification of all organs corresponding to the plant sampled.

D3.2 Observation models

Figure 3 shows the scatterplots of the relationships that gave basis to the observation models that we obtained. Although linear relationships may be observed, particularities of each cycle are noticeable, such as larger fruit biomass in Cycle 3 and lower leaf area in Cycle 1. For Cycle 2, excessive nitrogen fertilization at the beginning of the cycle, followed by mite attack after the beginning of the fruit stage, led to large leaf areas but low fruit mass.

As mentioned for the indirect observations, as plants reach the camera, one can no longer distinguish leaf area from images taken from the above view, which is an issue similar to the one of leaf area observed by satellites after leaf area reaches a certain value. In this sense, the relationship becomes non-linear, and images from the side view represent the leaf area better than from above. One can also see that in all cases of observations extracted from images, but particularly for fruits, observed values are concentrated in the lower range, making it harder to obtain good relationships for larger values. This may also have been caused by our choice of not compensating for occlusion and only including areas in which there was confidence the area corresponded to the plant, which led total organ area identified in images to being smaller than the total area that the organs occupy on plants. This did not impair our attainment of a reasonably good linear relationships between said areas and their corresponding observed state within a cycle. For aboveground biomass, although the linear relationship is very visible, uncertainty relates to the other aspect of conversion, which concerns the fraction of system biomass ascribed to aboveground biomass and which could not be measured.

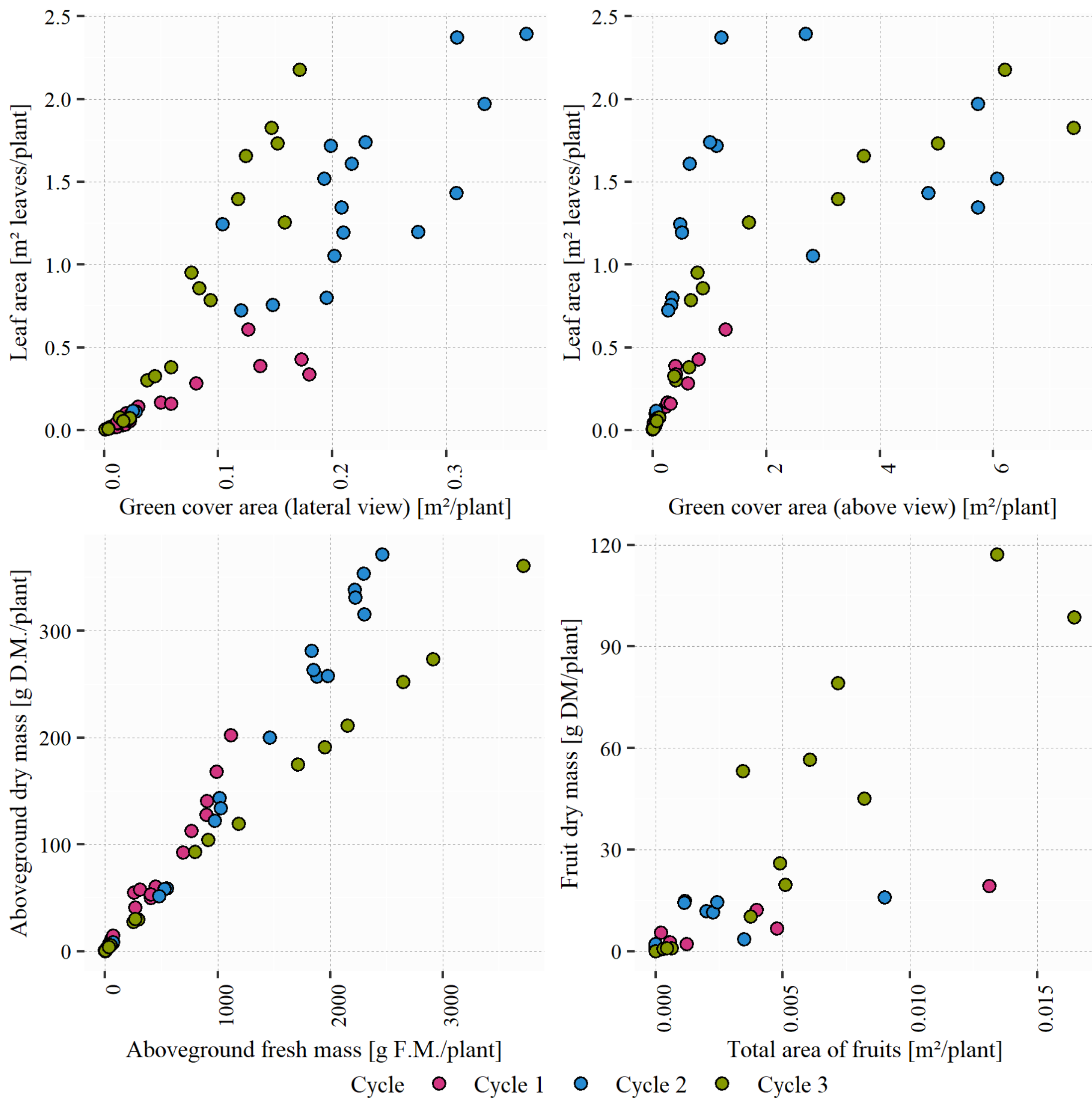

Figure 3. Scatterplots of relationships between observations of plants used in the destructive analyses, used for the development of observation models in each growth cycle. Observations that refer to an area were extracted from images and aboveground fresh mass was obtained by weighting plants before drying.

Table 2 shows the metrics from the observation models after excluding data from the cycle. While correlations are compatible with what is visible from the scatterplots, error metrics point to large uncertainties. Since these models are used to convert the state variable into the same unit of the observation, they should be evaluated in the observations' unit. And while an error of 0.40 g FM m^{-2} may be considered very small when compared to the mass of the weighting system, 0.61 [m^2 m^{-2}] is very large for the area visible on images, and is likely caused by the different behaviors from the three growth cycles. Mean Absolute Percentage Errors confirm that the error in the unseen cycle is very large and suggests that using these models to convert state variables in the assimilation may lead to lower efficiency of the process.

Table 2. Standard error (SE), mean absolute percentage error (MAPE) and coefficient of determination (R^2) from each observation model for data from each cycle. SE is reported from training in the other cycles and MAPE is reported from validation in the same cycle.

Assimilated variable		LAI	LAI	W	Wf
Observed Variable		GC Abv [m^2 m^{-2}]	GC Lat [m^2 m^{-2}]	W_fm [g FM m^{-2}]	Area Wf [m^2 m^{-2}]
Cycle 1	SE (training)	0.988	0.311	0.395	0.062
Cycle 2		0.597	0.613	0.339	0.084
Cycle 3		0.921	0.436	0.257	0.252
Cycle 1	R^2 (training)	0.64	0.73	0.94	0.81
Cycle 2		0.86	0.82	0.98	0.77
Cycle 3		0.44	0.87	0.99	0.36
Cycle 1	MAPE (validation)	30 %	41 %	34 %	373 %
Cycle 2		122 %	55 %	29 %	82 %
Cycle 3		26 %	113 %	58 %	122 %

*Observations as: GC Lat: green cover (lateral view), GC Abv: green cover (above view), W_fm fresh mass from destructive analyses, Area Wf: total area of fruits.

D3.3 Assimilation

Table 3 highlights the cases in which RMSE of the growth cycle for a state variable was lower with assimilation of that variable than without, regardless of calibration. Overall, calibration led to the lowest errors, but in almost all cases, assimilation slightly improved the results. No technique was consistently better either across variables or across growth cycles.

Although calibration is expected to improve model performance, this was not observed in some cases, as growth did not correspond to the situation for which the model was developed. In Cycle 1, in which total biomass was affected by irrigation, the optimization used in calibration could not determine parameters that would generate compatible estimates between all variables. In Cycle 2, similarly, excessive nitrogen led to much lower fruit production, and this effect was not properly captured by the parameters selected. Assimilation results in both cases depended on the quality of observations. In Cycle 1, in which the system biomass was affected by irrigation, the large errors also led to poor estimates and, therefore, the best results came from the non-calibrated simulation. In Cycle 2, on the other hand, assimilation of the images led to the adjustment of the estimates to the lower values that actually happened.

The errors in the weighting system of Cycle 1 were a particularity of that growth cycle, but since it should be the most precise measurement, it led to the largest improvements, and the results in Cycle 2 were very similar to the calibrated estimates, while on Cycle 3, errors were reduced in almost 50%. As for the uncertainties in observations from images that were discussed in the previous sections, they would affect all image-based assimilation. However, as these are permeated through the observation models, one should look to the models with lower validation errors to better understand this potential. In this case, the best example comes from using the pictures from above and the EnKF to estimate the leaf area index in Cycle 3. The large error by the end of the cycle is possibly caused by the absence of images, which led the model to simulate based on the last available update. It could also be noted that for Cycles 1 and 2, assimilation of images led to estimates as good as the ones obtained by calibration.

Table 3. Summary of errors for state variables assimilated in the evaluations.

Filter	Assim. state	Obs. variable*	Plant 1 - Cycle 1		Plant 2 - Cycle 1		Plant 1 - Cycle 2		Plant 2 - Cycle 2		Plant 1 - Cycle 3		Plant 2 - Cycle 3	
			Cycle RMSE	Final error	Cycle RMSE	Final error	Cycle RMSE	Final error	Cycle RMSE	Final error	Cycle RMSE	Final error	Cycle RMSE	Final error
None – Calib.	-	-	0.08	-0.21	0.08	-0.21	0.53	-0.02	0.53	0.00	0.24	0.50	0.30	0.60
None – Not Calib.	-	-	0.17	-0.21	0.17	-0.21	1.17	1.23	1.17	1.24	1.75	3.07	1.78	3.11
EnKF	LAI	GC Lat	**0.08**	-0.05	**0.08**	-0.20	**0.50**	-0.21	**0.91**	1.29	1.92	3.34	**1.75**	3.05
UKF			**0.12**	0.13	**0.08**	-0.21	**0.45**	1.02	**0.93**	1.48	1.93	3.33	**1.73**	2.99
EnKF		GC Abv	**0.06**	-0.15	**0.07**	-0.16	**1.02**	0.96	**1.11**	0.94	**0.78**	1.47	**0.71**	1.55
UKF			**0.09**	0.11	**0.08**	0.10	**1.07**	1.79	**1.06**	1.27	**1.60**	3.35	1.82	3.76
None – Calib.		-	47.81	103.68	37.01	71.86	32.56	-25.10	27.12	-8.96	71.73	136.83	68.85	129.62
None – Not Calib.	-	-	35.98	95.80	25.68	64.69	149.79	216.12	147.78	209.09	277.36	533.57	273.51	525.46
EnKF	W	W_fm_full	**45.71**	70.38	81.58	127.88	**41.18**	36.69	**68.69**	122.14	**141.98**	297.01	**142.70**	311.92
UKF	W		**53.44**	75.84	79.70	134.96	**52.34**	5.74	**77.99**	128.88	**119.08**	257.07	**128.45**	290.18
None – Calib.	-	-	12.31	-0.19	19.47	-25.18	88.72	-130.49	76.73	-109.63	2.66	5.12	0.90	-0.88
None – Not Calib.	-	-	27.36	85.70	24.26	76.98	35.86	-67.59	33.82	-63.32	90.84	164.10	89.33	160.55
EnKF	Wf	Area Wf	**25.89**	81.53	**22.82**	72.63	**28.55**	-54.75	**30.00**	-57.27	92.17	169.09	**88.47**	159.52
UKF	Wf		**24.86**	67.98	**22.42**	24.55	**13.70**	-20.28	**18.84**	-36.60	97.02	181.41	**75.35**	141.26

*Observations as: GC Lat: green cover (lateral view), GC Abv: green cover (above view), W_fm_full: weighting system, Area Wf: total area of fruits. Bold numbers refer to root mean squared errors lower than the larger RMSE between the non-calibrated and calibrated error.

When analyzing the results focusing on yield, overall, assimilation of either leaf area or aboveground biomass did not improve the estimates. But there are a few results that deserve further comments. The first result refers to the example from Cycle 3 (Figure 4), in which fruit area observations were apparently barely used, and the assimilated curve closely resembles the simulation without calibration. This is likely caused by bias in the observation model. Figure 1 showed that monitored plants in Cycle 3 had the largest areas of fruits by the end of the growth cycle. Still, the scatterplot from Figure 3 shows how a model obtained with data from the other two cycles would likely underestimate fruit mass. So even though there existed larger observations, this difference in magnitude of what was estimated by the model and the observation would not be captured in the residual calculation.

The second concerns the results of the Cycle 2, in which the calibrated model performed poorly, but UKF assimilation of fruit area in images, in part, improved the results (Figure 4). This was also observed for fruit biomass itself, but it is not necessarily the case that improvement of one state variable will cascade into improving the other. It should be noted that conversion by observation models also led to negative estimates, which is another point to the necessity of improving such models.

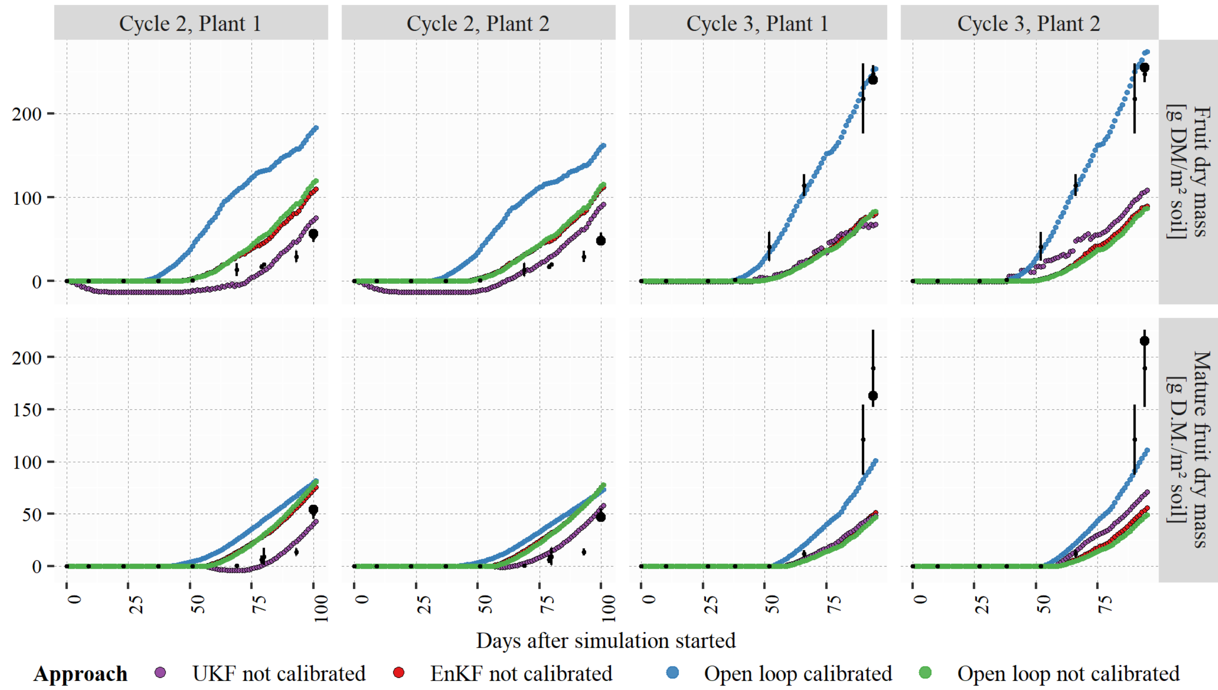

Figure 4. Growth curves for each monitored plant with the different methods used for assimilation of the indirect measurement of fruit dry biomass corresponding to the area of fruits in images. Dots refer to the average observation determined by destructive measurements, and the bar represents the associated standard deviation. The final value for the monitored plant is represented by a larger dot.

The last relevant result refers to the assimilation of aboveground biomass using the weighting system (Figure 5). Even though it thoroughly improved aboveground biomass, it had an adverse effect on fruit dry biomass. Because the Reduced Tomgro model calculates yield based on photosynthesis and respiration, instead of aboveground biomass previous values, the increase in biomass may lead to an increase in respiration that is not compensated by an increase in photosynthesis through LAI, thus decreasing assimilates available for fruits.

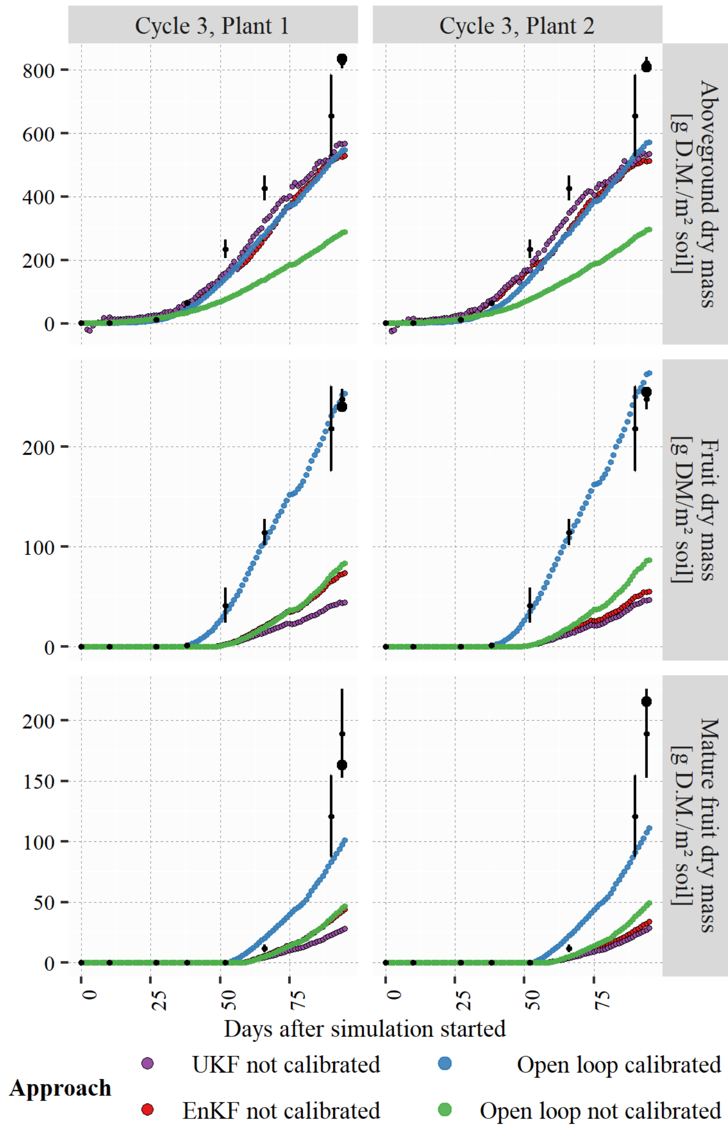

Figure 5. Growth curves for each monitored plant in Cycle 3 with the different methods used for assimilation of the indirect measurement of aboveground biomass corresponding to fresh plant weighting system. Dots refer to the values determined by destructive measurements, and the bar represents the associated standard deviation. The final value for the monitored plant is represented by a larger dot.

Another aspect to be observed is that it could be the case that for imprecise measurements, fewer observations may lead to similar outcomes of using all available data. Table 4 shows the results for assimilation using the UKF and its impact on yield, with the range of the observed RMSE in the repeated simulations. By reducing the frequency, ranges increase, as the usefulness of observations is not equal across time, and as later observations are often connected to poorer data quality, since the environment becomes more complex. Therefore, while fewer observations may lead to lower errors in most simulations, and the minimum observed RMSE in the multiple sampling is often similar to the one obtained using all observations, inferior results, i.e. larger errors, may also occur.

Table 4. Root mean squared error [g m^{-2}] for yield estimates assimilating data from different sources with the Unscented Kalman Filter. For 10% and 50% frequencies, observations were randomly sampled, so they are presented as the minimum and maximum RMSE obtained.

Frequency	Assim. state	Obs. variable*	Plant 1 - Cycle 1		Plant 2 - Cycle 1		Plant 1 - Cycle 2		Plant 2 - Cycle 2		Plant 1 - Cycle 3		Plant 2 - Cycle 3	
			Min	Max	Min	Max	Min	Max	Min	Max	Min	Max	Min	Max
-	None – Calib	-	5.05		10.11		29.05		25.34		4.65		5.50	
-	None – Not Calib.	-	20.48		17.95		22.45		21.72		62.21		61.12	
10%	LAI	GC Abv	24.64	26.42	22.99	25.41	**16.54**	29.20	**14.13**	**21.67**	**48.94**	**54.02**	**46.19**	61.99
50%	LAI	GC Abv	24.54	24.97	22.96	23.75	**24.57**	29.28	**19.66**	**22.41**	**48.98**	**52.40**	**46.21**	**53.98**
100%	LAI	GC Abv	24.59	24.59	23.01	23.01	**29.04**	**29.04**	**21.19**	**21.19**	**49.05**	**49.05**	**46.43**	**46.43**
10%	LAI	GC Lat	26.43	28.97	21.03	24.82	51.23	66.69	36.80	43.78	62.70	64.68	**56.75**	**59.76**
50%	LAI	GC Lat	26.83	27.66	20.46	21.79	62.02	65.58	39.26	43.07	63.50	63.90	**57.90**	**59.21**
100%	LAI	GC Lat	27.15	27.15	20.24	20.24	64.35	64.35	41.75	41.75	63.62	63.62	**58.76**	**58.76**
10%	W	W_fm_full	**17.99**	24.33	**9.23**	**13.62**	**7.43**	**10.20**	**11.78**	**15.41**	65.69	70.78	64.01	70.39
50%	W	W_fm_full	**19.52**	21.62	**9.45**	**11.43**	**6.99**	**7.40**	**11.22**	**12.14**	71.04	71.59	71.04	71.57
100%	W	W_fm_full	20.76	20.76	**9.85**	**9.85**	**7.19**	**7.19**	**11.40**	**11.40**	71.73	71.73	71.65	71.65
10%	Wf	Area Wf	**14.43**	24.77	**7.32**	**9.52**	**5.25**	**9.94**	**8.38**	**11.91**	**59.64**	**61.70**	**47.33**	**51.44**
50%	Wf	Area Wf	**13.87**	**16.38**	**7.79**	**9.64**	**5.50**	**5.92**	**8.46**	**9.70**	**60.73**	62.56	**48.01**	**51.59**
100%	Wf	Area Wf	**14.47**	**14.47**	**9.26**	**9.26**	**5.91**	**5.91**	**8.99**	**8.99**	**61.55**	**61.55**	**51.25**	**51.25**

*Observations as: GC Lat: green cover (lateral view), GC Abv: green cover (above view), W_fm_full: weighting system, Area Wf: total area of fruits. Bold numbers refer to root mean squared errors lower than the larger RMSE between the non-calibrated and calibrated error.

Finally, as the results observed are also a consequence of the reference used, we evaluated the results using another reference. The best example from the results is the case of the fruit estimates in Cycle 2 (Figure 6). One can see the model now overestimates fruit and mature biomass. Assimilation lowers the estimates while there are observations available, but as the rate of fruit biomass is calculated independently from the current value of the state, relying exclusively on net biomass, development stage, some parameters and air temperature, the steep increase observed in the non-calibrated estimates is then also observed in the curves of the assimilated cases.

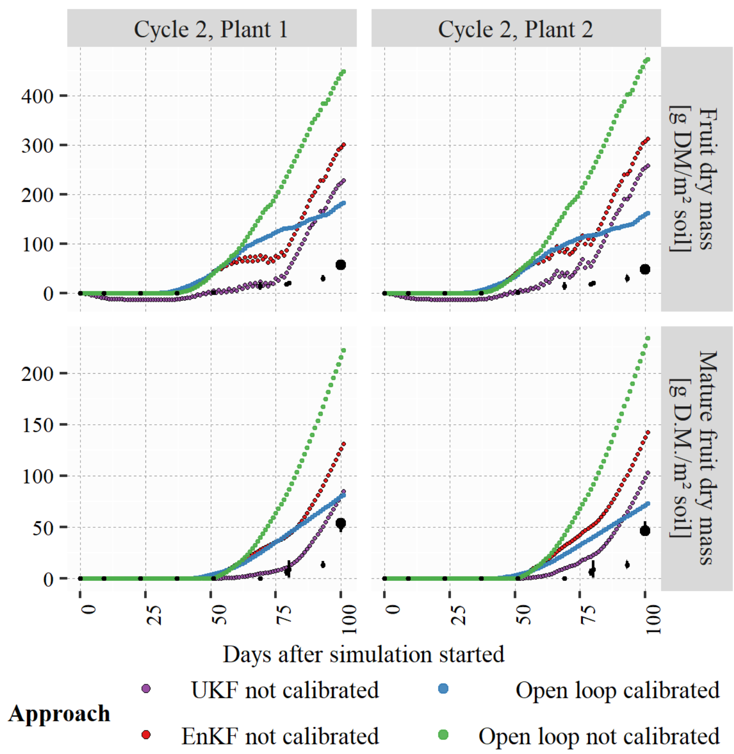

Figure 6. Growth curves for each monitored plant in Cycle 2 with the different methods used for assimilation of fruit dry biomass corresponding to the area of fruits in images. Dots refer to the values determined by destructive measurements and the bar represents the associated standard deviation. Final value for the monitored plant is represented by a larger dot.

D4. DISCUSSION

Calibration is usually a required step in assimilation, so that errors in the model are not as biased and the premises of the filters are not violated. However, this may be an excessively demanding step, as the parameters obtained from calibration with data from one population do not necessarily correspond to the true parameter values (Wallach, 2011), leading to the necessity of calibration for every different location and cultivar. Data assimilation of indirect measurements could replace this need if good data and good observation models are available.

Destructive measurements used for calibration could also be used in the development of observation models, so that for future work, these could be reused. Even in our case study, in which the three cycles were so different, often observations had similar magnitudes, so it should then be possible to obtain generalizable relationships. Furthermore, relationships may be improved: we focused on linear relationships, but fruit mass is proportional to volume, so treating them as linearly related to the area may be undermining how much information can be extracted.

As assimilation of a variable should impact their own estimates as well as the ones from other variables, we expected assimilation of several different state variables to improve yield outcomes in different ways. For instance, changes in leaf area index should affect aboveground biomass and fruit biomass as it affects photosynthesis. There are, however, several mechanisms that govern other state variables, such as respiration and fruit abortion, so that it is not necessarily the case that, even if there are improvements in the assimilated state, they are going to be propagated to other variables. It is then often unclear how assimilation may affect the results, since how much one state affects the other is not fixed even in potential growth, as changes in the weather inputs or cultivar could modify crop behavior. In our case, propagation led to two different outcomes after assimilation: both improvement and deterioration of the yield estimates. Our results suggest that for this greenhouse tomato model, the best approach should be assimilating fruit biomass: it is directly connected to yield and not only aboveground biomass could compromise the estimates as observed, but as the model expects leaf area to remain constant, so this data would stop being informative.

It could be the case that the high errors of observation models affected the ability of the techniques to extract information from the observations. These errors would lead to poorer estimates of the residuals and the gain, shifting how much the filter should rely on observations. Automatic annotation of images would allow for monitoring more plants and making the results more robust and based on more observations, which also impacts the observation models. Our observation models were limited, particularly for fruit area, as there were fewer observations, but they are promising, as suggested by the overall high correlations. When more observations are available, one can delve deeper into the question of which is the more appropriate timing for obtaining them, as it seems possible, with fewer observations, to achieve results as good as with observations every other day.

Hu et al. (2019) performed data assimilation in the SWAP-Wofost model, aiming to account for the interference in sugarcane LAI by artificial leaf stripping and natural storms, adjusting the potential growth provided by the model to real growth. In our case, we had three different scenarios: water stress, nutrient stress and adequate fertilization and irrigation. We observed the method was able to adjust the estimated variables obtained by the simulation, which expects potential growth, into more realistic values. And as yield variability in greenhouses may be even detected by models (Bojacá et al., 2009), this approach could be seen as a low-cost improvement of yield assessment by growers.

D5. Conclusions

In this work, we used data from different sources in a production-like environment to assimilate observations into a tomato growth model. Similarly to other data assimilation works, we observed that not all observations improve estimates, and the quality of observations and observation models greatly impact the outcome. But we showed how imperfect information from real-time observations could be used along with an imperfect model. Our work was a first attempt to use data assimilation techniques in a new context, and there are a few factors to disentangle from the observed outcomes — noisy observations and preliminary observation models —, and this work points to several venues of exploration.

D6. Acknowledgements

This study was financed in part by the Coordenação de Aperfeiçoamento de Pessoal de Nível Superior - Brasil (CAPES) - Finance Code 001 and by grant #2018/12050-6, São Paulo Research Foundation (FAPESP). We thank Dr James W Jones for providing access to the spreadsheet that was originally used to perform model calculations.

D7. References

Bojacá, C.R., Gil, R., Cooman, A., 2009. Use of geostatistical and crop growth modelling to assess the variability of greenhouse tomato yield caused by spatial temperature variations. Comput. Electron. Agric. 65, 219–227. https://doi.org/10.1016/j.compag.2008.10.001

Chen, W.-T., Yeh, Y.-H.F., Liu, T.-Y., Lin, T.-T., 2016. An Automated and Continuous Plant Weight Measurement System for Plant Factory. Front. Plant Sci. 7, 392. https://doi.org/10.3389/fpls.2016.00392

De Graaf, R., De Gelder, A., Blok, C., 2004. Advanced weighing equipment for water, crop growth and climate control management. Acta Hortic. 664, 163–167. https://doi.org/10.17660/ActaHortic.2004.664.17

de Koning, A.N.M., Bakker, J.C., 1992. In situ plant weight measurement of tomato with an electronic force gauge. Acta Hortic. 183–186. https://doi.org/10.17660/ActaHortic.1992.304.20

Dorigo, W.A., Zurita-Milla, R., de Wit, A.J.W., Brazile, J., Singh, R., Schaepman, M.E., 2007. A review on reflective remote sensing and data assimilation techniques for enhanced agroecosystem modeling. Int. J. Appl. Earth Obs. Geoinf. 9, 165–193. https://doi.org/10.1016/j.jag.2006.05.003

Gong, L., Yu, M., Jiang, S., Cutsuridis, V., Pearson, S., 2021. Deep Learning Based Prediction on Greenhouse Crop Yield Combined TCN and RNN. Sensors 21, 4537. https://doi.org/10.3390/s21134537

Helmer, T., Ehret, D.L., Bittman, S., 2005. CropAssist, an automated system for direct measurement of greenhouse tomato growth and water use. Comput. Electron. Agric. 48, 198–215. https://doi.org/10.1016/j.compag.2005.04.005

Hemming, S., de Zwart, F. de, Elings, A., Petropoulou, A., Righini, I., 2020. Cherry Tomato Production in Intelligent Greenhouses—Sensors and AI for Control of Climate, Irrigation, Crop Yield, and Quality. Sensors 20, 6430. https://doi.org/10.3390/s20226430

Hemming, S., de Zwart, F., Elings, A., Righini, I., Petropoulou, A., 2019. Remote Control of Greenhouse Vegetable Production with Artificial Intelligence—Greenhouse Climate, Irrigation, and Crop Production. Sensors 19, 1807. https://doi.org/10.3390/s19081807

Hu, S., Shi, L., Huang, K., Zha, Y., Hu, X., Ye, H., Yang, Q., 2019. Improvement of sugarcane crop simulation by SWAP-WOFOST model via data assimilation. F. Crop. Res. 232, 49–61. https://doi.org/10.1016/j.fcr.2018.12.009

Huang, J., Gómez-Dans, J.L., Huang, H., Ma, H., Wu, Q., Lewis, P.E., Liang, S., Chen, Z., Xue, J.-H., Wu, Y., Zhao, F., Wang, J., Xie, X., 2019. Assimilation of remote sensing into crop growth models: Current status and perspectives. Agric. For. Meteorol. 276–277, 107609. https://doi.org/10.1016/j.agrformet.2019.06.008

Jin, X., Kumar, L., Li, Z., Feng, H., Xu, X., Yang, G., Wang, J., 2018. A review of data assimilation of remote sensing and crop models. Eur. J. Agron. 92, 141–152. https://doi.org/10.1016/j.eja.2017.11.002

Jones, J.W., Dayan, E., Allen, L.H., Van Keulen, H., Challa, H., 1991. A dynamic tomato growth and yield model (TOMGRO). Trans. ASAE 34, 0663–0672. https://doi.org/10.13031/2013.31715

Jones, J.W., Kenig, A., Vallejos, C.E., 1999. Reduced state-variable tomato growth model.

Trans. ASAE 42, 255–265. https://doi.org/10.13031/2013.13203

Keating, B.A., Thorburn, P.J., 2018. Modelling crops and cropping systems—Evolving purpose, practice and prospects. Eur. J. Agron. 100, 163–176. https://doi.org/10.1016/j.eja.2018.04.007

Lee, J.W., Son, J.E., 2019. Nondestructive and Continuous Fresh Weight Measurements of Bell Peppers Grown in Soilless Culture Systems. Agronomy 9, 652. https://doi.org/10.3390/agronomy9100652

Linker, R., Ioslovich, I., 2017. Assimilation of canopy cover and biomass measurements in the crop model AquaCrop. Biosyst. Eng. 162, 57–66. https://doi.org/10.1016/j.biosystemseng.2017.08.003

Marcelis, L.F.M., van den Boogaard, R., Meinen, E., 2000. Control of Crop Growth and Nutrient Supply by the Combined Use of Crop Models and Plant Sensors. IFAC Proc. Vol. 33, 161–166. https://doi.org/10.1016/s1474-6670(17)40906-2

Pellenq, J., Boulet, G., 2004. A methodology to test the pertinence of remote-sensing data assimilation into vegetation models for water and energy exchange at the land surface. Agronomie 24, 197–204. https://doi.org/10.1051/agro:2004017

Ruíz-García, A., López-Cruz, I.L., Ramírez-Arias, A., Rico-Garcia, E., 2014. Modeling uncertainty of greenhouse crop lettuce growth model using Kalman Filtering. Acta Hortic. 1037, 361–368. https://doi.org/10.17660/ActaHortic.2014.1037.44

van Delden, S.H., SharathKumar, M., Butturini, M., Graamans, L.J.A., Heuvelink, E., Kacira, M., Kaiser, E., Klamer, R.S., Klerkx, L., Kootstra, G., Loeber, A., Schouten, R.E., Stanghellini, C., van Ieperen, W., Verdonk, J.C., Vialet-Chabrand, S., Woltering, E.J., van de Zedde, R., Zhang, Y., Marcelis, L.F.M., 2021. Current status and future challenges in implementing and upscaling vertical farming systems. Nat. Food 2021 1–13. https://doi.org/10.1038/s43016-021-00402-w

van Mourik, S., van Beveren, P.J.M., López-Cruz, I.L., van Henten, E.J., 2019. Improving climate monitoring in greenhouse cultivation via model based filtering. Biosyst. Eng. 181, 40–51. https://doi.org/10.1016/J.BIOSYSTEMSENG.2019.03.001

Verdouw, C., Tekinerdogan, B., Beulens, A., Wolfert, S., 2021. Digital twins in smart farming. Agric. Syst. 189, 103046. https://doi.org/10.1016/j.agsy.2020.103046

Wallach, D., 2011. Crop Model Calibration: A Statistical Perspective. Agron. J. 103, 1144–1151. https://doi.org/10.2134/agronj2010.0432

Yu, D., Zha, Y., Shi, L., Jin, X., Hu, S., Yang, Q., 2020. Improvement of sugarcane yield estimation by assimilating UAV-derived plant height observations. Eur. J. Agron. 121, 126159. https://doi.org/10.1016/j.eja.2020.126159

Appendix E — DATA ASSIMILATION IN CROP MODELS: OLD EXPERIENCES IN NEW CONTEXTS

ABSTRACT

Data assimilation has been used with remote sensing and crop models for decades, but often techniques requirements are not specified. As the concept may now be extrapolated to other contexts, such as greenhouse-grown plants or vertical farming, aided by computer vision to obtain data on plant growth, there is a great potential of these techniques being used for models to be available without the need for calibration. First, we delved into the requirements of assimilation techniques and how the particularities of remote sensing could be extrapolated to the protected environments context. Then, we performed an Observation System Synthetic Experiment to evaluate how assimilation of fruit or mature fruits in a greenhouse tomato growth model would impact the outcome, in the absence of calibration. We used three assimilation techniques — Ensemble Kalman Filter, Unscented Kalman Filter and Particle Filters — and evaluated different uncertainty characterizations, different observations assimilations, level of uncertainty acceptable and frequency of assimilation. We showed how filter uncertainty parameter choices greatly impacts outcomes and that their specification is also conditional on the frequency of observation availability.

E1. INTRODUCTION

Crop models are important tools but, as is the case with all models, their accuracy may be limited by the simplification of the processes they represent. One conclusion drawn from the theoretical evaluation of crop models' misspecification is that as the parameters obtained from calibration with data from one population do not necessarily correspond to the true parameters values, models should always be calibrated using a sample from the target population for them to show an improved performance (Wallach, 2011). Besides accuracy, model usage is also improved by reducing uncertainty in their estimates. To achieve the latter goal, (Wallach & Thorburn, 2017) mentioned the improvement of models, using the median of multi-model ensembles, redefining the quantity to be predicted. Evidently, if possible, other alternatives include using more data in the calibration step or higher quality input measurements.

One method that could tackle both uncertainty and accuracy issues, aligned to the new abundance of data, is called data assimilation (DA). Data assimilation on crop models has mostly been performed by the integration of remote sensing data into mechanistic models. The subject has been frequently revisited given the evolution in computational capacity and available state estimation techniques (Dorigo et al., 2007; Fischer, Kergoat, & Dedieu, 1997; Huang, Gómez-Dans, et al., 2019; Jin et al., 2018). The goals of data assimilation works are often connected to the improvement of agricultural systems' models predictive capability, differing in which variables are assimilated as well as the techniques used and the source of data that constitute the observations that will be assimilated.

The reviews that clarify how the approach has been used in crop modelling have looked into it from different perspectives: Previously, (Dorigo et al., 2007) had covered methods used to derive biophysical and biochemical canopy state variables from optical remote sensing data in the VNIR-SWIR regions. (Huang, Gómez-Dans, et al., 2019) recently detailed theoretical basis for methods as well as a walkthrough of the steps required to apply them. The authors suggest elements that should be considered when choosing the technique, the spatial and temporal scale, and presented an overview of uncertainty characterization. This last aspect is intimately connected to the discussion on (Jin et al., 2018), which also comment on sources of errors. All these works, however, emphasize aspects of satellite-derived observations, such as scale mismatches. In this sense, many of the lessons that have been learned by the crop modelling and remote sensing community could still be discussed and extended into other domains.

For instance, monitoring can happen frequently in greenhouse environments (Hemming, de Zwart, Elings, Petropoulou, & Righini, 2020; Hemming, de Zwart, Elings, Righini, & Petropoulou, 2019). And while the reviews previously mentioned point to multiple goals and approaches, such as assimilating soil moisture, leaf area index, vegetation indexes, leaf nitrogen accumulation and intended on improving yield, soil moisture, aboveground biomass, and leaf area index, many of the works are either very opaque for reproducing their methods or too specific to the problems of large areas.

It is often the case that works with simulations and artificial data are more detailed and their goals are more related to investigating the behaviour of the system with more methodological control. These have been called Observation System Synthetic Experiments (OSSE) (G. S. Nearing et al., 2012; Pellenq & Boulet, 2004) and synthetic twin (Lei et al., 2020) and have been used for answering questions such as if the assimilation of an observation improves all components of the model's simulations, if calibration errors can be compensated by assimilation (Pellenq & Boulet, 2004), which are limitations imposed by the model, the assimilation method, and uncertainty in model inputs and observations (G. S. Nearing et al., 2012), and appropriate ensemble size (Lei et al., 2020). In the greenhouse context, artificial data has also been used to emulate leaf area index measurements with the Reduced-State Tomgro model by (Torres-Monsivais, López-Cruz, Ruíz-García, Ramírez-Arias, & Peña-Moreno, 2017), aiming at evaluating the Unscented Kalman Filter performance on the estimation of leaf area index, aboveground biomass and number of nodes.

In this work, we aim at learning from satellite large scale experiences and bring these lessons to the other context of protected cultivation, revisiting aspects of data assimilation that are often not detailed in other reviews, as they focus on larger spatial scales and the issues associated to them, discussing theoretical aspects, along with an application with artificial data. We use greenhouse tomato growth as an example and the Reduced-State Tomgro model (Jones, Kenig, & Vallejos, 1999), aiming at improving yield estimates through assimilating simulated images of tomato in a greenhouse environment.

E2. THEORY

The reviews of data assimilation in crop models previously mentioned refer to three types of data assimilation: forcing, calibration and update. As there are several sources for better understanding them, this section will only briefly present the approaches, focusing on strategies for updating.

E2.1 Filter methods and their requirements

E2.1.1 The Kalman Filter (KF)

The main assumptions of the Kalman Filter are that the model estimates and the observations follow a normal distribution, and that the process model and the observation function are linear. Huang et al. (2019a) clarify the linearity requirement stating that if the crop model can be assumed locally linear between adjacent time steps, the standard Kalman Filter could be a viable choice.

Given its restrictions, there are fewer examples of the application of this technique. In some of them, the premise of the filter is used, but with modifications. Instead of calculating the gain, Vazifedoust et al., (2009) tested different values, using the best one as fixed, circumventing the need for identifying the source error values. This approach was repeated by

Chen Zhang and Tao (2018), who also normalized simulated and observation values according to the maximum value obtained so that they would be in the same range. Operating in this normalized space allowed them to focus on spatial variability and, in part, trends, instead of absolute values. Later, Chen and Tao (2020) explored more approaches for defining an appropriate value for the fixed gain, by a grid search of an optimal value, as well as exploring historical values.

E2.1.2 Extended Kalman Filter (EKF)

The Extended Kalman Filter is an adaptation of the Kalman Filter to deal with non-linear cases. To do so, it takes advantage of local linearization by replacing the model and the measurement function by their partial derivatives. The use of this technique is limited, as it requires access to the Jacobian of the model or, in some cases, to an approximation by finite differences that often will not scale to higher dimensions (Huang, Gómez-Dans, et al., 2019), so there are also few examples on crop modeling that apply this technique and most of those which use the method give few details of the implementation. One of the few examples in which there is an explanation of how the filter was used is the work of Linker and Ioslovich (2017). The authors used data from growth experiments of cotton and potatoes aiming at improving estimates of canopy cover and biomass through state assimilation and through the recalibration of three parameters from the Aquacrop model. They used dry biomass direct measurements and the images used as canopy cover observations were comprised of digital images taken 1.5 m and 2 m above canopy.

Given there were two different approaches for improving estimates, they estimated the covariance matrix of the errors in the state variables in two ways. For the assimilation process, by calculating the difference between the square of the model residuals and the dispersion of the measurements. They chose not to propagate the matrix along the process, given its strong nonlinearity, and recalculated it at each new time of measurement. They justified this choice by claiming the propagation without assimilation of new measurements would only increase the uncertainty related to the linearization and to the unknown initial data of the model errors. For the recalibration process, the matrix was calculated using an assumption that the corresponding standard deviation of each of the chosen parameters is equal to 20% of the current value of corresponding parameter. In their assimilation approach, the H matrix corresponded to the unit matrix, as the measurements directly corresponded to the states and, in the recalibration one, the components of the partial derivatives matrix H were calculated numerically at each instance of canopy cover measurement.

E2.1.3 Ensemble Kalman Filter (EnKF)

Overall, in the Ensemble Kalman Filter, an ensemble of initial states is generated and each individual ensemble member is propagated through the model until an observation is available. Then the update step is performed individually in each member. This allows for recalculation of the ensemble mean for the states and generation of a new ensemble. The ensemble approach comes from the premise that at least some of the particles will represent the true state. There are, however, different ways of approaching this problem and the elements of uncertainty are intimately connected to other decisions.

- Composition of ensemble elements

Huang et al. (2016) observed that two common methods to generate ensemble members are by directly adding a Gaussian perturbation to the state and by adding a Gaussian perturbation to the uncertain input parameters, which are then used by the model for the simulation. These methods have been explored in different ways. Input perturbation examples come from Lei et al. (2020), who perturbed precipitation and irrigation inputs via multiplicative rescaling with mean-unity lognormally distributed random errors that have a standard deviation equal to 20% of the corresponding input, and from De Wit and Van Diepen (2007), who generated precipitation ensembles based on a highly accurate precipitation dataset that was perturbed with an additive error component and a multiplicative component that generated binary rain or no-rain events on locations in which the records pointed to the absence of precipitation.

In cases in which states are perturbed, Xie et al. (2017) input the initial states and parameters into the CERES-Wheat and, at the beginning of the green-up stage, LAI and soil moisture were perturbed according to the errors between the field measurements and the simulated LAI and soil moisture. Ines et al. (2013) randomly sampled, at the start of the simulation, values of leaf weight at emergence and plant leaf area at emergence, to increase the variability of the ensemble. Beyond inputs, Lei et al. (2020) also applied direct perturbations to soil moisture states at all depths independently with random errors sampled from a mean-zero, normal distribution with temporally varying standard deviation equal to 10% of the state value, followed by the introduction of a vertical auto-correlation at the different depths.

Researchers have used multiple ways of ascribing uncertainty to parameters. Huang et al. (2016) chose the parameters based on the results of a sensitivity analysis and set the values of the standard deviations of two parameters according to the results of a previous study. Ines et al. (2013) identified which parameters had major influence in the model and, with an uncertainty level of 10%, perturbed each model parameter using a Gaussian distribution, generating ensemble members by randomly sampling model parameter combinations from the perturbed arrays. Zhao, Chen and Shen (2013) even tried to evaluate the impact of using parameter uncertainty to generate the ensembles. They chose one parameter that was mostly correlated to crop yield and ascribed a distribution to it, multiplying its standard deviation by different fixed values. Lu et al. (2021) took advantage of the existing uncertainty in parameters and used this as an artifact to generate ensembles without calibrating the model. They sampled parameters that they called variant as well as a fixed factor to scale phenological parameters for the canopy in a given year.

One issue in perturbing parameters or inputs for generating the ensembles is what Curnel et al. (2011) denominated phenological shift. This effect refers to ensemble members presenting ensemble elements that are in different phenological stages, which leads, at the same point in the simulation, to different modules in the model to be active and, therefore, the assimilation of an observation having different a meaning for each ensemble member.

As for observations, Ines et al., (2013) state that the variance used in the perturbation is based on the uncertainty of the data. But more precisely, Huang et al. (2016) mentions that the standard deviation of the Gaussian white noise error needs to be a realistic value for it to represent the uncertainty of the remotely sensed observation. In section 3.4.2, errors are more thoroughly described, but as an example, Xie et al. (2017) used the errors between the measurements and observations to determine the standard deviations of the observed LAI and soil moisture.

- Ensemble size

The choice of ensemble size is often performed in three different ways: testing, referencing a theoretical result or referencing other assimilation work on the literature. Pellenq and Boulet (2004) affirmed a preliminary study must be performed to find the minimum ensemble size that ensures particles may follow the same trajectory as the true state. They say the number usually corresponds to value above which assimilation results are identical. With this approach, Nearing et al. (2012) showed an example in which the number depended on the goal of the assimilation. The authors tested different values when assimilating LAI and soil moisture aiming at improving estimates of wheat yield, LAI and soil moisture. In the cases of assimilation of the state variable, RMSE became stable with number of elements of 25. In the other cases, the stability came with an ensemble of 100 elements. Lu et al. (2021) evaluated ensemble sizes for simultaneous assimilation of canopy cover and soil moisture from 10 to 400 and overall observed little improvement for more than 200, even though in some years 10 elements were enough for stable results.

Several works, however, refer to the experiences of other authors. Frequently, authors refer to De Wit and Van Diepen (2007) when commenting on their choice for the ensemble size (Bai et al., 2019; Y. Li et al., 2014; Zhao et al., 2013) The work by De Wit and Van Diepen (2007), however, applies to assimilating soil moisture with an ensemble obtained by perturbing precipitation and with an initial state ascribed by sampling a calculated Gaussian acceptable value and it is possible that they do not generalize for other approaches. Additionally, the authors mention that although they observed reduced RMSE in soil moisture estimates, this was not applied to the variance. Despite that, their results were compatible with other results for soil moisture, and recently, Mishra, Cruise and Mecikalski (2021) followed the suggestion from the work of Yin et al. (2015), who theoretically and through an example showed that the ideal ensemble size for assimilating soil moisture is 12, which suggests 50 would be a reasonable estimate in similar situations.

E2.1.4 Unscented Kalman Filter (UKF)

Similarly to the EnKF, the Unscented Kalman Filter uses the average of an ensemble as the state estimate, instead of the direct estimates provided by the model. However, the ensemble is not just sampled from a distribution. It uses what is called the unscented transform to generate particles — the sigma points — and weights for those particles that, when combined, are more representative of the expected state value. These sigma points are propagated through the non-linear model, which provides more accurate approximations of the mean and covariance matrix of the state vector, and thus more accurate state estimation. (Mansouri, Dumont, & Destain, 2013).

The Unscented Kalman Filter has been used in the context of crop growth with tomatoes and lettuce. Torres-Monsivais et al., (2017) evaluated the technique along with data simulated with the Reduced State Tomgro model, perturbed by several noise levels, representing measurements. Ruíz-García et al. (2014) used data from destructive analyses of lettuce in a greenhouse to assess uncertainty of the NICOLET model. In the work with tomato, the authors ascribed lower errors to the model and higher to the measurements, which were then subjected to a tuning process, while in the work with lettuce, the values were tuned until reasonable results were obtained.

E2.2 Errors and uncertainty

How to identify errors in the elements involved in assimilation and their uncertainties is widely discussed by Jin et al. (2018) and Huang et al. (2019a), as they are central in filtering approaches. For crop models, the sources of uncertainty they list include both the issues presented in section 3.3 as well as the difference between simulations and actual growth, which is impacted by pests and diseases. For observations, they mention errors in the measurement themselves and in retrieval methods. In both cases, often their works emphasize aspects of satellite-derived observations, such as errors in spatial data and scale mismatches. This section aims to revisit this topic, with more details and examples on how these uncertainties have been quantified and applied in data assimilation works. Although the discussion in this section focus on trying to ascribe meaning and understanding the uncertainties, these are filter hyperparameters that may be estimated from data (Wallach, Makowski, Jones, & Brun, 2019a).

- Observation errors

Overall, data assimilation in crop models rely on observations retrieved from satellite monitoring of Earth's surface. Dorigo et al. (2007) covered methods used to derive canopy state variables from optical remote sensing data in the visible to near-infrared and shortwave infrared regions. These methods either rely on statistical relationships between the spectral signature and the measured biophysical or biochemical properties of the canopy or they derive the states from the known behaviors of leaf reflectance and radiation propagation through the canopy. Both are used to obtain remote sensing products, which directly estimate the state for the final user. And both remote sensing products and reflectance itself, are used in assimilation. For those products, Huang et al. (2019a) mention how guidelines for uncertainty quantification are still being established by the community and that many EO-derived products have poor or no uncertainty information available. Particularly for satellite-derived leaf area index (LAI) products, Fang et al. (2019) also comment on how given the complexity associated to the retrieval process, a comprehensive quantitative assessment of the quality of LAI products is still missing. In the case of assimilating reflectance or albedo, the crop model is coupled with a radiative-transfer model (RTM), which allows for quantifying uncertainty in the measurements directly (Huang, Ma, et al., 2019).

By assimilating products, several works (Huang et al., 2016; Ines et al., 2013; Zhao et al., 2013) are able to consider the assimilation of the product as the assimilation of the state directly, which means the relationship between states and observations may be obtained by the unit matrix, simplifying the approach. However, this choice could affect the outcome as it may lead to bias in the residual and to the cross-variance term not taking any effect of dispersion caused by the observation model into account when determining the gain. Bias in the residual leads the updated estimate to the wrong value and in the gain, to the wrong weight of the residuals in the new estimate. These effects are not often discussed and the only example found that mentions them comes from the work of De Wit and Van Diepen (2007), which makes it explicit that the variance they ascribed to observations did not account for deficiencies in the conversion model itself, later concluding that the value they ascribed to the variance was indeed underestimated. Nevertheless, errors in retrieval have been acknowledged (Jin et al., 2018) and an alternative to avoid them is operating in the measurement space, which leads to avoiding the error in the inversion process (Guo et al., 2018). Additionally, Huang et al. (2019b) used the RTM PROSAIL, arguing this is a good way to avoid the process of regional LAI retrieval and Li et al. (2017) used the PROSAIL model and characterized errors in the observations, pointing to errors from 0.09 to 0.51 m^2 m^{-2} of error in LAI in the different development stages of wheat.

For those who develop their own measurement functions, they often establish them with empirical relationships and characterize their uncertainty based on field data. So works such as the one by Huang et al. (2016), which converted vegetation indices into LAI, obtained field measurements and used the regression error between LAI field observations and the indices to estimate errors in each phenological stage. As the problems that have been addressed often refer to large areas, estimates of observation uncertainty may be established as the variability across fields. For instance, Zhao, Chen and Shen (2013) understood that neighboring pixels had similar uncertainties for the same period and used the variance among fields as uncertainty of remote sensing LAI.

Other than satellite retrieved data, there are other sources for observations to which error is ascribed in other ways. For instance, Linker and Ioslovich (2017) and Ruíz-García et al. (2014) used destructive measurements of the assimilated state. In the first case, the authors used direct measurements of aboveground biomass of potatoes and cotton and in the second case, of lettuces. As for non-destructive measurements, Linker and Ioslovich (2017) also used pictures taken from 1.5 and 2 m above the crop to determine canopy cover, which, as a fraction of the fraction of the soil surface covered by the canopy, may also be considered a direct measurement of the state. On these cases, errors corresponded to variance from measurements. Data retrieved by unmanned aerial vehicles (UAVs) often have similar limitations as satellites regarding scale, but brings into discussions other aspects, particularly, as cameras are able to capture other types of data. For instance, Yu et al. (2020) used plant height detected by UAVs as well as field measured and discussed the effects of multiple values ascribed to errors, arguing the trial-and-error procedure could provide a guideline when the true field observation error is unknown.

Finally, one relevant aspect refers to how soil-crop systems may not have a constant value for the error. Nearing et al. (2012) explain how the soil moisture observation uncertainty is variable throughout time, since measurement accuracy degrades as vegetation water content increases throughout the season. They ascribed to error measurement a value derived from the relationship between variance in the soil moisture retrieval and this fraction of plant population and plant biomass that corresponds to water. Lei et al. (2020) evaluated a time-varying error for soil moisture observations as a function of LAI. They observed an overall improvement in soil moisture estimates, but also a somewhat less stable DA performance. Also for soil moisture, Mishra; Cruise and Mecikalski (2021), chose a constant error for the observation, but they were aware that the errors in the sensors used behaved in contrasting ways over crop growth stages, and that this choice may have led to errors that were too low in the early growth season and larger later in the season. Lu et al. (2021) used the multi-year average value of the daily standard deviation of the observations from the 4 soil moisture profiles. But for canopy cover, they noted the error varies dramatically during the growing season, with significant variability in the exponential growth stage and the decay period canopy cover, and only marginal when the canopy was near maximum. So, they assumed canopy cover observation error as dynamic, and the standard deviation of the samplings from the different zones on each sampling day was used separately. Li et al. (2017) considered the standard deviation of the LAI observations as 10% of the measured value, based one their observations of LAI, and Curnel et al. (2011) used a coefficient of variation to characterize uncertainty, thus ascribing to this hyperparameter of the filter a value that corresponded to a fraction of the observation.

- Model errors

As mentioned in section 3.3, model uncertainty may be ascribed to its parameters, inputs, and structure. In the case of Pellenq and Boulet (2004), they had two situations, and the differences in model behavior, regarding soil moisture and biomass, required different approaches for determining sources of model uncertainty. When analyzing the effects of initial input values, they observed that for biomass, as the state value is propagated throughout growth, there is no compensation for previous errors, and errors in the estimates of initial conditions could impact the following behavior. And while for soil water, the reliance on previous values is lower, with shorter "memory" of the system, in the coupled case, the initial water content could strongly impact biomass evolution. As for crop model noise, they assumed there would be at least one parameter set in the ensemble that could satisfactorily reproduce natural conditions. So, they decided by generating ensembles ascribing uncertainty to parameters and to inputs. On the other hand, in the case of soil moisture, since it tends towards low variance and equilibrium, they suggested including model noise as well, which should be nonetheless calibrated to avoid the loss of model integrity. Nearing et al. (2012) evaluated uncertainty in weather inputs, through correlated perturbations in weather time-series. Their results were not conclusive as in one of their systems, the assimilation of LAI improved yield estimates, but not the exclusive assimilation of soil moisture.

Uncertain inputs also manifest through unusual events, which are often not included in models. Therefore, for some authors, an advantage of filter assimilation methods is that they can incorporate these dynamic changes (Y. Li et al., 2014). For example, Hu et al. (2019) improved sugarcane yield estimates by assimilating leaf area index into the SWAP-Wofost model, after the interference in LAI caused by artificial leaf stripping and natural storms, and in Zhao, Chen and Shen (2013), the authors observed high errors when simulating yield for four regions in which meteorological disasters had occurred, which were then reduced to some extent by assimilating observations.

Calibration is an issue that is often mentioned regarding model errors, as it makes the model more consistent with the spatially limited field measurements and calculated uncertainty in parameters could be propagated through the model (Huang, Gómez-Dans, et al., 2019). Kang and Özdoğan (2019) identified that over large areas, calibration is no longer specific for cultivar, sowing dates or management. They commented on how the bias in model estimates this generates leads to violating the assumptions of assimilation techniques that require model errors to have zero means. The authors analyzed the impact of high model bias and uncertainty on yield estimates obtained by LAI assimilation and observed that bias with the same sign for

LAI and yield led to lower errors after assimilation than the open-loop reference, while opposite signs led to assimilation enlarging the errors. It is nevertheless the case that before performing assimilation, models are frequently calibrated. Lu et al. (2021) believed the standard was lower, aiming at having an ensemble of non-calibrated simulations that could capture the dynamics of key model states and that its spread reflected the model state variability. Their assimilation of canopy cover and soil moisture was able to improve yield when compared to the no-assimilation case.

E2.3 Variables

In a way, the largest restrictions to performing data assimilation in crop models are which additional data is available and if the knowledge or ability of how to relate them to models' state variables exists. This is one reason why LAI, canopy cover and soil moisture are frequently explored as observations, as there are several satellite products available for them. But being able to perform data assimilation does not mean that assimilation will be effective. As summarized by Lei et al. (2020), the performance of any data assimilation algorithm is fundamentally related to the strength of the relationship between observations and model states.

For Mishra; Cruise and Mecikalski (2021), assimilation of soil moisture, especially in irrigated areas, led to improvements in yield estimates, which is a very direct relationship, but for Ines et al. (2013), they expected assimilation of soil moisture in the DSSAT-CSM-Maize model to update the rootzone soil moisture, affecting soil nitrogen and, therefore, yield. There is then no guarantee that the included observations will improve estimates. For instance, Linker and Ioslovich (2017) discuss how since the Aquacrop model is water-driven, and as such, solar radiation is not considered explicitly, which may lead to underestimating the effect of canopy cover on crop development. And if assimilation not improving the outcomes is undesirable, it should be noted that it could even have an adverse effect on the estimates, depending on how variables interact with each other. Tewes et al. (2020a) argue that as model complexity rises, sequential update of only one or few state variables could threaten the model's integrity and cause an undefined state of the model, such as when the simulation triggers a new module by reaching a threshold value, but the filter updates the estimate to a value lower than the threshold.

Time-averaged correlation has been suggested as not very helpful when determining best assimilating state variables by Nearing et al. (2012). In their experiments, they point to several cases, using different realistic uncertainty scenarios, in which high correlation is not connected to improvement in yield estimates. Nearing et al. (2018) framed this discussion by relying on concepts of information theory, proposing a method to quantify how efficient data assimilation may be, through the quantification of information content on simulated model states and of the retrieval data relative to the imperfect evaluation data, and then measuring the fraction of this information that is extracted by a given DA implementation or algorithm.

E2.4 Timing and frequency

An issue that interacts with which variable is going to be assimilated to improve an estimate is at what time of growth and how often should the estimate be updated. Frequently, the discussion is connected to at which moment of the cycle the observation available will be most informative. Dente et al. (2008) evaluated the exclusion of one more precise image and observed that for wheat, within the conditions they observed, the data should include images from either the end of stem elongation stage or the beginning of heading, when the LAI reaches the maximum value. Timing of assimilation in wheat has been widely discussed (Curnel et al., 2011; Dente et al., 2008; Guo et al., 2019; Kang & Özdoğan, 2019; H. Li et al., 2017; Xie et al., 2017) with some authors reaching the conclusion that images from the whole cycle presented the best results (Kang & Özdoğan, 2019; H. Li et al., 2017). For sugarcane, on the other hand, Yu et al. (2020) concluded that assimilation of height in the late period of the elongation stage, involving the maximum plant height, can be the most useful, without the need for its sampling over the whole development stage.

As remote sensing observations are often only available with large intervals between them, their assimilation allows for the model to adjust to the updates, but local assimilation of, for example, soil moisture, would present a different situation. Lu et al. (2021) commented on how their use of local probes for monitoring soil moisture allowed for daily assimilation of this state, which likely improved their results. As crop systems models often present daily steps, it is not the case that assimilation would be performed in more frequent intervals, but in other contexts, such as weather forecasts, it has been argued that very frequent updates could insert noise in models, degrading forecasts (He, Lei, Whitaker, & Tan, 2020).

E3. MATERIALS AND METHODS

E3.1 Data sources

Environmental data collection was performed in research greenhouses at the School of Agricultural Engineering of the University of Campinas (22º 49' 06” S, 47º 03' 40” W, 635 m altitude), cultivated with tomatoes. Dry mass and leaf area index from destructive analyses of a tomato growth cycle was also collected for calibration of the models.

E3.2 Crop models

With the environmental data from greenhouses, we simulated growth using the Reduced State Tomgro model (Jones et al., 1999) and the Vanthoor model (Vanthoor, de Visser, Stanghellini, & van Henten, 2011). We performed assimilation in the Reduced Tomgro model with calibrated parameters from the original experiment in Gainesville, using two different sources of simulated observations, as explained in section 3.3. Calibration was performed in both models through minimizing the relative squared error.

Code was implemented in python language and difference equations were integrated by the Euler method. Model code, as all code used in this work, is available in https://github.com/mnqoliveira/data-assimilation-iot/.

E3.3 Data assimilation

We evaluated the impacts of different approaches for performing data assimilation for yield estimates. Ground truth values corresponded to the simulation performed in each of the four environments with the calibrated Reduced Tomgro. For the different approaches for assimilation, we included:

- Three assimilation techniques: Ensemble Kalman Filter (EnKF), Unscented Kalman Filter (UKF), Particle Filters (PF).
- Two assimilated variables: Fruit dry weight (Wf) and Mature fruit dry weight (Wm)
- Two sources of observations: one in which three noise levels were ascribed to the simulations of the calibrated Reduced Tomgro in the respective environments (Case 1) and one in which calibrated Vanthoor model was used for simulations (Case 2).

- Uncertainty in crop model: UKF requires determining a value for uncertainty in model estimates. In both Cases, as assimilation was performed in the non-calibrated Reduced Tomgro model, these were ascribed as the root mean squared error from the non-calibrated Reduced Tomgro model for the assimilated variable. This error was both tested as fixed and as a value variable through the cycle, corresponding to the error of the non-calibrated model to the samples used for calibration. For the EnKF, as this uncertainty could be ascribed in four different ways, we made an assessment of the different approaches: ascribing to the initial states the standard deviation of the observed initial values, ascribing to a parameter, conditioned to which state variable would be assimilated, a perturbation of 10% of its value, ascribing to the hourly photosynthetically active radiation a perturbation of 10% of its value and ascribing the values used in the variable case of the UKF directly to the model state.

- Uncertainty in observations: In Case 1, we ascribed the root mean squared error from the calibrated Vanthoor model for the assimilated variable, either using the RMSE of the whole cycle or the RMSE of the different observations in one day (Table 1). In Case 2, three different noise levels (10%, 30% and 50%) were ascribed to observations of the calibrated Reduced Tomgro Model. The level multiplied by the observation was treated as the standard deviation of a normal distribution from which the perturbation was sampled, as well as treated as uncertainty ascribed to that observation.

- We subsampled the observations to determine the effect of frequency. Subsampling used 50% and 10% of the data available in the cycle and in one of the repetitions, sampling was regularly spaced through the cycle while in the others, it was random.

In both Cases, we repeated the process 20 times to avoid biasing the results due to sampling. In the case of controlled error, we included additional random perturbations — N(1, 0.09) — in the observations and account for the variability of sampling the noise. The number of elements in Particle Filters was of 10.000 and in the Ensemble Kalman Filter, of 500.

Table 15. Errors ascribed to the filters as uncertainty estimates.

	Simulation day	Model		Observations (Case 1)	
State variable		Wf	Wm	Wf	Wm
Fixed – Non-calibrated model	All	90	60	45	20
Variable	10	0	0	0	0
	27	0	0	0	0
	38	1.73	0	2.85	0.0260
	52	38.7	0	6.20	2.01

	66	93.4	6.00	22.3	2.38
	90	144	82.5	8.21	45.6
	94	164	142	19.5	98.3

We evaluated our approaches by calculating the daily absolute relative error through growth. Our focus on evaluating daily results is related to the indeterminate growth. Differently from other crops in which one value is ascribed to yield, harvest for indeterminate crops is continuous, and therefore, model errors through the growth cycle affect estimates along harvests. As the excess of zeros from the vegetative phase could skew these results, they were not included in the calculation.

E4. RESULTS AND DISCUSSION

We have identified in the Theory section that even when the problem is well established, ascribing the covariances of filters' parameters is performed in multiple ways. In our evaluation of strategies to determine how to ascribe uncertainty to model and observations, we aimed at observing how imperfect measurements can allow for improvements on estimates of tomato yield, when compared to using the model without calibration (Open Loop). In general, Open Loop simulations in Experiments 1 and 2 underestimated the assumed truth a lot less than in Experiments 3 and 4. And as observations followed the trends in the truth, the larger differences in observations and model estimates would be observed in these two growth cycles. As for observations obtained from the Vanthoor model, there are differences depending on the variable. For fruits, they are overall slightly larger than the estimates of the non-calibrated model in Experiments 1 to 3 and much closer to the simulated truth in Experiment 4; for mature fruits, they are close to the non-calibrated model in Experiment 1, slightly larger than the model estimates in Experiments 2 and 3 and close to the simulate truth in Experiment 4.

We begin by the case in which we had no control on the error of the observation, Case 1, and attempt to understand and generalize them based on the results of Case 2. Figure 1 shows the relative errors of daily estimates through each cycle of all repetitions. One can observe how assimilation using both the UKF and the EnKF and fruits' observations in general improved the outcomes in comparison to the model without calibration and that assimilation of mature fruits' observations also showed improvements for most experiments. On the other hand, particle filters could not improve the estimates with assimilation of fruits, even deteriorating them, and only in some experiments it could improve estimates, particularly when all observations of mature fruit were available.

As in this first case errors on observations are not designed, uncertainty ascribed to them was evaluated as variable or fixed. Kalman filter methods are an optimized approach for performing a weighted average, in which the weights are related to the covariance of each estimate. If the residual magnitude is amplified by large uncertainties in the measurement, the impact on the updated value will be large, unless the uncertainty of the model is much lower than in the measurement, to guarantee the updated estimate would not be modified. As we used the non-calibrated model to provide models' estimates, which differs from the usual protocol, one could already expect, from Table 1, that models' larger covariances would lead assimilation to take more advantage of observations when their covariances are low. As it is often the case that crop models do not have constant variance (Wallach, Makowski, Jones, & Brun, 2019b), it is to be expected that errors grow through the cycle, so it seems that the process is more informed if covariances could vary with the magnitude of the observations and estimates. So, for the Kalman Filters, in this scenario, if model uncertainty is treated as variable, by ascribing the fixed value from Table 1 to the uncertainty in observations, the beginning of the growth cycle would mostly rely on the model and only final observations would be explored by the filter. On the other hand, if both are considered variable or if both are considered fixed, lower covariances of observations would move estimates towards them. Figure 1 shows that in Case 1, differences in the outcomes caused by uncertainty configuration depend both on the technique and frequency of assimilation. The EnKF should be mostly insensitive to the approaches evaluated regarding model covariance — unless if the perturbation was directly applied to the states, but in this case, it was applied to parameters —, as it calculates models' covariance based on the ensemble. The results then show marked differences based on how the observation covariance was treated. For the UKF, the ascribed uncertainty values led to very similar outcomes regardless of configuration, except for Experiment 4, in which the observations were the most different from the model estimates. In this case, allowing observation uncertainty to be lower than the model's led assimilation to rely more on them.

For the particle filter, the quality of the model estimates also affect the performance, but in a different way. In this case, instead of acting as a weight, model uncertainty spreads the particles of estimates for possible state variables' values and large covariances entail a very large spread. This spread is reduced by the selection of particles that are compatible to observations' uncertainties and values. Particles are then weighted considering their probability given the distribution of observation and, in this example, only in a few experiments it was possible to take advantage of both model estimates and observations to improve results through assimilation. Overall, divergence happened because the large spread of particles led to continuous resampling, without observations being used.

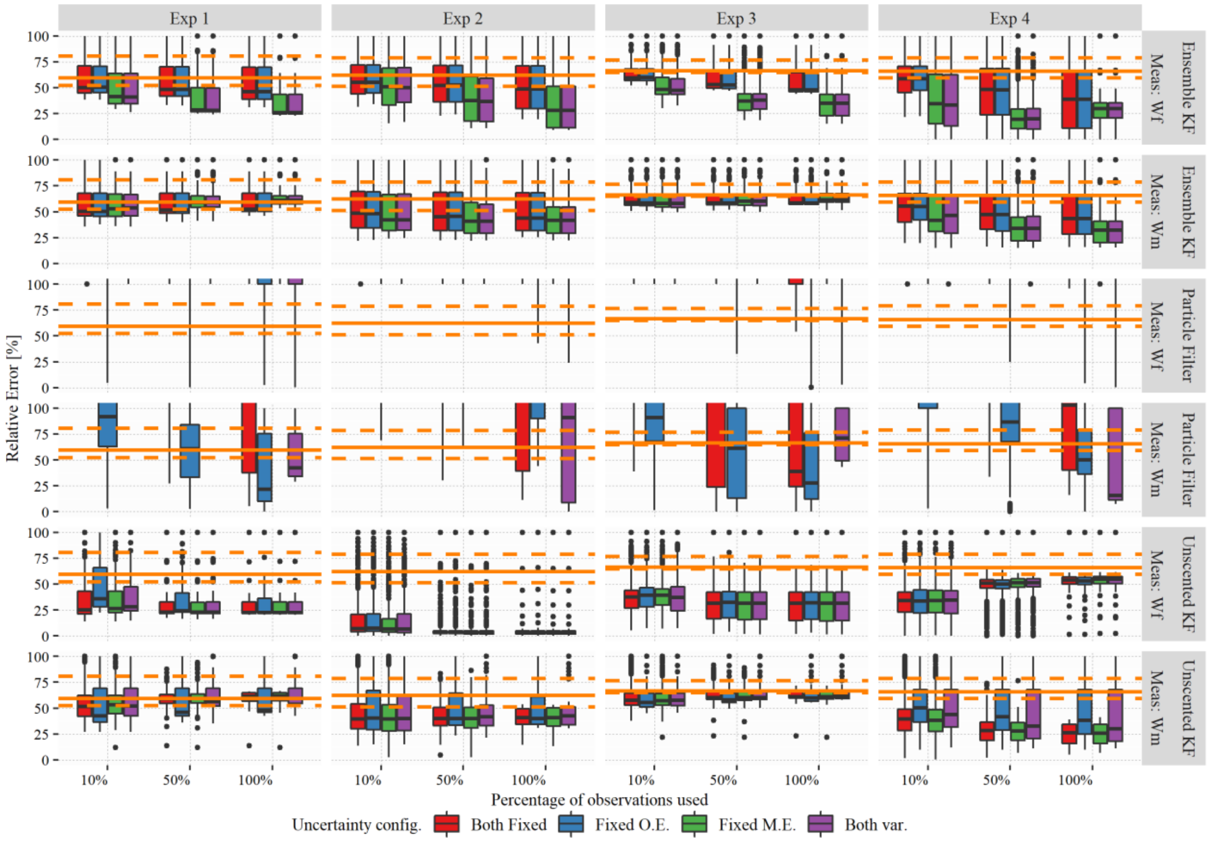

Figure 1. Relative errors for daily estimates of mature fruit dry mass obtained by assimilation of fruit dry biomass (Wf) or mature fruit dry biomass (Wm) as estimated by the Vanthoor model using the Ensemble Kalman Filter (EnKF), the Unscented Kalman Filter (UKF) or Particle Filters (PF) through the whole cycle with different fractions of the complete observation dataset for the four weather experiments and four different approaches of ascribing uncertainty (Model error and observation error fixed, only observation error fixed, only model error fixed and both varying through the cycle). Horizontal orange lines refer to the relative errors of the Reduced Tomgro model in estimating mature fruits without assimilation: full line corresponds to the median and dashed lines to the 25th and 75th percentiles. Y-axis is truncated at 100%.

Assimilation frequency may be considered complementary to uncertainty estimates, since assimilating an observation with large errors very frequently may not allow for the model to correct the estimates. As in most experiments of Case 1, observations were expected to improve estimates, except for assimilation of mature fruits in Experiment 1, which may be used as an example of fewer observations leading to slightly better results. On the other hand, in some cases, the difference between assimilation with half or 100% of observations of either variable for the Kalman Filters does not seem large, even in Experiment 4, in which observations lower relative errors the most.

With controlled errors, one can see the points previously made. It was expected that increasing noise would lead to deterioration of filter performance and that this is conditioned on model covariance, i.e., the larger the covariance is, more reliant the estimate is going to be on the observation. And that, except for large discrepancies, there will be a compromise between the two values. Figure 2 includes plots for relative error distribution in both fixed and variable model error cases in all four experiments for the assimilation of all observations available. Regarding the strategy of ascribing uncertainty to models, the previously mentioned effect of the EnKF is observed again. But the strategies lead to visibly different results for UKF and mature fruits. In this case, as observations are reasonably similar to the truth, they vastly improve the results of assimilation and the more the process is allowed to rely on them, by fixing model covariance as a large value, the lower the errors, similarly to what happened in Experiment 4 of Case 1. One can also note an interesting case for 30% of noise in fruits' observations and the Ensemble Kalman Filter in which the compromise between both model and observation uncertainty leads to yield estimates with lower relative errors than the lowest noise level. Before we delve into this issue, there is a comment to be made regarding assimilation frequency.

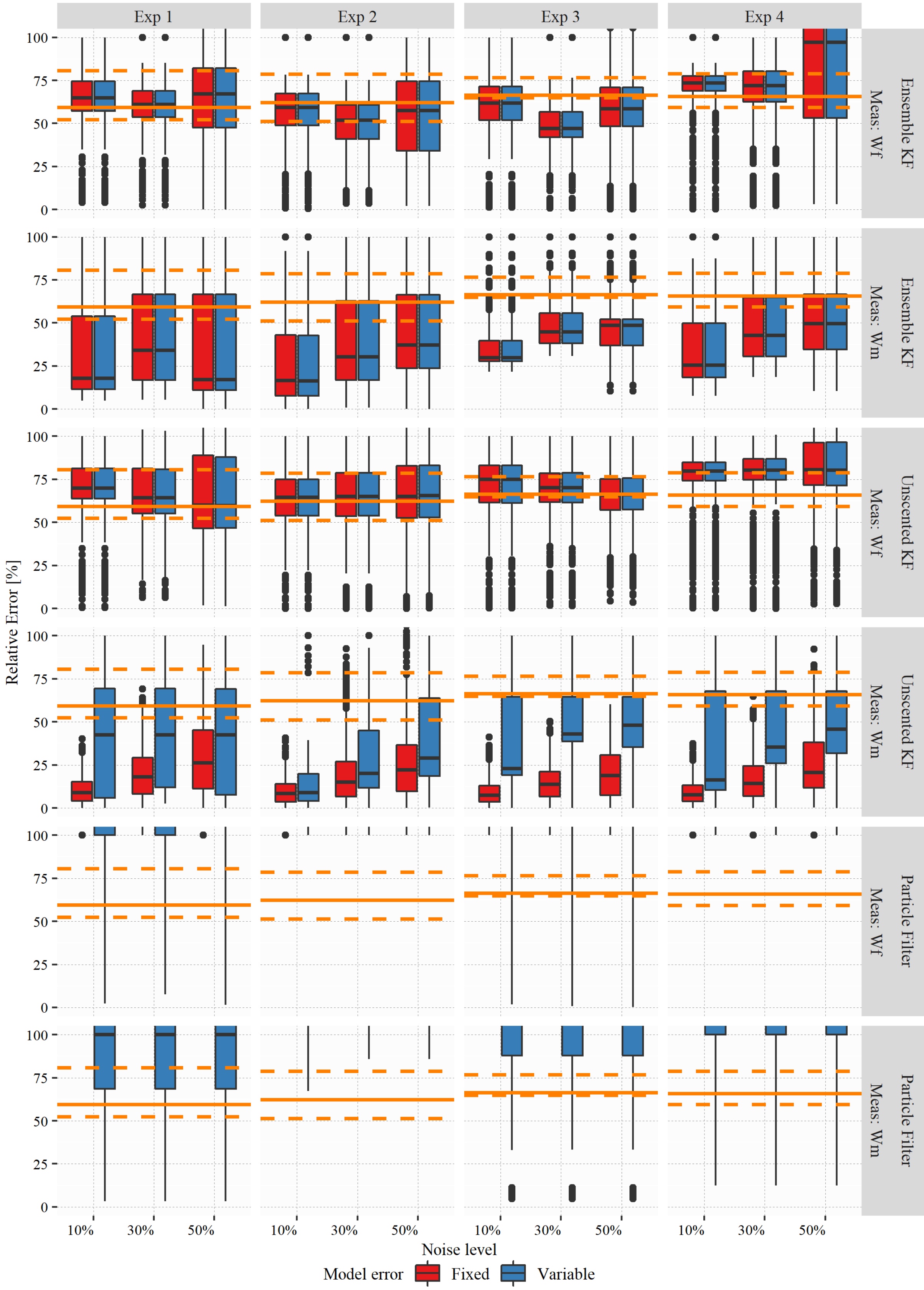

Figure 2. Relative errors for daily estimates of mature fruit dry mass obtained by assimilation of fruit dry biomass (Wf) or mature fruit dry biomass (Wm) as estimated by perturbations of different levels in the outputs of the Reduced Tomgro model using the Ensemble Kalman Filter (EnKF), the Unscented Kalman Filter (UKF) and Particle Filters (PF) through the whole cycle with different fractions of the

complete observation dataset for the four weather experiments and two different approaches of ascribing uncertainty (Model error fixed and model varying through the cycle). Horizontal orange lines refer to the relative errors of the Reduced Tomgro model in estimating mature fruits without assimilation: full line corresponds to the median and dashed lines to the 25th and 75th percentiles. Y-axis is truncated at 100%.

The effect of removing observations in the relative error over the growth cycle may be seen in Figure 3, in which the variable model uncertainty strategy is used. The main difference in outcomes relate to which variable is being assimilated, with worse outcomes for the more frequent assimilation of fruits' observations and the opposite being true for the assimilation of mature fruits. One can note that for both variables, as long as observations are not frequently used, outcomes are often similar regardless of noise level. This brings back the point of 30% of noise level in fruits observations leading to better outcomes with the EnKF noted in Figure 2, which is also clarified in Figure 4.

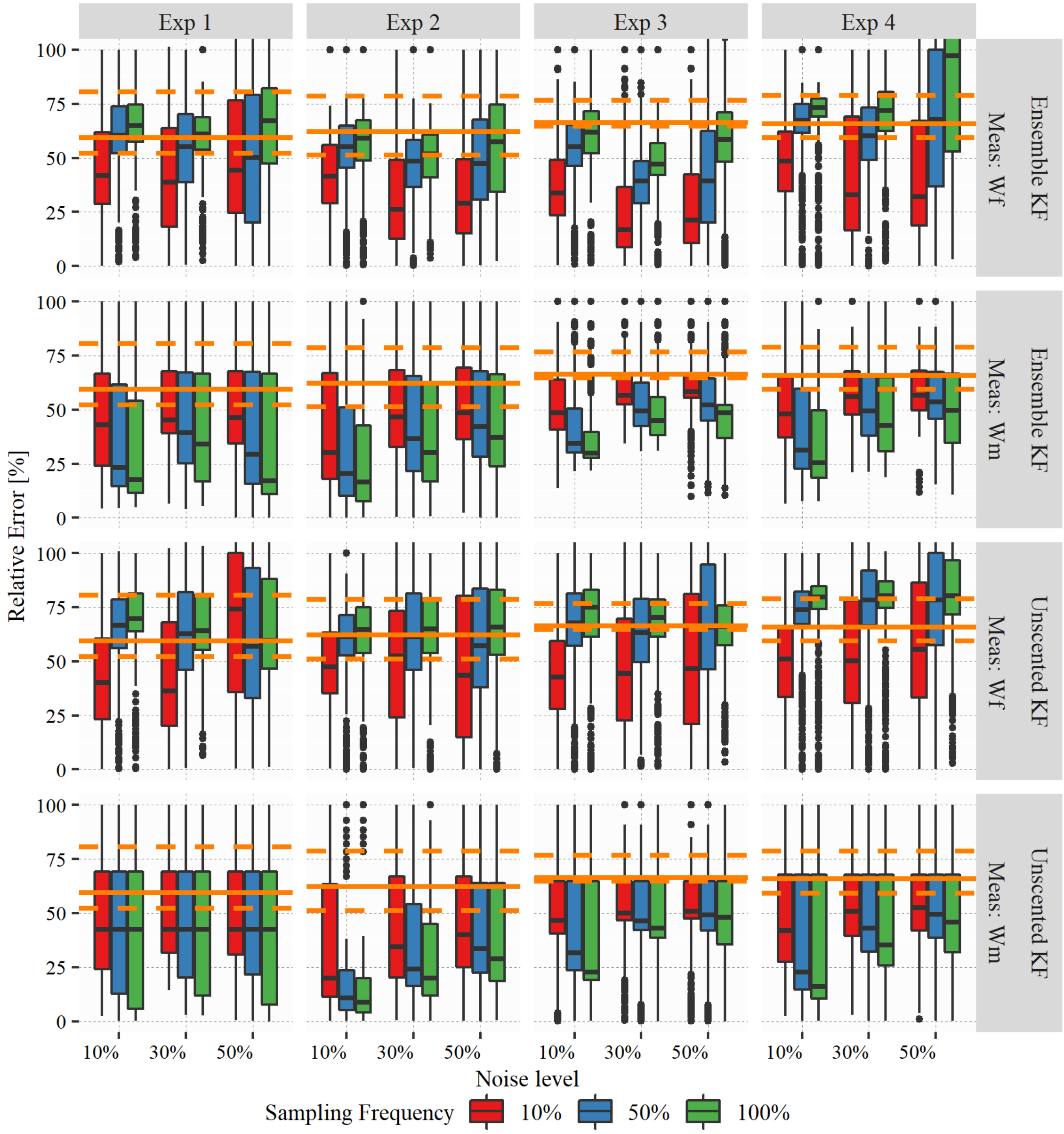

Figure 3. Relative errors for daily estimates of mature fruit dry mass obtained by assimilation of fruit dry biomass (Wf) or mature fruit dry biomass (Wm) as estimated by perturbations of different levels in the outputs of the Reduced Tomgro model using the Ensemble Kalman Filter (EnKF) and the Unscented Kalman Filter (UKF) through the whole cycle with different fractions of the complete observation dataset for the four weather experiments and ascribing variable model uncertainty to the filter. Horizontal orange lines refer to the relative errors of the Reduced Tomgro model in estimating mature fruits without assimilation: full line corresponds to the median and dashed lines to the 25th and 75th percentiles. Y-axis is truncated at 100%.

As assimilation relies both on observation quality and model performance, Figure 4 highlights the difference between experiments and how observations influence them. We selected for Case 1 the example of 100% of observations in which both uncertainty values are allowed to vary through growth. One can see in all experiments, that as the non-calibrated model underestimated both state variables, improvement provided by assimilation would come from taking advantage of the larger magnitude of observations to enlarge the estimates. But while it is evident that this would happen in Experiment 4, in which the variable of interest is the same as the one being assimilated, so there is no additional step of processing, this is less clear for the assimilation of fruits. Experiment 2 is a good example of this issue. In this experiment, even though observations of fruits were lower than the truth, the outcome when evaluating yield was much better than without assimilation. On the other hand, in Experiment 4, as observations of fruits were larger, this led to overestimating mature fruits after assimilation. This happens because assimilation does not change how the non-calibrated model relates fruits and mature fruits. This result is similar to the one of 30% of noise producing better results for yield, since it relates to how the updated state will impact the desired variable. In this sense, the idea of using few observations for the case of fruits relate to slightly changing magnitude but also capturing the trend with the model, causing an indirect positive effect on yield estimates.

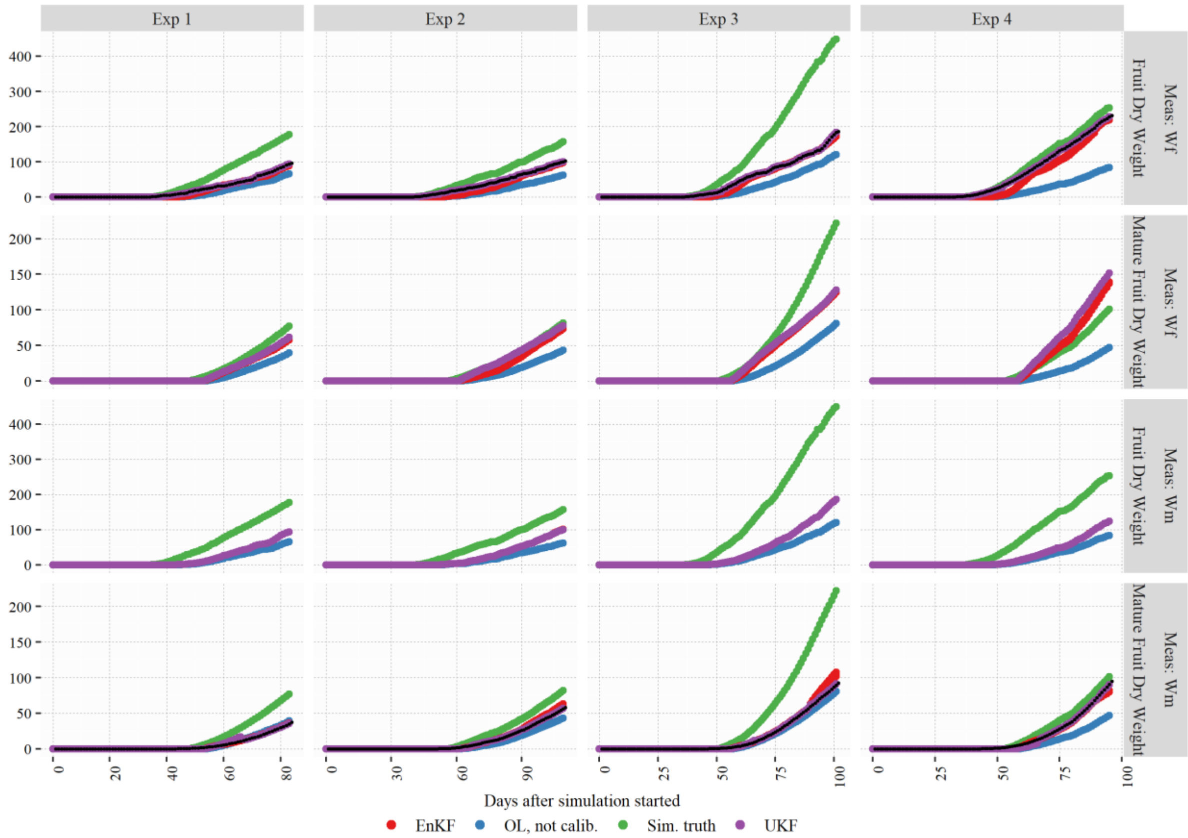

Figure 4. Growth curves for fruit and mature fruit dry mass obtained by assimilation of fruit dry biomass (Meas: Wf) or mature fruit dry biomass (Meas: Wm) estimated by the Vanthoor model as observations, using the Ensemble Kalman Filter (EnKF) or the Unscented Kalman Filter (UKF) with the complete observation dataset for the four weather experiments and ascribing variable uncertainty for both model and observations. Curves refer to all repetitions of the experiment.

Finally, in the previous discussions we focused on the generation of ensembles by using parameter perturbation. Figure 5 shows an example of the impact of the other approaches evaluated. Perturbating initial states had negligible effect in shifting estimates and perturbating states directly caused large variability on the values and if mature fruit is of interest, this is not desirable. This left inputs and parameters as possibilities, and we opted by the latter as outcomes seemed better.

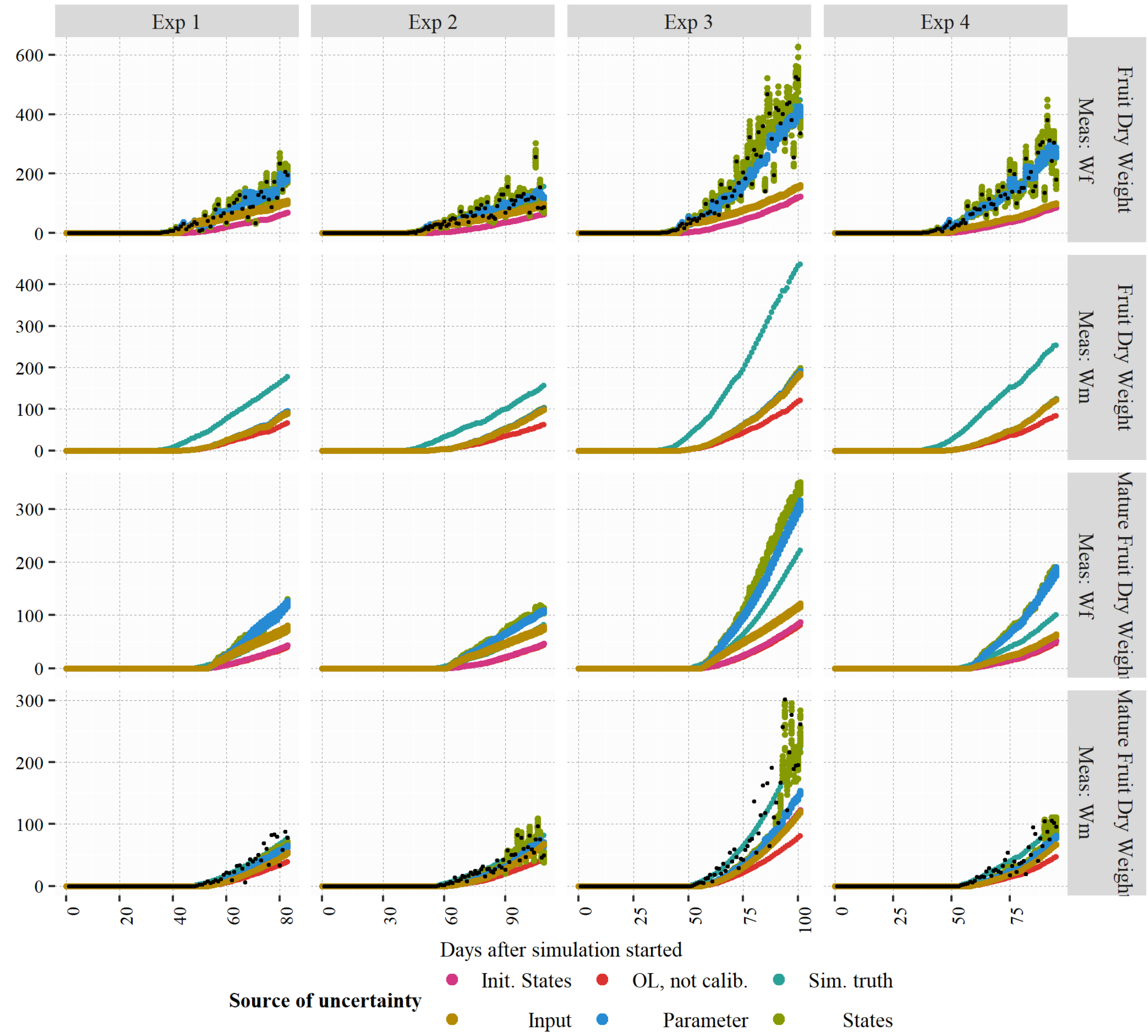

Figure 5. Growth curves for the estimates of both state variables evaluated, by assimilation of fruit dry biomass (Meas: Wf) or mature fruit dry biomass (Meas: Wm) using the Ensemble Kalman Filter with different approaches for ascribing uncertainty to the model, in all repetitions in each of the four weather experiments, for the case of variable model uncertainty in simulations using 30% of noise in observations. Smaller black dots represent the observations assimilated.

E5. CONCLUSION

Even though our focus was on discussing the new sources of data, assimilation with greenhouse tomato models is mostly new, so there is little information as to how different variables may impact the results. In this work we focused on assimilating fruit and mature fruit masses. It would be expected that direct assimilation of mature fruits could lead to the largest improvements, but we observed that intermittent assimilation of fruit mass also led to better estimates of mature fruit mass when compared to no assimilation.

We also aimed at enhancing clarity as to how to perform data assimilation and focused on a new field of application, in protected environments. The main characteristics of this new context for application are the new data sources, that could, for instance, rely on digital images to estimate fruit mass, as well as the frequency for obtaining them, which in this example could be daily. In this new context, in which availability of observations is not a restriction, some aspects of the process must be revaluated. Filter uncertainty parameter choices really impacts outcomes, and its specification is also conditional on the frequency of observation availability.

E6. ACKNOWLEDGEMENTS

This study was financed in part by the Coordenação de Aperfeiçoamento de Pessoal de Nível Superior - Brasil (CAPES) - Finance Code 001 and by grant #2018/12050-6, São Paulo Research Foundation (FAPESP). The funding sources had no role in the study design; the collection, analysis and interpretation of data; the writing of the report; or the decision to submit the article for publication.

E7. LITERATURE CITED

Bai, T., Wang, S., Meng, W., Zhang, N., Wang, T., Chen, Y., & Mercatoris, B. (2019). Assimilation of Remotely-Sensed LAI into WOFOST Model with the SUBPLEX Algorithm for Improving the Field-Scale Jujube Yield Forecasts. *Remote Sensing*, *11*(16), 1945. https://doi.org/10.3390/rs11161945

Chen, Y., & Tao, F. (2020). Improving the practicability of remote sensing data-assimilation-based crop yield estimations over a large area using a spatial assimilation algorithm and ensemble assimilation strategies. *Agricultural and Forest Meteorology*, *291*, 108082. https://doi.org/10.1016/j.agrformet.2020.108082

Chen, Y., Zhang, Z., & Tao, F. (2018). Improving regional winter wheat yield estimation through assimilation of phenology and leaf area index from remote sensing data. *European Journal of Agronomy*, *101*, 163–173. https://doi.org/10.1016/J.EJA.2018.09.006

Curnel, Y., de Wit, A. J. W., Duveiller, G., & Defourny, P. (2011). Potential performances of remotely sensed LAI assimilation in WOFOST model based on an OSS Experiment. *Agricultural and Forest Meteorology*, *151*(12), 1843–1855. https://doi.org/10.1016/j.agrformet.2011.08.002

de Wit, A. J. W., & van Diepen, C. A. (2007). Crop model data assimilation with the Ensemble Kalman filter for improving regional crop yield forecasts. *Agricultural and Forest Meteorology*, *146*(1–2), 38–56. https://doi.org/10.1016/j.agrformet.2007.05.004

Dente, L., Satalino, G., Mattia, F., & Rinaldi, M. (2008). Assimilation of leaf area index derived from ASAR and MERIS data into CERES-Wheat model to map wheat yield. *Remote Sensing of Environment*, *112*(4), 1395–1407. https://doi.org/10.1016/j.rse.2007.05.023

Dorigo, W. A., Zurita-Milla, R., de Wit, A. J. W., Brazile, J., Singh, R., & Schaepman, M. E. (2007). A review on reflective remote sensing and data assimilation techniques for enhanced agroecosystem modeling. *International Journal of Applied Earth Observation and Geoinformation*, *9*(2), 165–193. https://doi.org/10.1016/j.jag.2006.05.003

Fang, H., Baret, F., Plummer, S., & Schaepman-Strub, G. (2019). An Overview of Global Leaf Area Index (LAI): Methods, Products, Validation, and Applications. *Reviews of Geophysics*, *57*(3), 739–799. https://doi.org/10.1029/2018RG000608

Fischer, A., Kergoat, L., & Dedieu, G. (1997). Coupling Satellite Data with Vegetation Functional Models: Review of Different Approaches and Perspectives Suggested by the Assimilation Strategy. *Remote Sensing Reviews*, *15*(1–4), 283–303. https://doi.org/10.1080/02757259709532343

Guo, C., Tang, Y., Lu, J., Zhu, Y., Cao, W., Cheng, T., … Tian, Y. (2019). Predicting wheat productivity: Integrating time series of vegetation indices into crop modeling via sequential assimilation. *Agricultural and Forest Meteorology*, *272–273*, 69–80. https://doi.org/10.1016/J.AGRFORMET.2019.01.023

Guo, C., Zhang, L., Zhou, X., Zhu, Y., Cao, W., Qiu, X., … Tian, Y. (2018). Integrating remote sensing information with crop model to monitor wheat growth and yield based on simulation zone partitioning. *Precision Agriculture*, *19*(1), 55–78. https://doi.org/10.1007/s11119-017-9498-5

He, H., Lei, L., Whitaker, J. S., & Tan, Z. (2020). Impacts of Assimilation Frequency on

Ensemble Kalman Filter Data Assimilation and Imbalances. *Journal of Advances in Modeling Earth Systems*, *12*(10). https://doi.org/10.1029/2020MS002187

Hemming, S., de Zwart, F. de, Elings, A., Petropoulou, A., & Righini, I. (2020). Cherry Tomato Production in Intelligent Greenhouses—Sensors and AI for Control of Climate, Irrigation, Crop Yield, and Quality. *Sensors*, *20*(22), 6430. https://doi.org/10.3390/s20226430

Hemming, S., de Zwart, F., Elings, A., Righini, I., & Petropoulou, A. (2019). Remote Control of Greenhouse Vegetable Production with Artificial Intelligence—Greenhouse Climate, Irrigation, and Crop Production. *Sensors*, *19*(8), 1807. https://doi.org/10.3390/s19081807

Hu, S., Shi, L., Huang, K., Zha, Y., Hu, X., Ye, H., & Yang, Q. (2019). Improvement of sugarcane crop simulation by SWAP-WOFOST model via data assimilation. *Field Crops Research*, *232*, 49–61. https://doi.org/10.1016/j.fcr.2018.12.009

Huang, J., Gómez-Dans, J. L., Huang, H., Ma, H., Wu, Q., Lewis, P. E., … Xie, X. (2019). Assimilation of remote sensing into crop growth models: Current status and perspectives. *Agricultural and Forest Meteorology*, *276–277*, 107609. https://doi.org/10.1016/j.agrformet.2019.06.008

Huang, J., Ma, H., Sedano, F., Lewis, P., Liang, S., Wu, Q., … Zhu, D. (2019). Evaluation of regional estimates of winter wheat yield by assimilating three remotely sensed reflectance datasets into the coupled WOFOST–PROSAIL model. *European Journal of Agronomy*, *102*, 1–13. https://doi.org/10.1016/J.EJA.2018.10.008

Huang, J., Sedano, F., Huang, Y., Ma, H., Li, X., Liang, S., … Wu, W. (2016). Assimilating a synthetic Kalman filter leaf area index series into the WOFOST model to improve regional winter wheat yield estimation. *Agricultural and Forest Meteorology*, *216*, 188–202. https://doi.org/10.1016/j.agrformet.2015.10.013

Ines, A. V. M., Das, N. N., Hansen, J. W., & Njoku, E. G. (2013). Assimilation of remotely sensed soil moisture and vegetation with a crop simulation model for maize yield prediction. *Remote Sensing of Environment*, *138*, 149–164. https://doi.org/10.1016/J.RSE.2013.07.018

Jin, X., Kumar, L., Li, Z., Feng, H., Xu, X., Yang, G., & Wang, J. (2018). A review of data assimilation of remote sensing and crop models. *European Journal of Agronomy*, *92*(November 2017), 141–152. https://doi.org/10.1016/j.eja.2017.11.002

Jones, J. W., Kenig, A., & Vallejos, C. E. (1999). Reduced state-variable tomato growth model. *Transactions of the ASAE*, *42*(1), 255–265. https://doi.org/10.13031/2013.13203

Kang, Y., & Özdoğan, M. (2019). Field-level crop yield mapping with Landsat using a hierarchical data assimilation approach. *Remote Sensing of Environment*, *228*, 144–163. https://doi.org/10.1016/J.RSE.2019.04.005

Lei, F., Crow, W. T., Kustas, W. P., Dong, J., Yang, Y., Knipper, K. R., … Dokoozlian, N. (2020). Data assimilation of high-resolution thermal and radar remote sensing retrievals for soil moisture monitoring in a drip-irrigated vineyard. *Remote Sensing of Environment*, *239*, 111622. https://doi.org/10.1016/j.rse.2019.111622

Li, H., Chen, Z., Liu, G., Jiang, Z., & Huang, C. (2017). Improving Winter Wheat Yield Estimation from the CERES-Wheat Model to Assimilate Leaf Area Index with Different Assimilation Methods and Spatio-Temporal Scales. *Remote Sensing*, *9*(3), 190. https://doi.org/10.3390/rs9030190

Li, Y., Zhou, Q., Zhou, J., Zhang, G., Chen, C., & Wang, J. (2014). Assimilating remote sensing information into a coupled hydrology-crop growth model to estimate regional maize yield in arid regions. *Ecological Modelling*, *291*. https://doi.org/10.1016/j.ecolmodel.2014.07.013

Linker, R., & Ioslovich, I. (2017). Assimilation of canopy cover and biomass measurements in the crop model AquaCrop. *Biosystems Engineering*, *162*, 57–66. https://doi.org/10.1016/j.biosystemseng.2017.08.003

Lu, Y., Chibarabada, T. P., Ziliani, M. G., Onema, J. K., Mccabe, M. F., & Sheffield, J. (2021). Assimilation of soil moisture and canopy cover data improves maize simulation using an under-calibrated crop model. *Agricultural Water Management*, *252*(April), 106884. https://doi.org/10.1016/j.agwat.2021.106884

Mansouri, M., Dumont, B., & Destain, M.-F. (2013). Modeling and prediction of nonlinear environmental system using Bayesian methods. *Computers and Electronics in Agriculture*, *92*, 16–31. https://doi.org/10.1016/j.compag.2012.12.013

Mishra, V., Cruise, J. F., & Mecikalski, J. R. (2021). Assimilation of coupled microwave / thermal infrared soil moisture profiles into a crop model for robust maize yield estimates over Southeast United States. *European Journal of Agronomy*, *123*, 126208. https://doi.org/10.1016/j.eja.2020.126208

Nearing, G. S., Crow, W. T., Thorp, K. R., Moran, M. S., Reichle, R. H., & Gupta, H. V. (2012). Assimilating remote sensing observations of leaf area index and soil moisture for wheat yield estimates: An observing system simulation experiment. *Water Resources Research*, *48*(5). https://doi.org/10.1029/2011WR011420

Nearing, G., Yatheendradas, S., Crow, W., Zhan, X., Liu, J., & Chen, F. (2018). The Efficiency of Data Assimilation. *Water Resources Research*. https://doi.org/10.1029/2017WR020991

Pellenq, J., & Boulet, G. (2004). A methodology to test the pertinence of remote-sensing data assimilation into vegetation models for water and energy exchange at the land surface. *Agronomie*, *24*(4), 197–204. https://doi.org/10.1051/agro:2004017

Ruíz-García, A., López-Cruz, I. L., Ramírez-Arias, A., & Rico-Garcia, E. (2014). Modeling uncertainty of greenhouse crop lettuce growth model using Kalman Filtering. *Acta Horticulturae*, *1037*(1037), 361–368. https://doi.org/10.17660/ActaHortic.2014.1037.44

Tewes, A., Hoffmann, H., Krauss, G., Schäfer, F., Kerkhoff, C., & Gaiser, T. (2020). New Approaches for the Assimilation of LAI Measurements into a Crop Model Ensemble to Improve Wheat Biomass Estimations. *Agronomy*, *10*(3), 446. https://doi.org/10.3390/agronomy10030446

Torres-Monsivais, J. C., López-Cruz, I. L., Ruíz-García, A., Ramírez-Arias, J. A., & Peña-Moreno, R. D. (2017). Data assimilation to improve states estimation of a dynamic greenhouse tomatoes crop growth model. *Acta Horticulturae*, (1170), 433–440. https://doi.org/10.17660/ActaHortic.2017.1170.53

Vanthoor, B. H. E., de Visser, P. H. B., Stanghellini, C., & van Henten, E. J. (2011). A methodology for model-based greenhouse design: Part 2, description and validation of a tomato yield model. *Biosystems Engineering*, *110*(4), 378–395. https://doi.org/10.1016/j.biosystemseng.2011.08.005

Vazifedoust, M., van Dam, J. C., Bastiaanssen, W. G. M., & Feddes, R. A. (2009). Assimilation of satellite data into agrohydrological models to improve crop yield forecasts. *International Journal of Remote Sensing*, *30*(10), 2523–2545. https://doi.org/10.1080/01431160802552769

Wallach, D. (2011). Crop Model Calibration: A Statistical Perspective. *Agronomy Journal*, *103*(4), 1144–1151. https://doi.org/10.2134/agronj2010.0432

Wallach, D., Makowski, D., Jones, J. W., & Brun, F. (2019a). Data Assimilation for Dynamic Models. In D. Wallach, D. Makowski, J. W. Jones, & F. Brun (Eds.), *Working with Dynamic Crop Models* (Third Edit, pp. 487–518). https://doi.org/10.1016/B978-0-12-811756-9.00014-9

Wallach, D., Makowski, D., Jones, J. W., & Brun, F. (2019b). Regression Analysis, Frequentist. In D. Wallach, D. Makowski, J. W. Jones, & F. Brun (Eds.), *Working with Dynamic Crop Models* (Third Edit, pp. 161–205). https://doi.org/10.1016/B978-0-12-811756-9.00005-8

Wallach, D., & Thorburn, P. J. (2017). Estimating uncertainty in crop model predictions:

Current situation and future prospects. *European Journal of Agronomy*, *88*(October), A1–A7. https://doi.org/10.1016/j.eja.2017.06.001

Xie, Y., Wang, P., Bai, X., Khan, J., Zhang, S., Li, L., & Wang, L. (2017). Assimilation of the leaf area index and vegetation temperature condition index for winter wheat yield estimation using Landsat imagery and the CERES-Wheat model. *Agricultural and Forest Meteorology*, *246*, 194–206. https://doi.org/10.1016/J.AGRFORMET.2017.06.015

Yin, J., Zhan, X., Zheng, Y., Hain, C. R., Liu, J., & Fang, L. (2015). Optimal ensemble size of ensemble Kalman filter in sequential soil moisture data assimilation. *Geophysical Research Letters*, *42*(16), 6710–6715. https://doi.org/10.1002/2015GL063366

Yu, D., Zha, Y., Shi, L., Jin, X., Hu, S., & Yang, Q. (2020). Improvement of sugarcane yield estimation by assimilating UAV-derived plant height observations. *European Journal of Agronomy*, *121*(February), 126159. https://doi.org/10.1016/j.eja.2020.126159

Zhao, Y., Chen, S., & Shen, S. (2013). Assimilating remote sensing information with crop model using Ensemble Kalman Filter for improving LAI monitoring and yield estimation. *Ecological Modelling*, *270*, 30–42. https://doi.org/10.1016/j.ecolmodel.2013.08.016